

INFORMATION TO USERS

This manuscript has been reproduced from the microfilm master. UMI films the text directly from the original or copy submitted. Thus, some thesis and dissertation copies are in typewriter face, while others may be from any type of computer printer.

The quality of this reproduction is dependent upon the quality of the copy submitted. Broken or indistinct print, colored or poor quality illustrations and photographs, print bleedthrough, substandard margins, and improper alignment can adversely affect reproduction.

In the unlikely event that the author did not send UMI a complete manuscript and there are missing pages, these will be noted. Also, if unauthorized copyright material had to be removed, a note will indicate the deletion.

Oversize materials (e.g., maps, drawings, charts) are reproduced by sectioning the original, beginning at the upper left-hand corner and continuing from left to right in equal sections with small overlaps. Each original is also photographed in one exposure and is included in reduced form at the back of the book.

Photographs included in the original manuscript have been reproduced xerographically in this copy. Higher quality 6" x 9" black and white photographic prints are available for any photographs or illustrations appearing in this copy for an additional charge. Contact UMI directly to order.

U·M·I

University Microfilms International
A Bell & Howell Information Company
300 North Zeeb Road, Ann Arbor, MI 48106-1346 USA
313/761-4700 800/521-0600

Order Number 9136033

Analysis of combustion of pulverized coal by diffusion flame

Ji, Ching-China, Ph.D.

Rice University, 1991

U·M·I
300 N. Zeeb Rd.
Ann Arbor, MI 48106

RICE UNIVERSITY

**Analysis of Combustion of Pulverized Coal by
Diffusion Flame**

by

Ching-China Ji

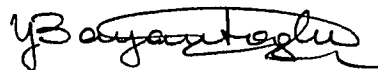
A THESIS SUBMITTED
IN PARTIAL FULFILLMENT OF THE
REQUIREMENTS FOR THE DEGREE

Doctor of Philosophy

APPROVED, THESIS COMMITTEE:



Dr. Cohen, Ruben D., Chairman
Associate Professor
Mechanical Engineering and Materials
Science



Dr. Bayazitoglu, Yildiz
Professor
Mechanical Engineering and Materials
Science



Dr. Chapman, Alan J.
Professor
Mechanical Engineering and Materials
Science



Dr. Miller, Clarence A.
Professor
Chemical Engineering

Houston, Texas

April, 1991

Analysis of Combustion of Pulverized Coal by Diffusion Flame

Ching-China Ji

Abstract

A two-dimensional theoretical model for the flow and combustion of pulverized coal by diffusion flames is presented. The model predicts gas flows, species concentrations and temperatures. The conservation equations are solved utilizing the κ - ϵ turbulence model. Coal devolatilization is modelled by two-competing-reactions scheme which generates two sets of volatiles and char, each by a specific rate constant which can be described in Arrhenius form, and char combustion from devolatilization occurs by reaction with oxygen, carbon dioxide, and water, and particle dispersion and radiative heat transfer between furnace wall and particles are studied.

The model is used to investigate the interaction between flow and combustion in flames produced by arranging the location of primary inlet and secondary inlet. The predictions, which could be valuable for designing furnaces, indicate that an off-center primary inlet, a large recirculation zone, and an asymmetric secondary air inlet are favorable for combustion.

Acknowledgments

I wish to express my gratitude and sincere thanks to my advisor Dr. Ruben D. Cohen for his guidance, advice, encouragement, and patience throughout this work. I would also like to thank Dr. Yildiz Bayazitoglu, Dr. Alan J. Chapman and Dr. Clarence A. Miller for serving on the dissertation committee.

Thanks are extended to the Department of Mechanical Engineering and Materials Science of Rice University for providing research environment and to the government of the Republic of China for financial support. An expression of appreciation is also due to Dr. Bala Ramaswamy, who is generous with suggestions and encouragement.

Finally, I would especially like to thank my wife, Hui-Chen, and daughter, Betty, for their patience and mental support during these years, and my family, for all their support.

Nomenclature

Symbols	Definition
a_1	constant
A	area for heat flow, recirculation area
A_F	preexponential factor
A_s	specific wetted surface area
b_1	constant
B	preexponential factor
B_{hr1}	preexponential factor for reaction $hr1$
B_{hr2}	preexponential factor for reaction $hr2$
B_{hr3}	preexponential factor for reaction $hr3$
B_{hr4}	preexponential factor for reaction $hr4$
B_{vo1}	preexponential factor for reaction $py1$
B_{vo2}	preexponential factor for reaction $py2$
C_1	empirical constant appearing in the turbulent transport equation
C_2	empirical constant appearing in the turbulent transport equation
C_D	drag force coefficient
C_μ	empirical constant appearing in the turbulent transport equation
dE	increment of stored energy
D	diffusion coefficient
\tilde{D}	drag due to the relative velocity between gas and particles
D_o	diffusion coefficient at time $t = 0$

Symbols	Definition
d_p	diameter of particle
D_{vx}	drag force in x direction
D_{vy}	drag force in y direction
$\frac{D}{Dt}$	substantial derivative
E	activation energy
\hat{E}	constant appearing in the logarithmic law of the wall
E_c	Eckert number
E_F	activation energy
E_{hr1}	activation energy for reaction <i>hr1</i>
E_{hr2}	activation energy for reaction <i>hr2</i>
E_{hr3}	activation energy for reaction <i>hr3</i>
E_{hr4}	activation energy for reaction <i>hr4</i>
E_{vo1}	activation energy
E_{vo2}	activation energy
F	fuel
\hat{F}	view factor
G	generation of turbulent kinetic energy
h	dimension of furnace
\hat{h}	heat transfer coefficient for a particle of size d_p
H_{chem}	mass enthalpy due to gas phase reactions
$H_{ho,F}$	heat released by homogeneous reaction
H_{ref}	$C_p T_{go}$
J	mechanical equivalent of heat
K	reaction rate constant
k_1	kinetic rate constant for reaction <i>py1</i>

Symbols	Definition
k_2	kinetic rate constant for reaction <i>py2</i>
K_{cond}	thermal conductivity
K_{hr1}	specific reaction rate constant for reaction <i>hr1</i>
K_{hr2}	specific reaction rate constant for reaction <i>hr2</i>
K_{hr3}	specific reaction rate constant for reaction <i>hr3</i>
K_{hr4}	specific reaction rate constant for reaction <i>hr4</i>
K_{vo1}	specific reaction rate constant for reaction <i>py1</i>
K_{vo2}	specific reaction rate constant for reaction <i>py2</i>
l_o	length scale of turbulence
\dot{m}_c	rate of mass loss due to consumption of carbon
\dot{m}_v	rate of mass loss due to pyrolysis
M_{cu}	coal undergraded
$\dot{M}_{ho,F}$	mass of fuel consumed per unit volume due to homogeneous reaction
$\dot{M}_{ho,K}$	mass of K species consumed per unit volume due to jth homogeneous reaction
\dot{M}_{hr}	carbon consumption rate of heterogeneous reaction
\dot{M}_{hr1}	carbon consumption due to reaction <i>hr1</i>
\dot{M}_{hr2}	carbon consumption due to reaction <i>hr2</i>
\dot{M}_{hr3}	carbon consumption due to reaction <i>hr3</i>
\dot{M}_{hr4}	carbon consumption due to reaction <i>hr4</i>
M_p	particle mass
\dot{M}_p	rate of mass loss due to pyrolysis and carbon consumption per particle
M_{po}	mass of particle at time $t = 0$

Symbols	Definition
$\dot{M}_{pp,K}$	rate of mass loss of species K due to pyrolysis and heterogeneous reactions ($K = CO, O_2, CH_4$) etc
\dot{M}_{vo}	volatiles liberation rate
\dot{M}_{vo1}	volatiles liberation rate for reaction <i>vo1</i>
\dot{M}_{vo2}	volatiles liberation rate for reaction <i>vo2</i>
n	order of reaction
\tilde{n}	number density (number of particles per unit spatial volume)
n_F	order of reaction with respect to fuel
n_{H_2O}	order of reaction with respect to H_2O
n_I	order of reaction with respect to I
n_{O_2}	order of reaction with respect to O_2
N_u	Nusselt number
P	pressure
P_r	Prandtl number
q	heat
\vec{q}	heat transfer flux vector
\dot{q}_{cond}	conductive heat transfer between the particle and gas
\dot{q}_{conv}	convective heat transfer between the particle and gas
\dot{q}_{het}	thermal energy exchanged between solid and gas phase via heterogeneous reaction
\dot{q}_{rad}	radiative heat transfer between particle and wall
$(\dot{q}_{chem})_{gas}$	chemical heat transfer
$(\dot{q}_{cond})_{gas}$	conductive heat transfer from the particle to gas per unit volume
$(\dot{q}_{conv})_{gas}$	convective heat transfer from the particle to gas per unit volume
\dot{q}_{decomp}	thermal energy utilized for decomposition of solid phase to gas

Symbols	Definition
q_x	conduction in x direction
q_y	conduction in y direction
r_p	radius of particle
R_u	universal gas constant
Re	Reynolds number
Re_{dp}	Reynolds number based on particle diameter
Re_{Dx}	Reynolds number in x direction
Re_{Dy}	Reynolds number in y direction
Re_{pg}	Reynolds number at grid point pg
S_B	burning surface of a spherical particle
Sc	Schmidt number
$S_{\dot{\phi}}$	source or sink term
t	time
T	transpose
T_g	gas temperature
T_p	particle temperature
T_w	temperature at wall
U	velocity
U_1	$U_g - U_p$
U_g	gas velocity in the x-direction
U_p	particle velocity in the x-direction
U_{pg}	velocity at grid point pg
$v_{K,F}$	stoichiometric coefficient
$v_{K,j}$	stoichiometric coefficient of species K in the jth reaction
V_g	gas velocity in the y-direction

Symbols	Definition
\vec{V}_g	gas velocity vector
\vec{V}_K	velocity of Kth species with respect to stationary coordinate axes
\vec{V}_{mK}	mass fraction of species K
V_1	$V_g - V_p$
V_p	particle velocity in the y-direction
\vec{V}_p	particle velocity vector
VO_1	volatile 1 produced due to pyrolysis reaction <i>py1</i>
VO_2	volatile 2 produced due to pyrolysis reaction <i>py2</i>
W	work
\dot{W}_{CO}	source term or sink of species <i>CO</i>
\dot{W}_h	source term or sink of energy
\dot{W}_K	source term or sink of species K
\dot{W}_m	source term or sink of mass
x	coordinate
y	coordinate
y_{pg}	the distance between grid point pg and wall
Y_{CO}	mass fraction of species <i>CO</i>
Y_K	mass fraction of species K
$Y_{O_2,w}$	mass fraction of species <i>O₂</i> at the wall of particle
∂	partial operator
ρ	density
ρ_K	mass of species K per unit volume
ρ_p	density of particle
ϕ	porosity (void volume / total volume)
$\hat{\phi}$	arbitrary variable

Symbols	Definition
μ	viscosity
μ_t	turbulent viscosity
μ_w	viscosity at the wall
$\hat{\mu}_w$	pseudo-viscosity at the wall
κ	kinetic energy of turbulence
$\hat{\kappa}$	von Karman's constant
κ_{pg}	kinetic energy of turbulence at grid point <i>pg</i>
ϵ	dissipation of turbulent kinetic energy
$\hat{\epsilon}$	emissivity
ϵ_{pg}	dissipation of turbulent kinetic energy at grid point <i>pg</i>
$\hat{\sigma}$	Stefan-Boltzmann constant
σ_k	empirical constant appearing in the turbulent transport equation
σ_ϵ	empirical constant appearing in the turbulent transport equation
ν_o	kinematic viscosity at time $t = 0$
α_1	maximum possible volatile yield via pyrolysis reaction <i>py1</i>
α_2	maximum possible volatile yield via pyrolysis reaction <i>py2</i>
λ	ρD
θ	dimensionless temperature
θ_p	dimensionless temperature
δQ	increment of heat transfer
δW	increment of work
$\vec{\nabla}$	gradient operator
$\Delta \hat{H}_v$	enthalpy of coal devolatilization
$\Delta \hat{H}_{het}$	enthalpy of coal heterogeneous reaction
Δx	length increment in <i>x</i>

Symbols	Definition
Δy	length increment in y
Δz	length increment in z
τ_{xx}	normal viscous force in the x-direction
τ_{xy}	shear force in the y-direction
τ_{yx}	shear force in the x-direction
τ_{yy}	normal viscous force in the y-direction
τ_w	shear stress at the wall
$\underline{\underline{\tau}}$	shear tensor
Γ_{ϕ}	diffusivity

Subscripts	Definition
o	initial value
c	center
g	gas
i	coordinate
j	coordinate
p	particle
E	east point of numerical cell
N	north point of numerical cell
P	center point of numerical cell
S	south point of numerical cell
W	west point of numerical cell

Supscripts	Definition
\cdot	time rate
$/$	correction
$*$	dimensionless

Contents

Abstract	ii
Acknowledgments	iii
Nomenclature	iv
List of Illustrations	xvi
List of Tables	xxii
1 INTRODUCTION	1
1.1 ABOUT COAL	1
1.1.1 CHARACTERISTICS OF COAL	1
1.1.2 ELEMENTS OF COAL REACTIONS	3
1.1.3 PHYSICAL AND CHEMICAL PROCESSES IN FLAMES . .	4
1.2 PREVIOUS RESEARCH ON PULVERIZED COAL COMBUSTION	5
1.3 CURRENT INVESTIGATION	6
2 DERIVATION OF THE GOVERNING EQUATIONS	9
2.1 MODEL	9
2.1.1 ASSUMPTIONS	10
2.2 GOVERNING EQUATIONS*	11
2.2.1 GAS PHASE GOVERNING EQUATIONS	11
2.2.1.1 MASS	11
2.2.1.2 MOMENTUM	12

*For detailed derivation, see Appendix A.

2.2.1.3	ENERGY	12
2.2.1.4	SPECIES	13
2.2.1.5	TURBULENCE MODEL	14
2.2.2	SOLID PHASE GOVERNING EQUATIONS	15
2.2.2.1	MASS	15
2.2.2.2	MOMENTUM	16
2.2.2.3	ENERGY (PARTICLE TEMPERATURE)	16
2.2.3	SOURCE TERMS	18
2.2.3.1	MASS SOURCE \dot{W}_m	18
2.2.3.2	SPECIES SOURCES, \dot{W}_K	21
2.2.3.3	ENERGY SOURCE, \dot{W}_h	23
2.3	WALL FUNCTIONS	23
2.4	SUMMARY OF GOVERNING EQUATIONS	25
2.4.1	CORRECTIONS	25
2.4.2	GOVERNING EQUATIONS	26
3	SOLUTION PROCEDURE	34
3.1	GENERAL ALGORITHM	34
3.1.1	THE STAGGERED GRID	35
3.1.2	DESCRIPTION OF THE COMPUTER PROGRAM:	37
3.2	THE SIMPLER ALGORITHM:	38
3.3	FINITE DIFFERENCE EQUATIONS FOR SOLID-PHASE	39
4	RESULTS AND DISCUSSION	45
4.1	SUDDEN EXPANSION FLOW	45
4.2	EFFECT OF RECIRCULATION AREA ON COAL COMBUSTION	46
4.3	EFFECT OF THE LOCATION OF THE SECONDARY AIR FLOW ON COAL COMBUSTION	49

4.4	EFFECT OF THE LOCATION OF THE PRIMARY STREAMS ON COAL COMBUSTION	51
5	CONCLUSIONS AND RECOMMENDATIONS	128
5.1	CONCLUSIONS	128
5.2	RECOMMENDATIONS REGARDING NUMERICAL PROCEDURES	130
	Bibliography	131
A	DERIVATION OF THE GOVERNING EQUATIONS	137
A.1	GAS PHASE	137
A.1.1	MASS	137
A.1.2	MOMENTUM	138
A.1.3	ENERGY	140
A.2	SOLID PHASE	142
A.2.1	MASS	142
A.2.2	MOMENTUM	144
B	DIMENSIONLESS GOVERNING EQUATIONS	146
B.1	NONDIMENSIONAL VARIABLES	146
B.2	DIMENSIONLESS GOVERING EQUATIONS	148

Illustrations

1.1	Schematic of Coal Particle, Illustrating Constituents and Reaction Processes	8
2.1	Gas-Phase Control Volume.	29
2.2	Solid-Phase Control Volume	30
2.3	Energy Balance Surround a Spherical Particle	31
2.4	View Factor.	32
2.5	Near Wall Nodes.	33
3.1	Staggered Location for U_g , V_g	41
3.2	Pressure Field	42
3.3	Two-Dimensional Grid Pattern	43
3.4	Program Flow Chart	44
4.1	Test Chamber in X-Y Coordinate.	55
4.2	Variation of Velocity (a) Present Predictions (b) Experimental Data of Barbin and Jones (1963).	56
4.3	Velocity Profile in Four Locations (a) Present Predictions (b) Experimental Data of Barbin and Jones (1963)	57
4.4	Kinetic Energy (a) Present Predictions (b) Experimental Data of Laufer (1952).	58

4.5	Velocity Profile (a) Present Predictions (b) Experimental Data of Laufer (1952).	59
4.6	Model Furnace Geometry and Six Cases of Different Inlet Position. .	60
4.7	Variation of Circulation Area A_1 and A_2	61
4.8	Variation of Total Circulation Area.	62
4.9	Reattachment Length.	63
4.10.1	Predicted Gas Velocity Vectors (a) Case 1 (b) Case 2 (c) Case 3 . . .	64
4.10.2	Predicted Gas Velocity Vectors (d) Case 4 (e) Case 5 (f) Case 6 . . .	65
4.11.1	Predicted Contours of Gas Velocity in X-Direction (a) Case 1 (b) Case 2 (c) Case 3	66
4.11.2	Predicted Contours of Gas Velocity in X-Direction (d) Case 4 (e) Case 5 (f) Case 6	67
4.12.1	Predicted Contours of Gas Velocity in Y-Direction (a) Case 1 (b) Case 2 (c) Case 3	68
4.12.2	Predicted Contours of Gas Velocity in Y-Direction (d) Case 4 (e) Case 5 (f) Case 6	69
4.13.1	Predicted Contours of Pressure (a) Case 1 (b) Case 2 (c) Case 3 . . .	70
4.13.2	Predicted Contours of Pressure (d) Case 4 (e) Case 5 (f) Case 6 . . .	71
4.14.1	Predicted Contours of Gas Temperature (a) Case 1 (b) Case 2 (c) Case 3	72
4.14.2	Predicted Contours of Gas Temperature (d) Case 4 (e) Case 5 (f) Case 6	73
4.15.1	Predicted Contours of Turbulent Kinetic Energy (a) Case 1 (b) Case 2 (c) Case 3	74
4.15.2	Predicted Contours of Turbulent Kinetic Energy (d) Case 4 (e) Case 5 (f) Case 6	75
4.16.1	Predicted Contours of Turbulent Dissipation Rate (a) Case 1	

(b) Case 2 (c) Case 3	76
4.16.2 Predicted Contours of Turbulent Dissipation Rate (d) Case 4	
(e) Case 5 (f) Case 6.	77
4.17.1 Predicted Contours of CO Concentration (a) Case 1 (b) Case 2	
(c) Case 3	78
4.17.2 Predicted Contours of CO Concentration (d) Case 4 (e) Case 5	
(f) Case 6.	79
4.18.1 Predicted Contours of CO_2 Concentration (a) Case 1 (b) Case 2	
(c) Case 3	80
4.18.2 Predicted Contours of CO_2 Concentration (d) Case 4 (e) Case 5	
(f) Case 6	81
4.19.1 Predicted Contours of CH_4 Concentration (a) Case 1 (b) Case 2	
(c) Case 3.	82
4.19.2 Predicted Contours of CH_4 Concentration (d) Case 4 (e) Case 5	
(f) Case 6.	83
4.20.1 Predicted Contours of H_2O Concentration (a) Case 1 (b) Case 2	
(c) Case 3	84
4.20.2 Predicted Contours of H_2O Concentration (d) Case 4 (e) Case 5	
(f) Case 6.	85
4.21.1 Predicted Contours of O_2 Concentration (a) Case 1 (b) Case 2	
(c) Case 3	86
4.21.2 Predicted Contours of O_2 Concentration (d) Case 4 (e) Case 5	
(f) Case 6	87
4.22.1 Predicted Cross-Section Profile of Gas Temperature at Five	
Different Locations (a) Case 1 (b) Case 2	88
4.22.2 Predicted Cross-Section Profile of Gas Temperature at Five	
Different Locations (c) Case 3 (d) Case 4.	89

4.22.3 Predicted Cross-Section Profile of Gas Temperature at Five Different Locations (e) Case 5 (f) Case 6	90
4.23.1 Predicted Cross-Section Profile of O_2 Concentration at Five Different Locations (a) Case 1 (b) Case 2.	91
4.23.2 Predicted Cross-Section Profile of O_2 Concentration at Five Different Locations (c) Case 3 (d) Case 4.	92
4.23.3 Predicted Cross-Section Profile of O_2 Concentration at Five Different Locations (e) Case 5 (f) Case 6.	93
4.24 The Location of Secondary Air in Six Cases, The Inclined Angle = 15.456° :	94
4.25.1 Predicted Gas Velocity Vectors (a) Case 1 (b) Case 2 (c) Case 3. . . .	95
4.25.2 Predicted Gas Velocity Vectors (d) Case 4 (e) Case 5 (f) Case 6. . . .	96
4.26.1 Predicted Contours of Pressure (a) Case 1 (b) Case 2 (c) Case 3. . . .	97
4.26.2 Predicted Contours of Pressure (d) Case 4 (e) Case 5 (f) Case 6. . . .	98
4.27.1 Predicted Contours of Gas Temperature (a) Case 1 (b) Case 2 (c) Case 3	99
4.27.2 Predicted Contours of Gas Temperature (d) Case 4 (e) Case 5 (f) Case 6.	100
4.28.1 Predicted Contours of Turbulent Kinetic Energy (a) Case 1 (b) Case 2 (c) Case 3.	101
4.28.2 Predicted Contours of Turbulent Kinetic Energy (d) Case 4 (e) Case 5 (f) Case 6.	102
4.29.1 Predicted Contours of Turbulent Dissipation Rate (a) Case 1 (b) Case 2 (c) Case 3	103
4.29.2 Predicted Contours of Turbulent Dissipation Rate (d) Case 4 (e) Case 5 (f) Case 6	104
4.30.1 Predicted Contours of CO Concentration (a) Case 1 (b) Case 2	

(c) Case 3.	105
4.30.2 Predicted Contours of CO Concentration (d) Case 4 (e) Case 5	
(f) Case 6.	106
4.31.1 Predicted Contours of CO_2 Concentration (a) Case 1 (b) Case 2	
(c) Case 3	107
4.31.2 Predicted Contours of CO_2 Concentration (d) Case 4 (e) Case 5	
(f) Case 6.	108
4.32.1 Predicted Contours of H_2O Concentration (a) Case 1 (b) Case 2	
(c) Case 3	109
4.32.2 Predicted Contours of H_2O Concentration (d) Case 4 (e) Case 5	
(f) Case 6.	110
4.33.1 Predicted Contours of O_2 Concentration (a) Case 1 (b) Case 2	
(c) Case 3	111
4.33.2 Predicted Contours of O_2 Concentration (d) Case 4 (e) Case 5	
(f) Case 6.	112
4.34.1 Predicted Contours of CH_4 Concentration (a) Case 1 (b) Case 2	
(c) Case 3	113
4.34.2 Predicted Contours of CH_4 Concentration (d) Case 4 (e) Case 5	
(f) Case 6.	114
4.35 The Location of Primary Streams in Three Cases.	115
4.36 Predicted Gas Velocity Vectors (a) Case 1 (b) Case 2 (c) Case 3. . . .	116
4.37 Predicted Contours of Gas Velocity in X-Direction (a) Case 1	
(b) Case 2 (c) Case 3.	117
4.38 Predicted Contours of Gas Velocity in Y-Direction (a) Case 1	
(b) Case 2 (c) Case 3.	118
4.39 Predicted Contours of Pressure (a) Case 1 (b) Case 2 (c) Case 3. . . .	119
4.40 Predicted Contours of Gas Temperature (a) Case 1 (b) Case 2	

	(c) Case 3.	120
4.41	Predicted Contours of Turbulent Kinetic Energy (a) Case 1 (b) Case 2	
	(c) Case 3.	121
4.42	Predicted Contours of Turbulent Dissipation Rate (a) Case 1 (b) Case 2	
	(c) Case 3	122
4.43	Predicted Contours of CO Concentration (a) Case 1 (b) Case 2	
	(c) Case 3	123
4.44	Predicted Contours of CO_2 Concentration (a) Case 1 (b) Case 2	
	(c) Case 3	124
4.45	Predicted Contours of H_2O Concentration (a) Case 1 (b) Case 2	
	(c) Case 3	125
4.46	Predicted Contours of O_2 Concentration (a) Case 1 (b) Case 2	
	(c) Case 3	126
4.47	Predicted Contours of CH_4 Concentration (a) Case 1 (b) Case 2	
	(c) Case 3	127

Tables

3.1	Subroutines and Their Parameters	40
4.1	Modeling Parameters Used in Each Section	53
4.2	Properties	54
4.3	Boundary Conditions at Wall, Inlet, and Exit	54

Chapter 1

INTRODUCTION

Although coal is currently one of the major sources of energy for power generation, its efficient consumption remains a difficult task. Much effort has been expended to better understand the processes involved in the combustion and conversion of coal. Once this knowledge is gained, the behavior of coal combustion can be predicted, thereby leading to improved designs for furnaces and combustion chambers.

Previous technologies related to improving coal furnaces and combustors have relied heavily on empirical trial and error methods for assessing the complex flows and chemical reactions. Recent technical advances in computer speeds involving numerical techniques for predicting turbulent, multiphase flows with chemical reaction have opened new avenues for analyzing such complex combustion systems.

1.1 ABOUT COAL

1.1.1 CHARACTERISTICS OF COAL

Coal consists of a complex mixture of organic chemical substances containing carbon, hydrogen and oxygen in chemical combination, together with small amounts of nitrogen and sulphur, formed mainly by the action of temperature and pressure on plant materials over long periods of time. The components present in coals are influenced by the difference in plant materials and in the extent of their decomposition.

Coals vary greatly in their composition. Of 1200 coals categorized by the Bituminous Coal Research Institute, no two had exactly the same composition (Hendrickson, 1975) [1]. Typical compositions (mass percentage) of coal include 65-95

percent carbon, 2-7 percent hydrogen, up to 25 percent oxygen and 10 percent sulfur, and 1-2 percent nitrogen (Essenhigh, 1977) [2].

Coalification is the name given to the development of the series of substances, which are peat, lignite or brown coal, bituminous and, finally, anthracite. Hendrickson (1975) [1] provides the following description of some of these coal types:

Lignite, the lowest rank of coal, was formed from peat which was compacted and altered. Its color has become brown and black and it is composed of recognizable woody materials imbedded in pulverized (macerated) and partially decomposed vegetable matter. Lignite displays jointing, banding, a high moisture content, and a low heating value when compared with the higher coals.

Subbituminous coal is difficult to distinguish from bituminous and is dull, black colored, shows little woody material, is banded, and has developed bedding planes. The coal usually splits parallel to the bedding. It has lost some moisture content, but is still of relatively low heating value.

Bituminous coal is dense, compacted, banded, brittle, and displays columnar cleavage and dark black color. It is more resistant to disintegration in air than are subbituminous and lignite coals. Its moisture content is low, volatile matter content is variable from high to medium, and its heating value is high. Several varieties of bituminous coal are recognizable.

Anthracite is the highly metamorphosed coal, is jet black in color, is hard and brittle, breaks with a conchoidal fracture, and displays a high luster. Its moisture content is low and its carbon content is high.

Neither *peat* nor *graphite* are coal, but they are the initial and end products of the progressive coalification process.

Bituminous is subdivided into three types: high volatile, medium volatile and low volatile. In the lower groups, the coal is low in carbon and very high in oxygen contents. Each higher group is distinguished by an increase in carbon content and a decrease in oxygen and hydrogen contents. Oxygen and hydrogen contents are considered as impurities, because they have the same effect on the heat value of the coal as ash; hence, the lower groups have a much lower available heat value than the higher groups.

Lowry (1963) [3], Given (1964) [4], Hendrickson (1975) [1], Neavil (1979) [5], Spackman (1980) [6], Hamblen *et al.* (1980) [7], and Elliott (1981) [8] discuss further physical, mechanical, thermal, and chemical properties of coal.

1.1.2 ELEMENTS OF COAL REACTIONS

In order to describe coal processes, a coal particle reaction is required. This schematic diagram of a reacting coal particle is shown in Figure 1.1 (Smoot and Pratt, 1979) [9].

The model suggests that the particle consists of:

- (1) Moisture
- (2) Raw coal
- (3) Char, and
- (4) Ash (mineral material)

At any time, during the reaction process, the particle may be surrounded by volatilized matter. A general description of experimental observations for pulverized-coal particles, and assumptions used in developing this model, are outlined in detail by Smoot and Smith (1979) [10].

Coal reactions are generally divided into two distinct components (Gray et al., 1976) [11]. Smoot and Smith (1985) [12] describe these two components as:

1. Devolatilization of the Raw Coal. This part of the reaction cycle occurs as the raw coal is heated in an inert or oxidizing environment; the particle may soften (become plastic) and undergo internal transformation. Moisture present in the coal will evolve early as the temperature rises. As the temperature continues to increase, gases and heavy tarry substances are emitted. The extent of this "pyrolysis" can vary from a few percent up to 70-80 of the total particle weight and can take place in a few milliseconds or several minutes depending on coal size and type, and on temperature conditions. The residual mass, enriched in carbon and depleted in oxygen and hydrogen, and still containing some nitrogen, sulfur, and most of the mineral matter, is referred to as "char". The char particle is often spherical (especially for small particles), has many cracks or holes made by escaping gases, may have swelled to a larger size, and can be very porous internally.

The nature of the char is dependent on the original coal type and size and also on the conditions of pyrolysis.

2. Oxidation of the Residual Char. The residual char particles can be oxidized or burned away by direct contact with oxygen at sufficiently high temperature. This reaction of the char and the oxygen is thought to be heterogeneous, with gaseous oxygen diffusing to and into the particle, adsorbing and reacting on the particles surface. This heterogeneous process is often much slower than the devolatilization process, requiring seconds for small particles to several minutes or more for larger particles. These rates vary with coal type, temperature, pressure, char characteristics (size, surface area, etc.), and oxidizer concentration. Other reactants, including steam, CO_2 , and H_2 , will also react with char, but rates with these reactants are considerably slower than for oxygen. These two processes (i.e., devolatilization and char reaction) may take place simultaneously, especially at very high heating rates. If devolatilization takes place in an oxidizing environment (e.g., air), then the fuel-rich gaseous and tarry products react further in the gas phase to produce high temperatures in the vicinity of the coal particles.

1.1.3 PHYSICAL AND CHEMICAL PROCESSES IN FLAMES

One characteristic feature of flames is that several physical and chemical processes can occur simultaneously. These processes can include (Smoot and Smith, 1985) [12]:

- (1) Convective and conductive heat transfer,
- (2) Radiative heat transfer,
- (3) Turbulent fluid motion,
- (4) Coal particle devolatilization,
- (5) Volatiles-oxidizer reaction,
- (6) Char-oxidizer reaction,
- (7) Particle dispersion,
- (8) Ash/slag formation,
- (9) Soot formation, and others.

The types of flame and operating conditions influence these processes, therefore, control the coal reaction process.

Most of the coal produced is consumed in pulverized form. Flames with pulverized coal include premixed flames and diffusion flames. In diffusion flames, fuel and oxidizer, not completely premixed, are delivered to a reactor vessel.

1.2 PREVIOUS RESEARCH ON PULVERIZED COAL COMBUSTION

The work of Field, et al. (1967) [13] contains a brief historical review of models of combustion processes developed in 1960's, and takes into account many aspects of coal reaction processes based on overall global calculations. These were the best computations available prior to 1970.

Also, reviews of modeling of turbulent reaction processes for gaseous systems are given by Edelman and Harsha (1978) [14], Lilley (1979) [15], and Williams and Libby (1980) [16]. Pulverized coal reaction processes as influenced by turbulence have been studied. The key components of the most recent and complete models are (Smoot, 1981) [17]:

- (1) Turbulence,
- (2) Gaseous combustion,
- (3) Particle dispersion,
- (4) Coal devolatilization,
- (5) Char reaction, and
- (6) Radiation.

By using these component models, the behaviors of certain interesting properties can be predicted. For instance, for turbulence, the $\kappa - \epsilon$ two equation method; for gaseous combustion, instantaneous reaction of CO ; for particle dispersion, particle treated like a gas; for coal devolatilization, parallel reaction rates of Arrhenius form; for char reaction, an oxidation rate of Arrhenius form; and for radiation, two-flux model. Gibson and Mogan (1970) [18] extended the steady-state model of Gosman et

al. (1969) [19] to simulate two-dimensional steady-state axisymmetric pulverized coal combustion. Richter and Quack (1974) [20] used a similar approach for low-volatile coals. The PCGC-2 model for two-dimensional, steady-state coal combustors (Smith and Smoot, 1980 [21]; Smith et al. 1981 [22]), includes the effects of gas turbulence on gaseous combustion and particle motion. Lockwood et al. (1980) [23] did a steady, two-dimensional method for coal flames with computations for a pulverized-coal furnace. Three-dimensional transient modeling of turbulent gaseous combustion has been treated by Patankar (1975) [24] and by Gosman et al. (1980). A three-dimensional, transient coal gasification model by Blake et al. (1977,1979) [25] is based on a mixed finite-element/finite-difference scheme. The finite-element character of the model permits numerical analysis of a variety of geometries.

1.3 CURRENT INVESTIGATION

Coal reaction processes, as mentioned before, depend strongly on the type of flame and operating conditions. Therefore, by adjusting operating conditions, one can effectively control furnace performance. An analysis of this comprises the main objective of this work.

We begin the modeling of the pulverized coal diffusion flame in a turbulent environment by considering pyrolysis, devolatilization, gas-phase reaction of volatiles, and heterogeneous oxidation processes. The characteristic effects of certain parameters such as wall temperature, inlet gas velocity, gas temperature, pressure, density, and particle size are taken into account.

This dissertation is organized in the following order. In Chapter 2, a suitable two-phase flow model is discussed, and the governing equations of conservation of mass, momentum, turbulent kinetic energy, turbulence dissipation rate energy, and species in gas and solid phases, as well as the wall function, are derived.

In Chapter 3, an algorithm named SIMPLER [26] is used to solve the elliptic partial differential equations which have the following form:

$$\frac{\partial}{\partial x}(\rho U \hat{\phi}) + \frac{\partial}{\partial y}(\rho V \hat{\phi}) = S_{\hat{\phi}} + \frac{\partial}{\partial x}(\Gamma_{\hat{\phi}} \frac{\partial \hat{\phi}}{\partial x}) + \frac{\partial}{\partial y}(\Gamma_{\hat{\phi}} \frac{\partial \hat{\phi}}{\partial y})$$

in gas phase. In solid phase, U_p and V_p are solved by using explicit central scheme for the second derivative and forward for the first derivative.

In Chapter 4, four different cases, all dealing with sudden expansion flow, are studied; these include a test case to evaluate the program's ability to solve the governing equations, the effects of recirculation area on coal combustion, the effects of the location of the secondary air flow on coal combustion and the effects of the location of the primary streams on coal combustion. The inlet, boundary conditions and the results of calculation are also described.

Finally, the dissertation ends with conclusions and recommendations in Chapter 5.

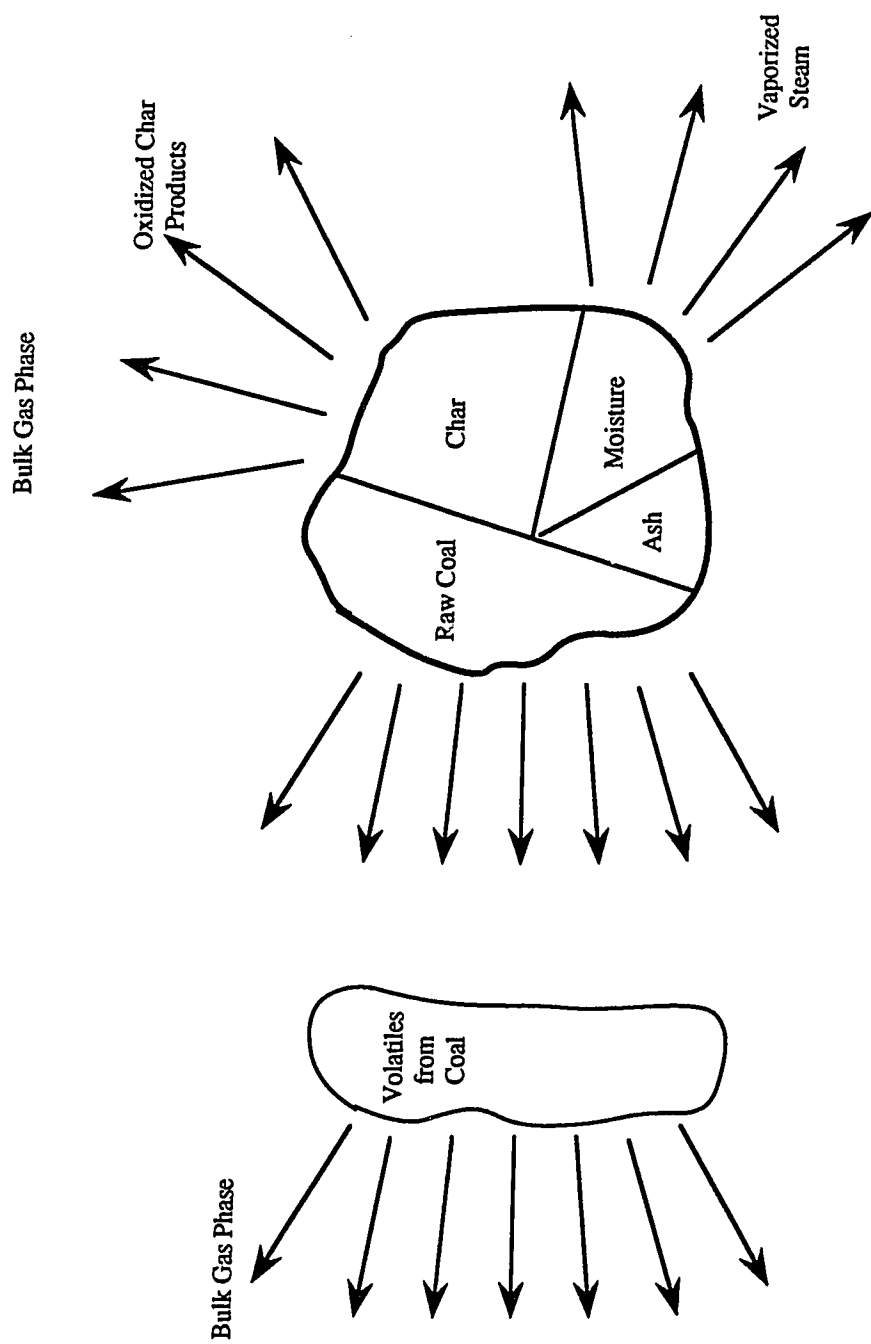


Figure 1.1 Schematic of Coal Particle, Illustrating Constituents and Reaction Processes.

Chapter 2

DERIVATION OF THE GOVERNING EQUATIONS

The objective of this chapter is to advance a detailed description of the model adopted. The assumptions used for this theoretical model are listed, the governing equations in the gas phase and solid phase for monosized particles flowing in the flow field are presented, and the gas-particle coupling is included through sources of mass, species and energy in the equations governing the gas flow are illustrated. The boundary conditions and the initial conditions for some particular problems are given in Chapter 4. With the help of some reference quantities, the governing equations are transferred into non-dimensional forms and presented in Appendix B.

2.1 MODEL

In order to investigate the interaction between flow and particle combustion in the flow field, the mass, momentum, energy and species equations for the gas phase, and the mass, momentum and energy equations for the solid phase are derived. They are approached by considering the balance of fluxes over a control volume. The control volume for the gas phase is the void volume occupied in a small elementary volume $\Delta x \Delta y \Delta z$ (Fig. 2.1); the remainder of which is occupied by the particles and, therefore, denoted as the particle phase control volume (Fig. 2.2).

The fractional porosity ϕ is defined as

$$\phi \equiv 1 - \frac{\tilde{n} M_p}{\rho_p} = \frac{\text{void volume}}{\text{total volume}} \quad (2.1)$$

where

\tilde{n} is the number density (number of particles per unit spatial volume)

M_p is the mass of each particle (M)

ρ_p is the density of particles (M/L³)

For a system of spherical particles of uniform size, we have

$$\phi = 1 - \frac{4}{3}\pi r_p^3 \tilde{n} \quad (2.2)$$

or

$$\tilde{n} = \frac{3(1 - \phi)}{4\pi r_p^3} \quad (2.3)$$

The specific wetted surface area, A_s , can be expressed as

$$A_s = S_B \tilde{n} = 4\pi r_p^2 \frac{3(1 - \phi)}{4\pi r_p^3} = \frac{3(1 - \phi)}{r_p} \quad (2.4)$$

where S_B is the burning surface of a spherical particle.

2.1.1 ASSUMPTIONS

The following aspects of pulverized-coal combustion and gasification have been incorporated in the model:

- (1) Two dimensional in x-y.
- (2) Monosized particles.
- (3) No soot is formed.
- (4) No particle fragmentation.
- (5) Steady-state condition apply.
- (6) Mixing of primary and secondary streams (specified as input).
- (7) Devolatilization of the coal.
- (8) Reaction of the char by oxygen, steam, carbon dioxide, and hydrogen.
- (9) Conductive and convective heat transfer between the coal particles and the gases.
- (10) Convective losses to the furnace wall.
- (11) Particle-wall radiation.
- (12) Oxidation of the coal devolatilization products.

2.2 GOVERNING EQUATIONS¹

2.2.1 GAS PHASE GOVERNING EQUATIONS

2.2.1.1 MASS

The equation for the conservation of mass may be stated as :

$$\left[\begin{array}{l} \text{the rate of gaseous mass} \\ \text{accumulation in the control} \\ \text{volume occupied by gases} \end{array} \right] = \left[\begin{array}{l} \text{the mass flux} \\ \text{convected into} \\ \text{control volume} \end{array} \right] + \left[\begin{array}{l} \text{the rate of gaseous mass addition} \\ \text{due to devolatilization and} \\ \text{heterogeneous reaction of solid particles} \end{array} \right]$$

The mass balance equation is :

$$\frac{\partial(\rho_g \phi)}{\partial t} + \vec{\nabla} \cdot (\rho_g \vec{V}_g \phi) = \dot{M}_p \tilde{n} = \dot{W}_m \quad (2.5)$$

where

ρ_g is the density of gas (M/L³)

\vec{V}_g is the gas velocity vector (L/T)

\dot{W}_m is the source term of mass (M/T)

\dot{M}_p is the rate of mass loss per particle due to pyrolysis and carbon consumption (M/T)

Note that when there are no particles in the spatial volume $\Delta x \Delta y \Delta z$, then $\phi = 1$ and $\dot{W}_m = 0$, so that the above equation reduces to the conventional continuity equation for unsteady, two dimensional flow.

¹For detailed derivation, see Appendix A.

2.2.1.2 MOMENTUM

The gas-phase momentum equation 2.6 is based upon the following :

$$\left[\begin{array}{c} \text{rate of increase} \\ \text{of momentum in} \\ \text{the control volume} \end{array} \right] = \left[\begin{array}{c} \text{net rate of} \\ \text{momentum flux into} \\ \text{control volume} \end{array} \right] + \left[\begin{array}{c} \text{summation of forces} \\ \text{acting on the} \\ \text{control volume} \end{array} \right]$$

In vector notation

$$\frac{D(\rho_g \vec{V}_g \phi)}{Dt} = \dot{W}_m \vec{V}_p - \vec{\nabla}(P\phi) + \vec{\nabla} \cdot (\underline{\tau}\phi) - \vec{D}_v A_s \quad (2.6)$$

where

$\frac{D}{Dt}$ is the substantial derivative

\vec{V}_g is the gas velocity vector (L/T)

\vec{V}_p is the particle velocity vector (L/T)

P is the atmospheric pressure

$\underline{\tau}$ is the stress tensor

\vec{D}_v is the drag due to the relative velocity between gas and particles

2.2.1.3 ENERGY

According to the first law of thermodynamics

$$\left[\begin{array}{c} \text{increase in stored} \\ \text{energy of} \\ \text{the system} \end{array} \right] = \left[\begin{array}{c} \text{work done} \\ \text{on system} \end{array} \right] + \left[\begin{array}{c} \text{energy} \\ \text{input to} \\ \text{system} \end{array} \right]$$

$$dE = \delta Q + \delta W \quad (2.7)$$

The rate of change of the total stored energy can then be written as

$$\frac{dE}{dt} = \frac{\delta Q}{\delta t} + \frac{\delta W}{\delta t} \quad (2.8)$$

In vector form the energy equation is given by:

$$\begin{aligned} \frac{D(\rho_g E \phi)}{Dt} = & \dot{W}_h - \vec{\nabla} \cdot (\vec{q} \phi) - \frac{1}{J} \vec{\nabla} \cdot (P \vec{V}_g \phi) - \frac{1}{J} \vec{\nabla} \cdot (\underline{\tau} \vec{V}_g \phi) \\ & - \frac{1}{J} A_s (\vec{D}_v \cdot \vec{V}_p) - \frac{P}{J} \frac{\partial \phi}{\partial t} + A_s \hat{h} (T_g - T_p) \end{aligned} \quad (2.9)$$

where

E is total stored energy,

\dot{W}_h is the source term of energy,

\vec{q} is the rate of heat conduction,

J is the unit transfer factor, and

\hat{h} is the convective heat transfer coefficient.

2.2.1.4 SPECIES

Derivation of the equation of continuity for each species in multicomponent mixture is done by using conservation of mass for each species in the mixture. The mass balance equation for species K is

$$\frac{\partial(\rho_K \phi)}{\partial t} + \vec{\nabla} \cdot (\rho_K \phi \vec{V}_K) = \dot{W}_K \quad (2.10)$$

For a multicomponent system, Eq. 2.10 (using the relationships that $\rho_K = Y_K \rho_g$ and $\vec{V}_K = \vec{V}_g + \vec{V}_{mK}$) becomes

$$\frac{\partial(\rho_g \phi Y_K)}{\partial t} + \vec{\nabla} \cdot \rho_g \phi Y_K (\vec{V}_g + \vec{V}_{mK}) = \dot{W}_K \quad (2.11)$$

or

$$\begin{aligned} \rho_g \phi \frac{\partial(Y_K)}{\partial t} + Y_K \frac{\partial(\rho_g \phi)}{\partial t} + Y_K \vec{\nabla} \cdot (\rho_g \phi \vec{V}_g) + \rho_g \phi \vec{V}_g \cdot \vec{\nabla} Y_K + \vec{\nabla} \cdot (\rho_g \phi Y_K \vec{V}_{mK}) \\ = \dot{W}_K \end{aligned} \quad (2.12)$$

From continuity equation,

$$Y_K \frac{\partial(\rho_g \phi)}{\partial t} + Y_K \vec{\nabla} \cdot (\rho_g \phi \vec{V}_g) = \dot{W}_m Y_K \quad (2.13)$$

and from Fick's law

$$\vec{V}_{mK} = \frac{D}{Y_K} \vec{\nabla} Y_K \quad (2.14)$$

Thus Eq. 2.10 simplifies to

$$\rho_g \phi \frac{D(Y_K)}{Dt} = \dot{W}_K - \dot{W}_m Y_K - \vec{\nabla} \cdot (\rho_g D \phi (\vec{\nabla} Y_K)) \quad (2.15)$$

where

ρ_K is the mass of species K per unit volume,

Y_K is the mass fraction of species K,

\vec{V}_K denotes the velocity of the Kth species with respect to the stationary coordinate axes,

D is the diffusion coefficient,

\vec{V}_{mK} is the mass diffusion velocity of Kth species, and

\dot{W}_K is the source term of species K. Here, K stands for CO, O_2 , CH_4 , H_2O , CO_2 etc.

For example, if K=CO, the equation becomes

$$\rho_g \phi \frac{D(Y_{CO})}{Dt} = \dot{W}_{CO} - \dot{W}_m Y_{CO} - \vec{\nabla} \cdot (\rho_g D \phi (\vec{\nabla} Y_{CO})) \quad (2.16)$$

2.2.1.5 TURBULENCE MODEL

The eddy viscosity hypothesis will be used in the equations of momentum and energy. The eddy or turbulent viscosity, μ_t , which in Eqs. 2.6 and 2.9, has to be specified by the turbulence model, has been defined using the two-equation κ - ϵ model of turbulence. The validity of the κ - ϵ model assumption has been tested for a wide range of flow configurations, [27], [28], [29], [30], [31], [32], and the agreement shown to be satisfactory for engineering purposes. According to this model, $\mu_t = C_\mu \rho \kappa^2 / \epsilon$ where C_μ is an empirical constant. κ and ϵ in Eqs. 2.17 and 2.18 are obtained from the following differential equations:

$$\vec{\nabla} \cdot (\rho_g \vec{V}_g \kappa \phi) = \vec{\nabla} \cdot \left[\left(\frac{\mu_t}{\sigma_\kappa} + \mu \right) \vec{\nabla} \kappa \phi \right] + G \phi - \rho_g \epsilon \phi \quad (2.17)$$

$$\vec{\nabla} \cdot (\rho_g \vec{V}_g \epsilon \phi) = \vec{\nabla} \cdot \left[\left(\frac{\mu_t}{\sigma_\epsilon} + \mu \right) \vec{\nabla} \epsilon \phi \right] + C_1 \frac{\epsilon}{\kappa} G \phi - \frac{C_2 \rho \epsilon^2}{\kappa} \phi \quad (2.18)$$

where $G = (\frac{\mu}{\sigma_\epsilon} + \mu) [\vec{\nabla} \vec{V}_g + [\vec{\nabla} \vec{V}_g]^T] : \vec{\nabla} \vec{V}_g$ which represents the generation of turbulent kinetic energy ;

Equations 2.17 and 2.18 are derived from the Navier-Stokes equations and the assumptions made in obtaining the above forms have been reported elsewhere [33]. The following values were used for the empirical constants [34] appearing in the two-equation $\kappa - \epsilon$ model $C_\mu = 0.09$, $\sigma_t=0.9$, $\sigma_\kappa=0.9$, $\sigma_\epsilon=1.22$.

2.2.2 SOLID PHASE GOVERNING EQUATIONS

2.2.2.1 MASS

From Fig. 2.2, the equation for the conservation of mass may be stated as:

$$\left[\begin{array}{l} \text{the rate of particle mass} \\ \text{accumulation in the control} \\ \text{volume occupied by particles} \end{array} \right] =$$

$$\left[\begin{array}{l} \text{the particle mass} \\ \text{convection into the} \\ \text{control volume} \\ \text{occupied by particles} \end{array} \right] + \left[\begin{array}{l} \text{the rate of particle mass} \\ \text{reduction due to gasification} \\ \text{of solid particles} \end{array} \right]$$

The mass balance is :

$$\frac{\partial(\rho_p(1 - \phi))}{\partial t} + \vec{\nabla} \cdot (\rho_p \vec{V}_p(1 - \phi)) = -\dot{W}_m = -\dot{M}_p \tilde{n} \quad (2.19)$$

where

ρ_p is the density of particle (M/L³),

\vec{V}_p is particle velocity vector (L/T),

\dot{W}_m is the source term of mass (M/T), and

\dot{M}_p is the rate of mass due to pyrolysis and devolatilization per

particle (M/T).

Note that the sign of source term in Eq. 2.5 is opposite of that in Eq. 2.19. When Eq. 2.5 and Eq. 2.19 are added, the source term vanishes, implying that the mass of gas-solid mixture is conserved.

2.2.2.2 MOMENTUM

The derivation of the solid-phase momentum equation 2.20 is based on the following balance :

$$\left[\begin{array}{c} \text{rate of increase} \\ \text{of particle momentum} \\ \text{in the control volume} \end{array} \right] =$$

$$\left[\begin{array}{c} \text{summation of forces} \\ \text{acting on the} \\ \text{control volume} \end{array} \right] + \left[\begin{array}{c} \text{net rate of} \\ \text{momentum flux into} \\ \text{control volume} \end{array} \right]$$

The momentum equation is:

$$\frac{D(\rho_p \vec{V}_p(1 - \phi))}{Dt} + \rho_p \vec{V}_p(1 - \phi) \vec{\nabla} \cdot \vec{V}_p = -\dot{W}_m \vec{V}_p + A_s \vec{D}_v \quad (2.20)$$

Uponing combining with mass equation, momentum equation can be finally written as

$$\frac{D(\rho_p \vec{V}_p(1 - \phi))}{Dt} = A_s \vec{D}_v \quad (2.21)$$

2.2.2.3 ENERGY (PARTICLE TEMPERATURE)

Consider a group of coal particles flowing with the gas stream through the black-body surface, temperature T_w , Fig. 2.3. The surface temperature is assumed to be constant in time. Heat is transported between gas and particles by convection

and conduction, and from wall surface by thermal radiative heat transfer. Thermal radiation exchange between particles and gas is assumed to be negligible. Some of the thermal energy received by the particles is consumed with thermal decomposition of solid coal matter to yield volatile matter and some of the thermal energy received by the particle by means of carbon heterogeneous reaction occurs on the surface of particle. The solid phase of the coal (particles) loses some of its sensible thermal energy due to transformation to gas at the solid phase temperature. The remaining net thermal energy increases the sensible energy content of the solid phase of coal particles. From energy balance around the individual particle, at any instant of time, t , conduction heat flux to the particle surface is

$$\dot{q}_{cond} = 2K_{cond}/d_p(T_g - T_p), \quad KJ/(m^2s) \quad (2.22)$$

The net thermal radiative heat flux to the particle surface from the wall surface is

$$\dot{q}_{rad} = \hat{F}\hat{\epsilon}\hat{\sigma}(T_w^4 - T_p^4), \quad KJ/(m^2s) \quad (2.23)$$

For a group of particles, with number density \tilde{n} , the view factor, \hat{F} , which is the distance between individual particle and wall surface Fig. 2.4 is a function of distance. $\hat{F} \equiv$ the fraction of surface area available for radiation to pass through. Analytically, therefore, \hat{F} can be calculated as follow

$$\hat{F} = \frac{\Delta x \cdot \Delta z - \tilde{n} \frac{\pi d_p^2}{4} \cdot \Delta x \cdot \Delta y \cdot \Delta z}{\Delta x \cdot \Delta z} = 1 - \tilde{n} \frac{\pi d_p^2}{4} \cdot \Delta y \quad (2.24)$$

The rate of thermal energy utilized for decomposition of solid phase to gas phase is

$$\dot{q}_{decomp} = -dM_p/dt(\Delta \bar{H}_v), \quad KJ/(s) \quad (2.25)$$

The rate of thermal energy exchanged between solid and gas via heterogeneous reaction is given by

$$\dot{q}_{het} = \sum_i -(dm/dt)_i \Delta \bar{H}_{het}, \quad KJ/(s) \quad (2.26)$$

The convective heat transfer flux to the particle surface is

$$\dot{q}_{conv} = N_u \pi d \lambda (T_g - T_p), \quad KJ/(s) \quad (2.27)$$

Thermal energy balance over the solid phase of particle is expressible by

Rate of change of the sensible energy content of the particle

$$\begin{aligned}
&= (\dot{q}_{cond} + \dot{q}_{rad}) \cdot (\text{particle exterior surface area}) \\
&\quad - \dot{q}_{decomp} + \dot{q}_{conv} + \dot{q}_{het}
\end{aligned} \tag{2.28}$$

Therefore,

$$\frac{d}{dt}(M_p \cdot C_p \cdot T_p) = (\dot{q}_{cond} + \dot{q}_{rad}) \cdot (\pi d_p^2) + \dot{q}_{conv} - \dot{q}_{decomp} + \dot{q}_{het} \tag{2.29}$$

Assuming that the mass loss occurs due to consumption of carbon at constant density, the particle of a single sphericle particle, d_p , changes as:

$$\frac{1}{2} \rho_p \pi d_p^2 \left[\frac{dd_p}{dt} \right] = \dot{M}_{hr} \tag{2.30}$$

Finally, assuming that the mass loss due to pyrolysis occurs volumetrically at constant particle size, the overall decrease in density, ρ_p , occurs according to

$$\left[\frac{\pi d_p^3}{6} \right] \left[\frac{d\rho_p}{dt} \right] = \dot{M}_{vo} \tag{2.31}$$

2.2.3 SOURCE TERMS

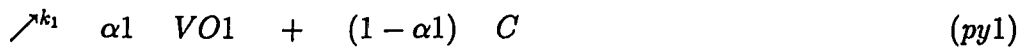
2.2.3.1 MASS SOURCE \dot{W}_m

The mass added to the unit volume of the bulk gas must be equal to the mass loss of solid particles per unit volume as long as quasi-steady assumption is valid. The mass loss rate (\dot{M}_p) is sum of volatiles liberation rate (\dot{M}_{vo}) and carbon consumption rate (\dot{M}_{hr}) due to the heterogeneous reaction.

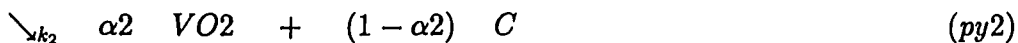
$$\dot{M}_p = \dot{M}_{vo} + \dot{M}_{hr} \tag{2.32}$$

(a) \dot{M}_{vo} loss rate of volatiles (pyrolysis model)

Anthony and Howard (1976) [35], Howard (1981) [36], Horton (1979) [37], and Wendt (1980) [38] provide reviews of coal devolatilization. Most of work has emphasized finely pulverized-coal particles at high temperatures. Devolatilization is modelled by the two-competing-reaction scheme suggested by Kobayashi *et al.* (1977) [39]:



Coal



The kinetic parameters for the rate constant K , which are expressed in Arrhenius form, i.e. $K = B \exp(-E/R_u T)$, are taken as: $B_{vo1}=3.7e5$ KJ/S, $E_{vo1}=7.37e4$ KJ/Kmole, $B_{vo2}=1.46e13$ KJ/S, $E_{vo2}=2.51e5$ KJ/Kmole [40] [41]. The stoichiometric factor $\alpha 1$ is taken to be the approximate volatile content of the coal, and $\alpha 2$ is chosen so that it reproduces the measured ultimate yield of volatiles under heating conditions similar to those encountered in the pulverized-coal flames. Typically, $\alpha 2 \approx 2\alpha 1$ [42] for medium to high volatile bituminous coals.

$$\dot{M}_{vo1} = \alpha 1 K_{vo1} M_{cu}$$

$$\dot{M}_{vo2} = \alpha 2 K_{vo2} M_{cu}$$

where

$$\begin{aligned} K_{vo1} &= B_{vo1} e^{\frac{-E_{vo1}}{R_u T_p}} \\ K_{vo2} &= B_{vo2} e^{\frac{-E_{vo2}}{R_u T_p}} \\ M_{cu} &= M_{po} - \int_0^t \left(\frac{\dot{M}_{vo1}}{\alpha 1} + \frac{\dot{M}_{vo2}}{\alpha 2} \right) dt \\ \dot{M}_{vo} &= \dot{M}_{vo1} + \dot{M}_{vo2} \end{aligned} \tag{2.33}$$

here, solving \dot{M}_{vo} by letting $M_{cu} = a1 e^{b1 t}$ and plugging into Eq. 2.33

$$\begin{aligned} a1 e^{b1 t} &= M_{po} - \int_0^t \left(a1 K_{vo1} e^{b1 t} + a1 K_{vo2} e^{b1 t} \right) dt \\ &= M_{po} - a1 K_{vo1} \int_0^t e^{b1 t} dt - a1 K_{vo2} \int_0^t e^{b1 t} dt \\ &= M_{po} - \frac{a1}{b1} K_{vo1} e^{b1 t} \Big|_0^t - \frac{a1}{b1} K_{vo2} e^{b1 t} \Big|_0^t \\ &= M_{po} - \frac{a1}{b1} e^{b1 t} (K_{vo1} + K_{vo2}) + \frac{a1}{b1} (K_{vo1} + K_{vo2}) \end{aligned}$$

comparing coefficients of constant and exponential terms:

$$\begin{aligned} a1 &= -\frac{a1}{b1} (K_{vo1} + K_{vo2}) \\ M_{po} &= -\frac{a1}{b1} (K_{vo1} + K_{vo2}) \end{aligned}$$

Therefore

$$a1 = M_{po}$$

$$b1 = -(K_{vo1} + K_{vo2})$$

giving the final result of

$$\begin{aligned}
 M_{cu} &= M_{po} e^{-(K_{vo1} + K_{vo2})t} \\
 \dot{M}_{vo} &= \dot{M}_{vo1} + \dot{M}_{vo2} \\
 &= (\alpha_1 K_{vo1} + \alpha_2 K_{vo2}) M_{cu} \\
 &= (\alpha_1 K_{vo1} + \alpha_2 K_{vo2}) M_{po} e^{-(K_{vo1} + K_{vo2})t}
 \end{aligned}$$

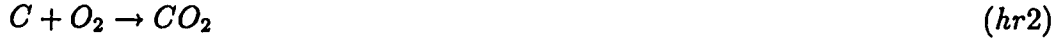
A significant advantage of the two-competing-reactions scheme is that once the empirical parameters have been determined for a particular type of coal, the model would then be capable of predicting the yield of volatiles as a function of coal heating conditions.

(b) \dot{M}_{hr} carbon consumption rate due to heterogeneous reactions

The total carbon consumption rate for a particle of size d_p is given as

$$\dot{M}_{hr} = \dot{M}_{hr1} + \dot{M}_{hr2} + \dot{M}_{hr3} + \dot{M}_{hr4} \quad (2.34)$$

The following heterogeneous reaction proceed at the surface of particles



The mass loss rate \dot{M}_{hr} due to heterogeneous char reactions is evaluated as follows.

For heterogeneous reaction $hr1$

$$\dot{M}_{hr1} = \rho_p K_{hr1} Y_{O_2,w}^{n_{O_2,hr1}} \pi d_p^2$$

where $Y_{O_2,w}^{n_{O_2,hr1}}$ is the concentration of oxygen at the wall of particle and K_{hr1} is the specific reaction rate constant for reaction $hr1$, and is given by

$$K_{hr1} = B_{hr1} \exp\left(\frac{-E_{hr1}}{R_u T_p}\right)$$

where B_{hr1} is the preexponential factor for reaction, $hr1$, $n_{O_2,hr1}$ is the order of reaction with respect to O_2 for reaction $hr1$, and \dot{M}_{hr} is the carbon consumption due to reaction $hr1$. Similarly

$$\dot{M}_{hr2} = \rho_p K_{hr2} Y_{O_2,w}^{n_{O_2,hr2}} \pi d_p^2$$

$$\begin{aligned}
\dot{M}_{hr3} &= \rho_p K_{hr3} Y_{CO_2,w}^{n_{CO_2,hr3}} \pi d_p^2 \\
\dot{M}_{hr4} &= \rho_p K_{hr4} Y_{H_2O,w}^{n_{H_2O,hr4}} \pi d_p^2 \\
K_{hr2} &= B_{hr2} \exp\left(\frac{-E_{hr2}}{R_u T_p}\right) \\
K_{hr3} &= B_{hr3} \exp\left(\frac{-E_{hr3}}{R_u T_p}\right) \\
K_{hr4} &= B_{hr4} \exp\left(\frac{-E_{hr4}}{R_u T_p}\right)
\end{aligned}$$

Note that B_{hri} ($i=1, 2, 3, 4$) must be selected such that it represents carbon consumption rate for the particular reaction. Finally,

$$\begin{aligned}
\dot{M}_p &= \dot{M}_{vo} + \dot{M}_{hr} \\
&= (\alpha_1 K_{vo1} + \alpha_2 K_{vo2}) m_{po} e^{-(K_{vo1} + K_{vo2})t} \\
&\quad + \dot{M}_{hr1} + \dot{M}_{hr2} + \dot{M}_{hr3} + \dot{M}_{hr4}
\end{aligned} \tag{2.35}$$

which results in

$$\begin{aligned}
\dot{W}_m &= \tilde{n} \dot{M}_p \\
&= \tilde{n} \left[(\alpha_1 K_{vo1} + \alpha_2 K_{vo2}) m_{po} e^{-(K_{vo1} + K_{vo2})t} \right. \\
&\quad \left. + \dot{M}_{hr1} + \dot{M}_{hr2} + \dot{M}_{hr3} + \dot{M}_{hr4} \right]
\end{aligned} \tag{2.36}$$

2.2.3.2 SPECIES SOURCES, \dot{W}_K

The species K added to the gas phase due to the pyrolysis and heterogeneous reactions are given as

$$\dot{M}_{pp,K} = Y_{K,v}(\tilde{n} \dot{M}_{vo}) + \tilde{n} \sum_j (\dot{M}_{hr,j} \nu_{K,j}) \tag{2.37}$$

where $j=j$ th heterogeneous reaction (for example if $K=CO$, then CO may be produced by the pyrolysis reactions, as well as heterogeneous reactions (hr1), (hr3), and (hr4).

Thus

$$\dot{M}_{pp,CO} = Y_{CO,v}(\tilde{n} \dot{M}_{vo}) + \tilde{n}(\dot{M}_{hr,1} \nu_{CO,1}) + \tilde{n}(\dot{M}_{hr,3} \nu_{CO,3}) + \tilde{n}(\dot{M}_{hr,4} \nu_{CO,4}) \tag{2.38}$$

While the species K are added to the gas phase from the particle or transported from the gas phase to the particles, they may also be consumed or added to the gas phase

by homogeneous reactions.

$$\dot{M}_{ho,K} = \sum_j \dot{M}_{ho,j} v_{K,j} \quad (2.39)$$

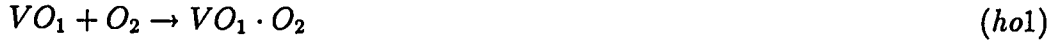
where $\dot{M}_{ho,K}$ is the mass of principal species consumed per unit volume due to j th homogeneous reaction, and $v_{K,j}$ is the stoichiometric coefficient of species K in the j th reaction taking place in the gas phase. The single global reaction of a fuel species F with an oxidizer is therefore

$$\dot{M}_{ho,K} = \dot{M}_{ho,F} v_{K,F} \quad (2.40)$$

where $\dot{M}_{ho,F}$ can be evaluated as follow

$$\dot{M}_{ho,F} = A_F \rho^n Y_F^{n_F} Y_{O_2}^{n_{O_2}} Y_I^{n_I} \exp\left(\frac{-E_F}{R_u T_g}\right) \quad (2.41)$$

where A_F is the preexponential factor. For example, for the CO wet scheme oxidation in which $Y_I = Y_{H_2O}$, $n_I = n_{H_2O}$, $Y_I = Y_{CO}$, the following homogeneous reactions can take place



where VO_1 are the volatiles produced by pyrolysis reaction *py1*. Thus, if $VO_1 = CH_4$ then



and if $VO_2 = C_6H_6$ then



Hence CO_2 production rate due to gas phase oxidation reaction is given as

$$\dot{M}_{ho,CO_2} = \dot{M}_{ho,CH_4} v_{CO_2,ho1} + \dot{M}_{ho,C_6H_6} v_{CO_2,ho2} + \dot{M}_{ho,CO} v_{CO_2,ho3}$$

where $v_{CO_2,ho1}$ is the stoichiometric mass of CO_2 per unit mass of CH_4 in reaction ho1. Subsequently the net rate of production of species K in the gas phase is given as

$$\dot{W}_K = \dot{M}_{pp,K} + \dot{M}_{ho,K} \quad (2.42)$$

2.2.3.3 ENERGY SOURCE, \dot{W}_h

The energy source in the gas phase is expressed as

$$\dot{W}_h = (\dot{q}_{cond})_{gas} + (\dot{q}_{conv})_{gas} + (\dot{q}_{chem})_{gas} \quad (2.43)$$

The conductive heat transfer from the particle to gas per unit volume is given as

$$(\dot{q}_{cond})_{gas} = \tilde{n} \dot{q}_{cond} \quad (2.44)$$

where $\dot{q}_{cond} = 2K_{cond}/d_p(T_p - T_g)$. The convective heat transfer from the particle to gas per unit volume is represented by

$$(\dot{q}_{conv})_{gas} = \tilde{n} \dot{q}_{conv} \quad (2.45)$$

where $\dot{q}_{conv} = N_u \pi d \lambda (T_p - T_g)$,

$$\dot{q}_{chem} = \sum_j \dot{M}_{ho,F} H_{ho,F} \quad (2.46)$$

and $H_{ho,F}$ is the heat value for j th gas phase reaction. Because, in Section 2.2.3.2, we have three gas phase reactions (ho1), (ho2), and (ho3), then

$$\dot{q}_{chem} = \dot{M}_{ho,CO} \cdot H_{chem,ho3} + \dot{M}_{ho,CH_4} \cdot H_{chem,ho1} + \dot{M}_{ho,C_6H_6} \cdot H_{chem,ho2} \quad (2.47)$$

While the first term $(\dot{q}_{cond})_{gas}$ and the second term $(\dot{q}_{conv})_{gas}$ on the right hand side of Eq. 2.43 are the heat sink or cooling of coal particles, the third term $(\dot{q}_{chem})_{gas}$ represents the heat generation per unit volume due to chemical reactions in the gas phase.

2.3 WALL FUNCTIONS

The $\kappa - \epsilon$ turbulence model presented above is intended for flow regions with high turbulence Reynolds number on the order of

$$Re = \frac{\rho_g \kappa^{\frac{1}{2}} l_0}{\mu} > 5000 \quad (2.48)$$

where l_0 is the length scale of turbulence, which is defined as $\frac{\kappa^{\frac{3}{2}}}{\epsilon}$. In the region of the flow near a solid wall, the local turbulence Reynolds number is so small that viscous effects dominate. If the exact momentum equations are to be solved in this region, then a large number of grid nodes are needed. In order to reduce the number of

grid nodes, conditions adjacent to the solid wall are often matched to some assumed boundary layer profiles of velocity, temperature and species concentrations. This approach assumes that just outside the viscous sublayer, the velocity component parallel to the wall follows the logarithmic law. This implies that the turbulence in this region is in local equilibrium, thereby resulting in a κ -production term which is equal to its dissipation term.

These assumptions yield the following relations in dimensionless form:

$$\frac{U_{pg}}{\sqrt{\frac{\tau_w}{\rho_g}}} = \frac{1}{\hat{\kappa}} \ln \left(\hat{E} \frac{\rho_g y_p \sqrt{\frac{\tau_w}{\rho_g}}}{\mu} \right) \quad (2.49)$$

$$\epsilon_{pg} = \frac{\sqrt{\frac{\tau_w}{\rho_g}}^{\frac{3}{2}}}{\kappa y_{pg}} \quad (2.50)$$

and

$$\frac{\kappa_{pg}}{\left(\frac{\tau_w}{\rho_g}\right)} = C_\mu^{-\frac{1}{2}} \quad (2.51)$$

where, (as illustrated in Fig. 2.5) the subscripts w and pg represent the conditions at the wall and at the adjacent grid node, respectively. τ_w is the shear stress at the wall, $\sqrt{\frac{\tau_w}{\rho_g}}$ is the friction velocity, $\hat{\kappa}$ is the von Karman's constant appearing in the logarithmic law of the wall, and \hat{E} is another constant that is a function of wall roughness (i.e. $\hat{E} \simeq 9$ for smooth walls). The values of $\hat{\kappa}$ and \hat{E} are taken to be 0.42 and 8.8 respectively as suggested by [43]. Eliminating $\left(\frac{\tau_w}{\rho_g}\right)$ from Eqs. 2.50 and 2.51 gives

$$\epsilon_{pg} = \frac{C_\mu^{\frac{3}{4}} \kappa_{pg}^{\frac{3}{2}}}{\hat{\kappa} y_{pg}} \quad (2.52)$$

Substituting Eq. 2.50 into 2.49 yields

$$\frac{U_{pg}}{\kappa_{pg}^{\frac{1}{2}}} = \frac{C_\mu^{\frac{1}{4}}}{\hat{\kappa}} \ln \left(\hat{E} \frac{\rho_g C_\mu^{\frac{1}{4}} \kappa_{pg}^{\frac{1}{2}} y_p}{\mu} \right) \quad (2.53)$$

We now define

$$\left(\frac{\tau_w}{\rho_g}\right) = \frac{\mu_w}{\rho_g} \left(\frac{\partial U}{\partial y}\right)_w = \frac{\hat{\mu}_w}{\rho_g} \frac{U_{pg}}{y_{pg}} \quad (2.54)$$

where $\hat{\mu}_w$ is the pseudo-viscosity at the wall, in order to simplify calculation of the shear stress in the momentum equation. Replacing the expression of $\left(\frac{\tau_w}{\rho_g}\right)$ by Eq. 2.54

yields

$$U_{pg} = \kappa_{pg} C_{\mu}^{\frac{1}{2}} \rho_g y_{pg} \hat{\mu}_w \quad (2.55)$$

Finally, inserting Eq. 2.55 into Eq. 2.53 leads to

$$\hat{\mu}_w = \frac{\hat{\kappa} C_{\mu}^{\frac{1}{4}} \kappa_{pg}^{\frac{1}{2}} \rho_g y_{pg}}{\ln \left(\hat{E} \frac{\rho_g C_{\mu}^{\frac{1}{4}} \kappa_{pg}^{\frac{1}{2}} y_{pg}}{\mu} \right)} \quad (2.56)$$

When using the wall-function method, one has to make certain that the grid node pg is sufficiently far from wall so that Re_{pg} would be much greater than unity; so much greater in fact that the viscous effects are entirely overcome by turbulence. If the value of $\frac{\rho_g C_{\mu}^{\frac{1}{4}} \kappa_{pg}^{\frac{1}{2}} y_{pg}}{\mu}$ is smaller than 15 [44], then the grid node, pg, is too close to the wall, and therefore located in the lamilar sublayer. In this case, we have $\hat{\mu}_w = \mu_w$.

2.4 SUMMARY OF GOVERNING EQUATIONS

2.4.1 CORRECTIONS

The following are some assumptions and correlations needed to close the problem:

1. Constitutive law for shear stress

$$\tau_{xx} = \left(\frac{\mu_t}{\sigma_t} + \mu \right) \left[2 \frac{\partial U_g}{\partial x} - \frac{2}{3} \left(\frac{\partial U_g}{\partial x} + \frac{\partial V_g}{\partial y} \right) \right] \quad (2.57)$$

$$\tau_{yx} = \left(\frac{\mu_t}{\sigma_t} + \mu \right) \left[\frac{\partial U_g}{\partial y} + \frac{\partial V_g}{\partial x} \right] \quad (2.58)$$

$$\tau_{yy} = \left(\frac{\mu_t}{\sigma_t} + \mu \right) \left[2 \frac{\partial V_g}{\partial y} - \frac{2}{3} \left(\frac{\partial U_g}{\partial x} + \frac{\partial V_g}{\partial y} \right) \right] \quad (2.59)$$

$$\tau_{xy} = \left(\frac{\mu_t}{\sigma_t} + \mu \right) \left[\frac{\partial V_g}{\partial x} + \frac{\partial U_g}{\partial y} \right] \quad (2.60)$$

2. Drag force

$$D_{ux} = \frac{3}{8} C_D \rho_g (U_g - U_p) |U_g - U_p| \quad (2.61)$$

$$D_{uy} = \frac{3}{8} C_D \rho_g (V_g - V_p) |V_g - V_p| \quad (2.62)$$

The drag coefficient for solid spheres is usually employed. An expression proposed by Putnam [45] is given as

$$\begin{aligned} C_D &= \frac{24}{Re_{dp}} \left[1 + Re_{dp}^{\frac{2}{3}} \right] & \text{for } Re_{dp} < 1000 \\ &= 0.44 & \text{for } Re_{dp} > 1000 \end{aligned} \quad (2.63)$$

where the Reynolds number , Re_{dp} , is defined as

$$Re_{dp} = \frac{d_p |U_p - U_g|}{\nu} \quad (2.64)$$

According to Faeth [46], the following expressions of Dickerson and Schuman [47]

with a broader Reynolds-number range yield similar results to Eq. 2.63

$$\begin{aligned} C_D &= \frac{27}{Re_{dp}^{0.84}} & \text{for } Re_{dp} < 80 \\ &= 0.271 Re_{dp}^{0.217} & \text{for } 80 \leq Re_{dp} \leq 10^4 \end{aligned} \quad (2.65)$$

3. Fourier law of conduction

$$q_x = -K_{cond} A \frac{\partial T_g}{\partial x} \quad (2.66)$$

$$q_y = -K_{cond} A \frac{\partial T_g}{\partial y} \quad (2.67)$$

2.4.2 GOVERNING EQUATIONS

The governing equations appearing in Section 2.2.1 and 2.2.2 are summarized as follows:

$$\frac{\partial(\rho_g \phi)}{\partial t} + \vec{\nabla} \cdot (\rho_g \vec{V}_g \phi) = \dot{M}_p \tilde{n} = \dot{W}_m$$

$$\frac{D(\rho_g \vec{V}_g \phi)}{Dt} = \dot{W}_m \vec{V}_p - \vec{\nabla}(P\phi) + \vec{\nabla} \cdot (\underline{\tau}\phi) - \vec{D}_v A_s$$

$$\begin{aligned} \frac{D(\rho_g E \phi)}{Dt} &= \dot{W}_h - \vec{\nabla} \cdot (\vec{q}\phi) - \frac{1}{J} \vec{\nabla} \cdot (p \vec{V}_g \phi) - \frac{1}{J} \vec{\nabla} \cdot (\underline{\tau} \vec{V}_g \phi) \\ &\quad - \frac{1}{J} A_s (\vec{D}_v \cdot \vec{V}_p) - \frac{P}{J} \frac{\partial \phi}{\partial t} + A_s \hat{h} (T_g - T_p) \end{aligned}$$

$$\rho_g \phi \frac{D(Y_K)}{Dt} = \dot{W}_K - \dot{W}_m Y_K - \vec{\nabla} \cdot (\rho_g D \phi (\vec{\nabla} Y_K))$$

$$\vec{\nabla} \cdot (\rho_g \vec{V}_g \kappa \phi) = \vec{\nabla} \cdot \left[\left(\frac{\mu_t}{\sigma_k} + \mu \right) \vec{\nabla} \kappa \phi \right] + G \phi - \rho_g \epsilon \phi$$

$$\vec{\nabla} \cdot (\rho_g \vec{V}_g \epsilon \phi) = \vec{\nabla} \cdot \left[\left(\frac{\mu_t}{\sigma_\epsilon} + \mu \right) \vec{\nabla} \epsilon \phi \right] + C_1 \frac{\epsilon}{\kappa} G \phi - \frac{C_2 \rho \epsilon^2}{\kappa} \phi$$

where $G = (\frac{\mu_i}{\sigma_i} + \mu) [\vec{\nabla} \vec{V}_g + [\vec{\nabla} \vec{V}_g]^T] : \vec{\nabla} \vec{V}_g$

$$\frac{\partial(\rho_p(1-\phi))}{\partial t} + \vec{\nabla} \cdot (\rho_p \vec{V}_p(1-\phi)) = -\dot{W}_m = -\dot{M}_p \tilde{n}$$

$$\frac{D(\rho_p \vec{V}_p(1-\phi))}{Dt} = A_s \vec{D}_v$$

$$\frac{d}{dt}(M_p \cdot C_p \cdot T_p) = (\dot{q}_{cond} + \dot{q}_{rad}) \cdot (\pi d_p^2) + \dot{q}_{conv} - \dot{q}_{decomp} + \dot{q}_{het}$$

$$\frac{1}{2} \rho_p \pi d_p^2 \left[\frac{dd_p}{dt} \right] = \dot{M}_{hr}$$

$$\left[\frac{\pi d_p^3}{6} \right] \left[\frac{d\rho_p}{dt} \right] = \dot{m}_{vo}$$

Using the corrections, the governing equations given above are re-written into scale forms.

$$\frac{\partial(\rho_g \phi)}{\partial t} + \frac{\partial(\rho_g U_g \phi)}{\partial x} + \frac{\partial(\rho_g V_g \phi)}{\partial y} = \dot{W}_m = \dot{M}_p \tilde{n} \quad (2.68)$$

$$\begin{aligned} & \frac{\partial(\rho_g U_g \phi)}{\partial t} + \frac{\partial(\rho_g U_g \phi U_g)}{\partial x} + \frac{\partial(\rho_g U_g \phi V_g)}{\partial y} = \dot{W}_m U_p - \frac{\partial(P\phi)}{\partial x} \\ & + \phi \mu \left[\frac{\partial^2 U_g}{\partial x^2} + \frac{\partial^2 U_g}{\partial y^2} \right] + \frac{1}{3} \phi \mu \frac{\partial}{\partial x} \left[\frac{\partial U_g}{\partial x} + \frac{\partial V_g}{\partial y} \right] + \frac{\partial(\phi \mu)}{\partial x} \left[\frac{4}{3} \frac{\partial U_g}{\partial x} - \frac{2}{3} \frac{\partial V_g}{\partial y} \right] \\ & + \frac{\partial(\phi \mu)}{\partial y} \left[\frac{\partial U_g}{\partial y} + \frac{\partial V_g}{\partial x} \right] - D_{vx} A_s \end{aligned} \quad (2.69)$$

$$\begin{aligned} & \frac{\partial(\rho_g V_g \phi)}{\partial t} + \frac{\partial(\rho_g U_g \phi V_g)}{\partial x} + \frac{\partial(\rho_g V_g \phi V_g)}{\partial y} = \dot{W}_m V_p - \frac{\partial(P\phi)}{\partial y} \\ & + \phi \mu \left[\frac{\partial^2 V_g}{\partial x^2} + \frac{\partial^2 V_g}{\partial y^2} \right] + \frac{1}{3} \phi \mu \frac{\partial}{\partial y} \left[\frac{\partial U_g}{\partial x} + \frac{\partial V_g}{\partial y} \right] + \frac{\partial(\phi \mu)}{\partial y} \left[\frac{4}{3} \frac{\partial V_g}{\partial y} - \frac{2}{3} \frac{\partial U_g}{\partial x} \right] \\ & + \frac{\partial(\phi \mu)}{\partial x} \left[\frac{\partial U_g}{\partial y} + \frac{\partial V_g}{\partial x} \right] - D_{vy} A_s \end{aligned} \quad (2.70)$$

$$\begin{aligned} & \frac{\partial(\rho_g C_p T_g \phi)}{\partial t} + \frac{\partial(\rho_g C_p T_g U_g \phi)}{\partial x} + \frac{\partial(\rho_g C_p T_g V_g \phi)}{\partial y} + \frac{\partial}{\partial x} \left(-\phi K \frac{\partial T_g}{\partial x} \right) \\ & + \frac{\partial}{\partial y} \left(-\phi K \frac{\partial T_g}{\partial y} \right) + \frac{1}{J} \frac{\partial(P U_g \phi)}{\partial x} + \frac{1}{J} \frac{\partial(P V_g \phi)}{\partial y} - \frac{1}{J} \frac{4}{3} \phi \mu \left[U_g \frac{\partial^2 U_g}{\partial x^2} + V_g \frac{\partial^2 V_g}{\partial y^2} \right] \end{aligned}$$

$$\begin{aligned}
& - \frac{1}{J} \frac{\partial \phi \mu U_g}{\partial x} \left[\frac{4}{3} \frac{\partial U_g}{\partial x} - \frac{2}{3} \frac{\partial V_g}{\partial y} \right] + \frac{1}{J} \frac{2}{3} \left[\frac{\partial U_g}{\partial x} \frac{\partial^2 V_g}{\partial x \partial y} + \frac{\partial V_g}{\partial y} \frac{\partial^2 U_g}{\partial x \partial y} \right] \\
& - \frac{1}{J} \frac{\partial \phi \mu V_g}{\partial y} \left[\frac{4}{3} \frac{\partial V_g}{\partial y} - \frac{2}{3} \frac{\partial U_g}{\partial x} \right] + \frac{P}{J} \frac{\partial \phi}{\partial t} = \dot{W}_h
\end{aligned} \tag{2.71}$$

$$\begin{aligned}
& \rho_g \phi \frac{Y_K}{\partial t} + \rho_g \phi U_g \frac{Y_K}{\partial x} + \rho_g \phi V_g \frac{Y_K}{\partial y} + \frac{\partial}{\partial x} (\rho_g \phi D \frac{\partial Y_K}{\partial x}) + \frac{\partial}{\partial y} (\rho_g \phi D \frac{\partial Y_K}{\partial y}) \\
& = \dot{W}_K - \dot{W}_m Y_K
\end{aligned} \tag{2.72}$$

$$\begin{aligned}
\frac{\partial}{\partial x} (\rho_g U_g \phi \kappa) + \frac{\partial}{\partial y} (\rho_g V_g \phi \kappa) &= \frac{\partial}{\partial x} \left[\left(\frac{\mu_t}{\sigma_k} + \mu \right) \frac{\partial \phi \kappa}{\partial x} \right] + \frac{\partial}{\partial y} \left[\left(\frac{\mu_t}{\sigma_k} + \mu \right) \frac{\partial \phi \kappa}{\partial y} \right] \\
&+ G \phi - \rho_g \epsilon \phi
\end{aligned} \tag{2.73}$$

$$\begin{aligned}
\frac{\partial}{\partial x} (\rho_g U_g \phi \epsilon) + \frac{\partial}{\partial y} (\rho_g V_g \phi \epsilon) &= \frac{\partial}{\partial x} \left[\left(\frac{\mu_t}{\sigma_\epsilon} + \mu \right) \frac{\partial \phi \epsilon}{\partial x} \right] + \frac{\partial}{\partial y} \left[\left(\frac{\mu_t}{\sigma_\epsilon} + \mu \right) \frac{\partial \phi \epsilon}{\partial y} \right] \\
&+ C_1 \frac{\epsilon}{\kappa} G \phi - \frac{C_2 \rho \epsilon^2}{\kappa} \phi
\end{aligned} \tag{2.74}$$

$$\text{where } G = \left(\frac{\mu_t}{\sigma_\epsilon} + \mu \right) \left[2 \left(\frac{\partial V_g}{\partial y} \right)^2 + 2 \left(\frac{\partial U_g}{\partial x} \right)^2 + \left(\frac{\partial V_g}{\partial x} + \frac{\partial U_g}{\partial y} \right)^2 \right]$$

$$\frac{\partial(\rho_p(1-\phi))}{\partial t} + \frac{\partial(\rho_p U_p(1-\phi))}{\partial x} + \frac{\partial(\rho_p V_p(1-\phi))}{\partial y} = -\dot{W}_m = -\dot{M}_p \tilde{n} \tag{2.75}$$

$$\rho_p(1-\phi) \left[\frac{\partial U_p}{\partial t} + U_p \frac{\partial U_p}{\partial x} + V_p \frac{\partial U_p}{\partial y} \right] = A_s D_{ux} \tag{2.76}$$

$$\rho_p(1-\phi) \left[\frac{\partial V_p}{\partial t} + U_p \frac{\partial V_p}{\partial x} + V_p \frac{\partial V_p}{\partial y} \right] = A_s D_{vy} \tag{2.77}$$

$$\frac{d}{dt} (M_p \cdot C_p \cdot T_p) = (\dot{q}_{cond} + \dot{q}_{rad}) \cdot (\pi d_p^2) + \dot{q}_{conv} - \dot{q}_{decomp} + \dot{q}_{het} \tag{2.78}$$

$$\frac{1}{2} \rho_p \pi d_p^2 \left[\frac{dd_p}{dt} \right] = \dot{M}_{hr} \tag{2.79}$$

$$\left[\frac{\pi d_p^3}{6} \right] \left[\frac{d\rho_p}{dt} \right] = \dot{M}_{vo} \tag{2.80}$$

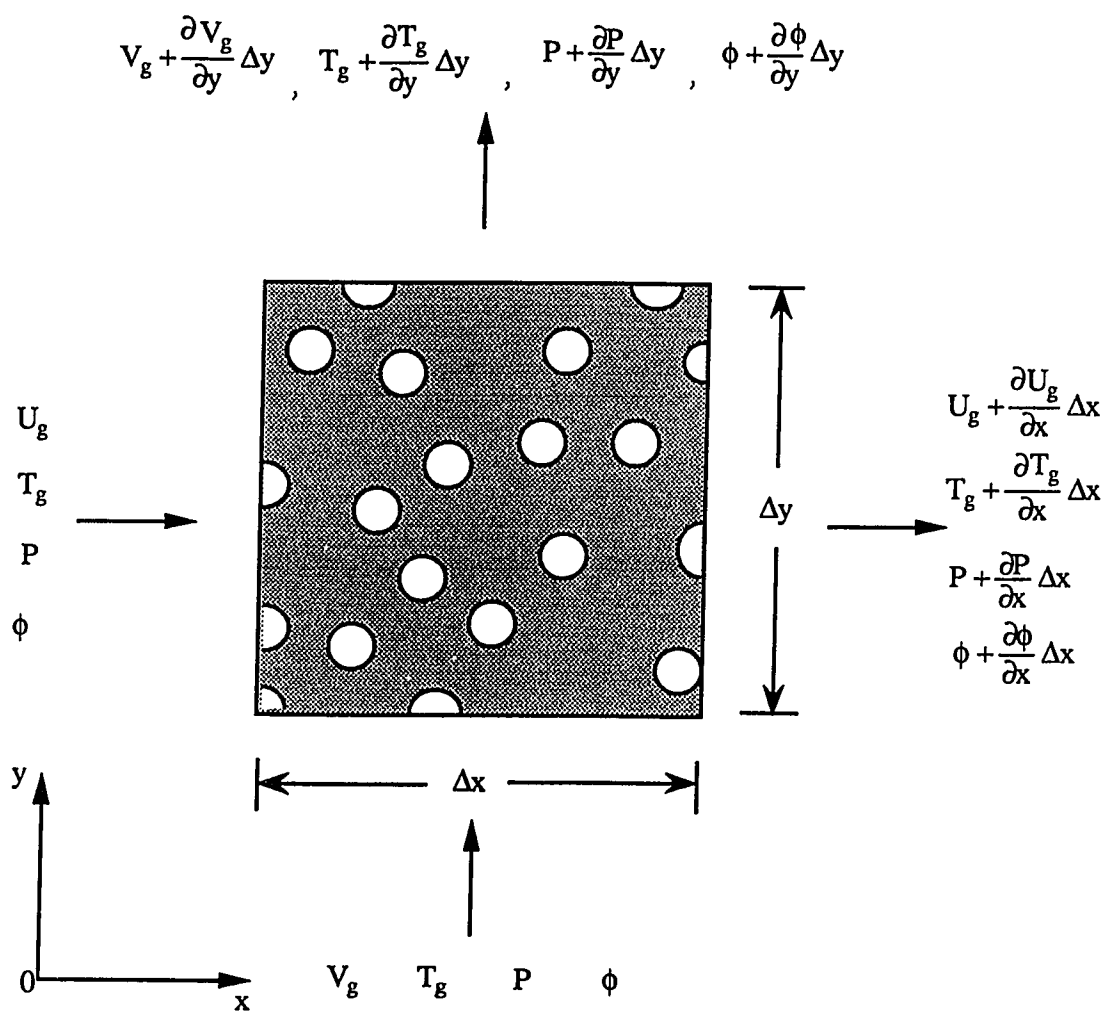


Figure 2.1 Gas-Phase Control Volume.

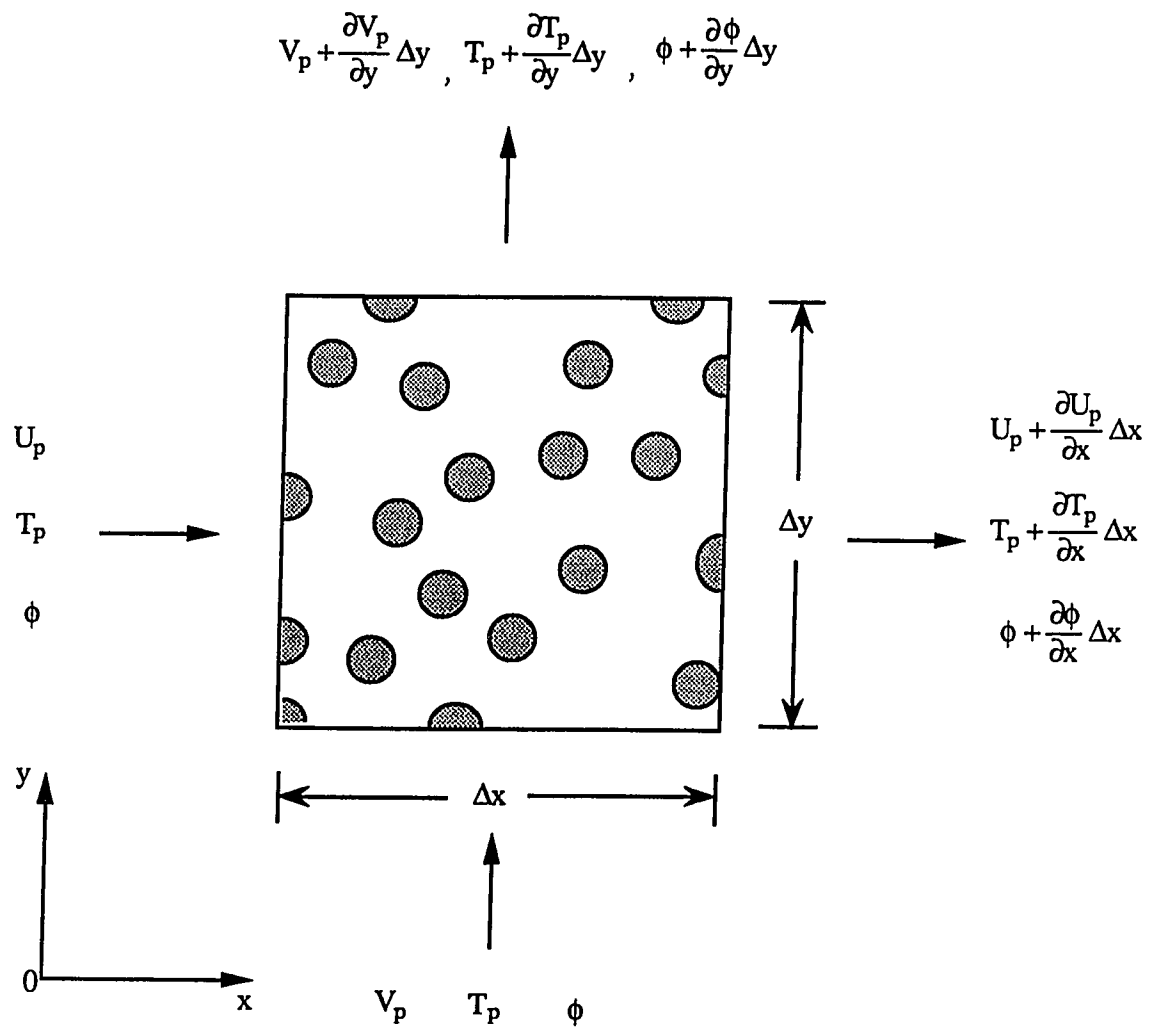


Figure 2.2 Solid- Phase Control Volume.

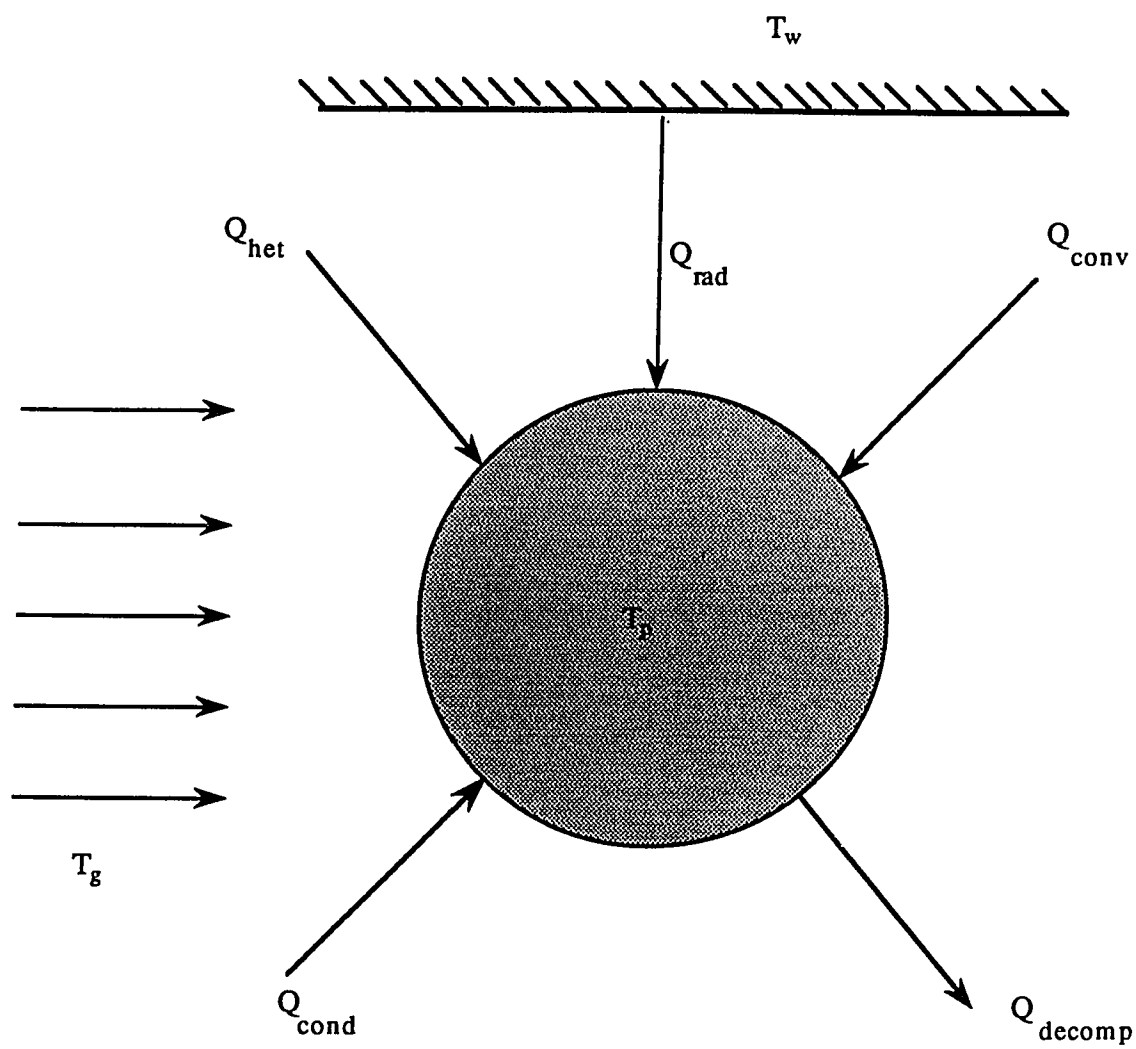


Figure 2.3 Energy Balance Surround a Spherical Particle.

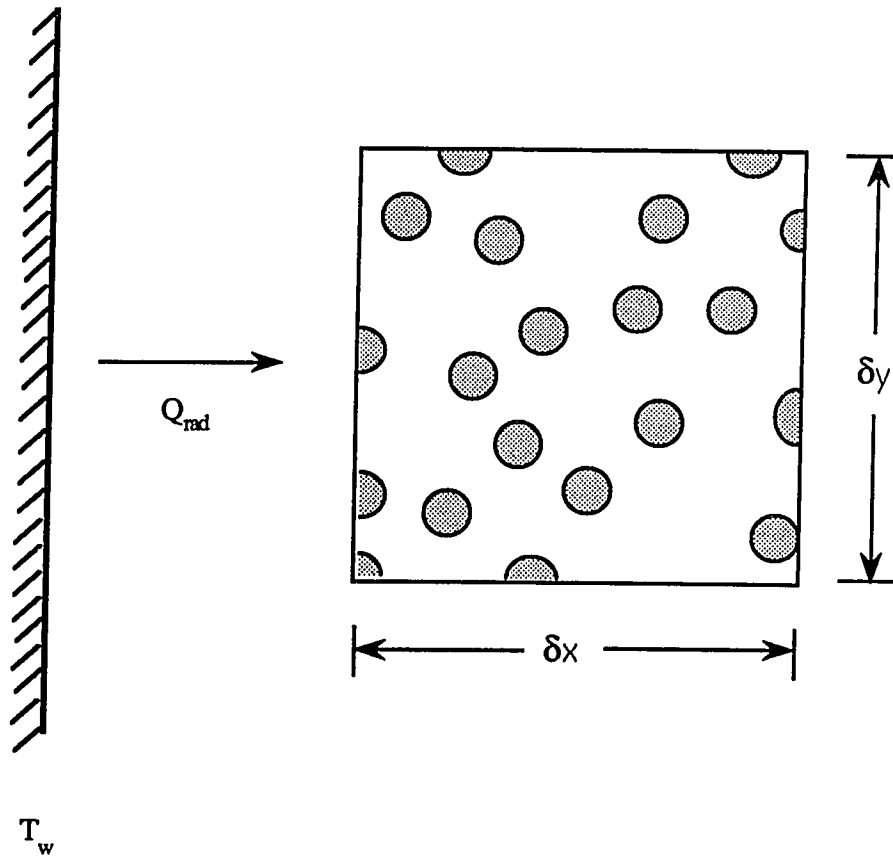


Figure 2.4 View Factor

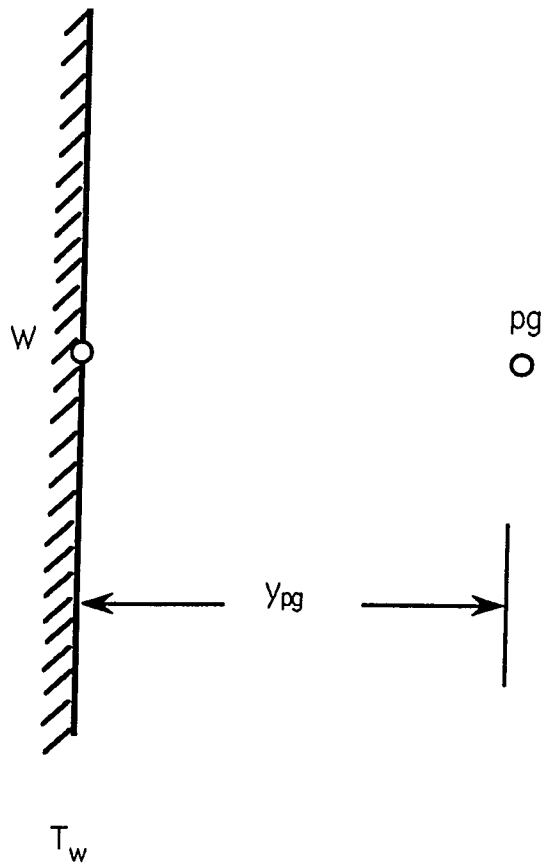


Figure 2.5 Near Wall Nodes.

Chapter 3

SOLUTION PROCEDURE

3.1 GENERAL ALGORITHM

The following is general algorithm used to solve the problem:

- (1) Input flow and particle parameters such as free-stream velocity, pressure, fluid density, viscosity, particle density, particle diameter, number of density, etc.
- (2) Input the length of x and y .
- (3) Input boundary values and a set of initial guess values.
- (4) Compute the source terms.
- (5) Solve the flow field properties by the "SIMPLER" procedure.
- (6) Calculate particle properties by using an explicit forward scheme.
- (7) Update all properties for the next time step.

Step (1) allows the user to change the flow velocity, and temperature, the particle velocity, temperature, number density etc.,

Step (2) generates the uniform "staggered grid", which is rectangular in Cartesian coordinates. Figure 3.1 shows how the points are arranged in the x - y plane. At each point, the variables U_g, V_g, P , etc., are stored.

Step (3) guess an initial flow field that conserves mass and satisfies the no-slip boundary condition at the wall surface, as well as the free-stream boundary condition on the inlet boundary.

Steps (4) and (5) compose most of the computational work at each time step. These are discussed in detail in Sections 3.3 and 3.4. Step (4) computes the source terms for mass, species, and energy in each time step. Step (5) solves the flow field

governing equation by the SIMPLER algorithm, i.e. using p-v corrections and TDMA (Tri-Diagonal Matrix Algorithm) line-by-line iterations with under-relaxations. Step (6) evaluates explicitly the particle mass, velocity, and diameter from the solid-phase governing equations which are discussed in Section 3.5

3.1.1 THE STAGGERED GRID

The staggered grid for velocity components was first used by Harlow and Weleh (1965). Before describing the staggered grid concept, let us look first at the two-dimensional pressure distribution shown in Figure 3.2. Here, the x-direction momentum is influenced by $P_W - P_E$, the y-direction momentum is affected by $P_S - P_N$, and the pressure P_P plays no role. The pressure field, which is composed of four arbitrary values of pressure arranged in a checkerboard pattern, would produce no pressure force in the x and y directions. Thus, a highly nonuniform pressure field would be treated as a uniform pressure field in the discretized form of the momentum equations.

Upon discretizing the continuity equation, we note that the troublesome hurdles in the numerical analysis seem to be associated with the first derivatives. The second derivatives always behave well and create no difficulties. In the staggered grid, however, by arranging velocity components on grids, all the difficulties described above will disappear.

In the staggered grid, the velocity components are calculated at the points that lie on the faces of the control volumes. Thus, the x-direction velocity U_g is calculated at the faces normal to the x-direction. In Figure 3.3, for example, a two-dimensional grid pattern is shown, with the locations for U_g and V_g placed on the respective control volume faces.

The finite difference counterpart¹ of the general P.D.E. is derived by supposing that each variable is enclosed in its own control volume or "cell", as illustrated in Fig. 3.3. The P.D.E. is integrated over the control volume, with the aid of assumptions about the relations between the nodal values of $\hat{\phi}$, the rates of creation/destruction of this entity within the cells, and its transport by convection and diffusion across the cell boundaries. The source term is represented in linearized form as:

$$S_{\hat{\phi}} \equiv \int_v S_{\hat{\phi}} dv = S_0 + S_P \hat{\phi}_P \quad (3.1)$$

and the transport at interface w can be expressed as,

$$(\rho U)_w \frac{(\hat{\phi}_P + \hat{\phi}_W)}{2} a_W - \Gamma_{\hat{\phi},w} \frac{(\hat{\phi}_P - \hat{\phi}_W)}{2} a_W \quad (3.2)$$

with the definition of ρU as strength of convection and $\Gamma_{\hat{\phi}}$ as diffusion conductance, when the quantity $F_{EW} \equiv (\rho U)_w \delta x_{PW} / \Gamma_{\hat{\phi},w}$ is small.

For large F_{EW} ,

$$\begin{aligned} \hat{\phi}_w &= \hat{\phi}_W & \text{if } (\rho U)_w > 0 \\ \hat{\phi}_w &= \hat{\phi}_P & \text{if } (\rho U)_w < 0 \end{aligned}$$

This is upwind scheme.

Where the subscripts P and W refer to the central and west nodes, respectively, and w denotes the intervening cell boundary. Combining the above and similar expression for the remaining boundaries yields the F.D.E.;

$$(A_P - S_P) \hat{\phi}_P = \sum_n A_n \hat{\phi}_n + S_0 \quad (3.3)$$

where \sum_n denotes summation over the neighbouring nodes, N, S, E , and W ; $A_P = \sum A_n$; and S_0 and S_P are deduced from the $S_{\hat{\phi}}'$'s.

An equation for the pressure, which still remains unknown, is obtained by combining the continuity and momentum equations in the manner explained in [48]; the entails connecting changes in pressure, denoted by P' with changes in velocity U' and V' by approximate formulae derived from the momentum F.D.E.s. Substitution

¹Excluding the continuity equation, which receives special treatment

of these formulae into the continuity equation therefore yields a F.D.E. for p' similar to 3.3, with S_0 now representing the local continuity imbalance in the prevailing velocity field.

3.1.2 DESCRIPTION OF THE COMPUTER PROGRAM:

The main program reads the input data from the various input files. It also calls the subroutines which are necessary for calculating several parameters. The gas phase differential equations are solved using the SIMPLER algorithm, and the solid phase differential equations are solved by the explicit scheme. The flow chart is given in Figure 3.4, and subroutines and their functions are presented in Table 3.1.

1. To determine the gas properties at $t = \delta t$ with the given initial conditions at $t=0$ ($T_o, Y_{K,o}, T_{p,o}, \rho_{p,o}$, and $d_{p,o}$). The main program calls the subroutine source to calculate the source terms ($\dot{W}_K, \dot{W}_m, \dot{W}_h$) with $T_{p,o}$. With \dot{W}_m being the sum of \dot{M}_{vo} and \dot{M}_{hr} , the volatiles liberation rate, \dot{M}_{vo} is found by the subroutine PYROM, and the heterogeneous production rate, \dot{M}_{hr} , is obtained from subroutine YIELDWALL. At the same time, the density of the particle is calculated by using subroutine DENSITYP, and the current diameter is established by using subroutine DIAMETERP. To compute \dot{W}_K , one has to find the mass production rate of species K in the gas phase due to pyrolysis and heterogeneous reaction at the particles surfaces, and also due to gas phase reactions. Subroutines YIELDWALL, PYROM and HETMASS, provide the necessary outputs for the species generation due to pyrolysis and heterogeneous reactions. The chemical production rate of species K due to gas phase reactions, $\dot{W}_{K,ch}$, is given by subroutine HOMASS (CO-oxidation reactions and volatile oxidation reactions). The term \dot{W}_h , corresponding to the gas phase oxidation, is computed from subroutine HOMASS. The subroutines calls QCONVP, QHET, QDECOMP and QRAD to find the heat transfer between the particles and the gas and wall. Then the main program calls subroutine SIMPLER which is to solve a common finite difference

equation for all variables of interest. This subroutine computes $U_g, V_g, P, T_g, \kappa, Y_K$ and ϵ at all time steps. Subroutine TEMPP gives the temperature of the particle at every point and step.

2. The program determines the mass loss of volatiles within Δt from the values of \dot{M}_{vo} at $t=0$, and the mass loss rate of carbon within Δt from \dot{M}_{hr} at $t=0$. Therefore, using \dot{M}_{vo} and \dot{M}_{hr} , the total mass flow rate \dot{M}_P , ρ_p and d_p at $t=\Delta t$ can be found.

3. The program then repeats step 1 and step 2 for subsequent time steps.

3.2 THE SIMPLER ALGORITHM:

SIMPLE stands for Semi-Implicit Method for Pressure-Linked Equations, and SIMPLER is for SIMPLE Revised, which has a faster convergence rate. This algorithm consists of solving the pressure equation to obtain the pressure field and solving the pressure-correction equation only to correct the velocities. The sequence of operations is the following:

1. Begin with a guessed velocity field.
2. Calculate the coefficients for the momentum equations and hence calculate \hat{u} , \hat{v} .
3. Calculate the coefficient for pressure equation, and solve it to obtain the pressure field.
4. Treating this pressure field as p^* , solve the momentum equations to obtain u^*, v^* .
5. Calculate the mass source and hence solve the p' equation.
6. Correct the velocity field.
7. Solve the discretization equations for other ϕ 's if necessary.
8. Return to step 2 and repeat until convergence

3.3 FINITE DIFFERENCE EQUATIONS FOR SOLID-PHASE

The finite difference used here to solve U_p and V_p is the explicit central scheme for second derivative and forward for first derivative. These can be expressed as

$$\begin{aligned}
 U_{p,i,j}^{n+1} = & U_{p,i,j}^n - U_{p,i,j}^n \cdot \frac{U_{p,i+1,j}^n - U_{p,i,j}^n}{\Delta x} - V_{p,i,j}^n \cdot \frac{U_{p,i,j+1}^n - U_{p,i,j}^n}{\Delta y} \\
 & + \frac{1}{(\rho_p(1-\phi))_{i,j}^n} \cdot \left[(A_s D_{ux})_{i,j}^n \right. \\
 & - U_{p,i,j}^n D_{i,j}^n \frac{(\rho_p(1-\phi))_{i+1,j}^n - 2 \cdot (\rho_p(1-\phi))_{i,j}^n + (\rho_p(1-\phi))_{i-1,j}^n}{\Delta x^2} \\
 & \left. - U_{p,i,j}^n D_{i,j}^n \frac{(\rho_p(1-\phi))_{i,j+1}^n - 2 \cdot (\rho_p(1-\phi))_{i,j}^n + (\rho_p(1-\phi))_{i,j-1}^n}{\Delta y^2} \right] \quad (3.4)
 \end{aligned}$$

$$\begin{aligned}
 V_{p,i,j}^{n+1} = & V_{p,i,j}^n - U_{p,i,j}^n \cdot \frac{V_{p,i+1,j}^n - V_{p,i,j}^n}{\Delta x} - V_{p,i,j}^n \cdot \frac{V_{p,i,j+1}^n - V_{p,i,j}^n}{\Delta y} \\
 & + \frac{1}{(\rho_p(1-\phi))_{i,j}^n} \cdot \left[(A_s D_{vy})_{i,j}^n \right. \\
 & - V_{p,i,j}^n D_{i,j}^n \frac{(\rho_p(1-\phi))_{i+1,j}^n - 2 \cdot (\rho_p(1-\phi))_{i,j}^n + (\rho_p(1-\phi))_{i-1,j}^n}{\Delta x^2} \\
 & \left. - V_{p,i,j}^n D_{i,j}^n \frac{(\rho_p(1-\phi))_{i,j+1}^n - 2 \cdot (\rho_p(1-\phi))_{i,j}^n + (\rho_p(1-\phi))_{i,j-1}^n}{\Delta y^2} \right] \quad (3.5)
 \end{aligned}$$

where n, i , and j stand for time step, x direction grid point and y direction grid point respectively.

Table 3.1: Subroutines and Their Parameters

SUBROUTINE	INPUT	OUTPUT
DENSITYP	$d_p, \rho_p, \dot{M}_{vo}$	d_p
DIAMETERP	$d_p, \rho_p, \dot{M}_{hr}$	ρ_p
HETMASS	\dot{M}_{hr}, \tilde{n}	$(\dot{M}_{CO}, \dot{M}_{O_2}, \dot{M}_{H_2O}, \dot{M}_{CO_2})_{HET}$
HOMASS	$\rho_g, A_{CO}, E_{CO}, A_{CH_4}, E_{CH_4}$	$(\dot{M}_{CO}, \dot{M}_{O_2}, \dot{M}_{H_2O}, \dot{M}_{CO_2}, \dot{M}_{CH_4})_{HOM}$
PYROM	T_P, E_{vo}, B_{vo}	\dot{M}_{vo}
PYROMASS	M_{vo}	$(\dot{M}_{CO}, \dot{M}_{O_2}, \dot{M}_{H_2O}, \dot{M}_{CO_2}, \dot{M}_{CH_4})_{VOL}$
QCHEMA	$M_{vo}, M_{hr}, \Delta H_{HET}, \Delta H_{PYR}$	\dot{q}_{HET}
QCONDP	T_g, T_p, D_p, K	\dot{q}_{COND}
QCONVP	$N_u, \rho D, C_p, T_g, T_p, \lambda, D_p$	\dot{q}_{CONV}
QDECOMP	$\dot{M}_{vo}, \Delta \bar{H}_{VOL}$	\dot{q}_{DECOMP}
QRADP	$T_g, T_p, \hat{F}, \hat{\sigma}, \hat{\epsilon}$	\dot{q}_{RAD}
SIMPLE	$\dot{W}_K, \dot{W}_h, \dot{W}_m$	$U_g, V_g, T_g, \kappa, \epsilon, P, \rho_g$
TEMPP	$\dot{q}_{HET}, \dot{q}_{COND}, \dot{q}_{CONV}, \dot{q}_{DECOMP}, \dot{q}_{RAD}$	T_p
YIELDWALL	ρ_p, d_p, M_{po}	\dot{M}_{hr}

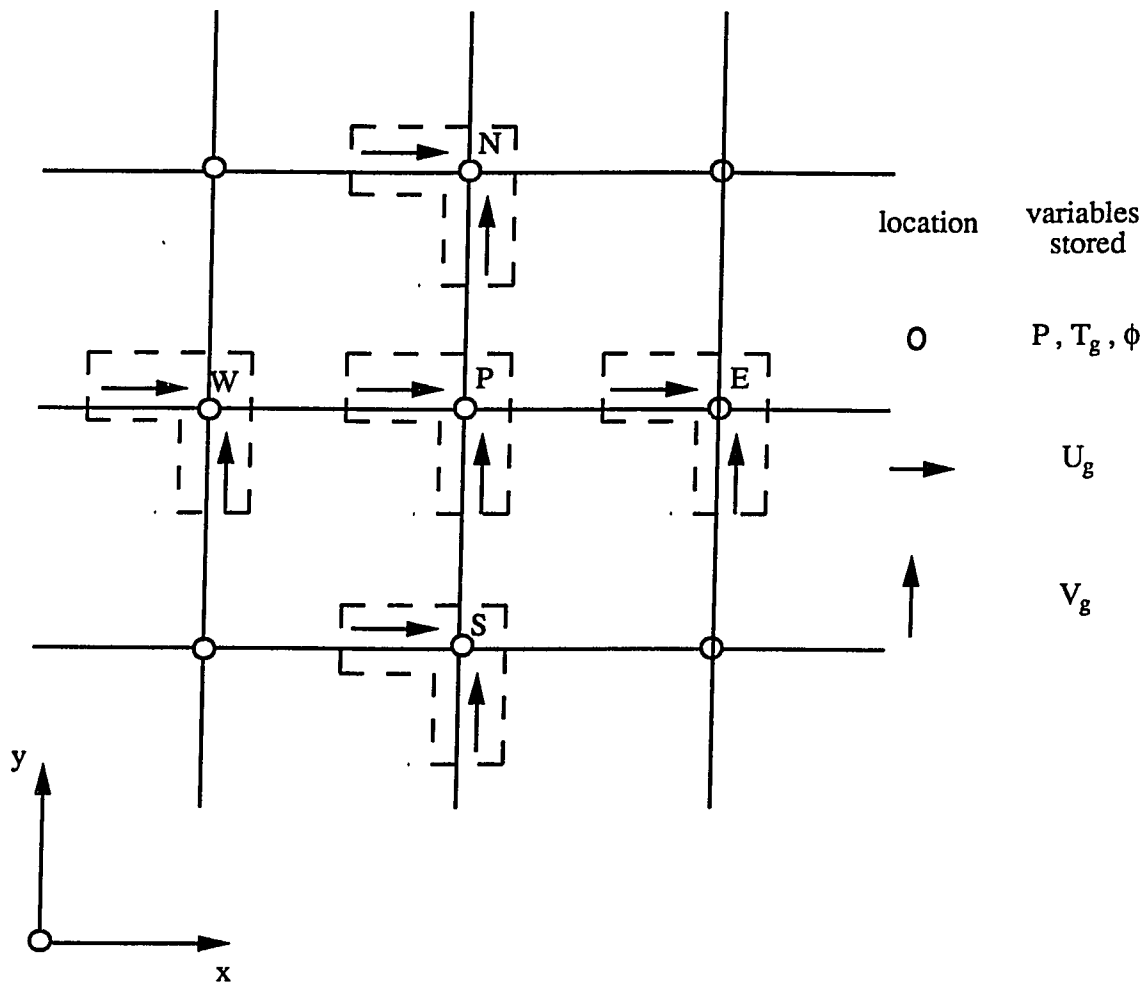


Figure 3.1 Staggered Location for U_g , V_g .

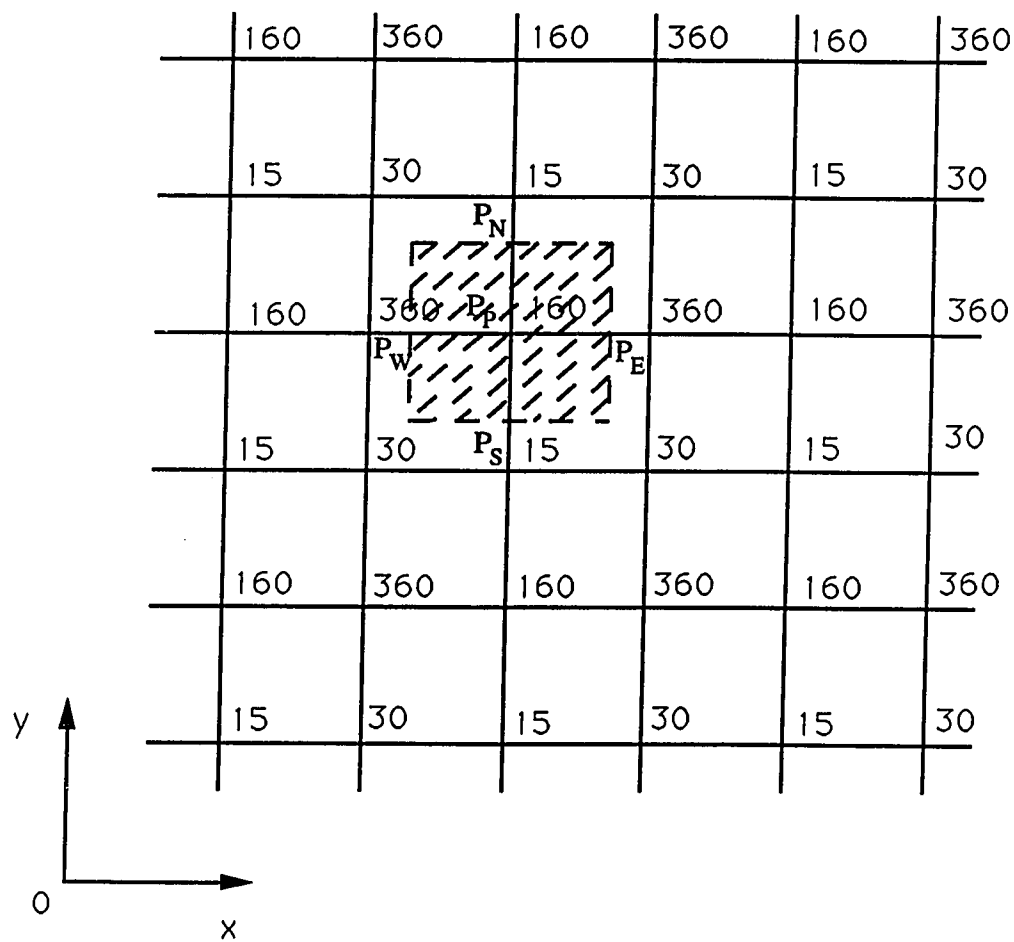


Figure 3.2 Pressure Field.

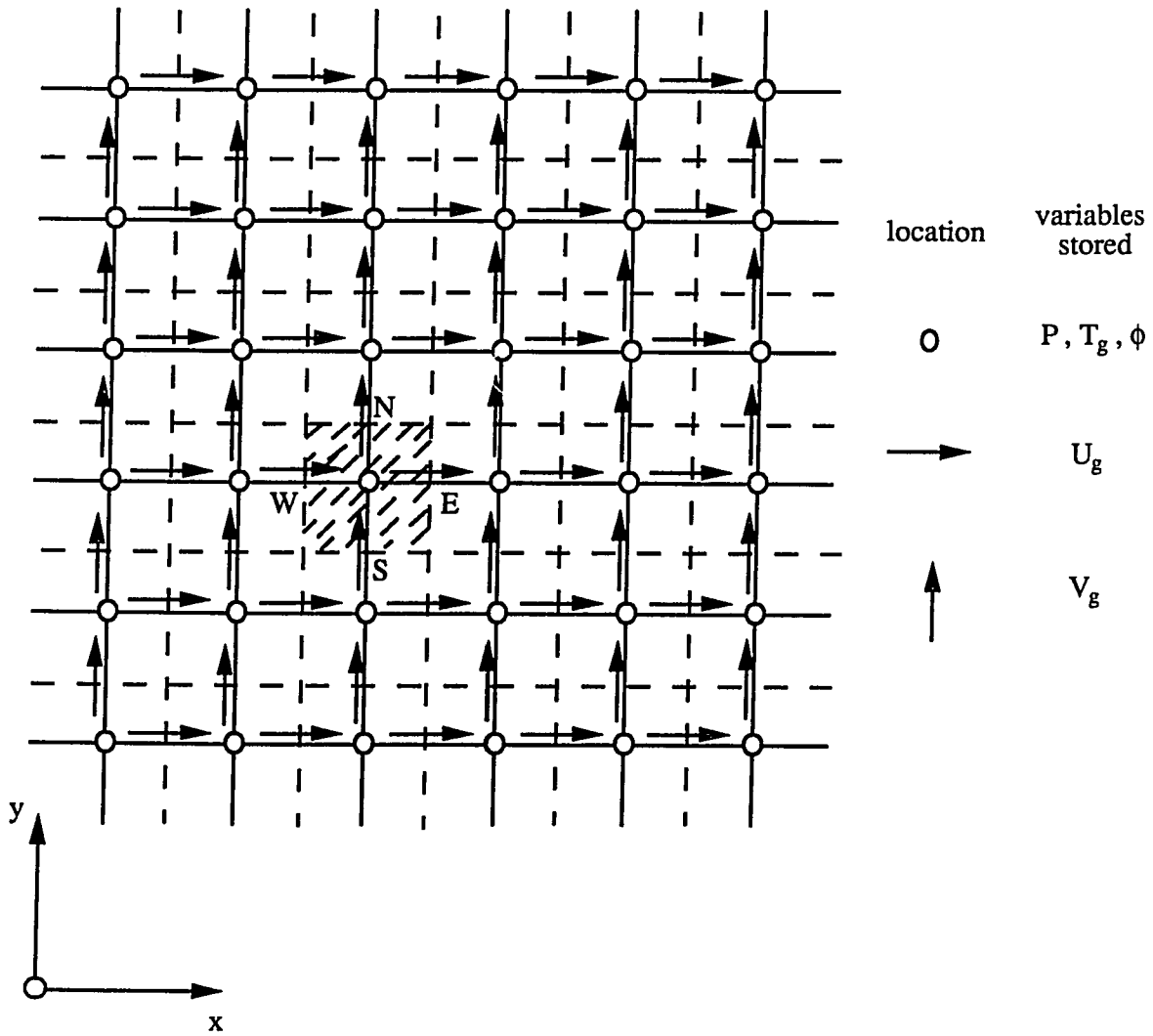


Figure 3.3 Two-Dimensional Grid Pattern.

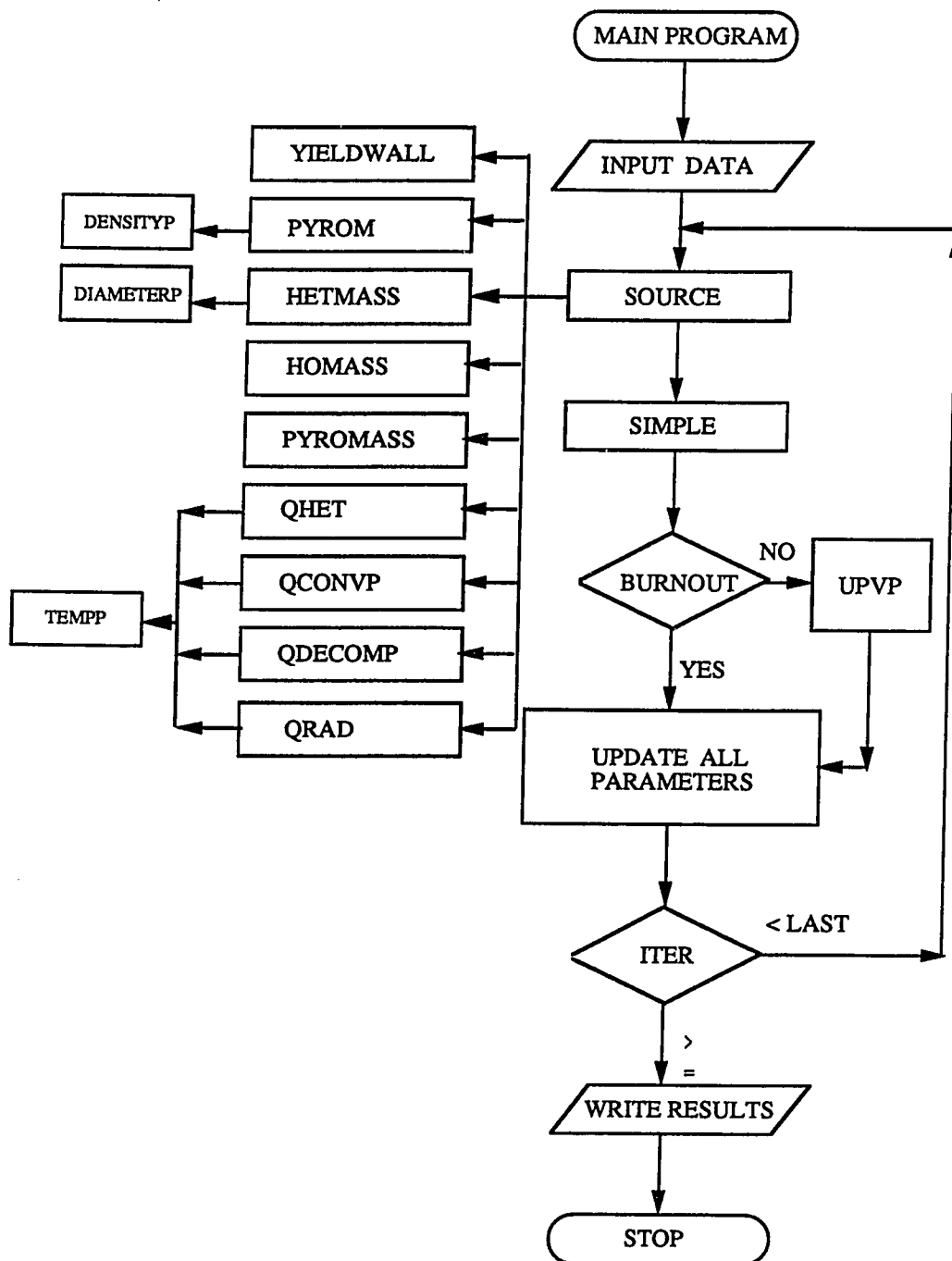


Figure 3.4 Program Flow Chart.

Chapter 4

RESULTS AND DISCUSSION

The modeling parameters, properties used, and boundary conditions employed at wall, inlet, and exit are tabulated in Table 4.1, Table 4.2 and Table 4.3 respectively.

4.1 SUDDEN EXPANSION FLOW

The purpose of this test case is to evaluate the program's ability to solve the conservation of mass, momentum, and energy equations using the κ - ϵ model to account for turbulence. The test chamber is 2-dimensional, as shown in Fig. 4.1.

The computational predictions for the variations in velocity and kinetic energy are illustrated in Figs. 4.2 to 4.5. The results are compared with the experimental data taken in cylindrical geometries since no experiments in two-dimensional ducts exist. We observe that the agreement is satisfactory.

The Reynolds number for Fig. 4.2 and Fig. 4.3 is 3.88e05 and is 5.0e05 for Fig. 4.4 and Fig. 4.5. The inlet velocity and temperature are assumed to be uniform and the inlet turbulence parameters are given by [29]:

$$\kappa_0 = C'U_0^2$$
$$\epsilon_0 = \frac{\kappa_0^{\frac{3}{2}}}{0.01h_3}$$

Where h_3 is the width of inlet; $C'=0.03$. A uniform grid system of 20×20 is employed for all of the study.

Fig. 4.2 [49] displays the predicted velocity distribution ratio, $\frac{U}{U_0}$, at four locations in the y-direction as a function of $\frac{x}{h_3}$. Fig. 4.3 [49] depicts the cross-sectional velocity

profile at four locations along the y direction, and the distribution of $\frac{\kappa}{U_c^2}$ (U_c is the centerline velocity) and velocity are shown in Fig. 4.4 [50], Fig. 4.5 [50].

4.2 EFFECT OF RECIRCULATION AREA ON COAL COMBUSTION

In this section we study the size of recirculation zone and its effect on coal combustion. The size of the recirculation zone can be controlled by varying the location of the inlet. Fig. 4.6 shows the geometry and six inlet locations.

The conditions are:

- (1) keep inlet width h_3 constant
- (2) decrease width h_2
- (3) increase width h_1

A summary of the results are as follows:

According to Fig. 4.7 (a) and (b), the recirculation area ratio, defined as the total flow field area over recirculation area, is linearly dependent on h_1 and h_3 . In Fig. 4.7 (a) recirculation area ratio, $\frac{A_1}{A}$, increases with increasing h_1 , while the area ratio, $\frac{A_2}{A}$, decreases with h_2 (b).

Interestingly, the sum $\frac{A_1+A_2}{A}$ increases almost linearly from 0.03 to 0.085 (Fig. 4.8). Therefore, to minimize the recirculation zone, the inlet must be centered.

Fig. 4.9 (a) and (b) show the reattachment lengths, defined by $\frac{x_{r1}}{h_1}$ or $\frac{x_{r2}}{h_2}$, to be nearly constants, equal to 1.9 and 2.25, respectively. This trend can be proven by the following order of magnitude analysis.

Outside the recirculation zone, we have

$$\rho U_0 h_3 = \rho U_2 h \quad (4.1)$$

$$P_1 + \rho \frac{U_0^2}{2} = P_2 + \rho \frac{U_2^2}{2} \quad (4.2)$$

Here, density is assume to be constant. Substituting Eq. 4.1 into Eq. 4.2 yields

$$P_2 - P_1 = \frac{\rho}{2} \left(1 - \frac{h_3^2}{h^2}\right) U_0^2 \quad (4.3)$$

Inside the recirculation zone, we have

$$\frac{\partial P}{\partial x} = \mu_t \frac{\partial^2 U}{\partial y^2} \quad (4.4)$$

By order of magnitude, the above relation can be approximated as

$$\frac{P_2 - P_1}{x_{r2}} \approx \mu_t \frac{U_0}{h_2^2} \quad (4.5)$$

Substituting $(P_2 - P_1)$ from Eq. 4.3 into Eq. 4.5 and arranging gets

$$\frac{x_{r2}}{h_2} \approx \frac{\rho U_0 h_3}{2\mu_t} \frac{h_2}{h_3} \left(1 - \frac{h_3^2}{h^2}\right) \quad (4.6)$$

For turbulence,

$$\mu_t = C_\mu \rho \frac{\kappa^2}{\epsilon} \quad (4.7)$$

where

$$\begin{aligned} \kappa &\approx \left(\frac{3}{2} U_0^2\right) \\ \epsilon &\approx \frac{C_\mu \kappa^{\frac{3}{2}}}{(0.01 h_3)} \\ C_\mu &= 0.09 \end{aligned}$$

Substituting these three terms into Eq. 4.7 yields

$$\mu_t = 0.01225 \rho U_0 h_3 \quad (4.8)$$

Plugging μ_t into Eq. 4.6, we get

$$\frac{x_{r2}}{h_2} \approx 40.82 \frac{h_2}{h_3} \left(1 - \frac{h_3^2}{h^2}\right) = \text{constant} \quad (4.9)$$

Figs. 4.10 to 4.21 show how the contours related to certain properties vary by changing the inlet locations (as shown in Fig. 4.6). Fig. 4.10 to 4.12 are the gas velocity vectors, contours of gas velocity U_g and V_g . From the three pictures, it is clear that the recirculation zones are initially identical, but lose this characteristic with asymmetric inlet condition. Fig. 4.13 shows the pressure contours. Past the inlet, the pressure increases in the direction of flow (adverse pressure gradient) owing to the presence of recirculation zone. Beyond this region, the pressure decreases in the direction of flow (favorable pressure gradient) down to the exit. Figs. 4.14 to 4.16 display the gas temperature contours, turbulence kinetic energy contours and turbulence dissipation contours. Species concentration contours of CO , CO_2 , H_2O , O_2 and CH_4 are shown in Figs. 4.17 to 4.21, respectively. The concentrations of O_2 (Fig. 4.20), CO (Fig. 4.17), and CH_4 (Fig. 4.21) decrease from inlet ($x=0$) to exit ($x=1.52$ meter). On the contrary, however, the concentrations of CO_2 (Fig. 4.18) and H_2O (Fig. 4.19) increase from inlet ($x=0$) to ($x=1.52$ meter).

The total recirculation area increases from case 1 ($h_1 = h_2$) to case 6 ($h_2 = 7.4h_1$).

This causes:

- (1) a large recirculation zone, instead of two small separated recirculation zones (Fig. 4.10), to form.
- (2) A high temperature burned gas to penetrate deep into the recirculation zone (Fig. 4.14). The recirculation zones, as a result, become quite hot.
- (3) Strong turbulence and through mixing occur cause faster burning (Figs. 4.15, 4.16).

We speculate that the above findings are favorable for stable and intensive combustion. Therefore, in order to meet this goal, the inlet must be highly off-centered. Fig. 4.22 shows the predicted cross-section distributions of gas temperature at five stations, $x=0.0423$ m; $x=0.381$ m; $x=0.7$ m; $x=1.06$ m; $x=1.4$ m, and provides a more complete picture of the influence of inlet location on coal combustion. Due

to the same inlet temperature, all six cases have similar bell-shaped distributions at $x=0.0423$ m. The bell-shape shifts from center to bottom as the location of the entrance changes. At $x=0.381$ m the bell-shaped distributions become inverted. For case 6, however, there is no qualitative variation in shape from $x=0.0423$ m to 0.381 m. This is believed to be due to wall friction. At the other succeeding stations, however, the distributions are inverted, and maintain, more or less, the same shape.

Fig. 4.23 shows the predicted distributions of O_2 concentration at five stations mentioned above. It is noted that where temperature is high, the concentration of O_2 is low, and vice versa. Interestingly, upon summing up the two (without considering the scale), a vertical line is obtained. The reason for this is that O_2 consumption increases at high temperatures.

4.3 EFFECT OF THE LOCATION OF THE SECONDARY AIR FLOW ON COAL COMBUSTION

In this section, we study the effect of the location of the secondary air flow on coal combustion. As will be demonstrated, the aerodynamics and combustion performance can be made different by varying the location of secondary air along the furnace wall. Fig. 4.24 shows the six inlets of secondary air flow locations that were investigated here.

The parameters used in this section are tabulated in Table 4.1. The only difference in these cases is the location of secondary air flow, while all others properties are kept the same. Fig. 4.25 to 4.34 show the variation of the gas velocity vectors and contours pertaining to some important properties with changing air inlet locations from $x=0.127$ meter to 0.55 meter (exit).

Fig. 4.25 illustrates the effects of the primary air and recirculation on the flow. In Fig. 4.25.1 (case 1, 2 and 3), the effect of inlet air on the velocity distribution is obvious in that cancelations in the y-component velocities lead to a more parallel flow

field. In Fig. 4.25.2 (case 4, 5 and 6), the effect of recirculation on the flow patterns when the secondary flow at $x=0.381$ m, $x=0.466$ m and $x=0.55$ m totally disappear, implying that the location of the inlet is quite important on the overall results. Also, it is interesting to note that the downstream flow pattern is the same in all six cases.

Fig. 4.26 shows the pressure contours. In all six cases, pressure increases from $x=0$ meter to the location of the secondary air where a maximum is reached. The pressure, ultimately, begins to drop all the way to $x=1.52$ meter. This suggests that the pressure gradient equal to zero around the location of the secondary air; left of it the pressure gradient is larger than zero and right of it the pressure gradient is smaller than zero.

Fig. 4.27 shows the temperature field where it is clear that the temperature distributions are highly dependent on the fluid mechanics. If the location of the secondary air is too far away from the recirculation zone (ie. case 4, 5 and 6) the oxidizer can not reach upstream. Since, there exists very little oxidizer volatiles in coal, then the temperature will not increase sufficiently to promote further combustion. As a result, it is important to locate the secondary air within the recirculation zone.

Fig. 4.28 and 4.29 shows the turbulence kinetic energy and turbulence dissipation contours, both of which display similar characteristics. Focusing on one isoline, for instance κ = line 4 in Fig. 4.28 and ϵ = line 3 in Fig. 4.29, we note that its shape accompanies the secondary flow. These isolines are, therefore, affected strongly by the inlet values of κ_0 and ϵ_0 .

Fig. 4.30 to 4.34 show the species concentration contours of CO , CO_2 , H_2O , O_2 and CH_4 . The characteristics of these species are same as in Section 4.2, however, from $x=0$ meter to the location of the secondary air inlet, the concentrations are very low for the same reasons discussed earlier.

In conclusion, if air is to be supplied from the side walls, the location of the (air) inlet must correspond to the region where flow re-attaches. This maximizes the combustibility by reducing the amount of unburnt products.

4.4 EFFECT OF THE LOCATION OF THE PRIMARY STREAMS ON COAL COMBUSTION

In this section, the effects of the location of the primary streams on coal combustion are examined. As noted earlier, the aerodynamics and combustion performance can undergo significant changes. Fig. 4.35 shows the three primary inlet locations investigated.

All parameters used in here, except for the locations of the primary streams, are similar to those tabulated in Table 4.1. Figs. 4.36 to 4.48 again show the variation of the gas velocity vectors and contours pertaining to some properties with changing primary streams inlet locations from $y=3.3$ cm to $y=16.6$ cm. In Fig. 4.36, the flow patterns for the three cases look quite different from $x=0$ meter to the location of secondary air flow. Afterwards, however they assume similar shapes. In case (a), a triangular shaped recirculation zone is formed. In case (b), two separated recirculation zones of different sizes form due to asymmetry; and in case (c), a large recirculation zone forms in upper corner.

Fig. 4.39 shows the pressure contours. In all three cases, pressure increases from $x=0$ meter to the location of the secondary air after which it begins to fall. Here, however, unlike the situation described in section 4.3 where the pressure decreases all the way to exit, the pressure increases again after passing through minimum.

Fig. 4.40 shows the temperature contours. In cases (a) and (c), the temperature changes gradually from inlet to exit. Furthermore, due to the location of secondary air flow at the lower wall, the high temperature region is pushed towards the opposite wall. In case (b), however, the temperature in the upstream is low except near

the furnace walls. Therefore, in order to get a more stable and intensive combustion, the favorable configuration are case (a) and (c).

Finally, Figs. 4.41 to 4.47 depict the contours of turbulence kinetic energy, turbulence dissipation and species concentration of CO , CO_2 , H_2O , O_2 and CH_4 , respectively.

Table 4.1: Modeling Parameters Used in Each Section

Parameters	Section 4.1	Section 4.2	Section 4.3	Section 4.4
Furnace Length	152 cm	152 cm	152 cm	152 cm
Furnace Width	20.3 cm	20.3 cm	20.3 cm	20.3 cm
Primary Width	6.8 cm	2.3 cm	2.3 cm	2.3 cm
Secondary Width	0	2.3 cm	8.5 cm	17cm
X Grid	20 nodes	20 nodes	20 nodes	20 nodes
Y Grid	20 nodes	20 nodes	20 nodes	20 nodes
Fuel Mass Fractions (Kg species/Kg fuel)				
CH_4		0.0208	0.0208	0.0208
CO		0.29875	0.29875	0.29875
$C(S)$		0.6617	0.6617	0.6617
N_2		0.01876	0.01876	0.01876
Oxidant Mass Factions (species/oxidant) Kg				
N_2		0.755	0.755	0.755
O_2		0.231	0.231	0.231
Ar		0.014	0.014	0.014
Wall Temperature	1500 K	1500 K	1500 K	1500 K
Fuel Temp.		356 K	356 K	356 K
Oxidant Temp.		589 K	589 K	589 K
Fuel Vel.		33.6 m/s	33.6 m/s	33.6 m/s
Oxidant Vel.		34.1 m/s	34.1 m/s	34.1 m/s
$\dot{m}_{primary}(air)$		0.0056 Kg/s	0.0056 Kg/s	0.0056 Kg/s
$\dot{m}_{primary}(coal)$		0.00121 Kg/s	0.00121 Kg/s	0.00121 Kg/s
$\dot{m}_{second}(air)$		0.0361 Kg/s	0.0361 Kg/s	0.0361 Kg/s

Table 4.2: Properties

Properties	Values	Properties	Values
A_{co}	0.45e3 m/s	B_{hr2}	0
B_{hr1}	0.45e3 m/s	B_{hr2}	0
B_{hr3}	0.39e3 m/s	B_{hr4}	0
B_{vo1}	3.7e5 1/s	B_{vo2}	1.46e13 1/s
E_{hr1}	0.664e5 KJ/Kmole	E_{hr2}	0
E_{hr3}	1.09e5 KJ/Kmole	E_{hr4}	0
E_{vo1}	7.37e4 KJ/Kmole	E_{vo2}	2.51e5 KJ/Kmole
K_{cond}	6.84e-5 KJ/(m s K)	D	4.17e-5 m ² /s
C_p	1.05 KJ/(Kg K)	d_p	100e-6 m
P	1.0132e5 Kg/(s ² m)	\tilde{n}	5.552e8 particles/m ³
R_u	8.28 KJ/(Kmole K)	N_u	2
ρ_g	1.2 Kg/m ³	ρ_p	1.3e3 Kg/m ³
ρD	0.5e-4 Kg/m-s	λ	0.59e-4 Kw/(m K)
Volatiles of Species (Weight % of Coal)			
CH_4	1.25 %	H_2O	16.5 %
CO_2	8.5 %	CO	7 %

Table 4.3: Boundary Conditions at Wall, Inlet, and Exit

Parameters	Wall Condition	Inlet Condition	Exit Condition
U_g	0	U_{g0}	$\frac{\partial U_g}{\partial x} = 0$
V_g	0	0	$\frac{\partial V_g}{\partial x} = 0$
U_p	0	U_{p0}	$\frac{\partial U_p}{\partial x} = 0$
V_p	0	0	$\frac{\partial V_p}{\partial x} = 0$
T_g	T_w	T_{g0}	$\frac{\partial T_g}{\partial x} = 0$
κ	$\frac{\partial \kappa}{\partial x} = 0$	κ_0	$\frac{\partial \kappa}{\partial x} = 0$
ϵ	$\epsilon = \frac{C_\mu^{\frac{3}{4}} \kappa^{\frac{3}{2}}}{l_n}$	ϵ_0	$\frac{\partial \epsilon}{\partial x} = 0$
Y_K	$\frac{\partial Y_K}{\partial y} = 0$	Y_{K0}	$\frac{\partial Y_K}{\partial x} = 0$

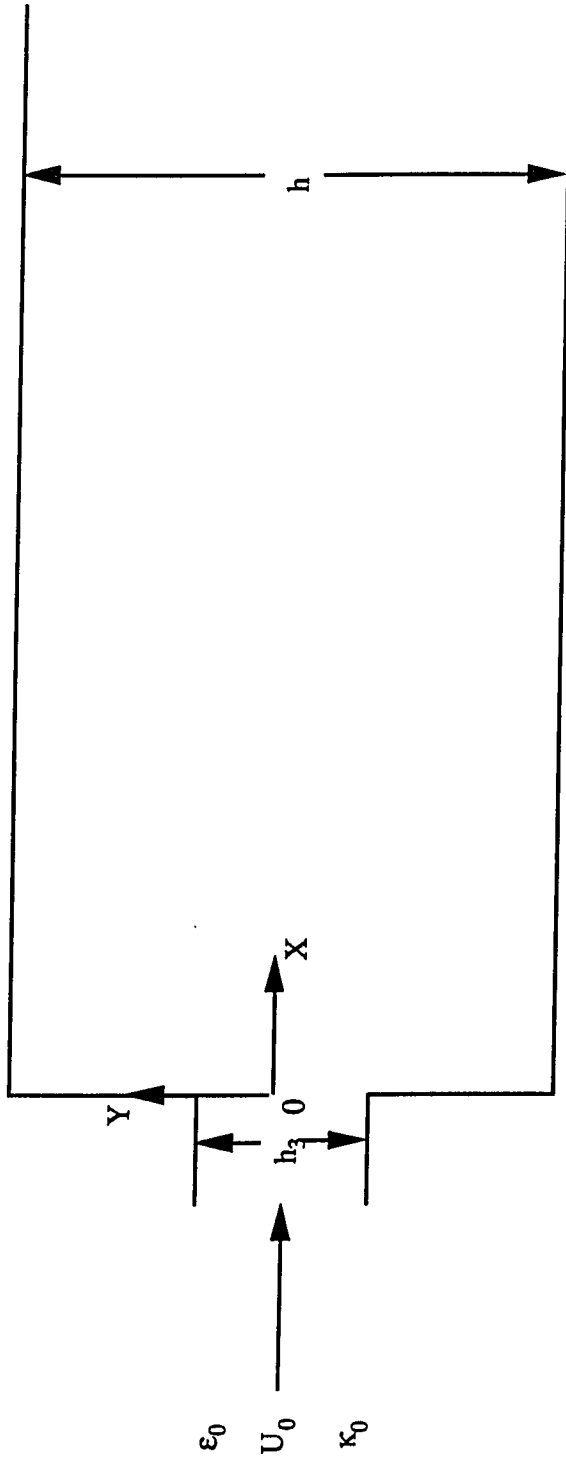


Figure 4.1 Test Chamber in X-Y Coordinate

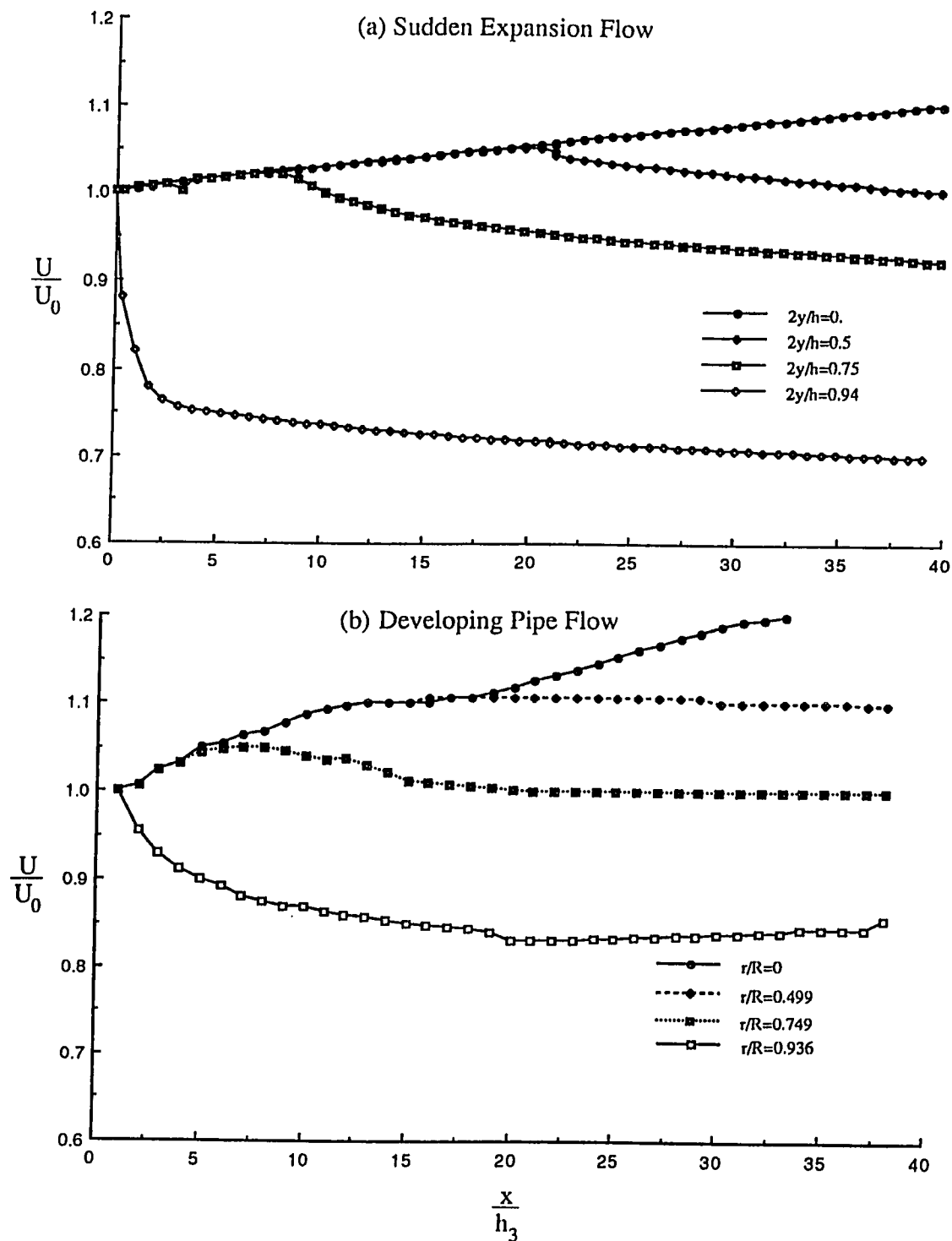


Figure 4.2 Variation of Velocity (a) Present Predictions
(b) Experimental Data of Barbin and Jones (1963)

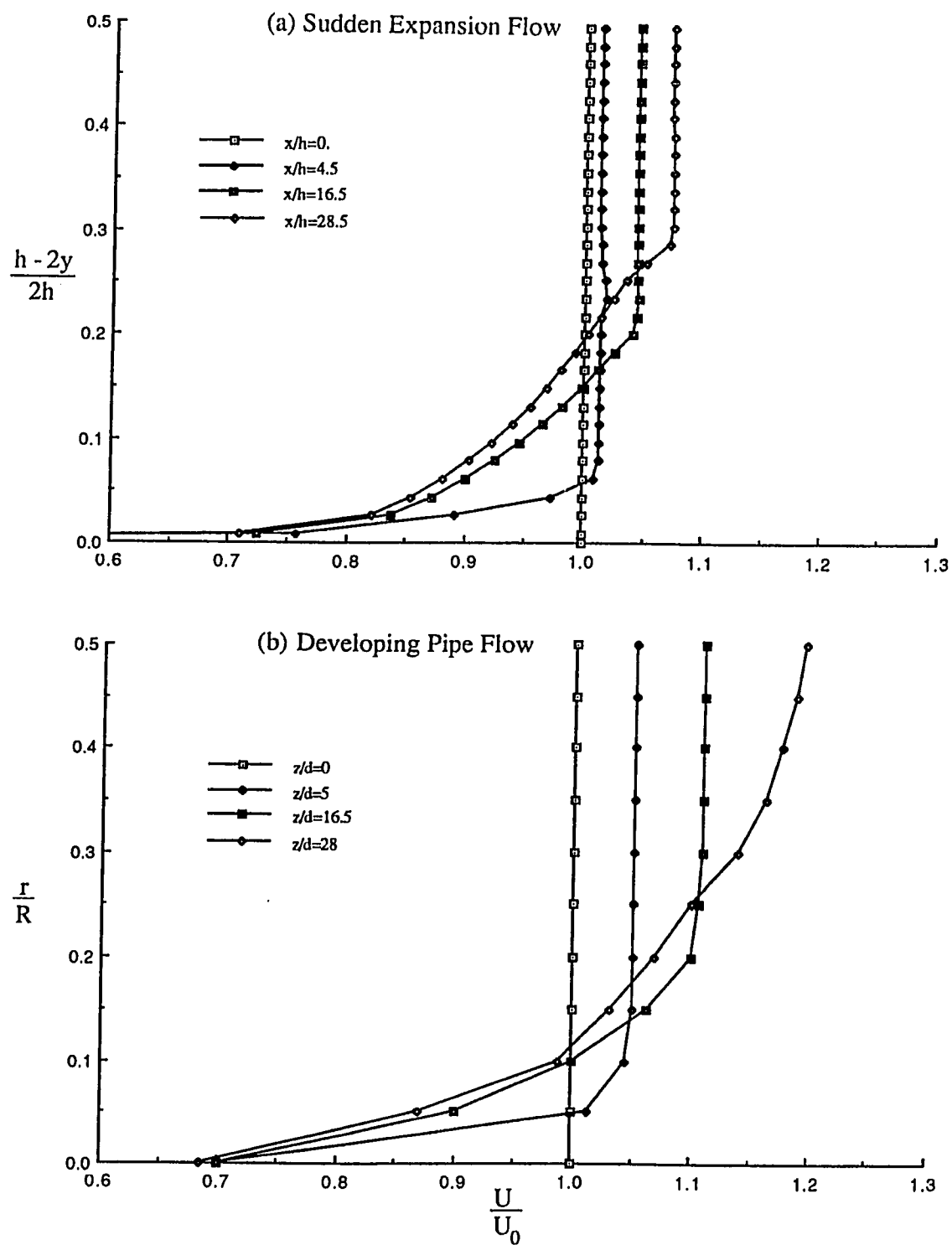


Figure 4.3 Velocity Profile in Four Locations (a) Present Predictions
(b) Experimental Data of Barbin and Jones (1963)

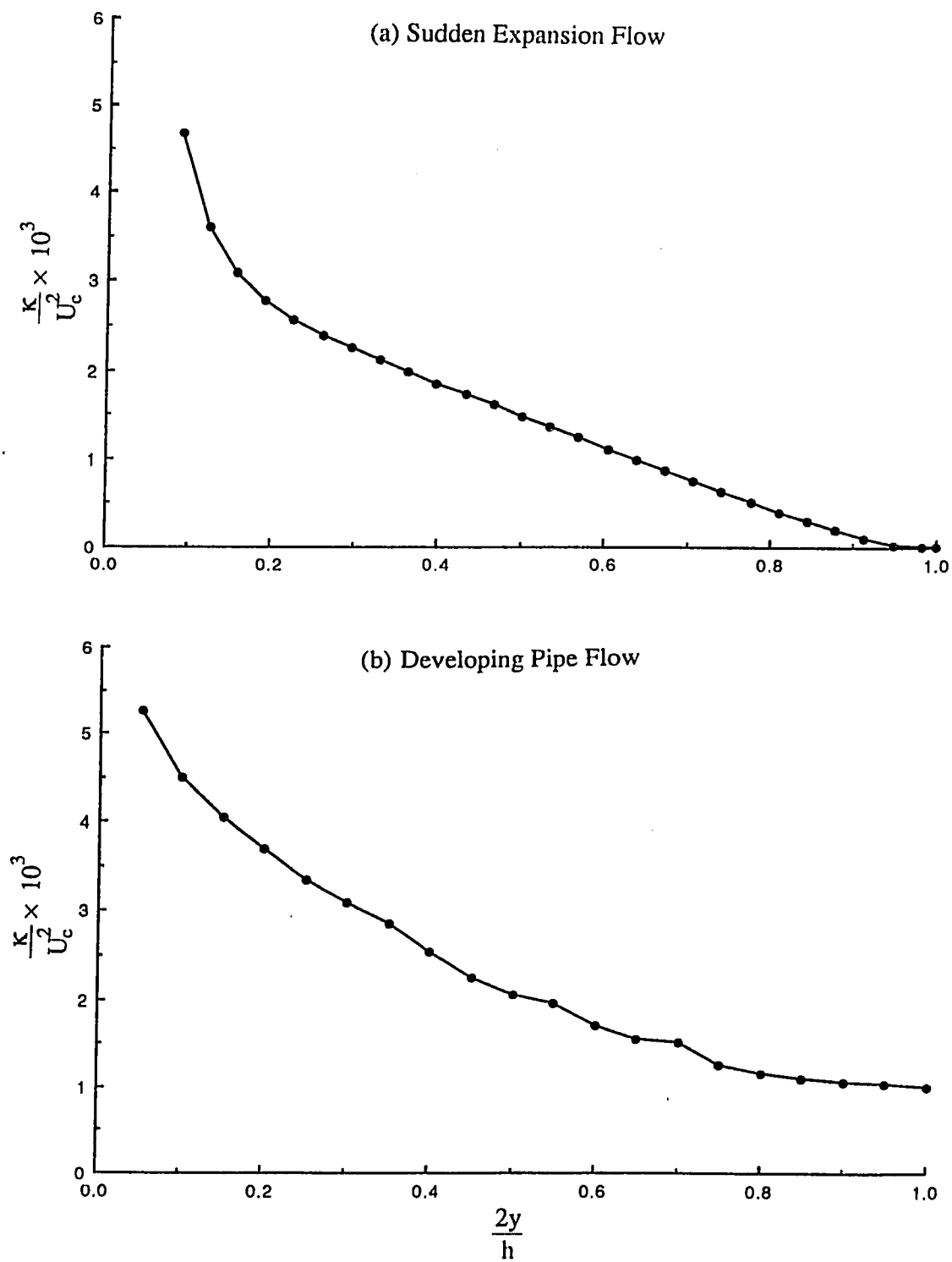


Figure 4.4 Kinetic Energy (a) Present Predictions
(b) Experimental Data of Laufer (1952)

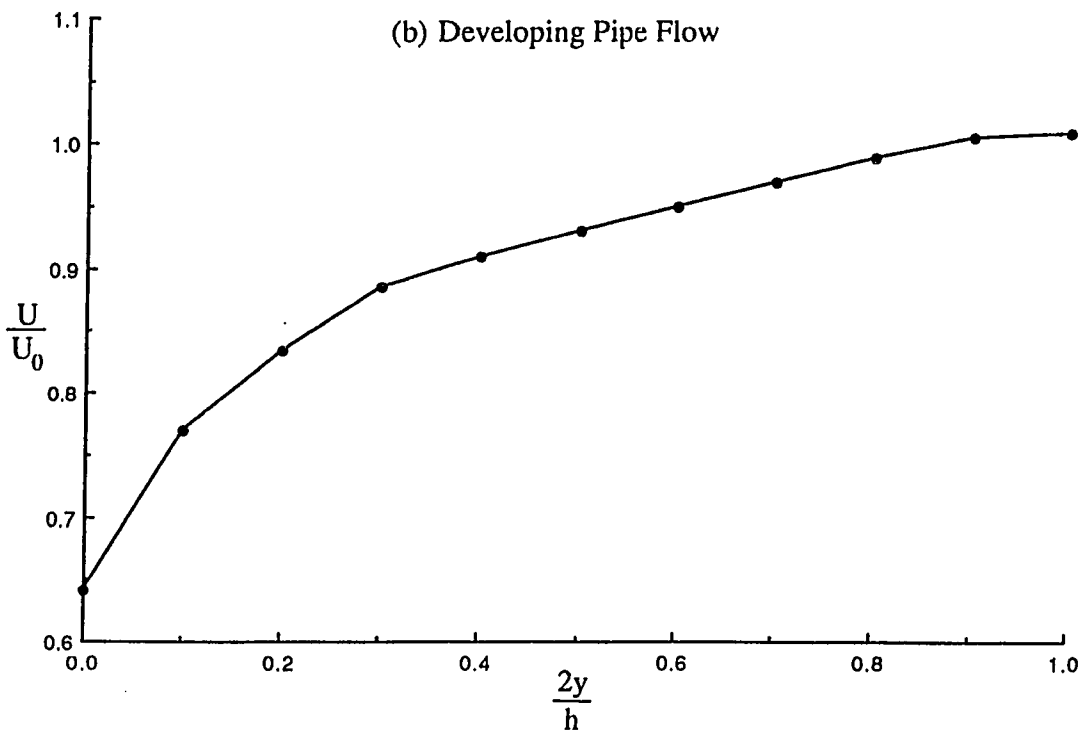
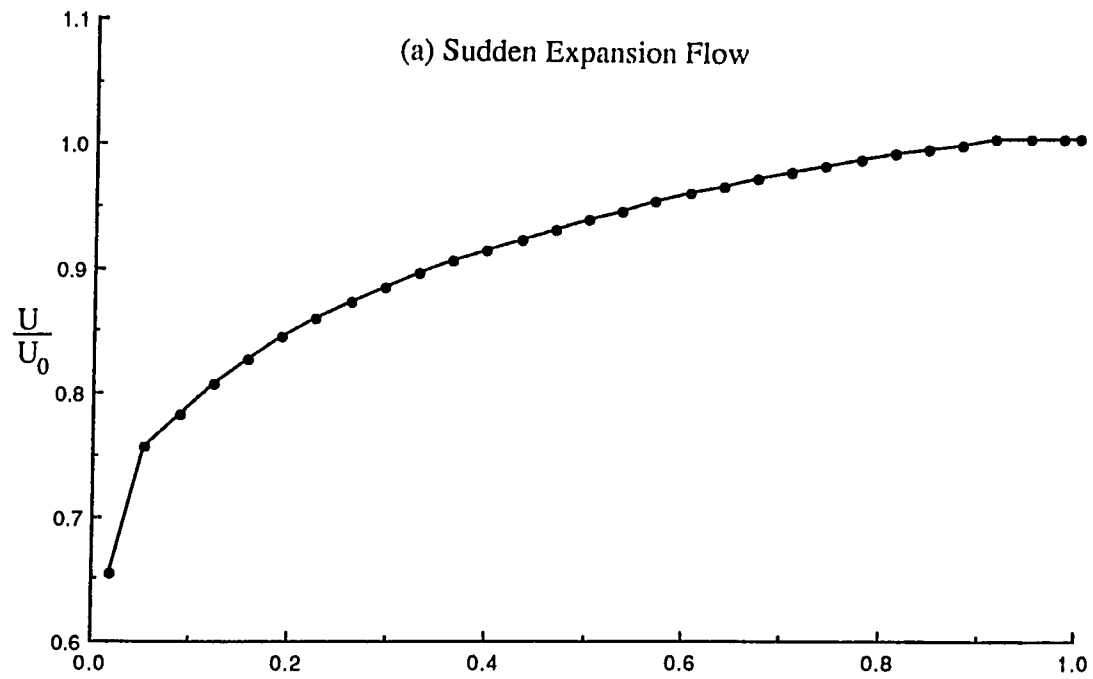


Figure 4.5 Velocity profile (a) Present predictions
(b) Experimental Data of Laufer (1952)

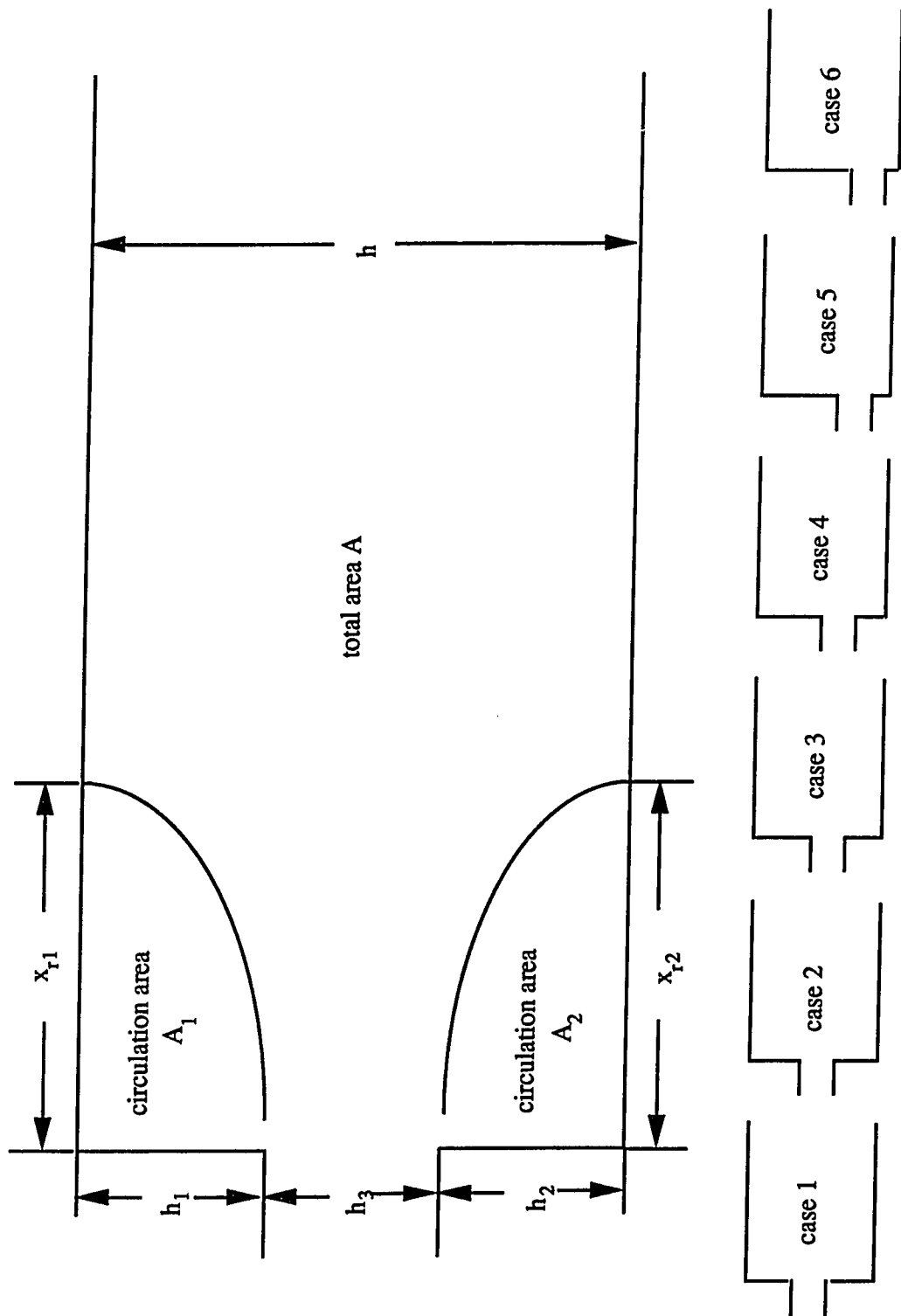


Figure 4.6 Model Furnace Geometry and Six Cases of Different Inlet Position

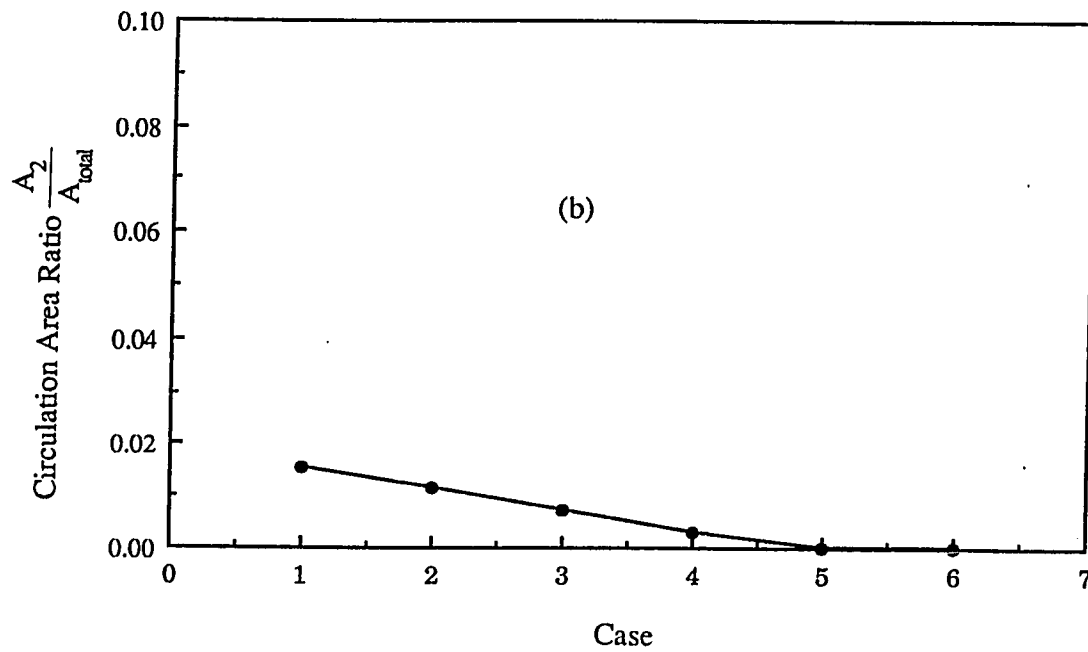
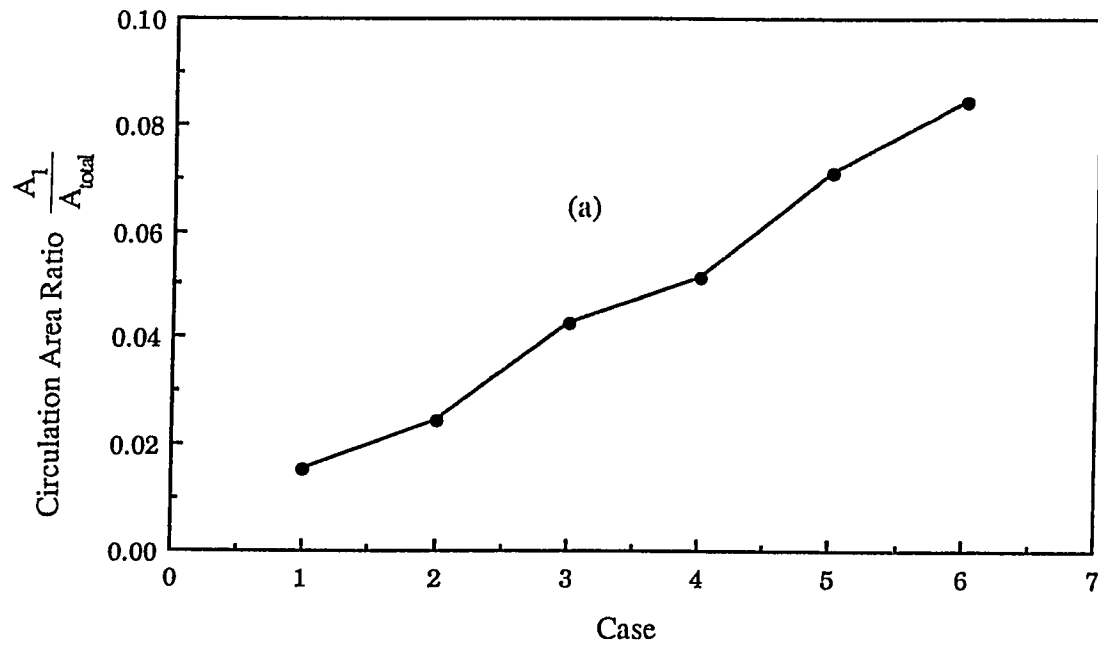


Figure 4.7 Variation of Circulation Area A_1 and A_2

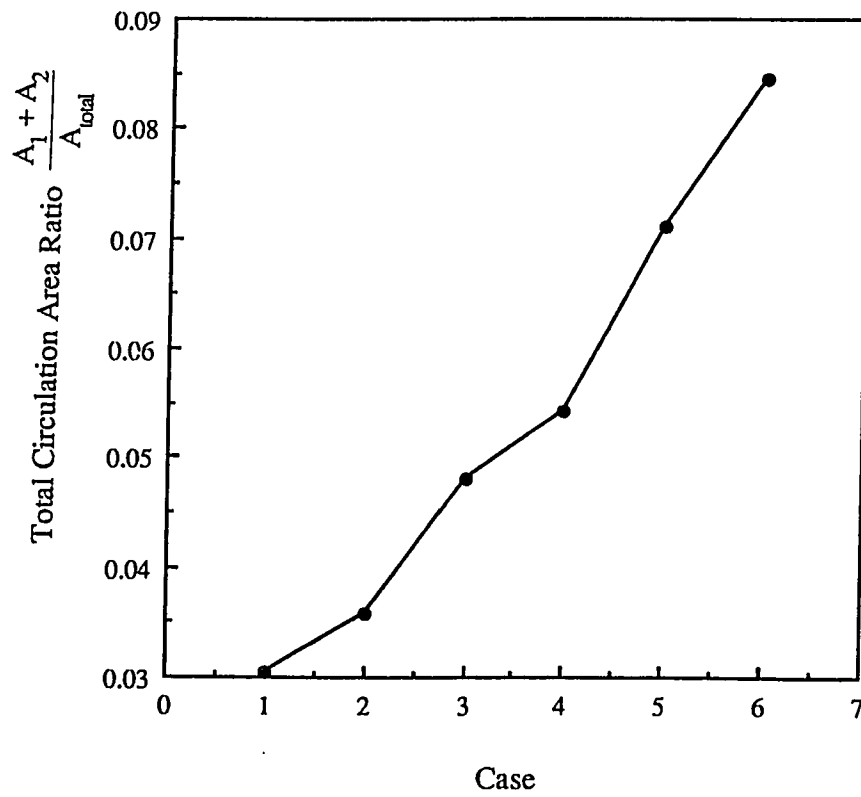


Figure 4.8 Variation of Total Circulation Area

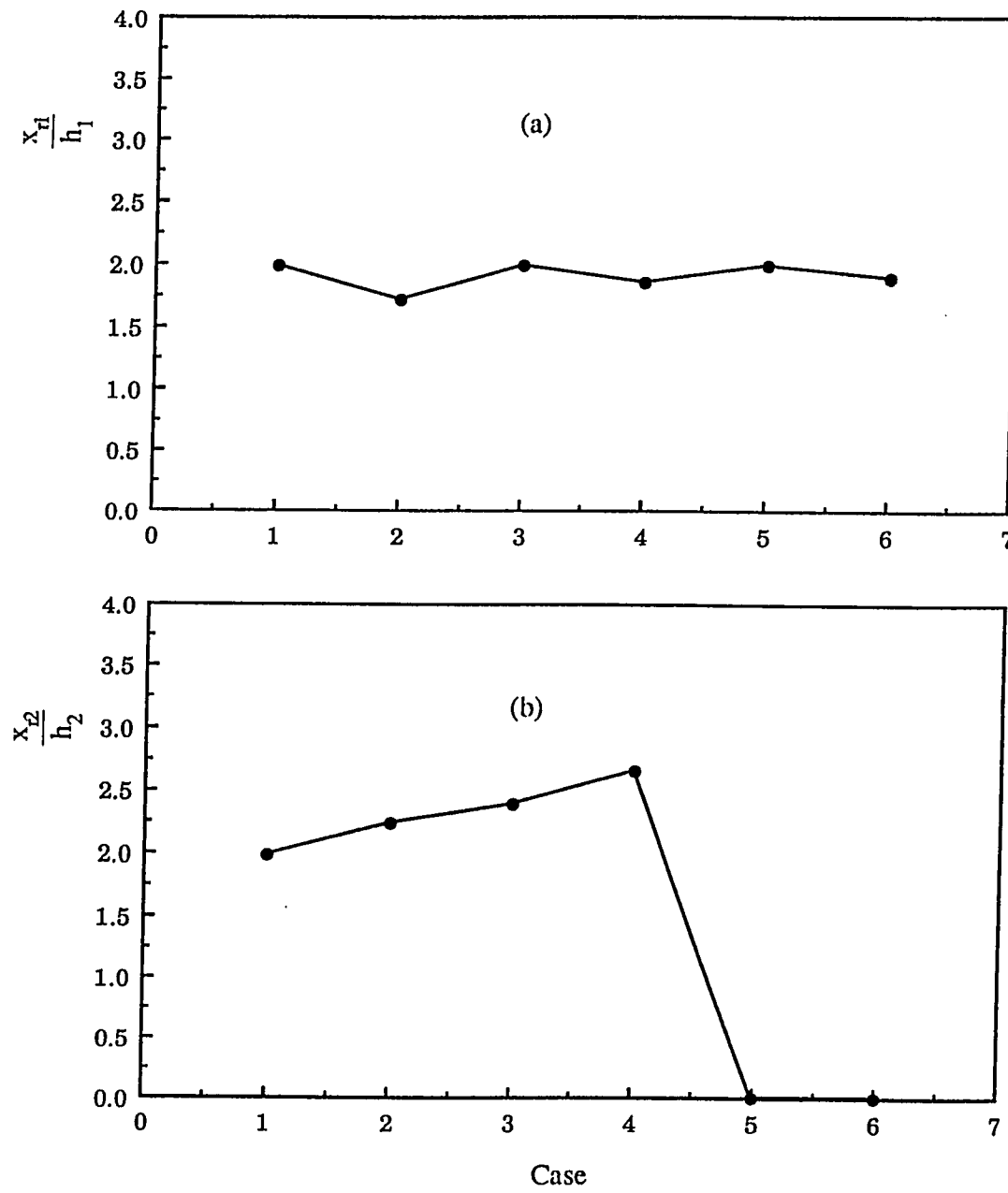


Figure 4.9 Reattachment Length

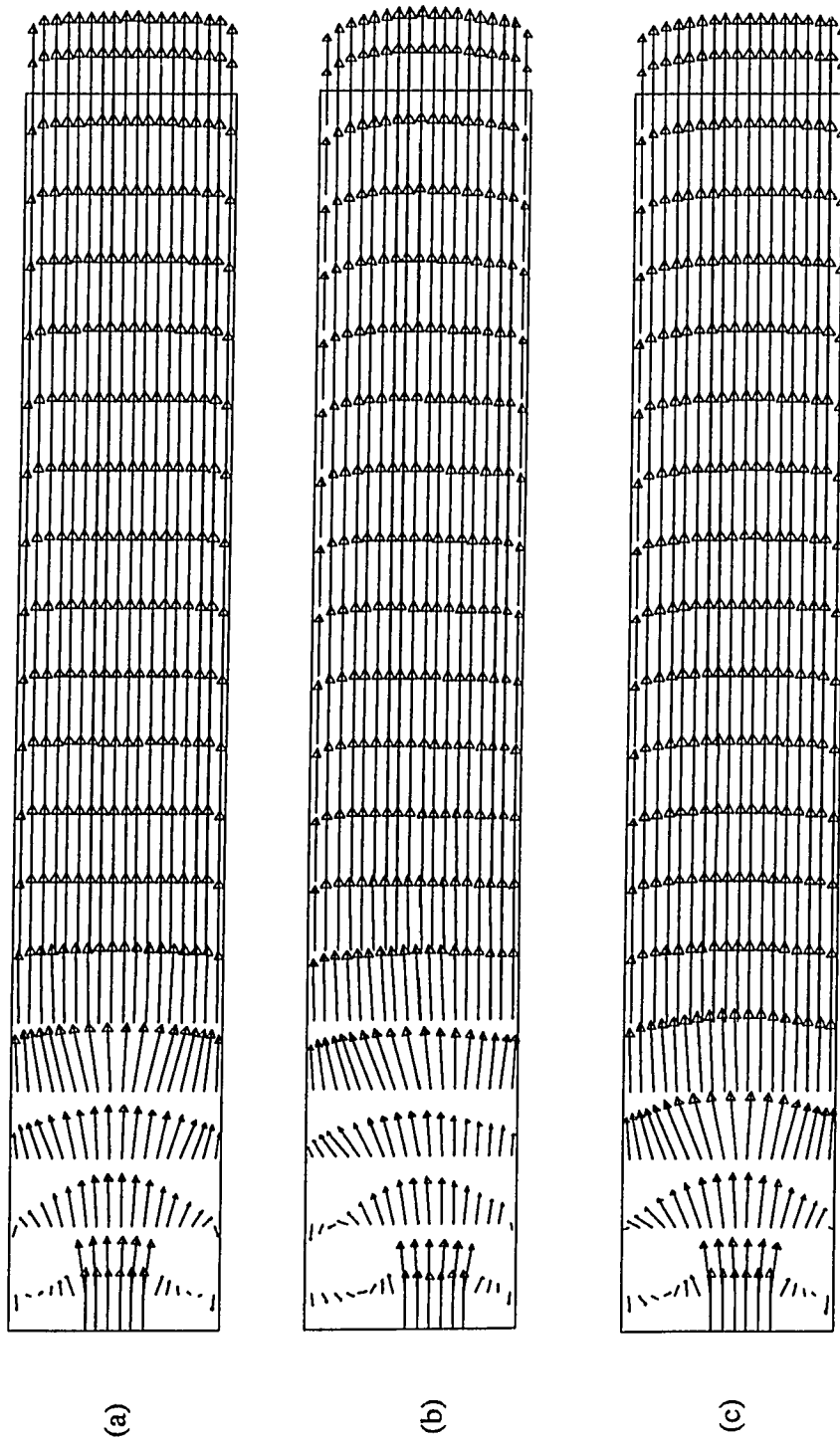


Figure 4.10.1 Predicted Gas Velocity Vectors (a) case 1 (b) case 2 (c) case 3.

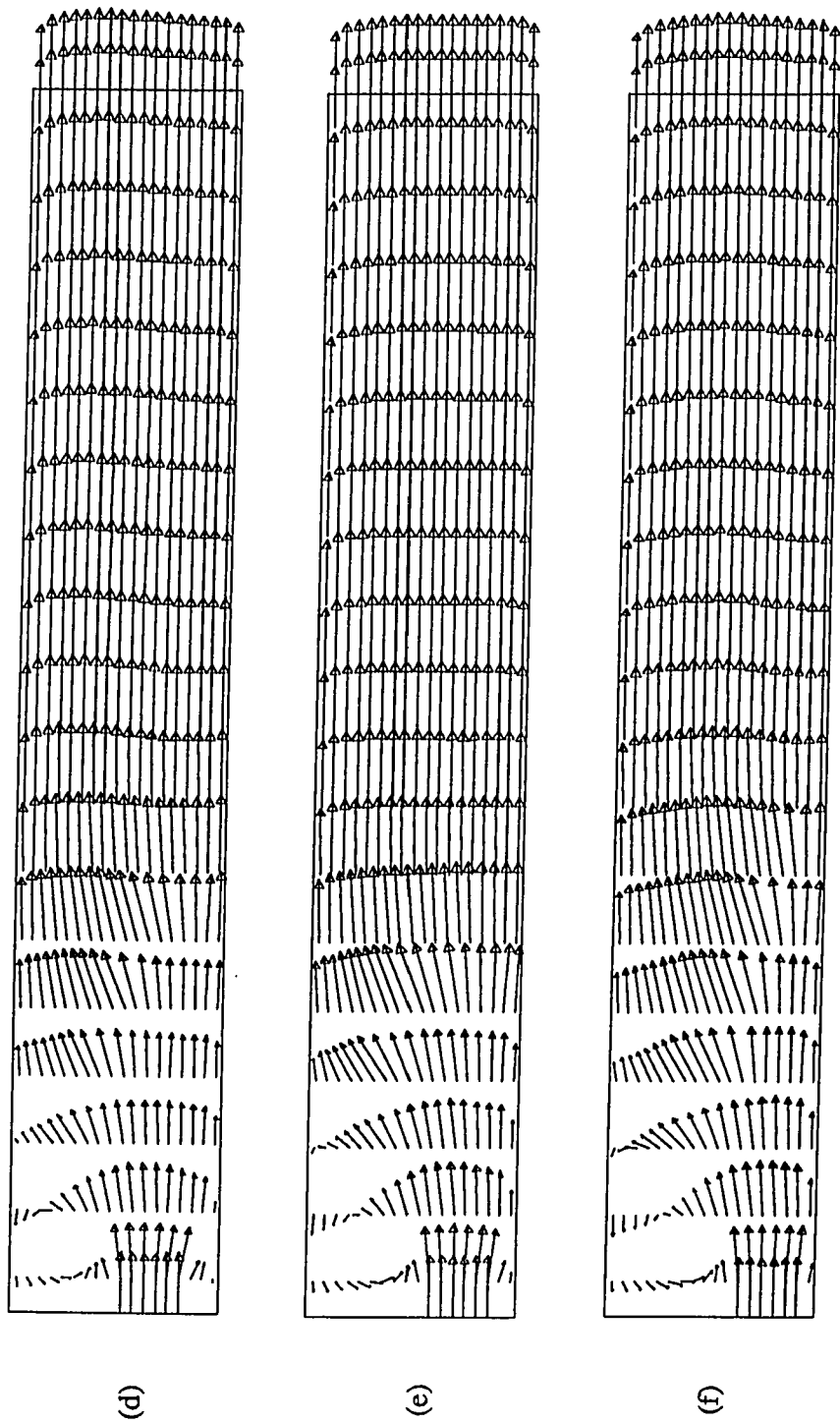
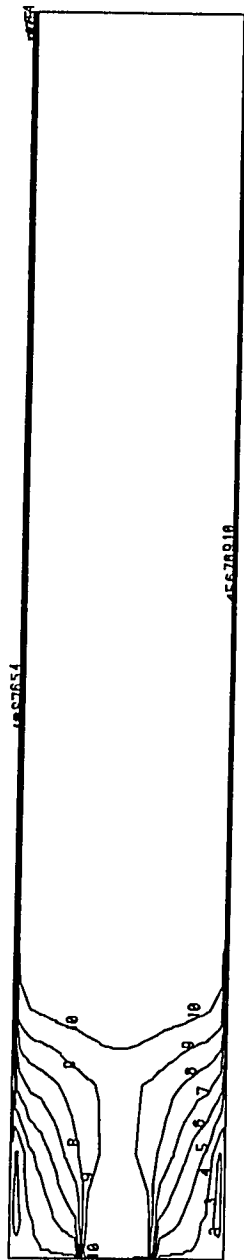


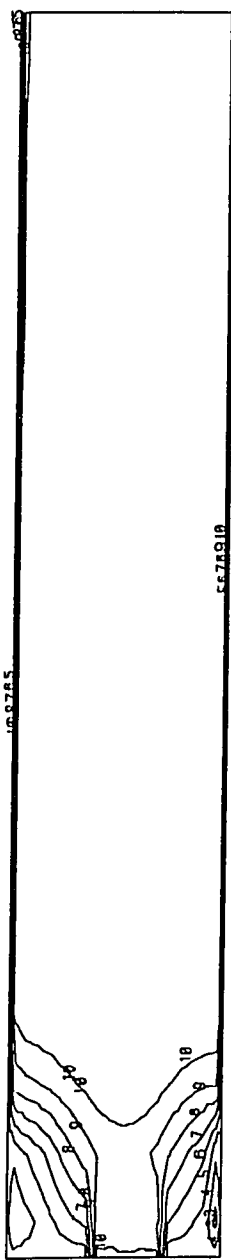
Figure 4.10.2 Predicted Gas Velocity Vectors (d) case 4 (e) case 5 (f) case 6.

3 -4.78891E+00
4 7.83035E+01
5 6.31811E+00
6 1.18727E+01
7 1.74273E+01
8 2.28815E+01
9 2.85364E+01
10 3.48808E+01



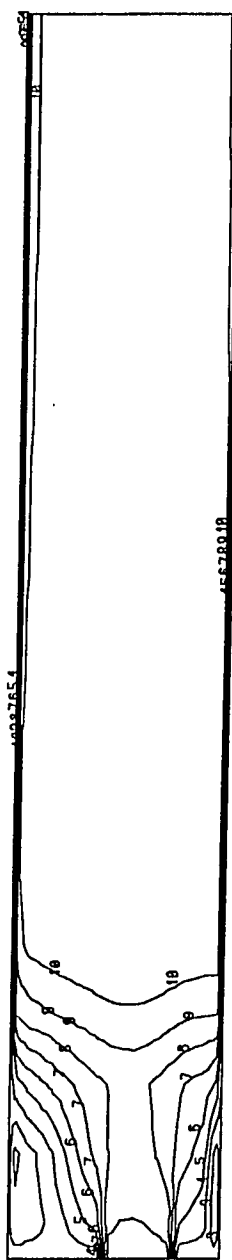
(a)

3 -7.81818E+00
4 -1.92727E+00
5 3.95364E+00
6 9.85455E+00
7 1.57455E+01
8 2.18364E+01
9 2.75273E+01
10 3.34182E+01



(b)

3 -2.18182E+00
4 3.52727E+00
5 9.23635E+00
6 1.49455E+01
7 2.06545E+01
8 2.63635E+01
9 3.20727E+01
10 3.77818E+01



(c)

Figure 4.11.1 Predicted Contours of Gas Velocity in X-Direction (a) case 1 (b) case 2 (c) case 3.

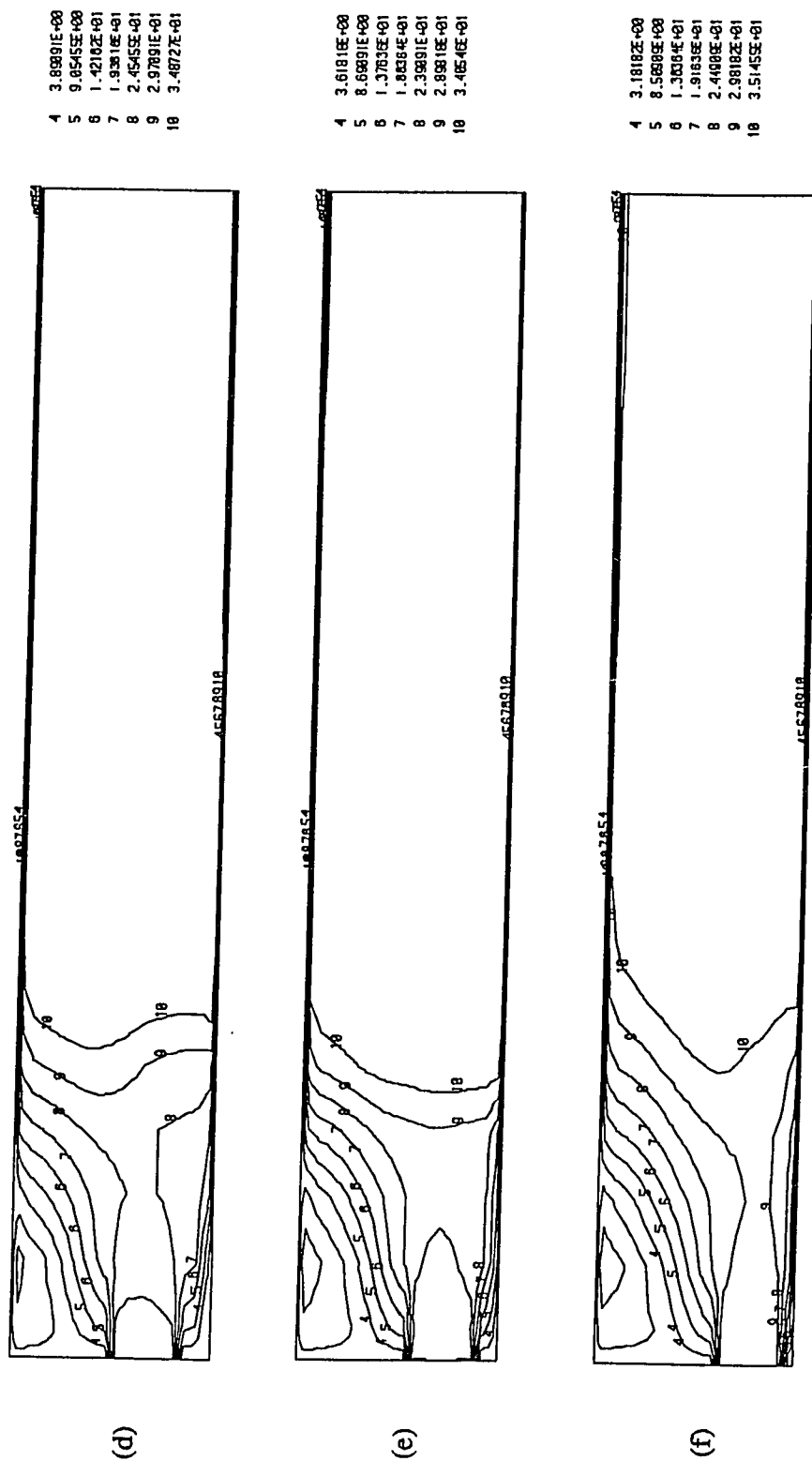
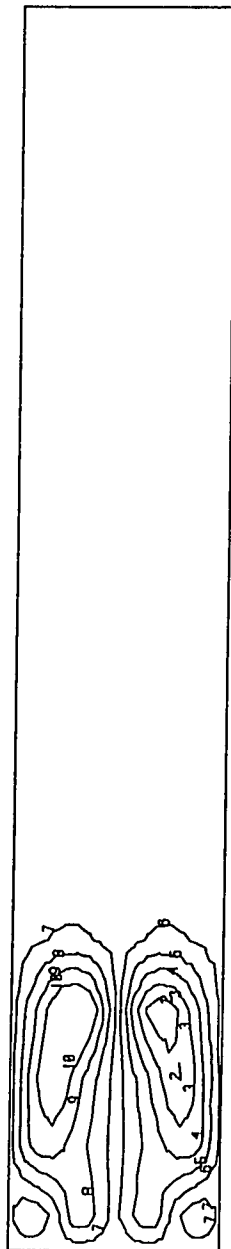


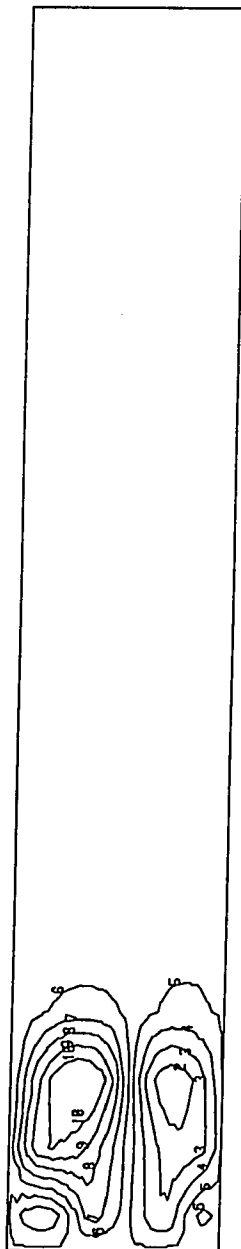
Figure 4.11.2 Predicted Contours of Gas Velocity in X-Direction (d) case 4 (e) case 5 (f) case 6.

2 -8.4628E+00
3 -5.0205E+00
4 -3.5394E+00
5 -2.1542E+00
6 -7.1869E-01
7 7.1869E-01
8 2.1542E+00
9 3.5394E+00
10 5.0205E+00



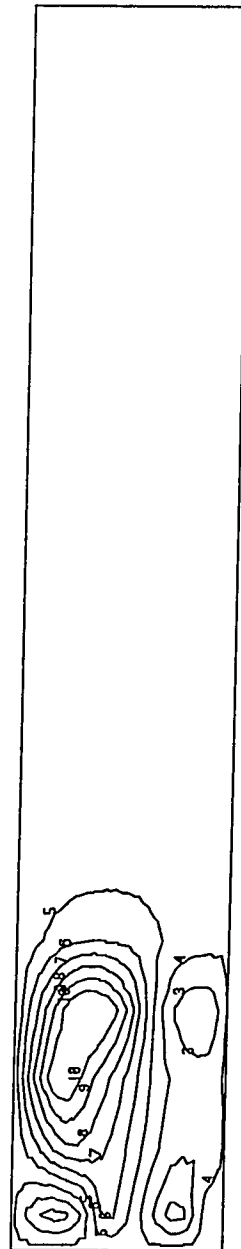
(a)

2 -5.0810E+00
3 -3.4638E+00
4 -1.8458E+00
5 -2.2788E-01
6 1.3918E+00
7 3.0688E+00
8 4.6278E+00
9 6.2458E+00
10 7.8638E+00



(b)

3 -1.8206E+00
4 -3.9845E-01
5 1.0457E+00
6 2.4819E+00
7 3.9188E+00
8 5.3542E+00
9 6.7904E+00
10 8.2265E+00



(c)

Figure 4.12.1 Predicted Contours of Gas Velocity in Y-Direction (a) case 1 (b) case 2 (c) case 3.

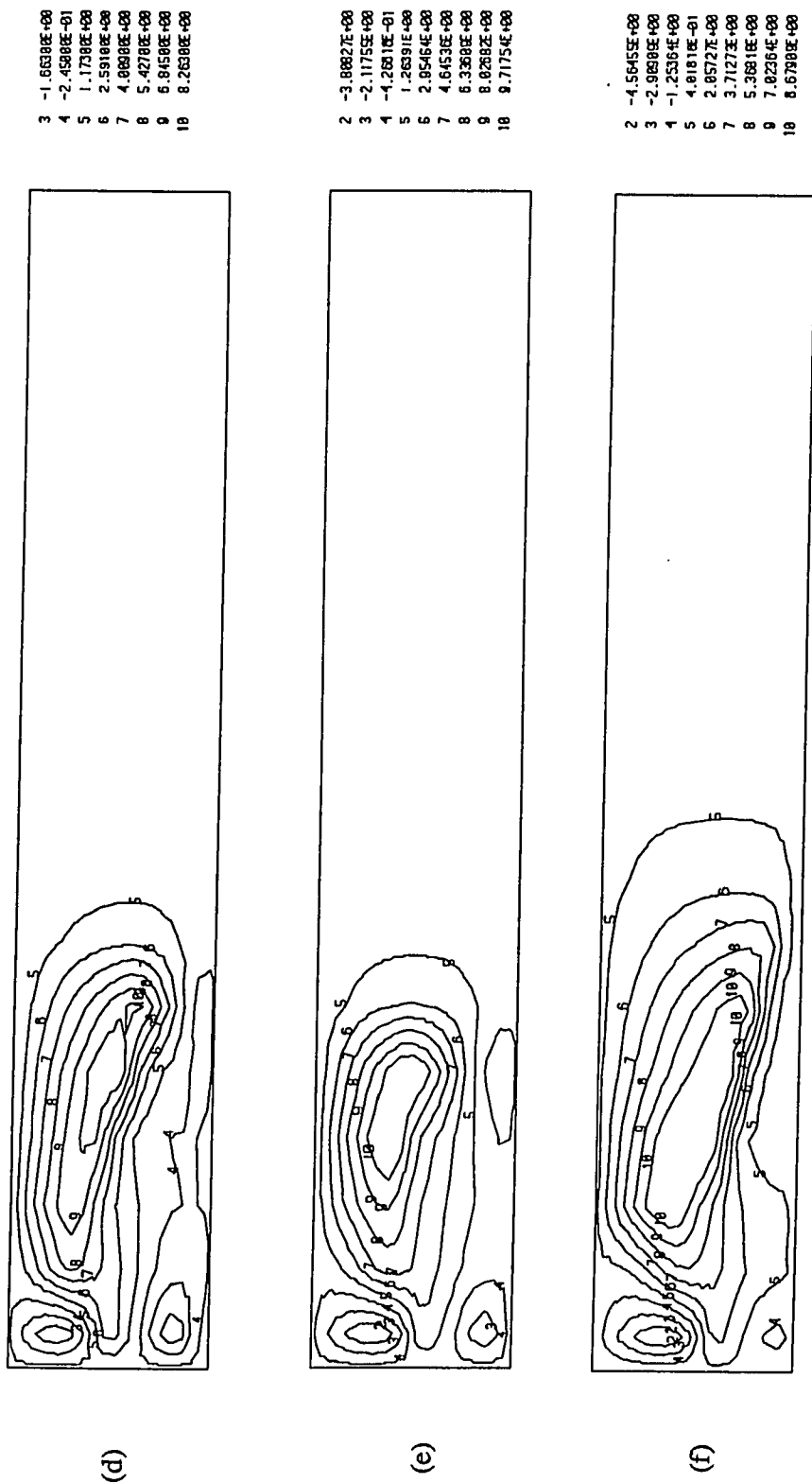


Figure 4.12.2 Predicted Contours of Gas Velocity in Y-Direction (d) case 4 (e) case 5 (f) case 6.

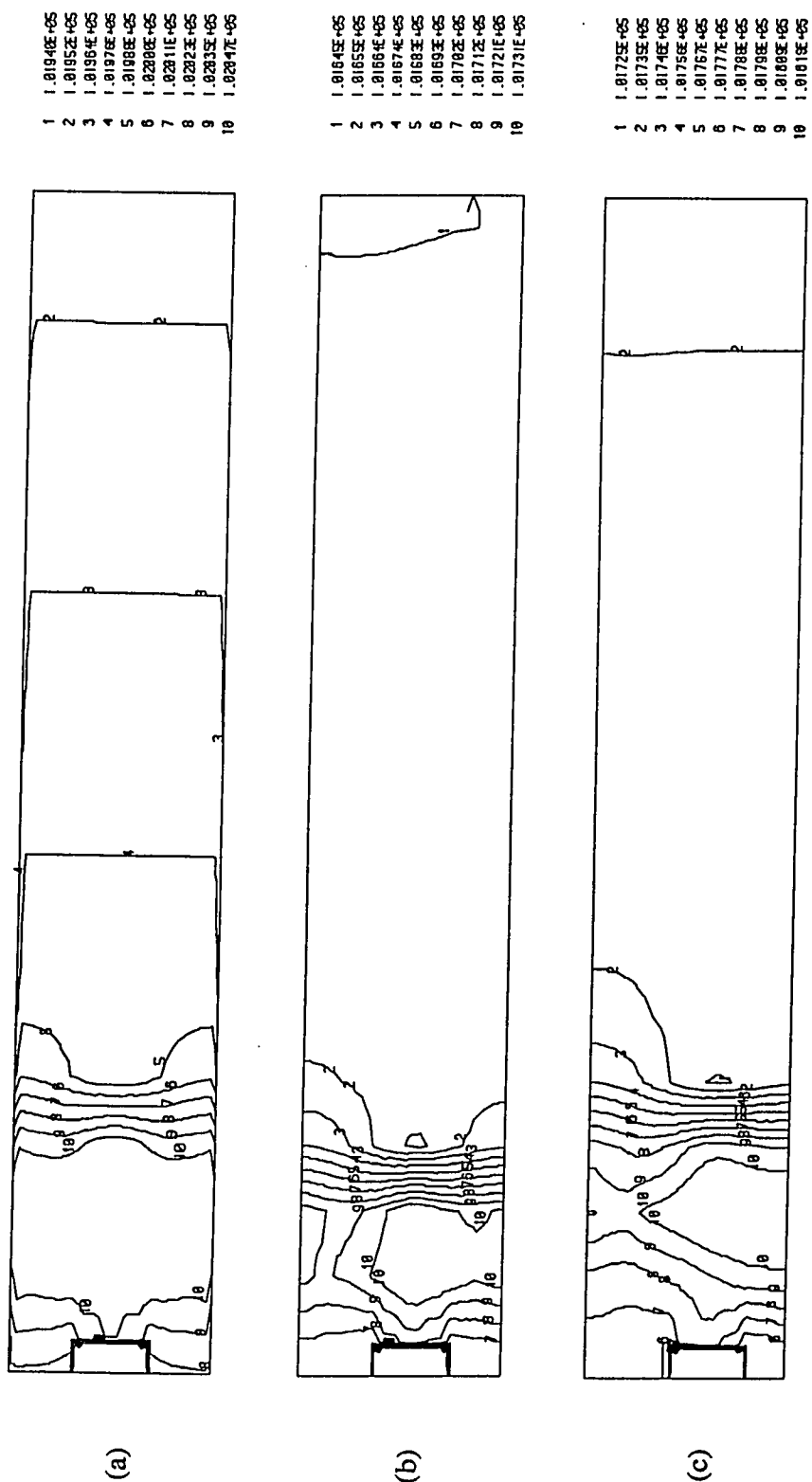


Figure 4.13.1 Predicted Contours of Pressure (a) case 1 (b) case 2 (c) case 3.

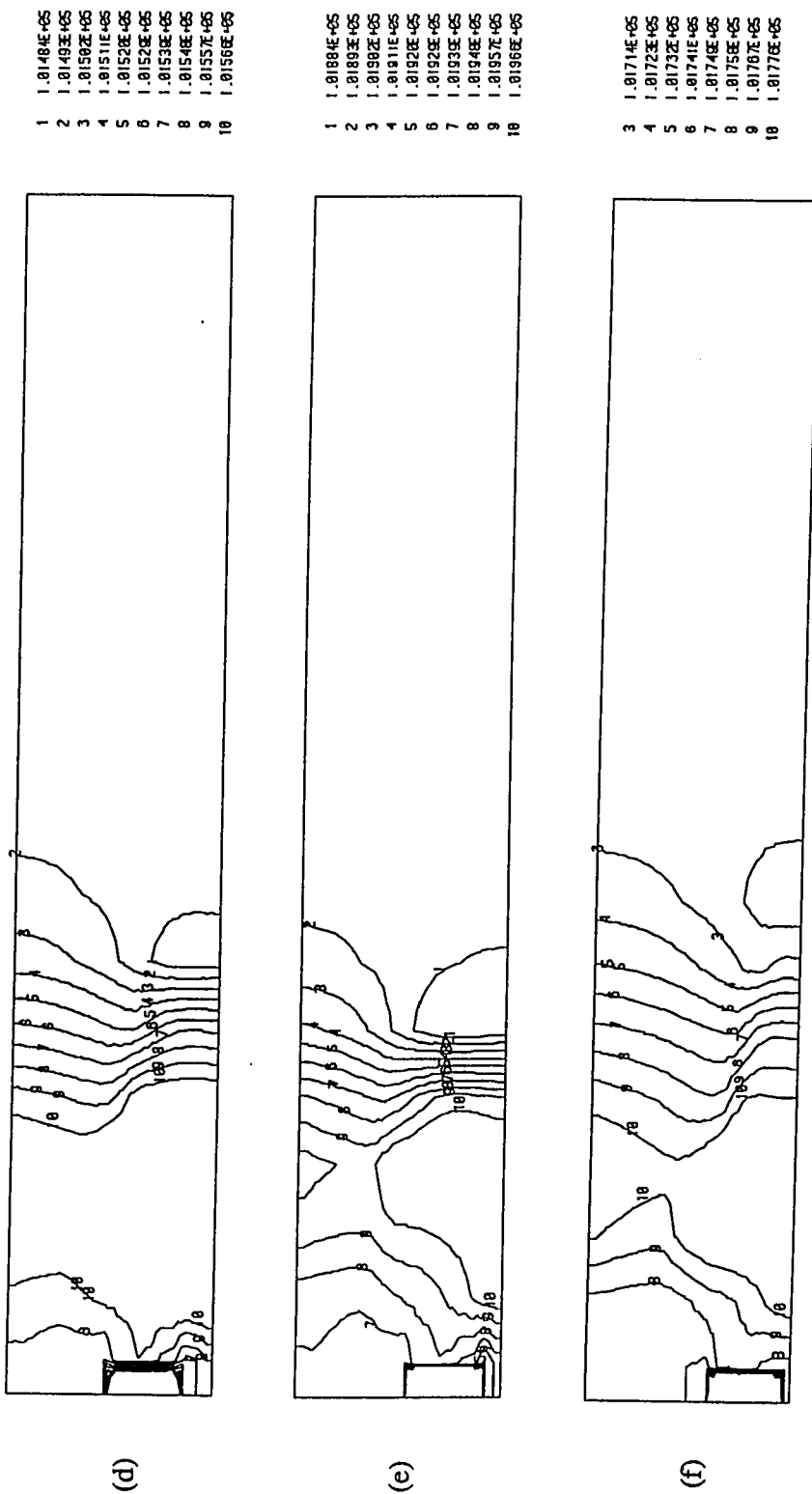


Figure 4.13.2 Predicted Contours of Pressure (d) case 4 (e) case 5 (f) case 6.

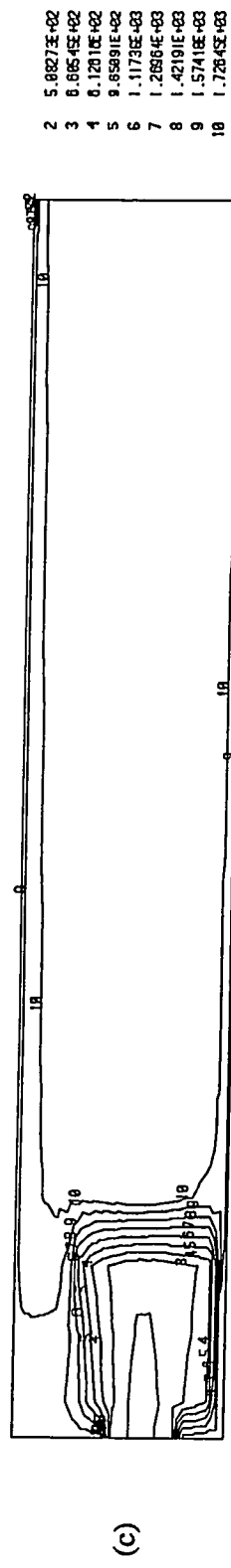
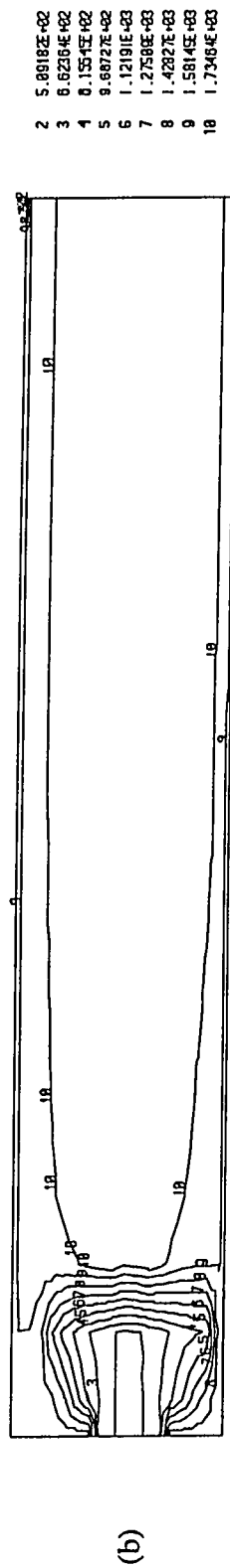
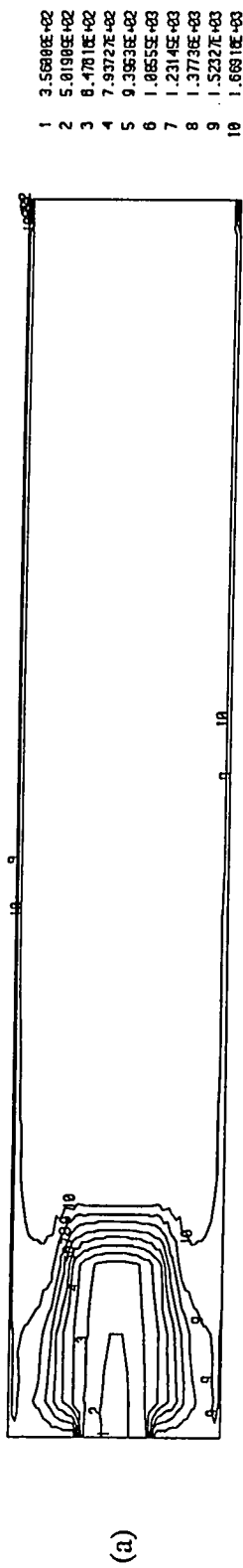


Figure 4.14.1 Predicted Contours of Temperature (a) case 1 (b) case 2 (c) case 3.

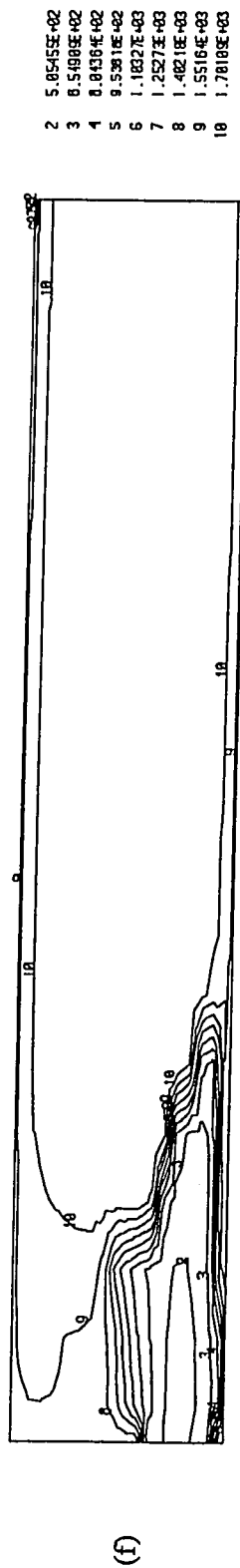
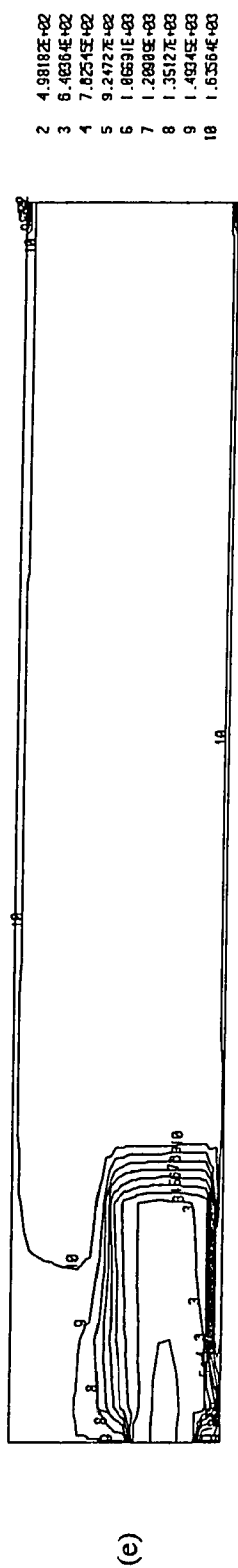
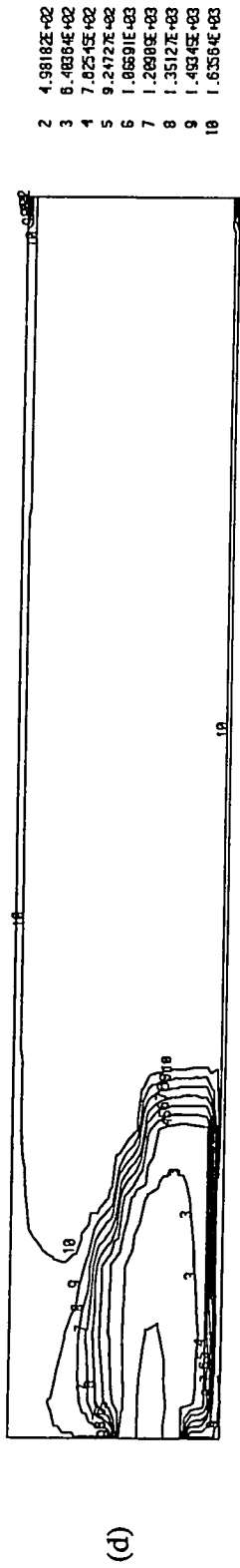


Figure 4.14.2 Predicted Contours of Temperature (d) case 4 (e) case 5 (f) case 6.

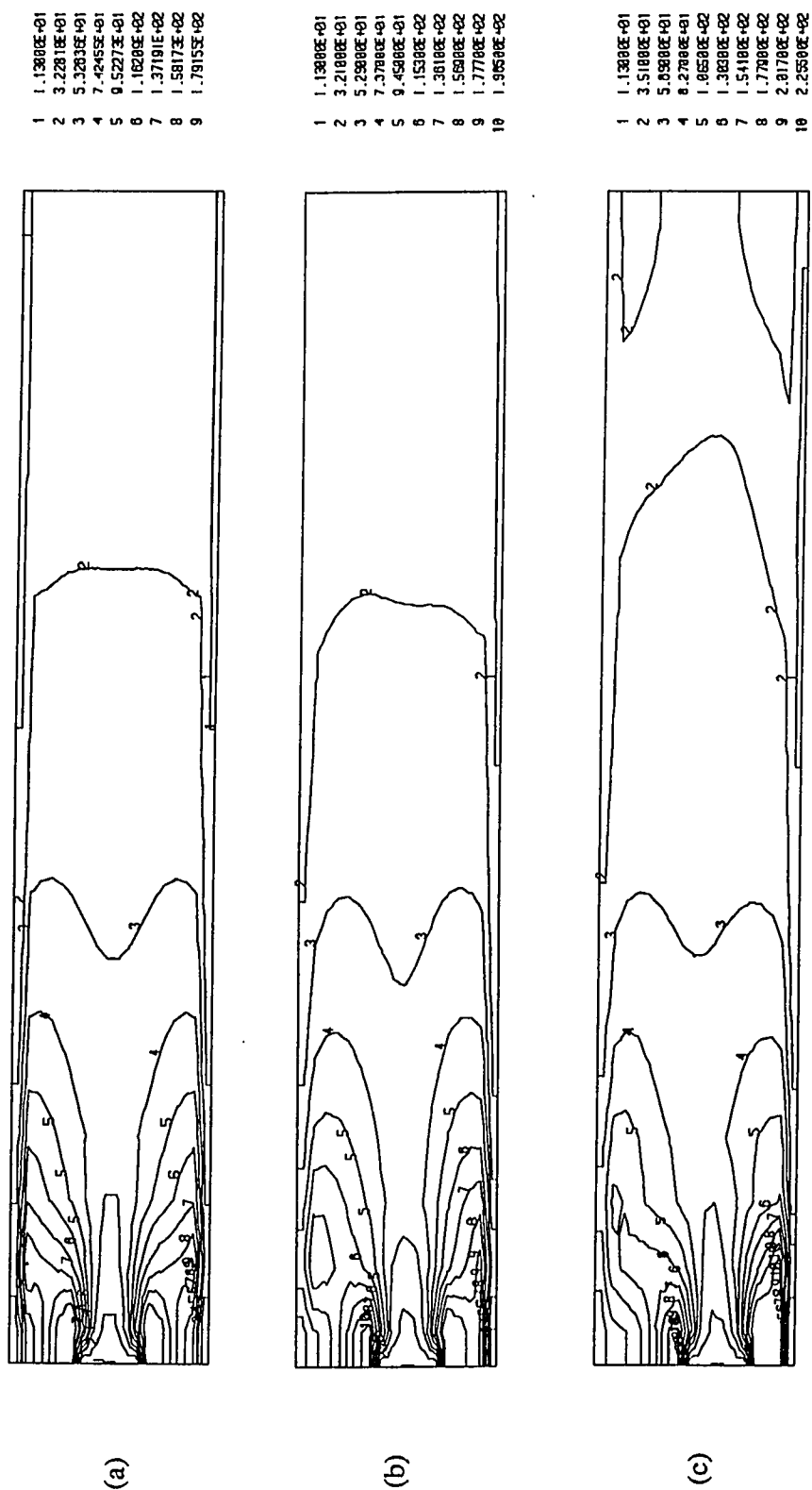


Figure 4.15.1 Predicted Contours of Turbulence Kinetic Energy (a) case 1 (b) case 2 (c) case 3.

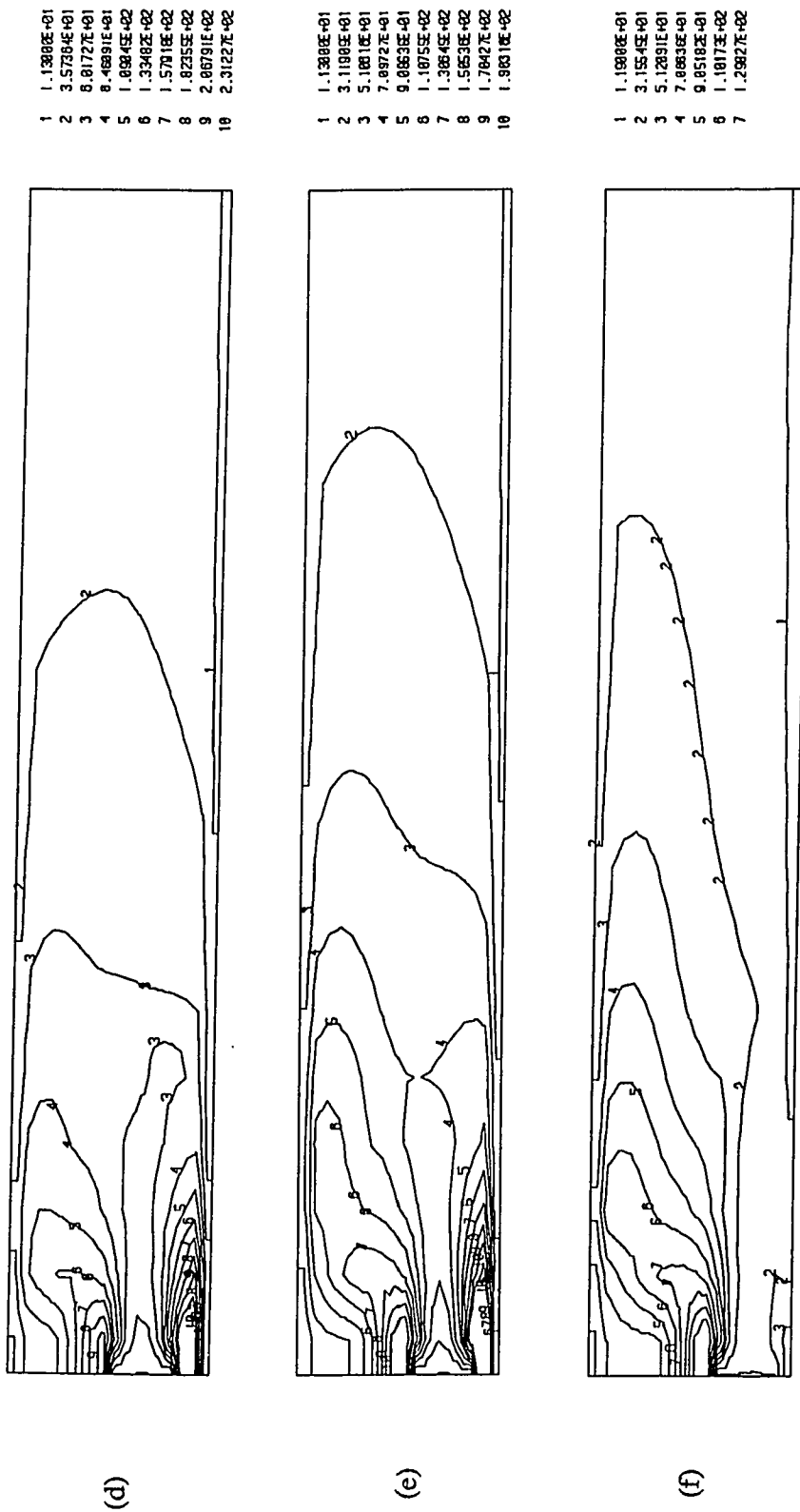


Figure 4.15.2 Predicted Contours of Turbulence Kinetic Energy (d) case 4 (e) case 5 (f) case 6.

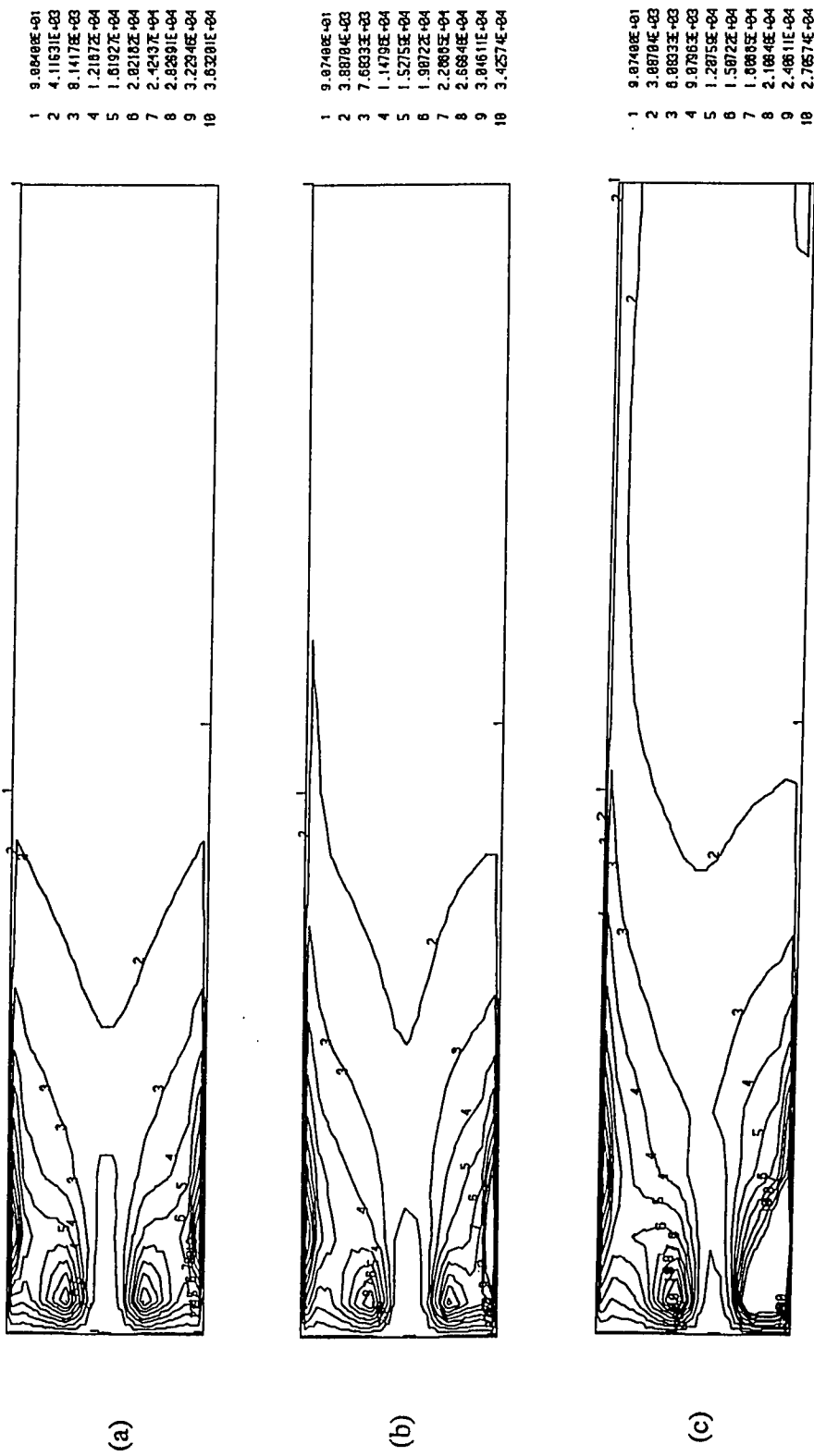


Figure 4.16.1 Predicted Contours of Turbulence Dissipation Rate (a) case 1 (b) case 2 (c) case 3.



Figure 4.16.2 Predicted Contours of Turbulence Dissipation Rate (d) case 4 (e) case 5 (f) case 6.

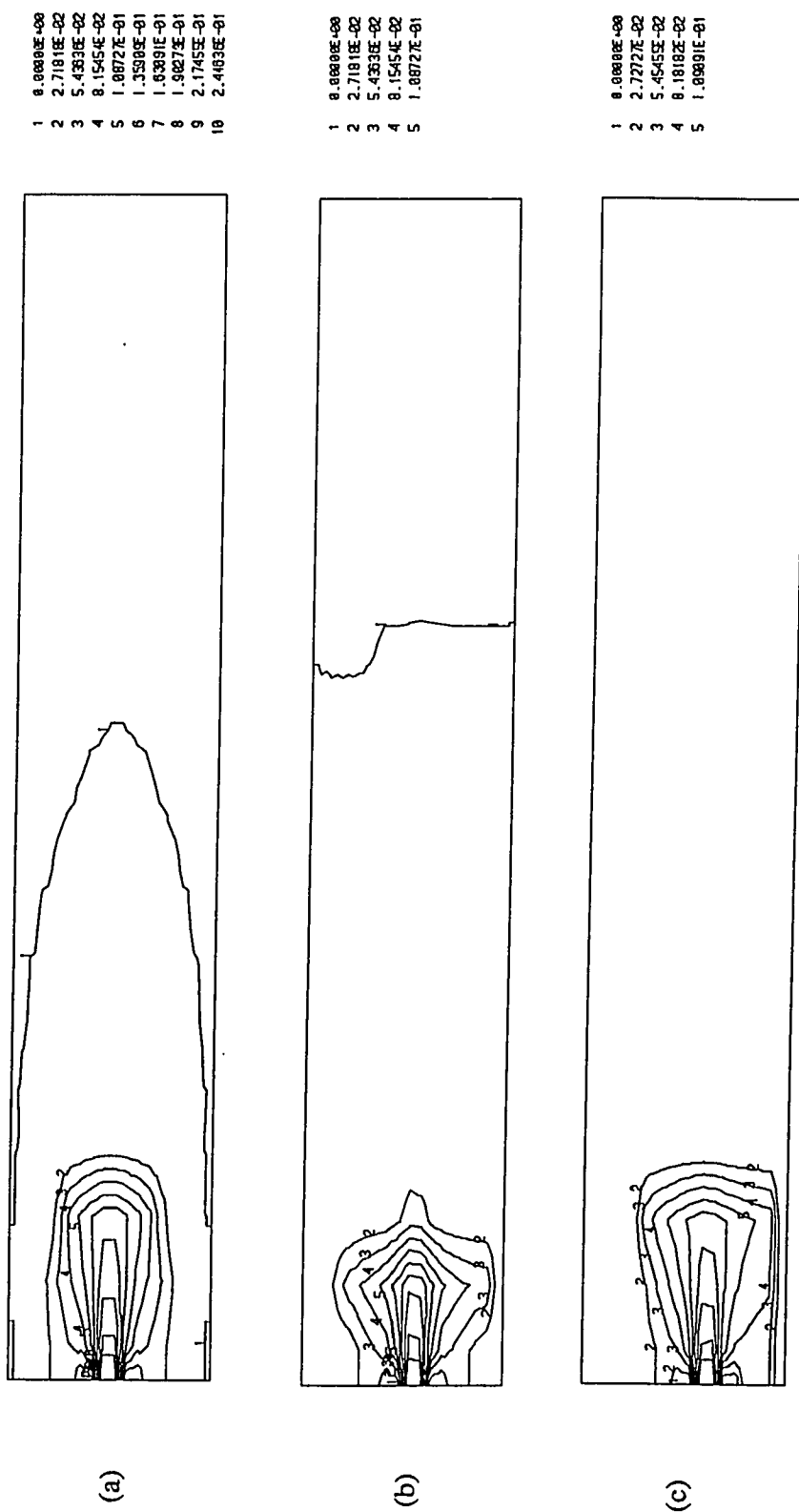


Figure 4.17.1 Predicted Contours of CO Concentration (a) case 1 (b) case 2 (c) case 3.

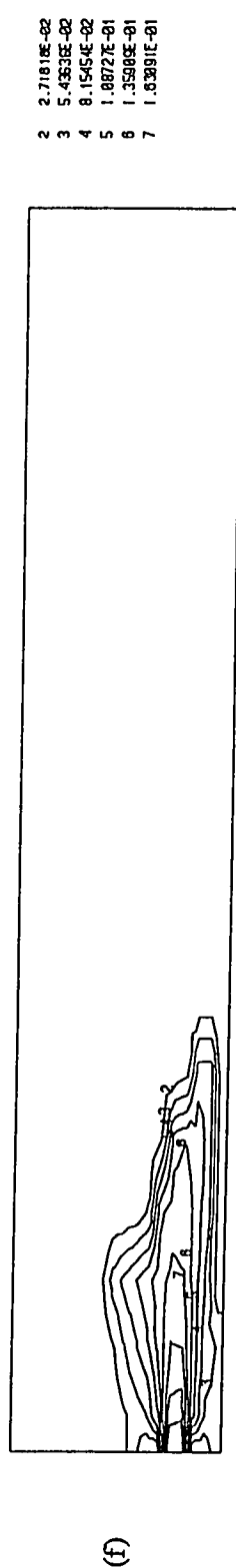
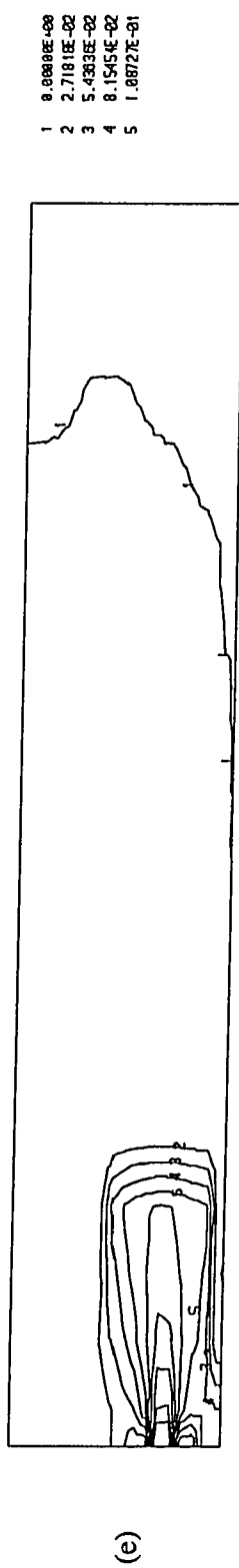
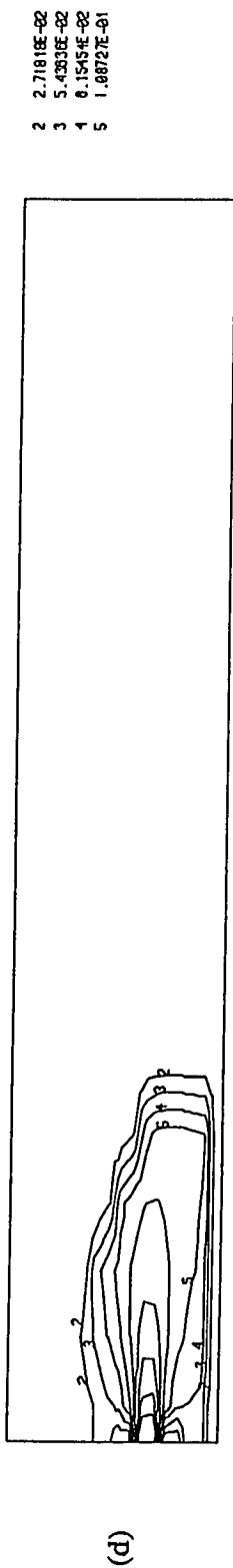


Figure 4.17.2 Predicted Contours of CO Concentration (d) case 4 (e) case 5 (f) case 6.

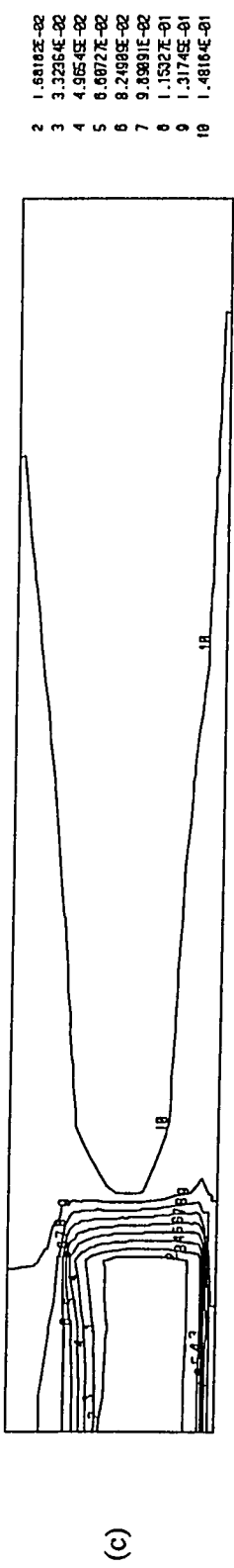
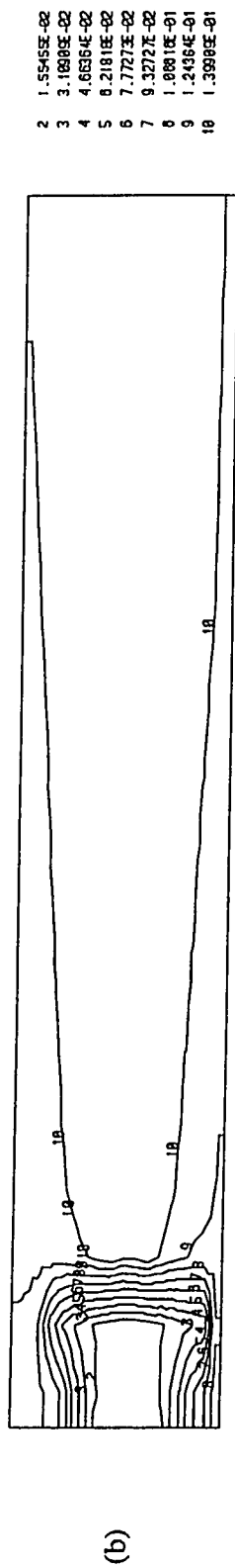
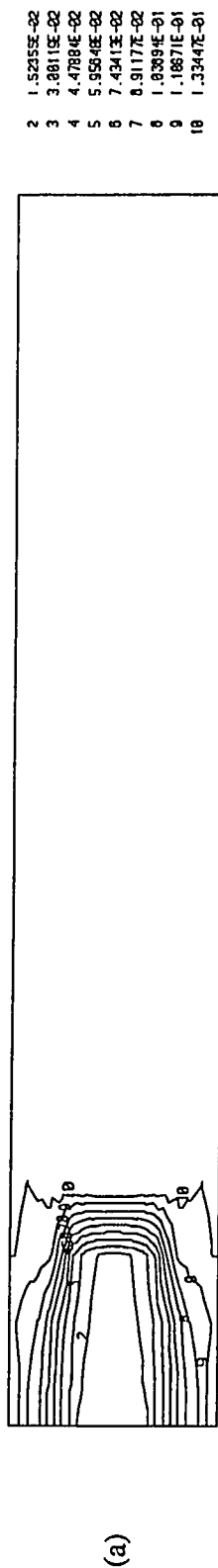


Figure 4.18.1 Predicted Contours of CO₂ Concentration (a) case 1 (b) case 2 (c) case 3.

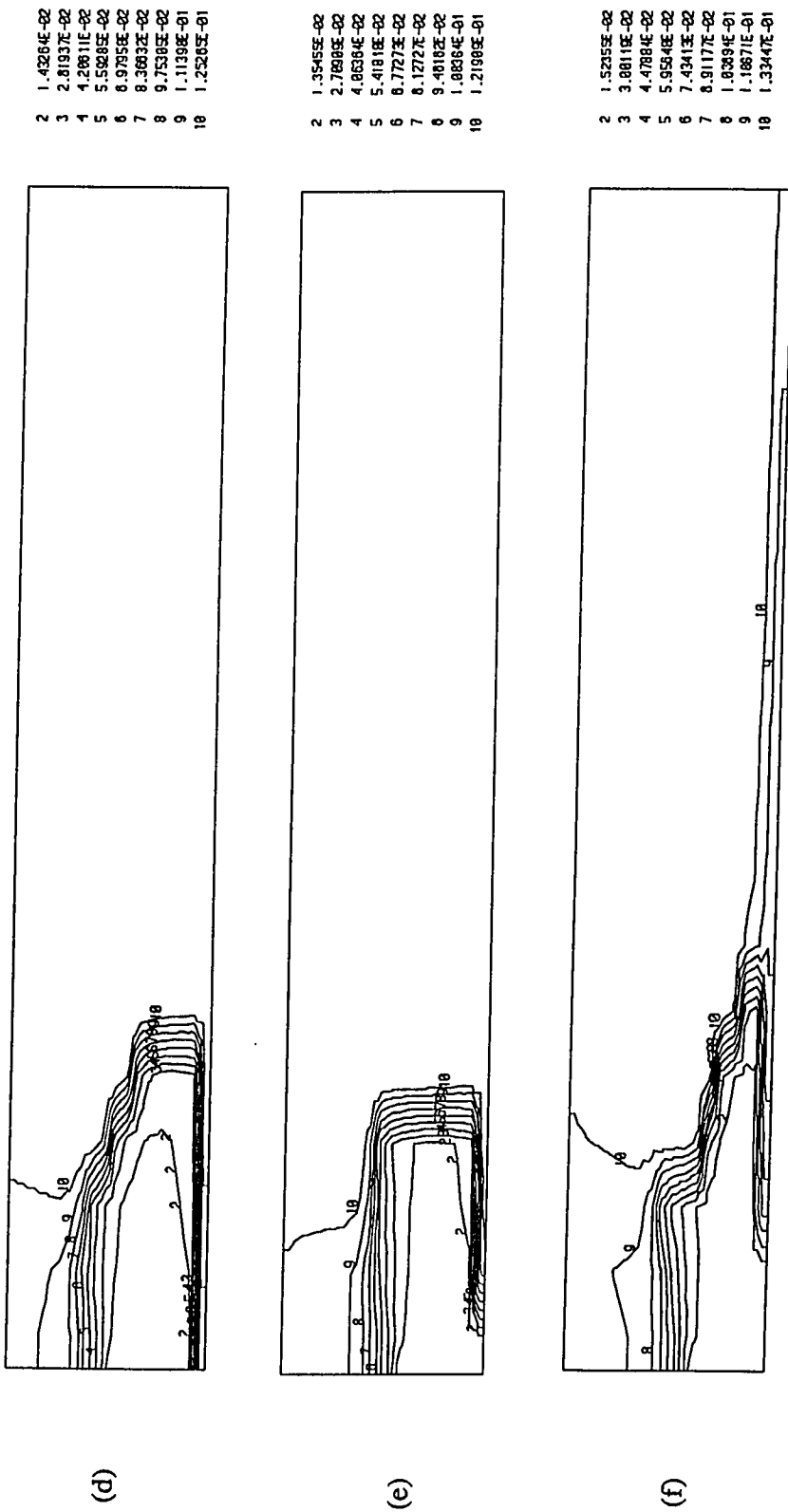


Figure 4.18.2 Predicted Contours of CO₂ Concentration (d) case 4 (e) case 5 (f) case 6.

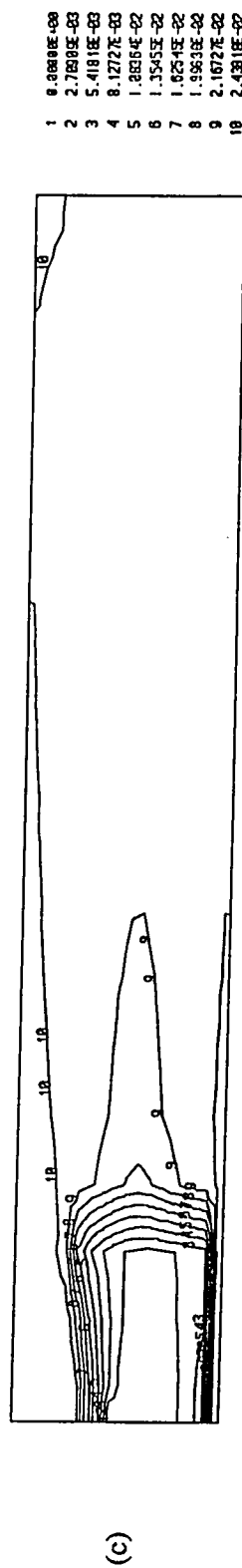
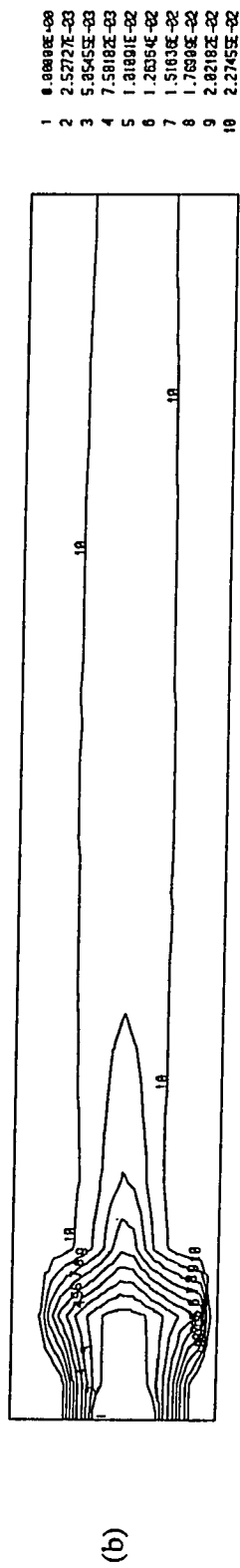
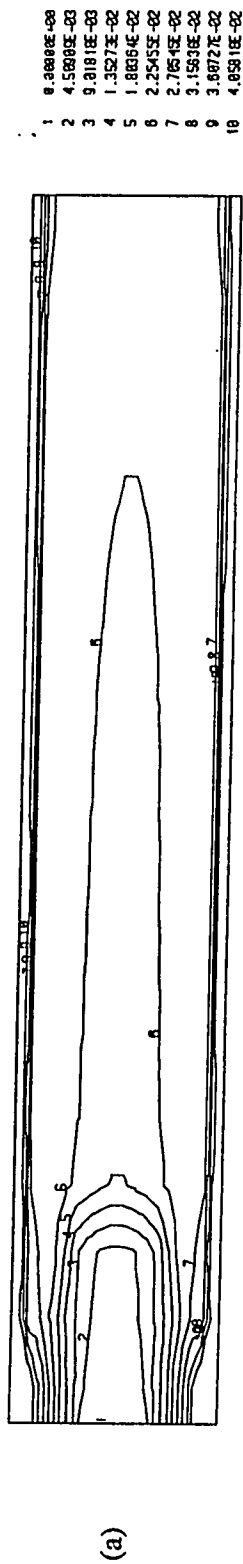


Figure 4.19.1 Predicted Contours of H_2O Concentration (a) case 1 (b) case 2 (c) case 3.

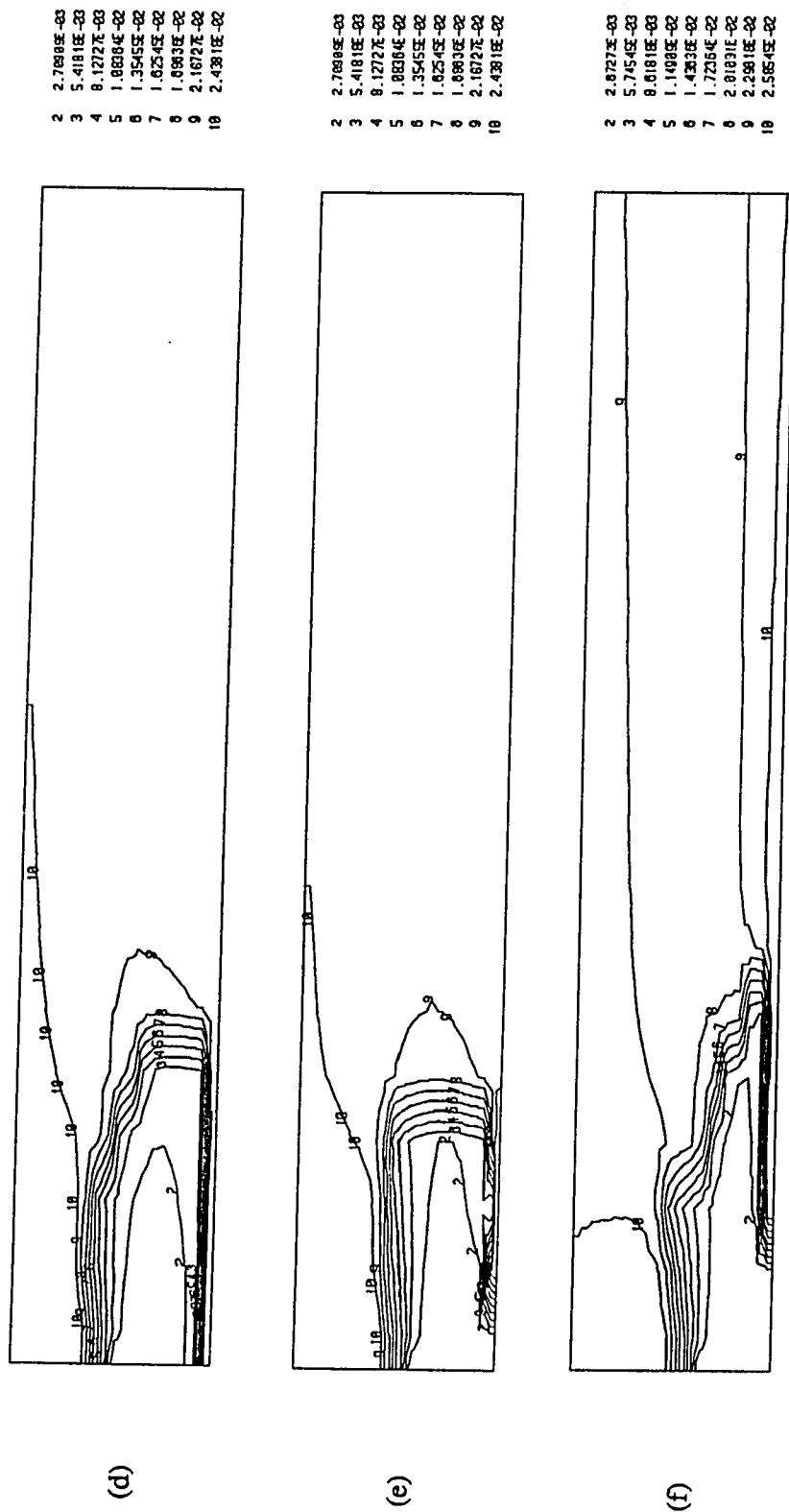


Figure 4.19.2 Predicted Contours of H_2O Concentration (d) case 4 (e) case 5 (f) case 6.

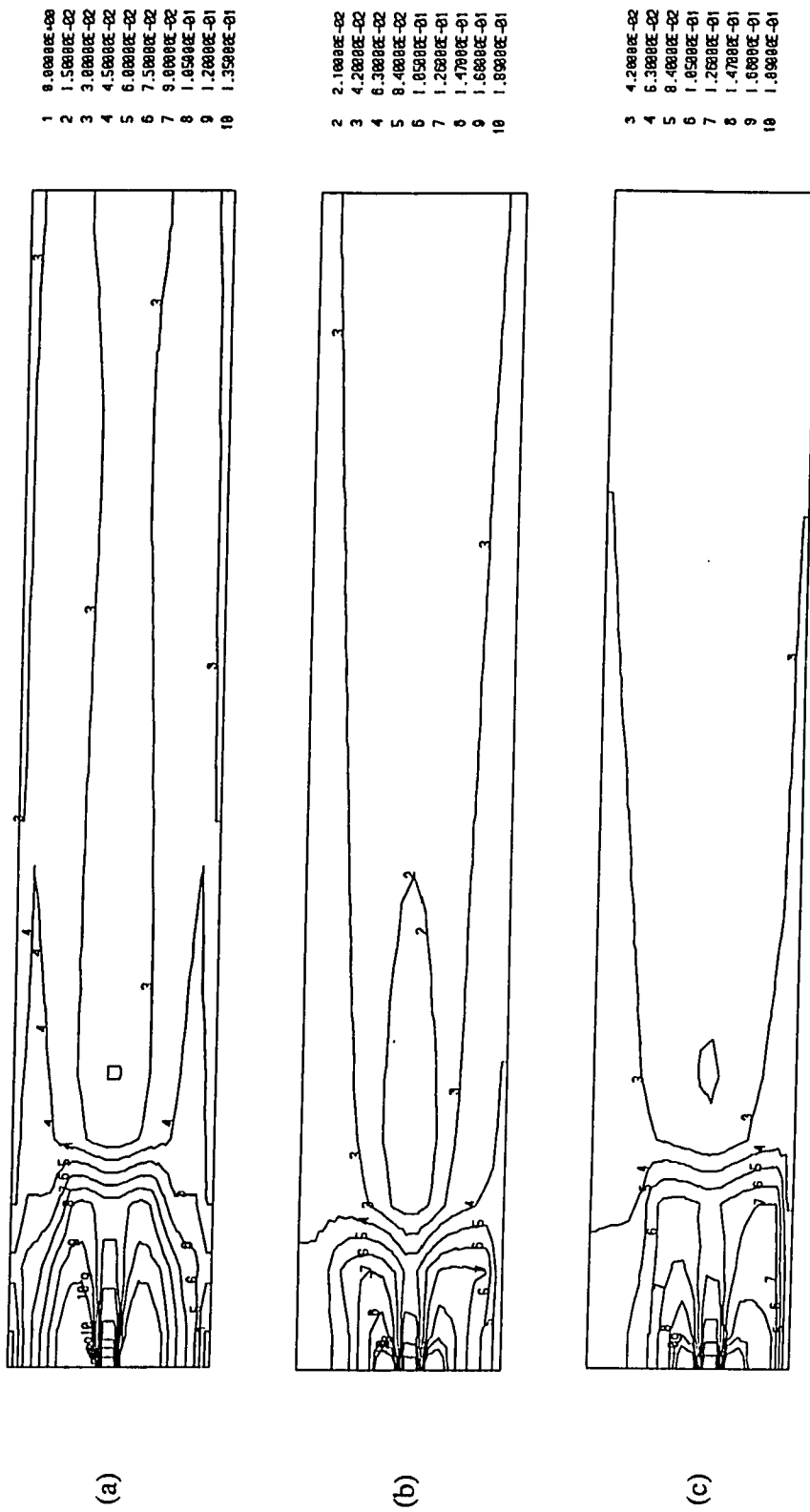


Figure 4.20.1 Predicted Contours of O₂ Concentration (a) case 1 (b) case 2 (c) case 3.

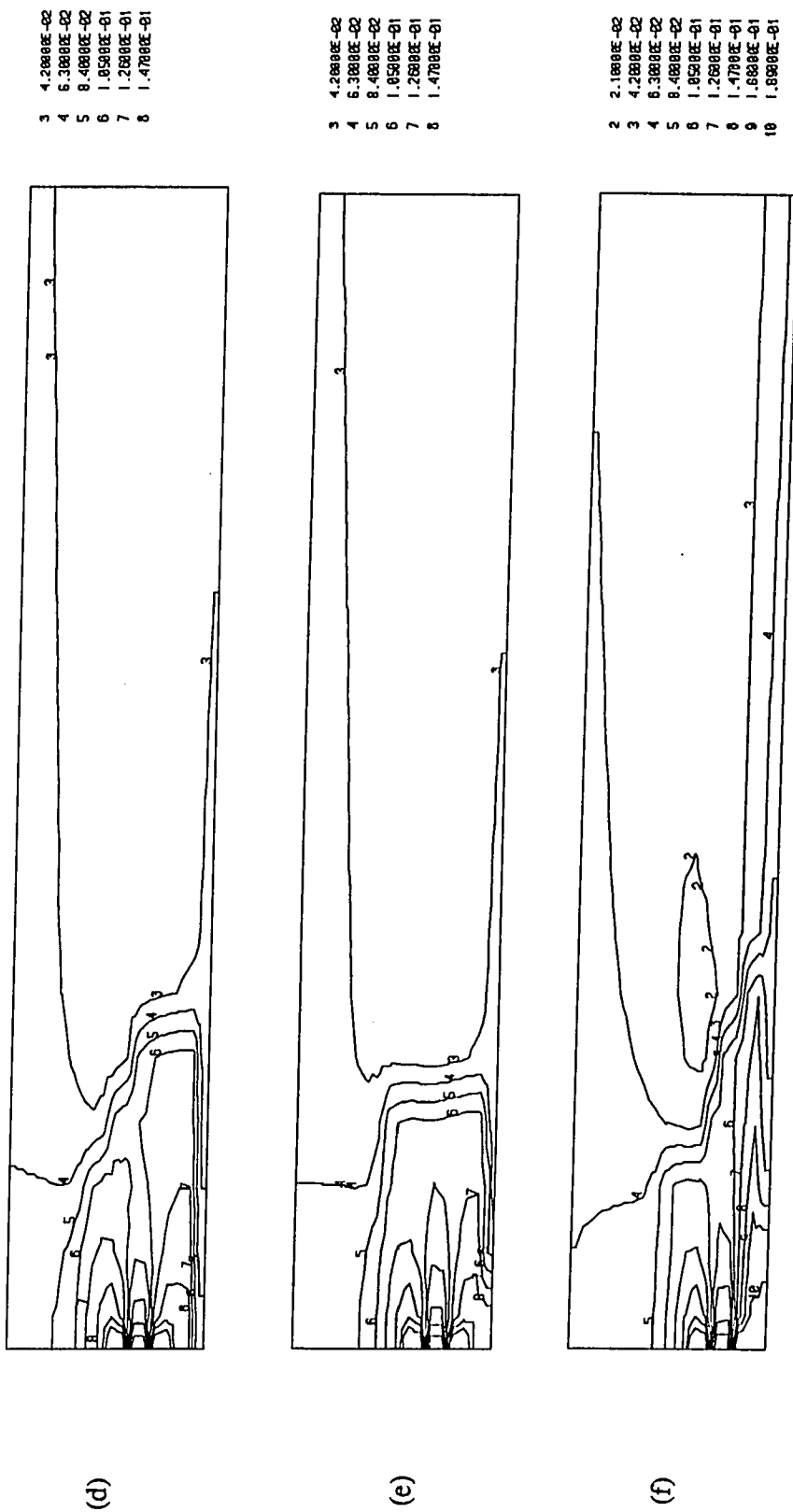


Figure 4.20.2 Predicted Contours of O₂ Concentration (d) case 4 (e) case 5 (f) case 6.

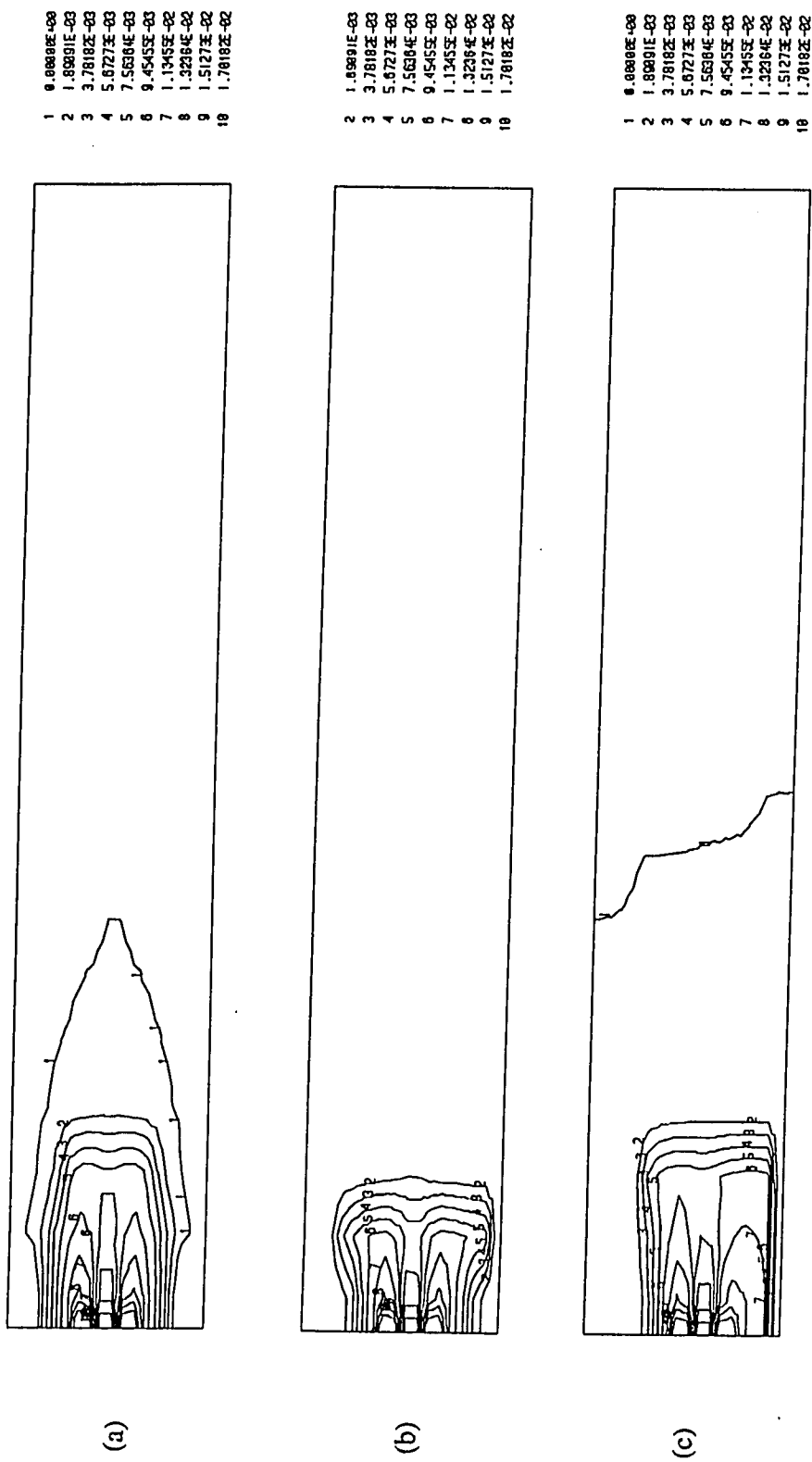


Figure 4.21.1 Predicted Contours of CH₄ Concentration (a) case 1 (b) case 2 (c) case 3.

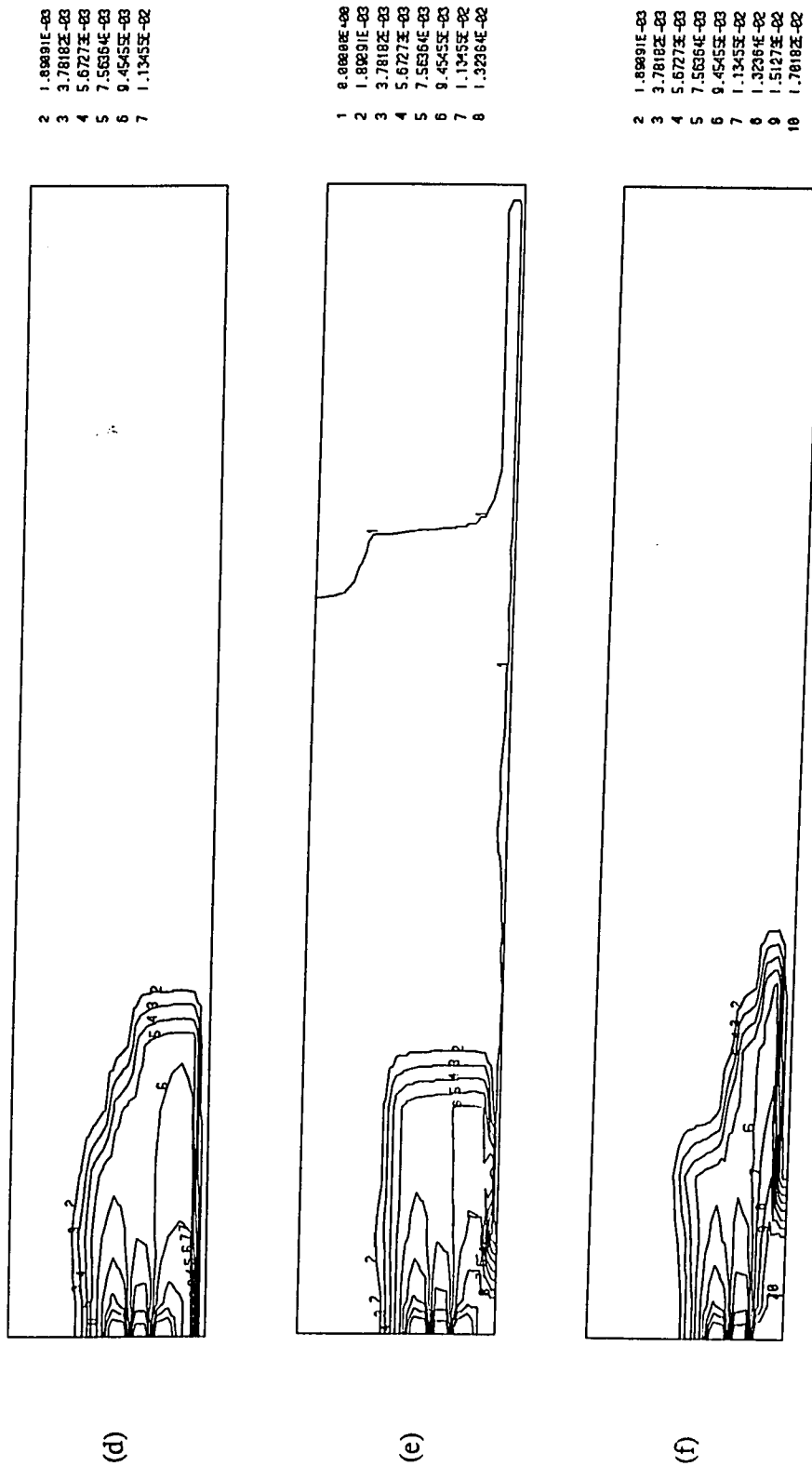


Figure 4.21.2 Predicted Contours of CH_4 Concentration (d) case 4 (e) case 5 (f) case 6.

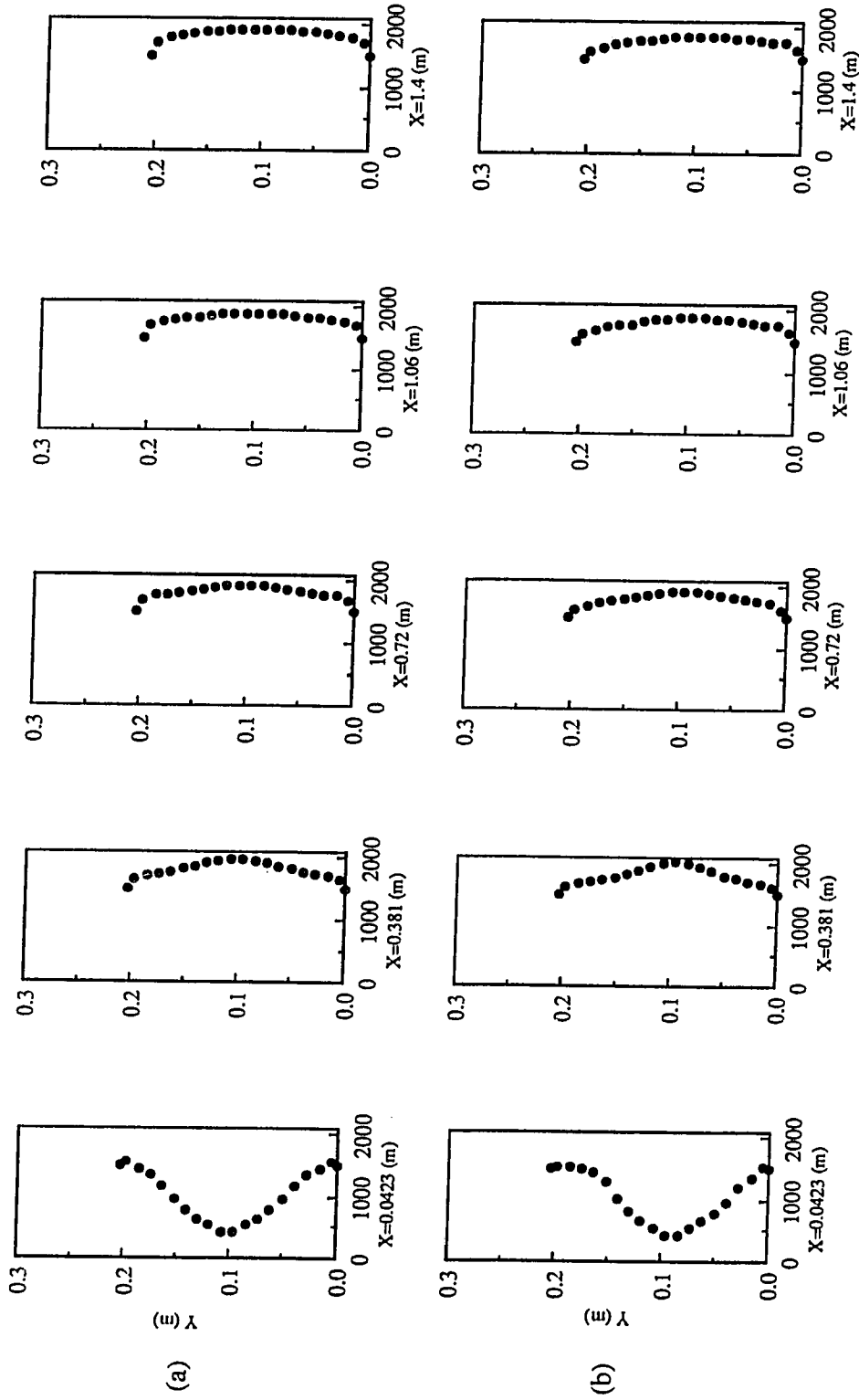


Figure 4.22.1 Predicted Cross-Section Profile of Gas Temperature at Five Different Locations (a) case 1 (b) case 2.

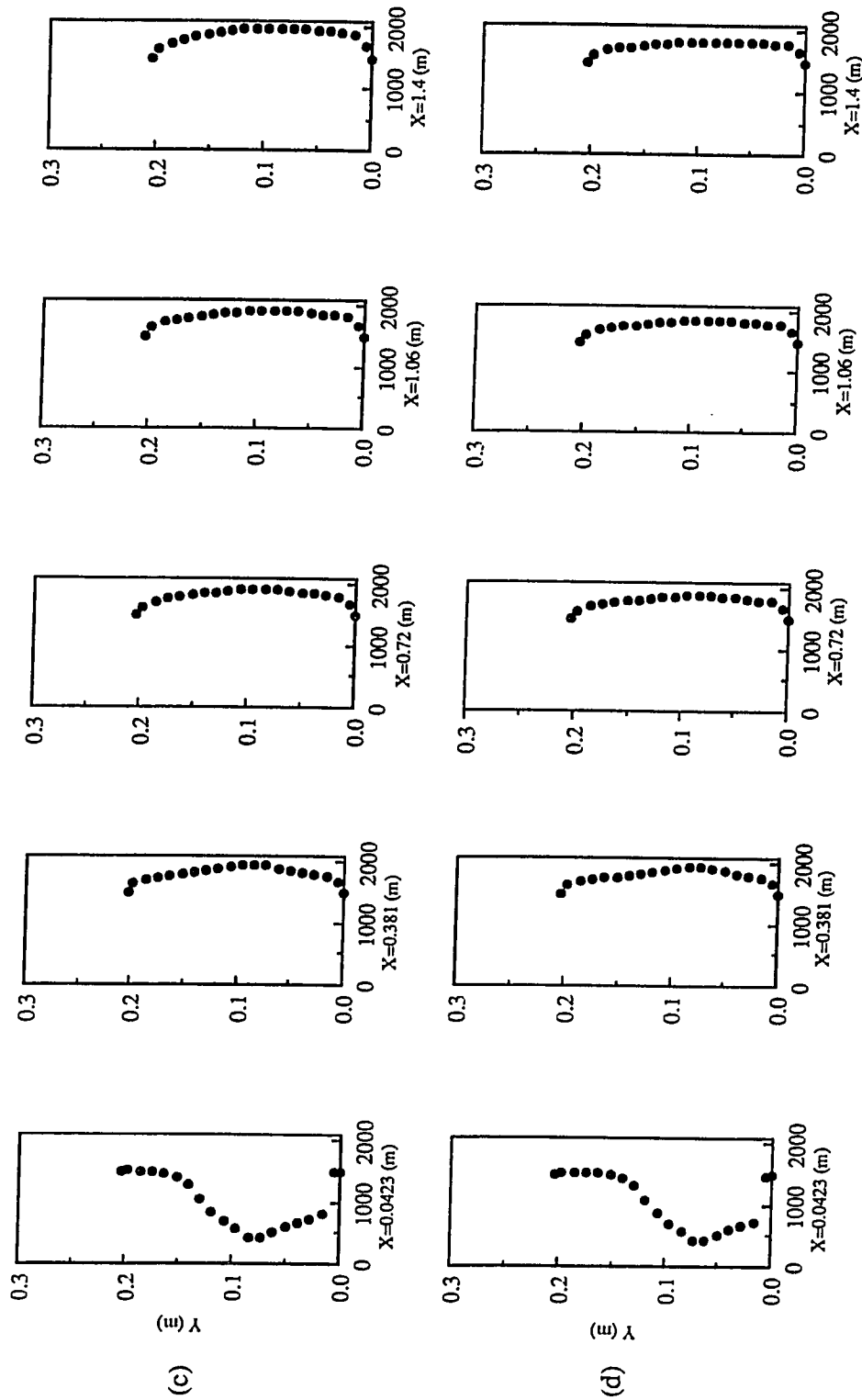


Figure 4.22.2 Predicted Cross-Section Profile of Gas Temperature at Five Different Locations (c) case 3 (d) case 4.

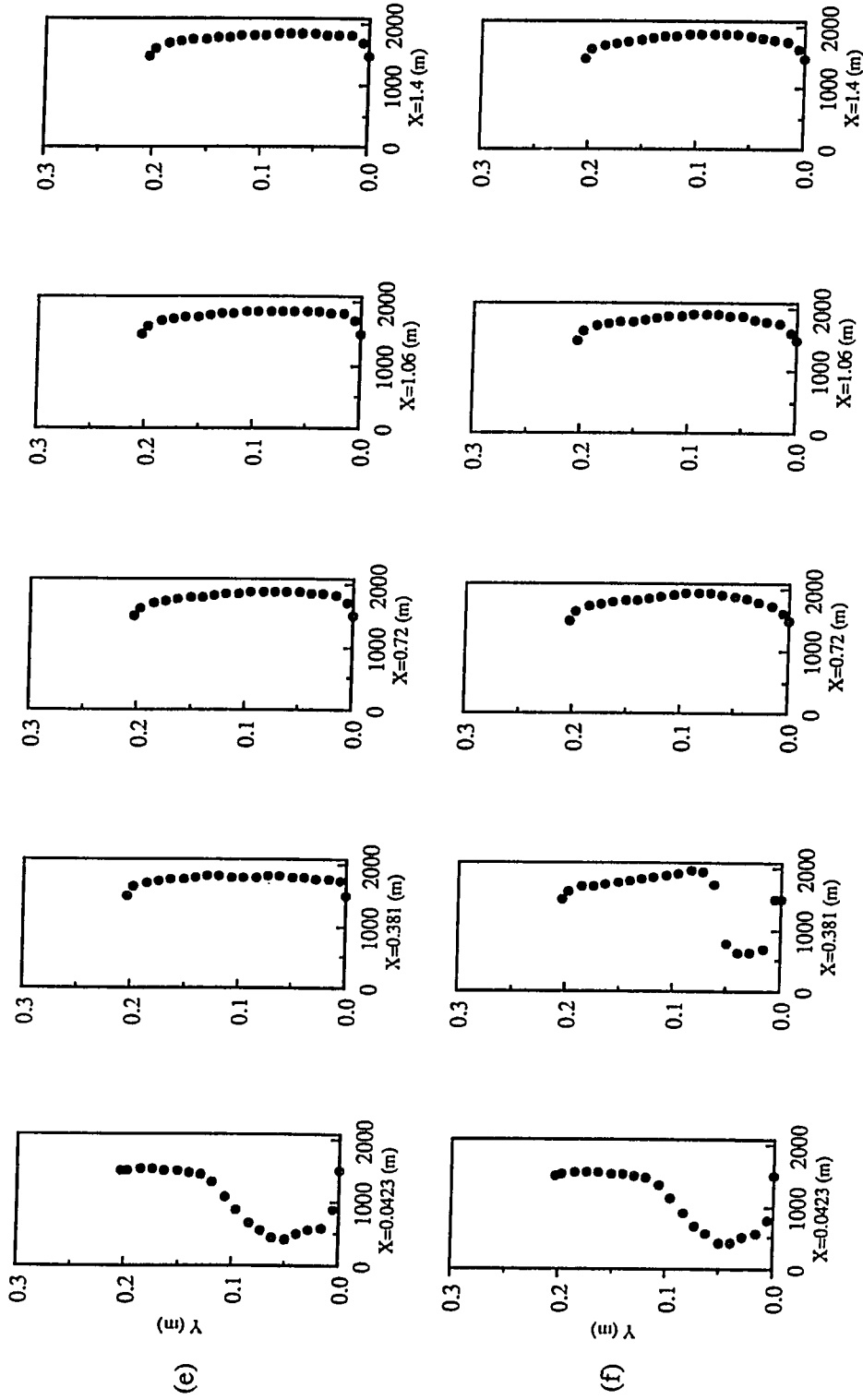


Figure 4.22.3 Predicted Cross-Section Profile of Gas Temperature at Five Different Locations (e) case 5 (f) case 6.

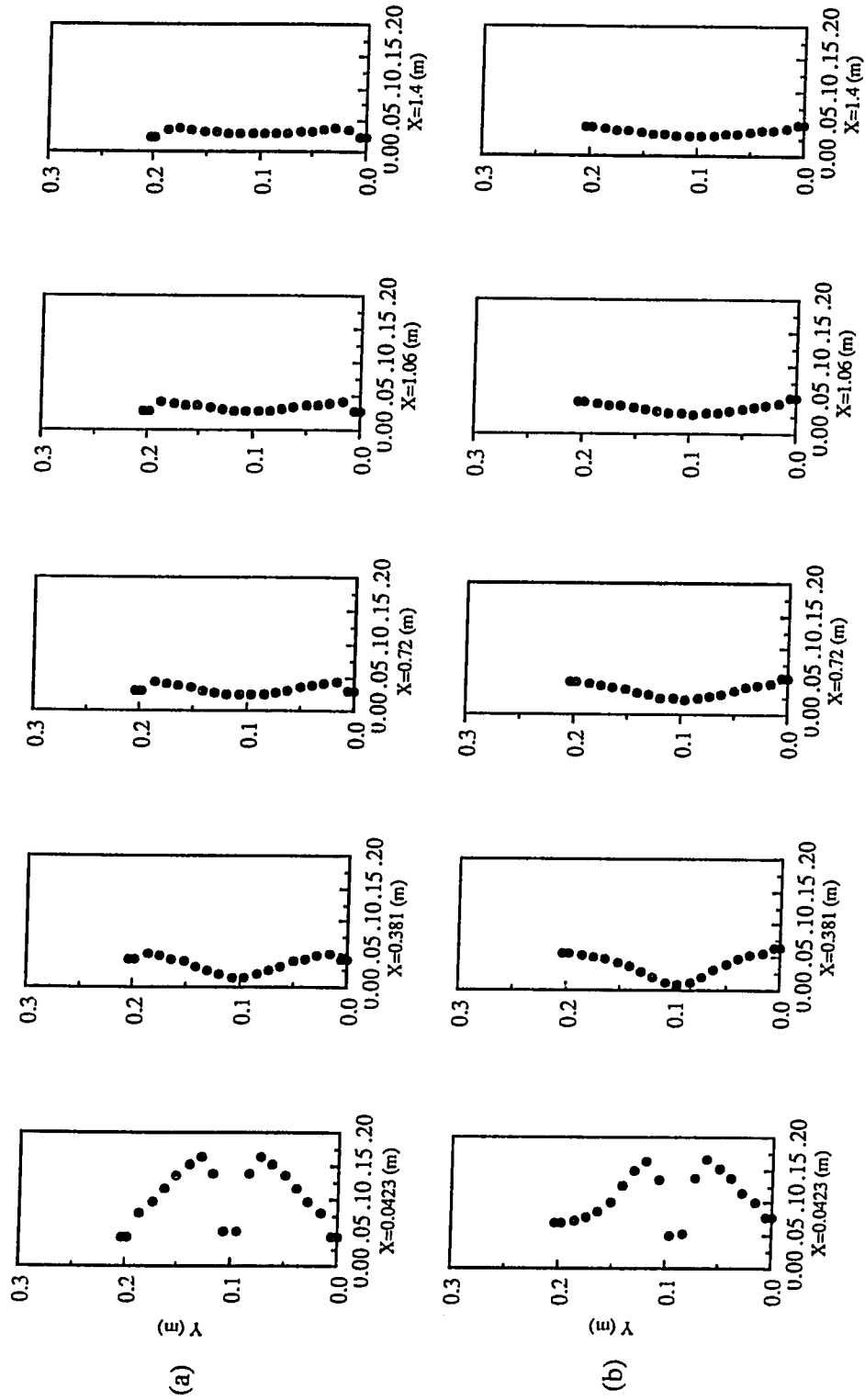


Figure 4.23.1 Predicted Cross-Section Profile of O_2 Concentration at Five Different Locations (a) case 1 (b) case 2.

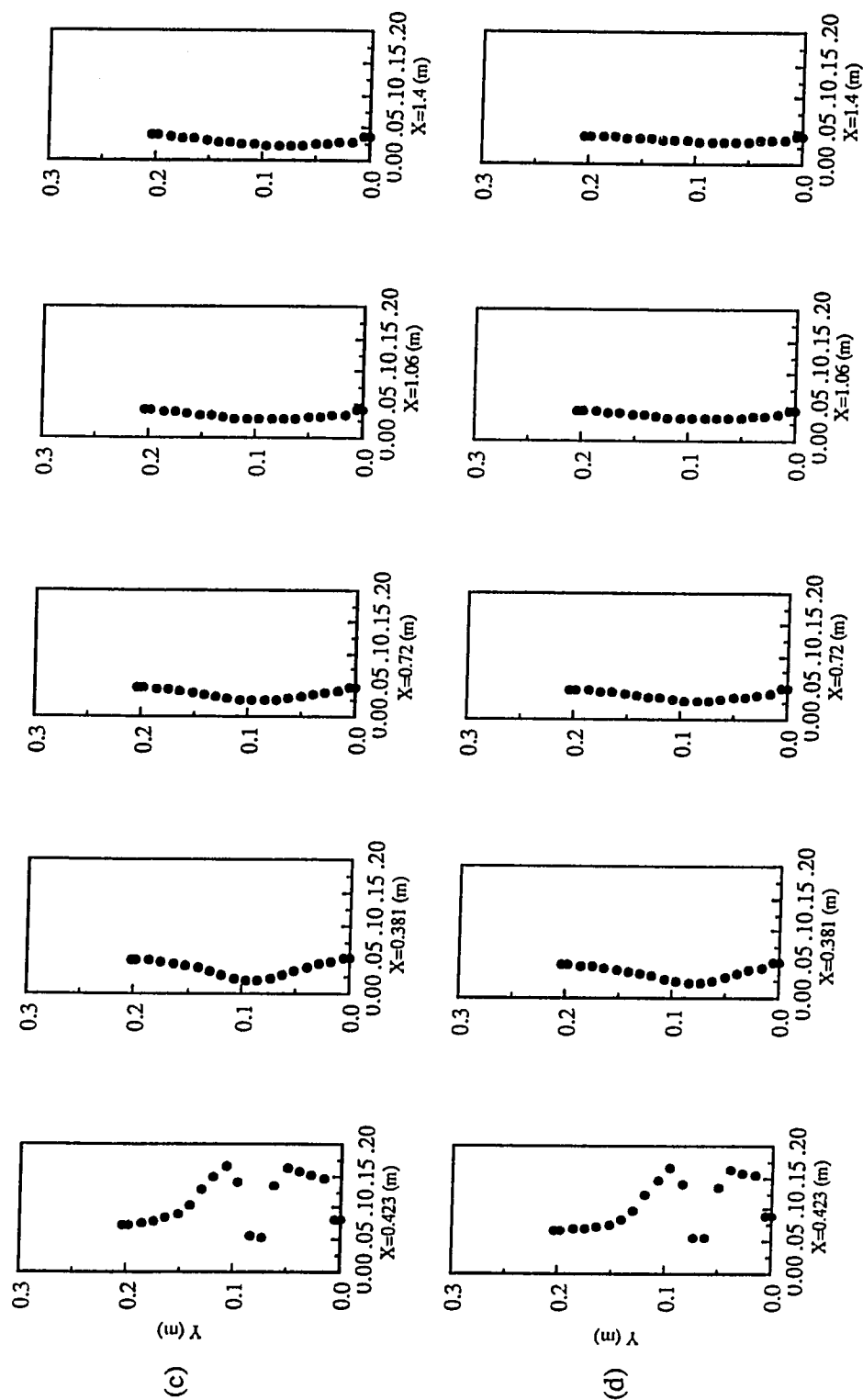


Figure 4.23.2 Predicted Cross-Section Profile of O_2 Concentration at Five Different Locations (c) case 3 (d) case 4.

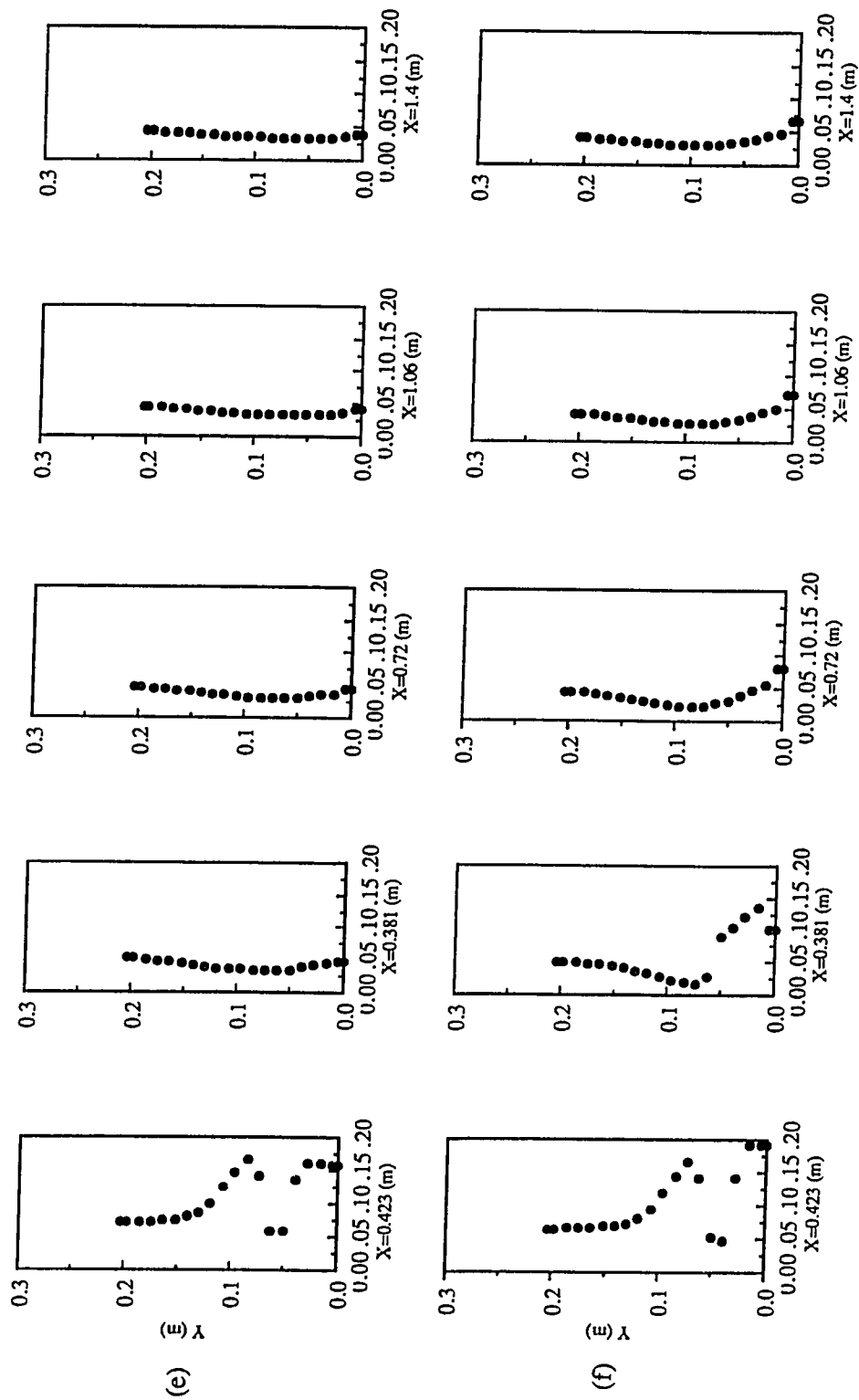


Figure 4.23.3 Predicted Cross-Section Profile of O_2 Concentration at Five Different Locations (e) case 5 (f) case 6.

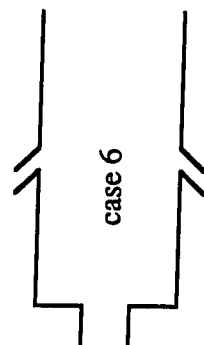
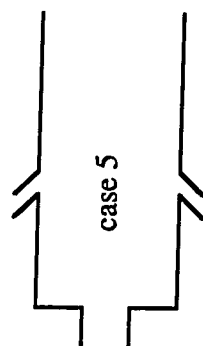
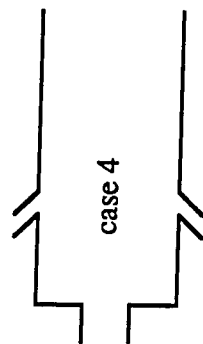
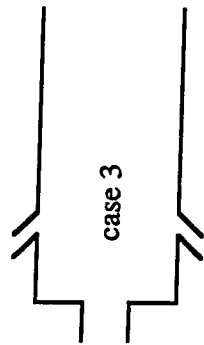
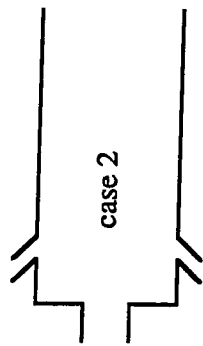
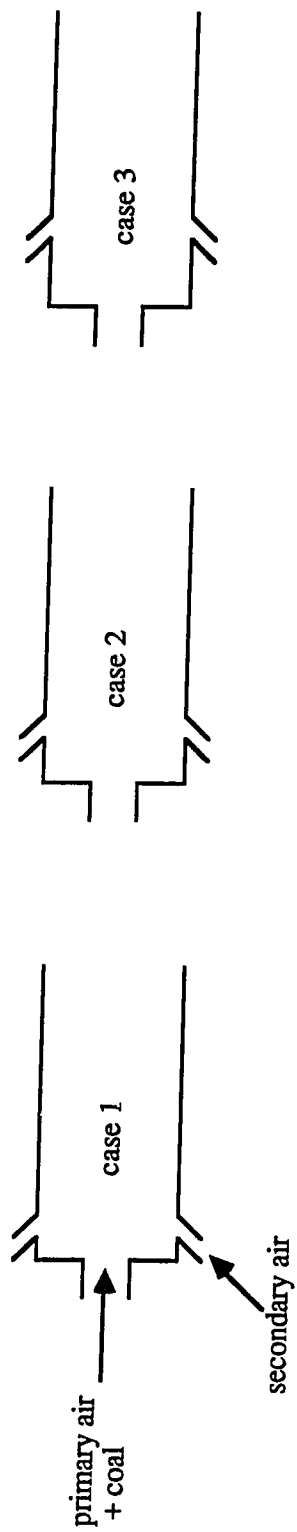


Figure 4.24 The Location of Secondary Air in Six Cases, The Inclined Angle = 15.456

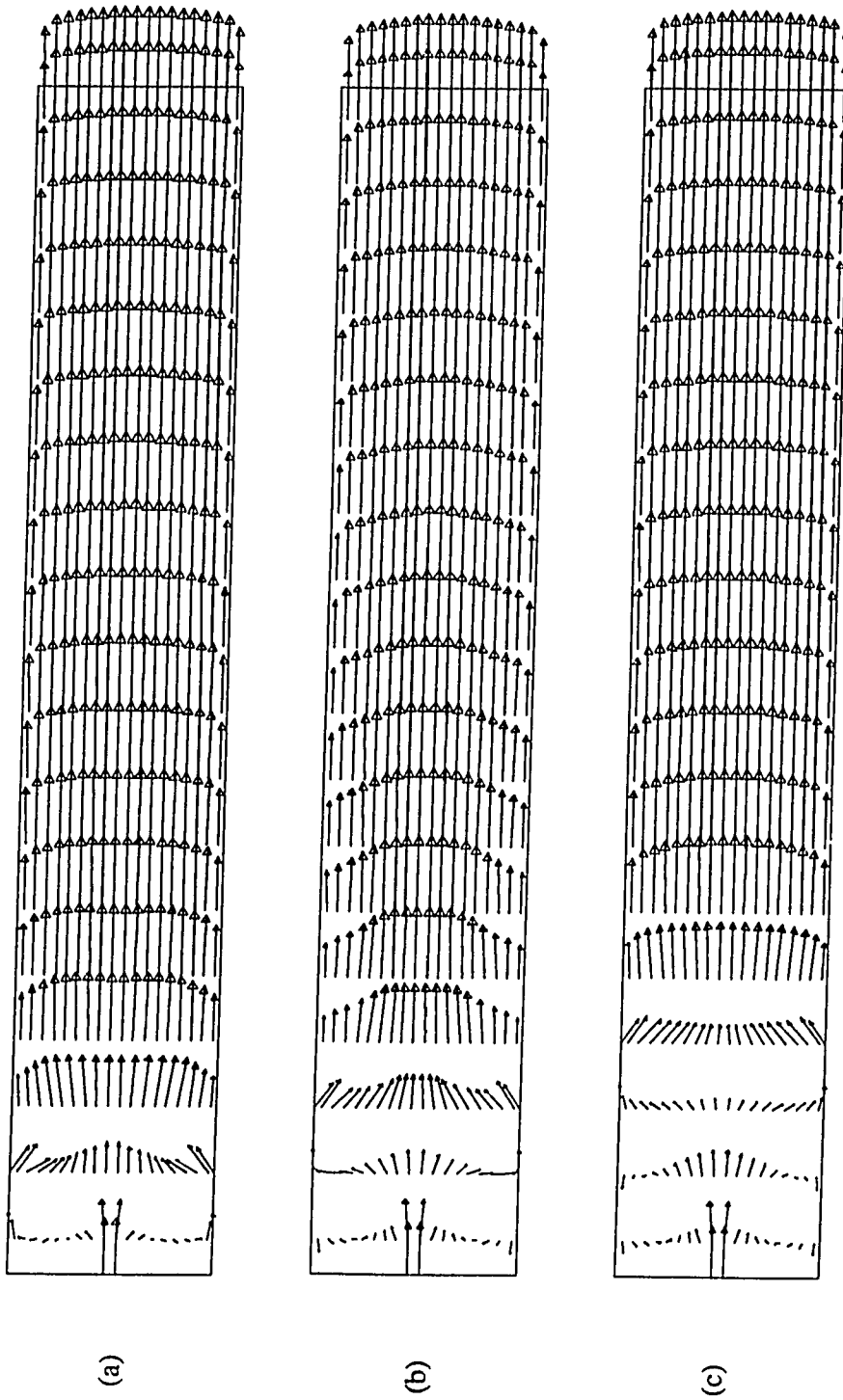


Figure 4.25.1 Predicted Gas Velocity Vectors (a) case 1 (b) case 2 (c) case 3.

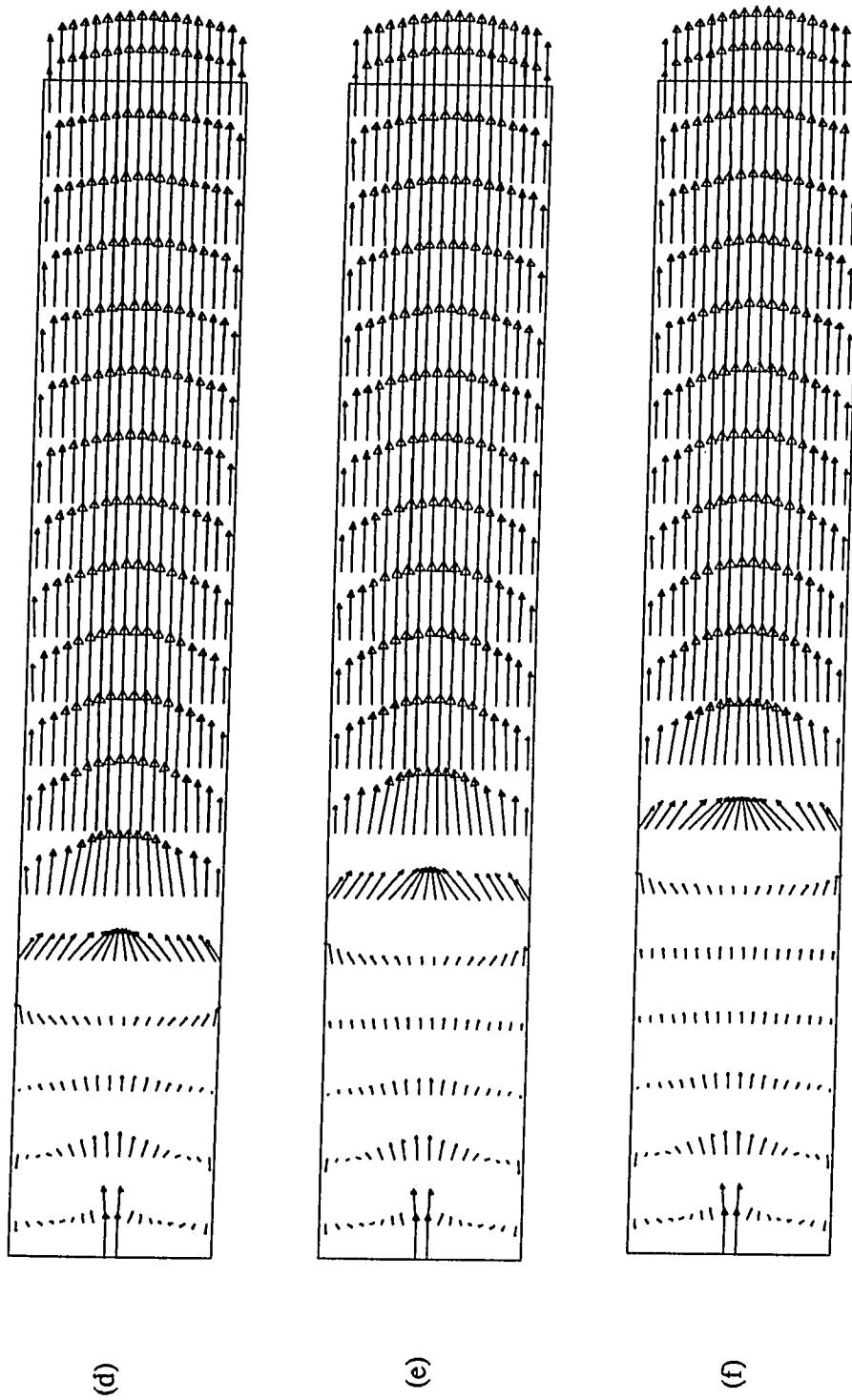


Figure 4.25.2 Predicted Gas Velocity Vectors (d) case 4 (e) case 5 (f) case 6.

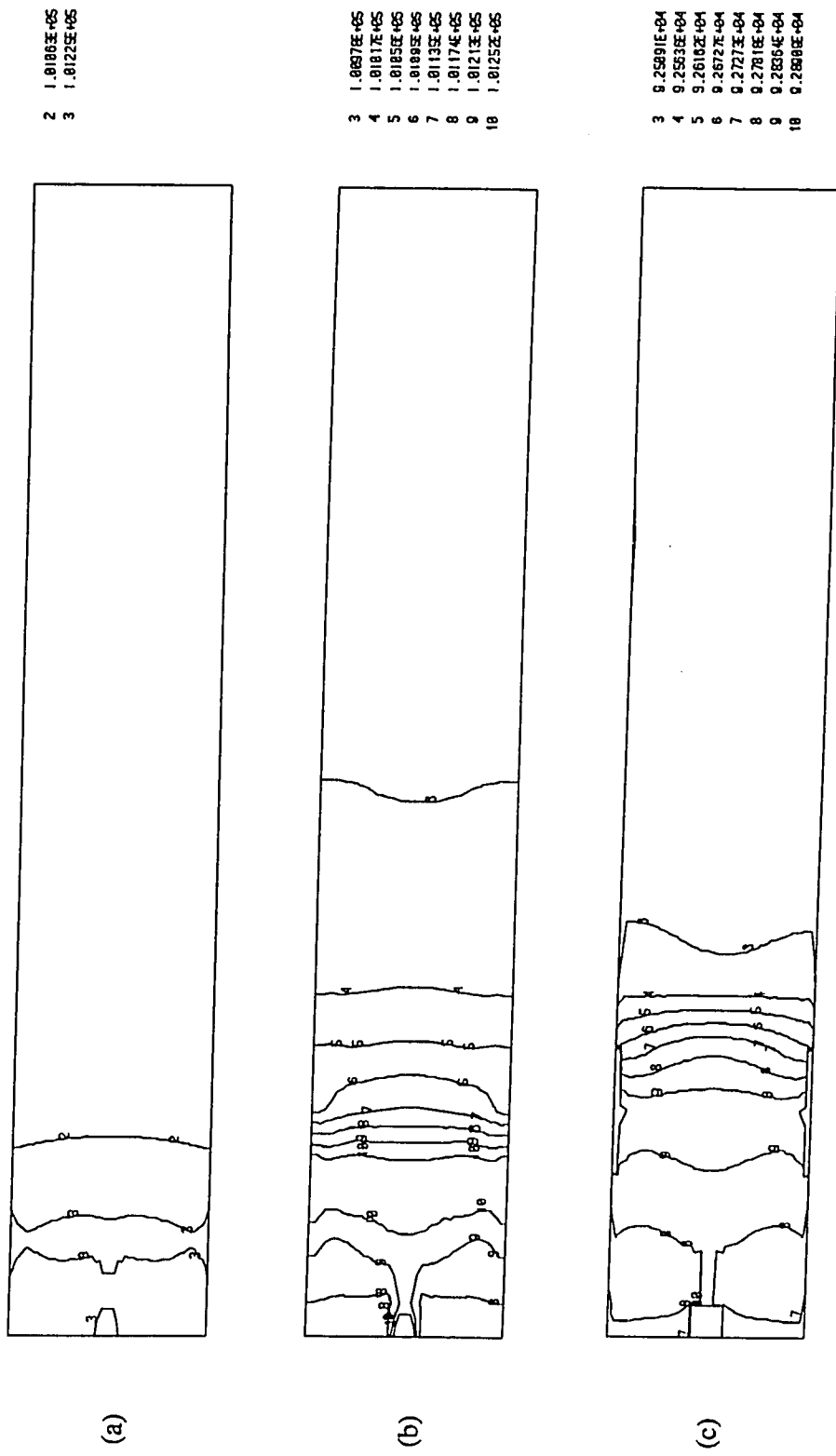
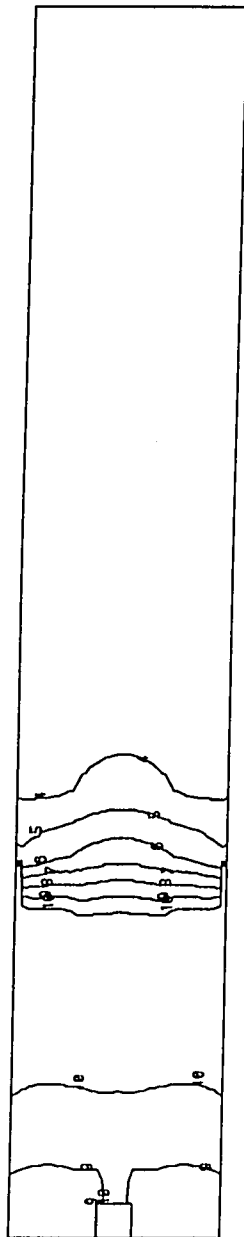


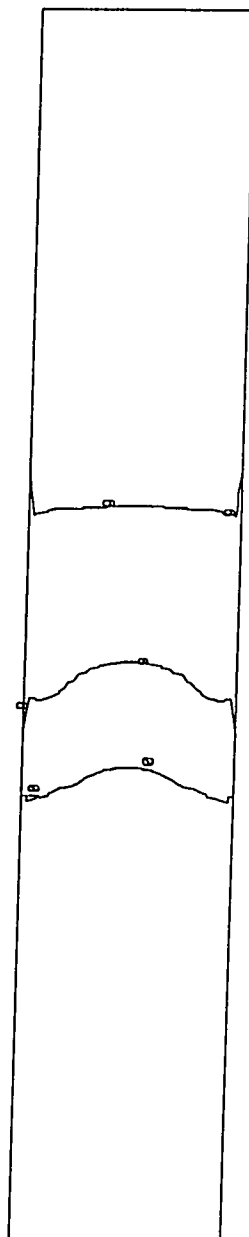
Figure 4.26.1 Predicted Contours of Pressure (a) case 1 (b) case 2 (c) case 3.

4 0.5333E+04
5 0.5378E+04
6 0.5422E+04
7 0.5467E+04
8 0.5511E+04
9 0.5556E+04
10 0.5600E+04



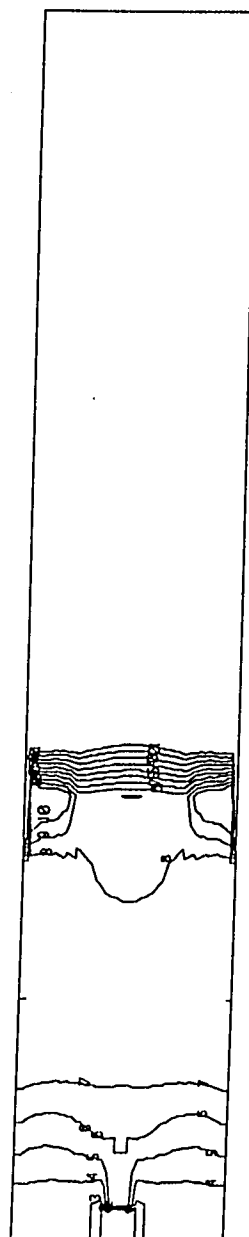
(d)

9 0.6777E+04
10 0.6818E+04



(e)

1 1.0190E+05
2 1.0191E+05
3 1.0193E+05
4 1.0185E+05
5 1.0197E+05
6 1.0190E+05
7 1.0200E+05
8 1.0202E+05
9 1.0204E+05
10 1.0206E+05



(f)

Figure 4.26.2 Predicted Contours of Pressure (d) case 4 (e) case 5 (f) case 6.

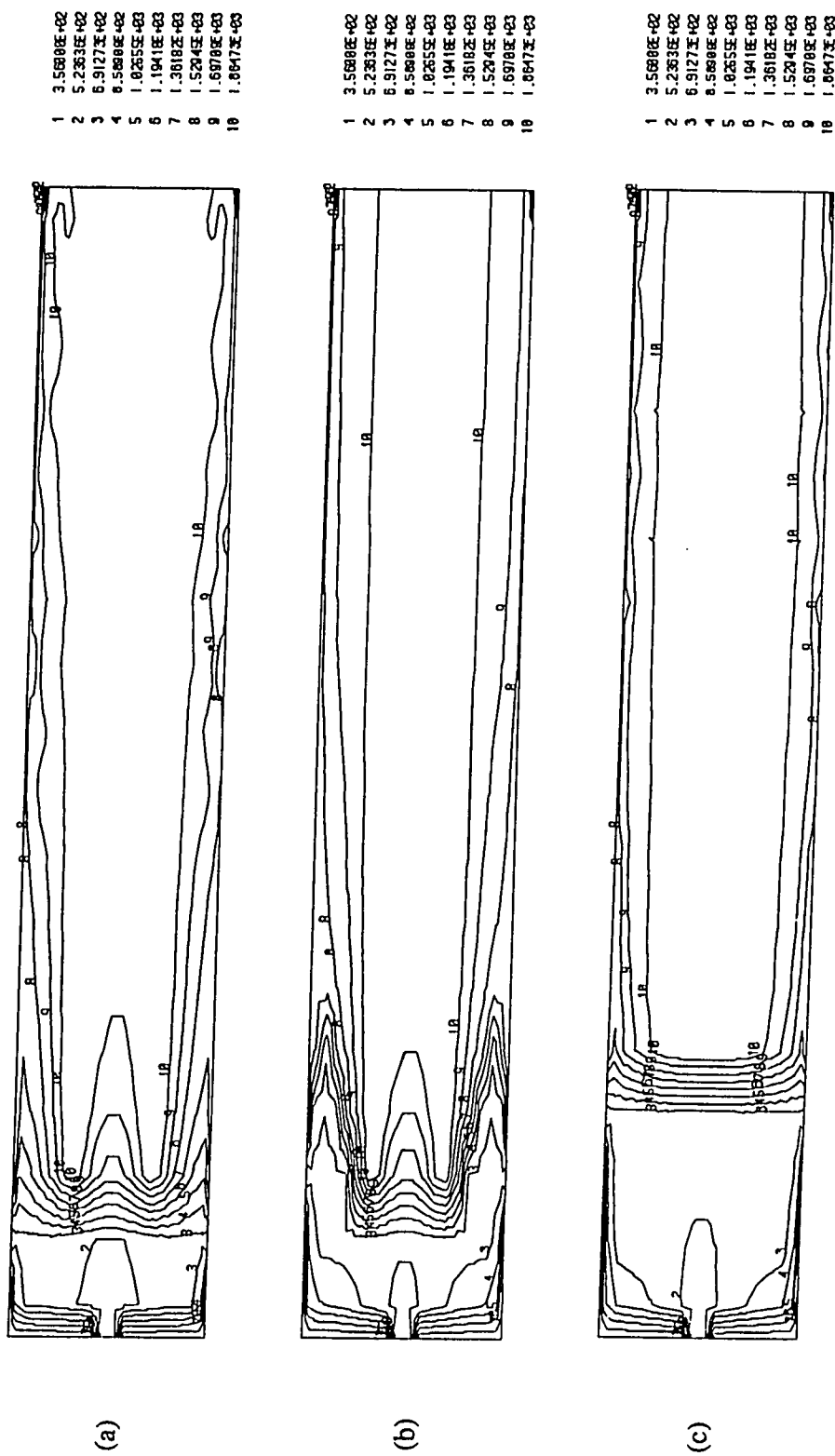


Figure 4.27.1 Predicted Contours of Temperature (a) case 1 (b) case 2 (c) case 3.

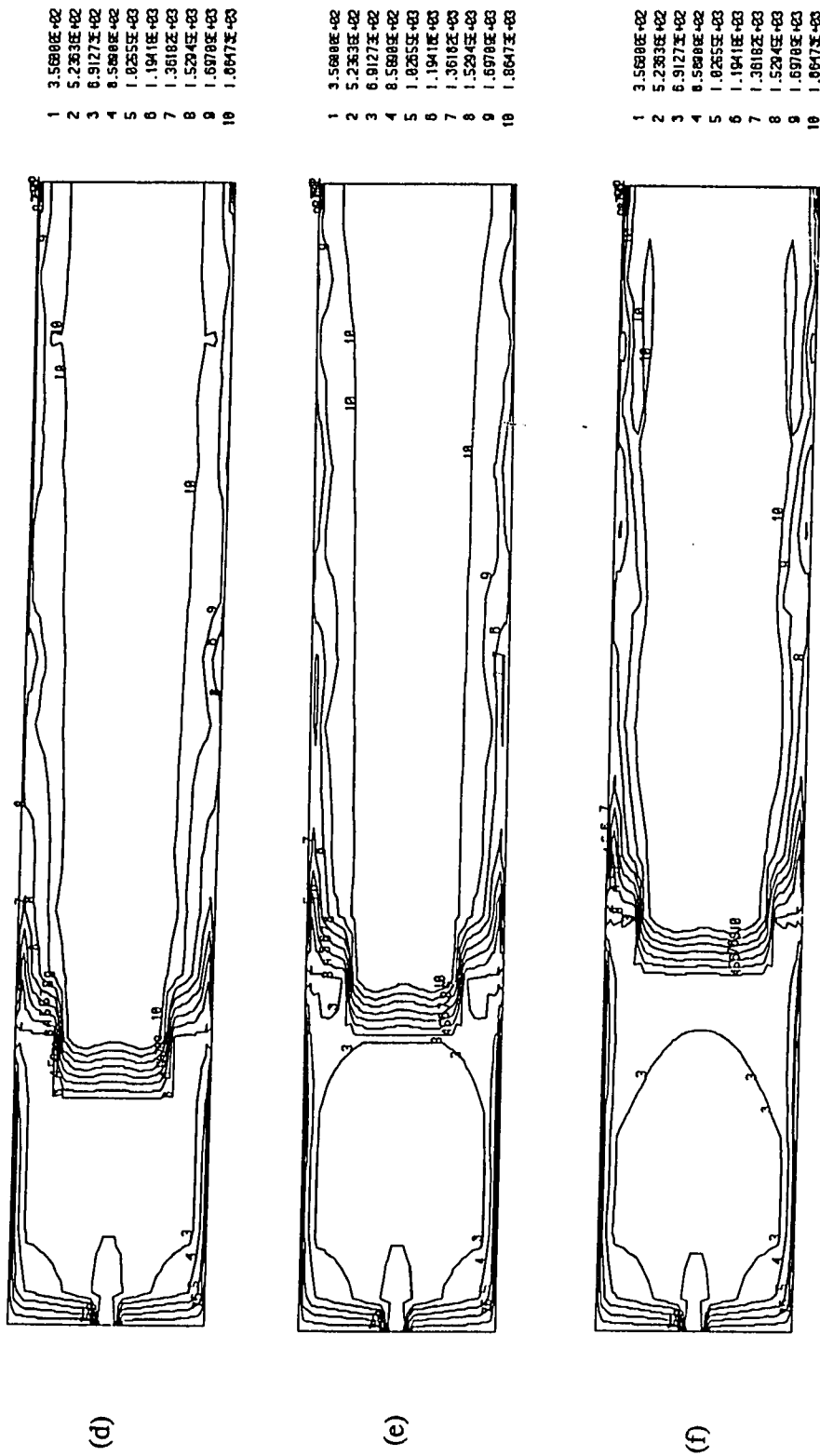


Figure 4.27.2 Predicted Contours of Temperature (d) case 4 (e) case 5 (f) case 6.

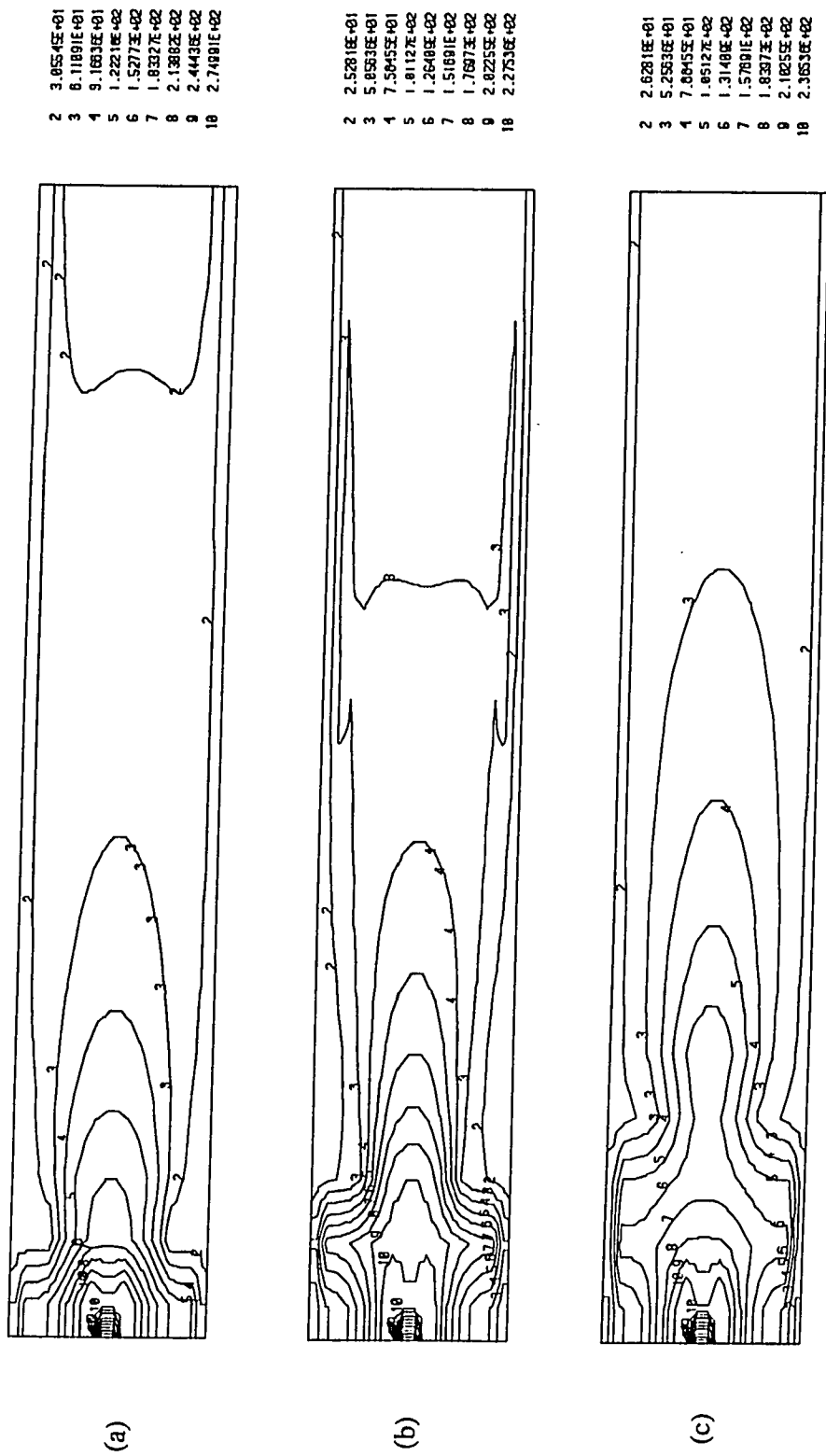


Figure 4.28.1 Predicted Contours of Turbulence Kinetic Energy (a) case 1 (b) case 2 (c) case 3.

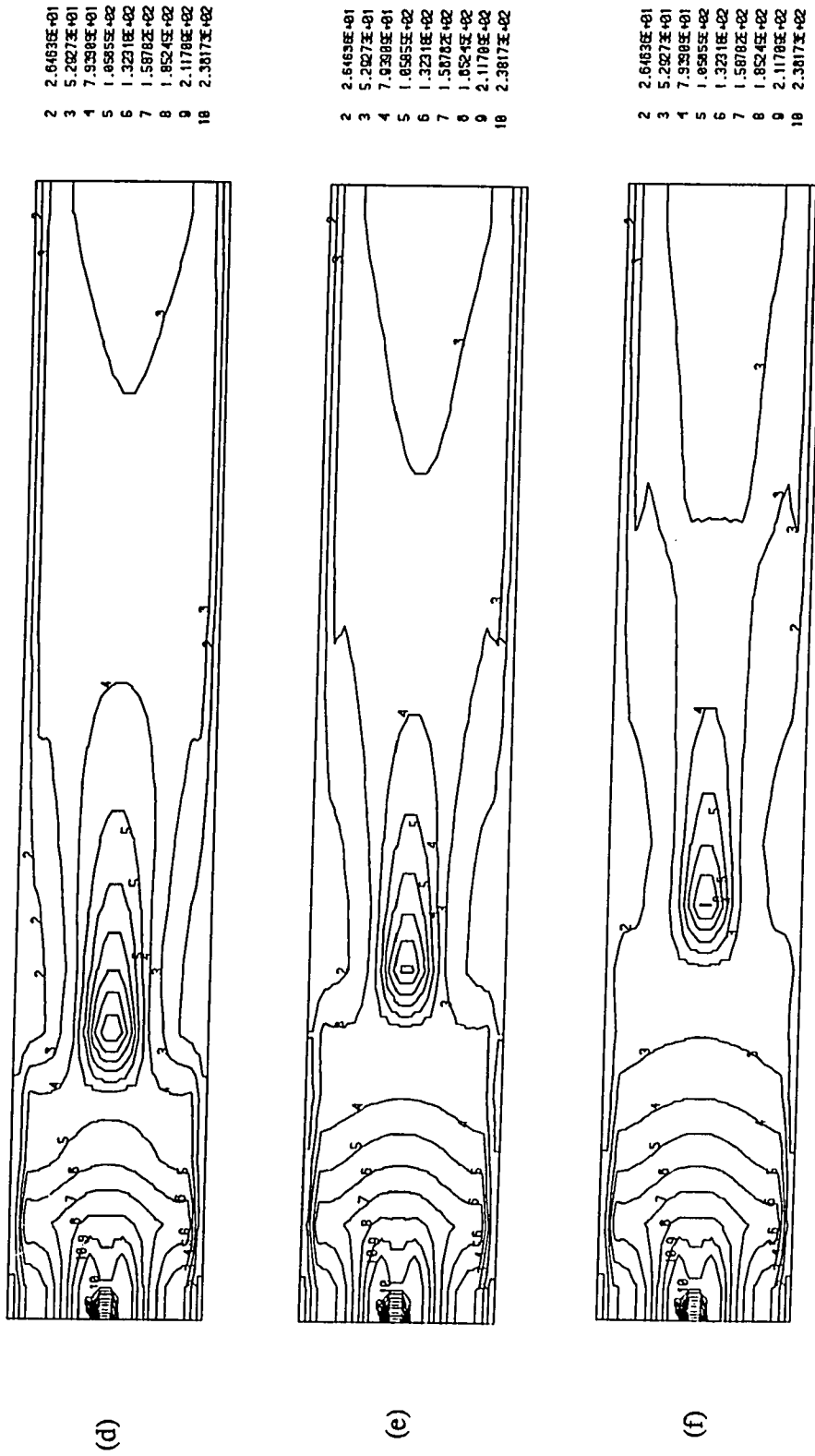


Figure 4.28.2 Predicted Contours of Turbulence Kinetic Energy (d) case 4 (e) case 5 (f) case 6.

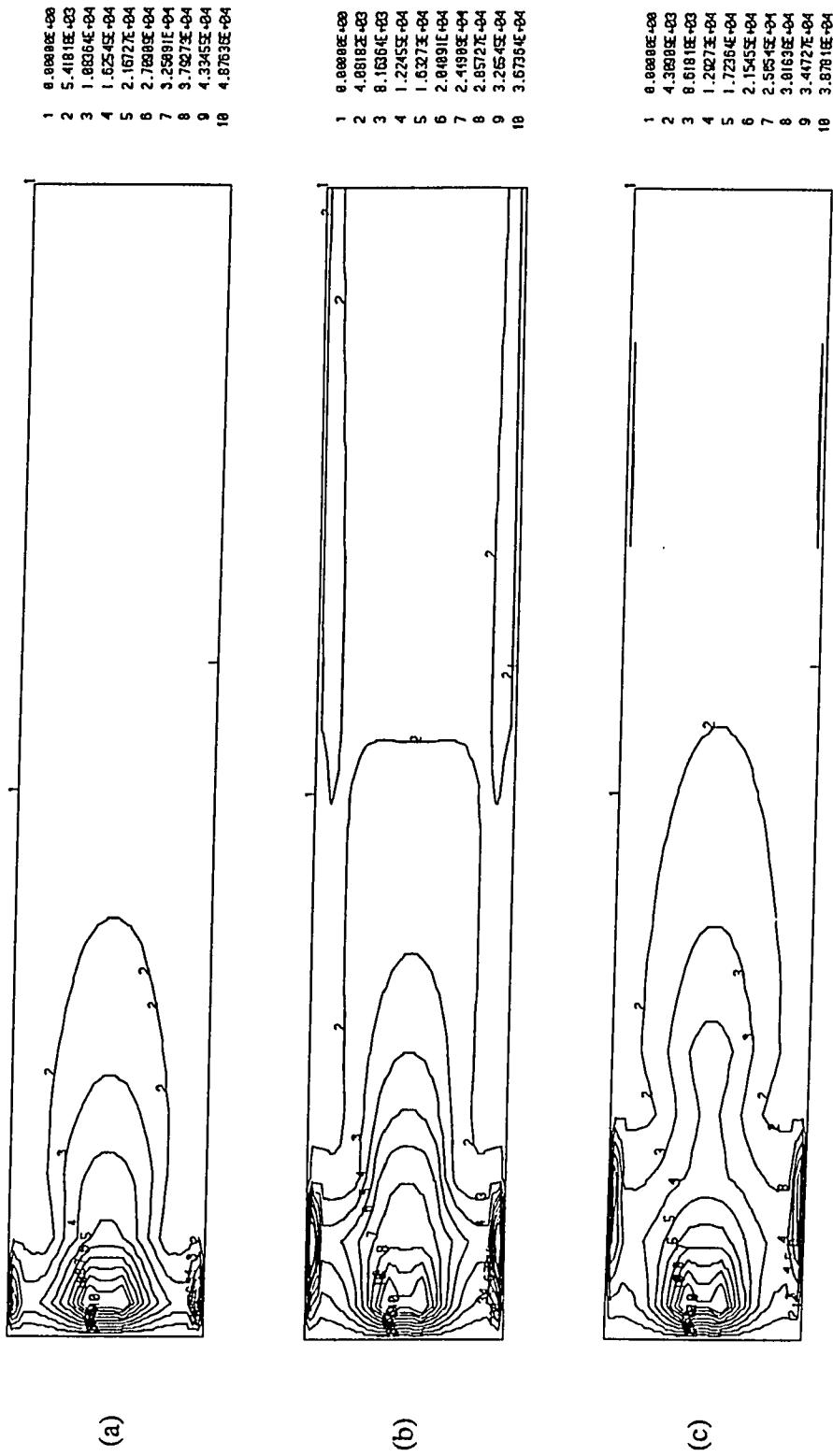


Figure 4.29.1 Predicted Contours of Turbulence Dissipation Rate (a) case 1 (b) case 2 (c) case 3.

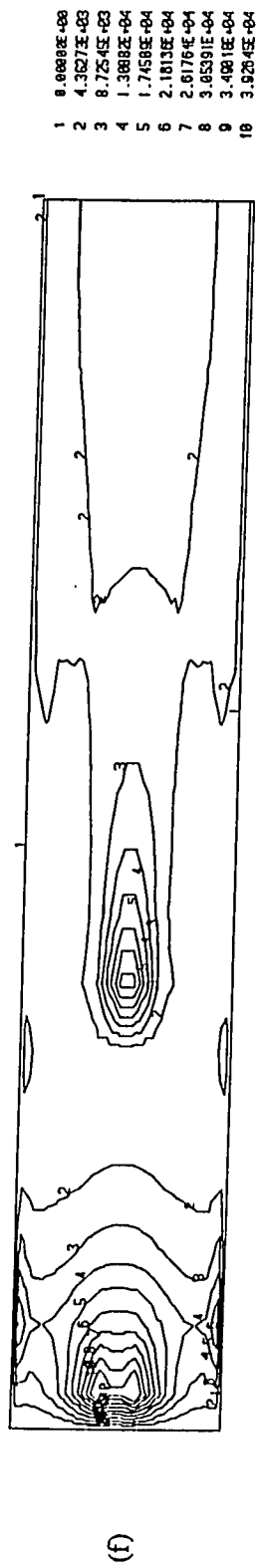
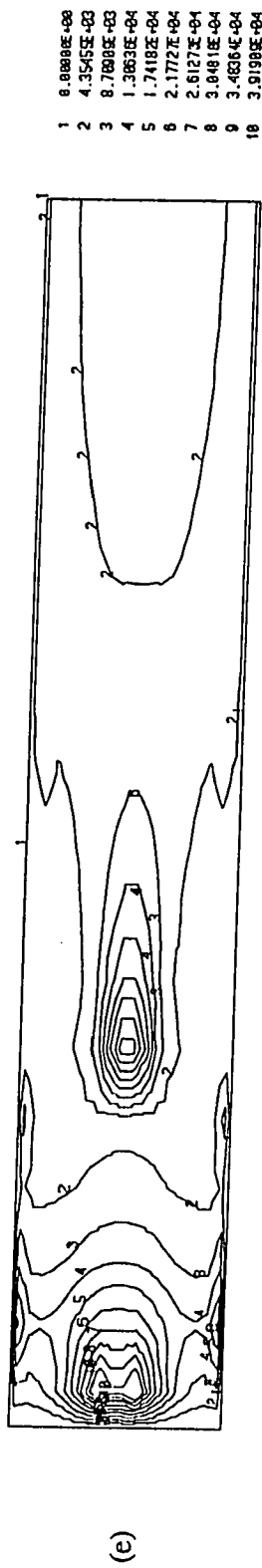
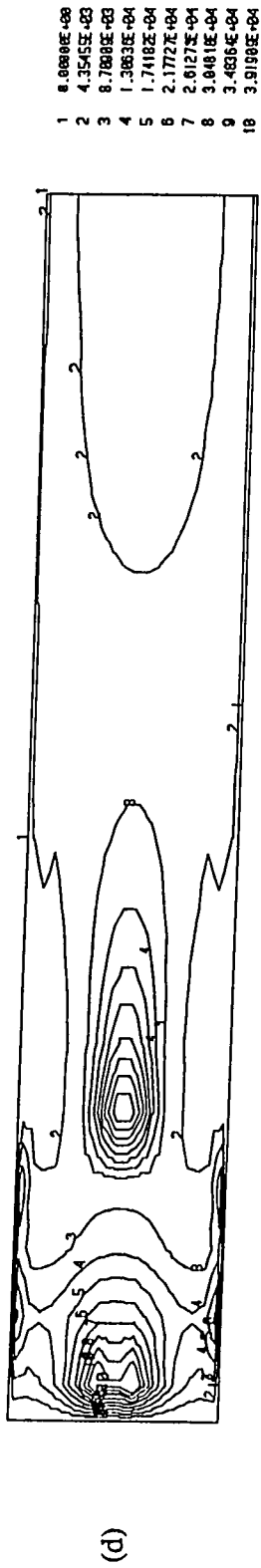


Figure 4.29.2 Predicted Contours of Turbulence Dissipation Rate (d) case 4 (e) case 5 (f) case 6.

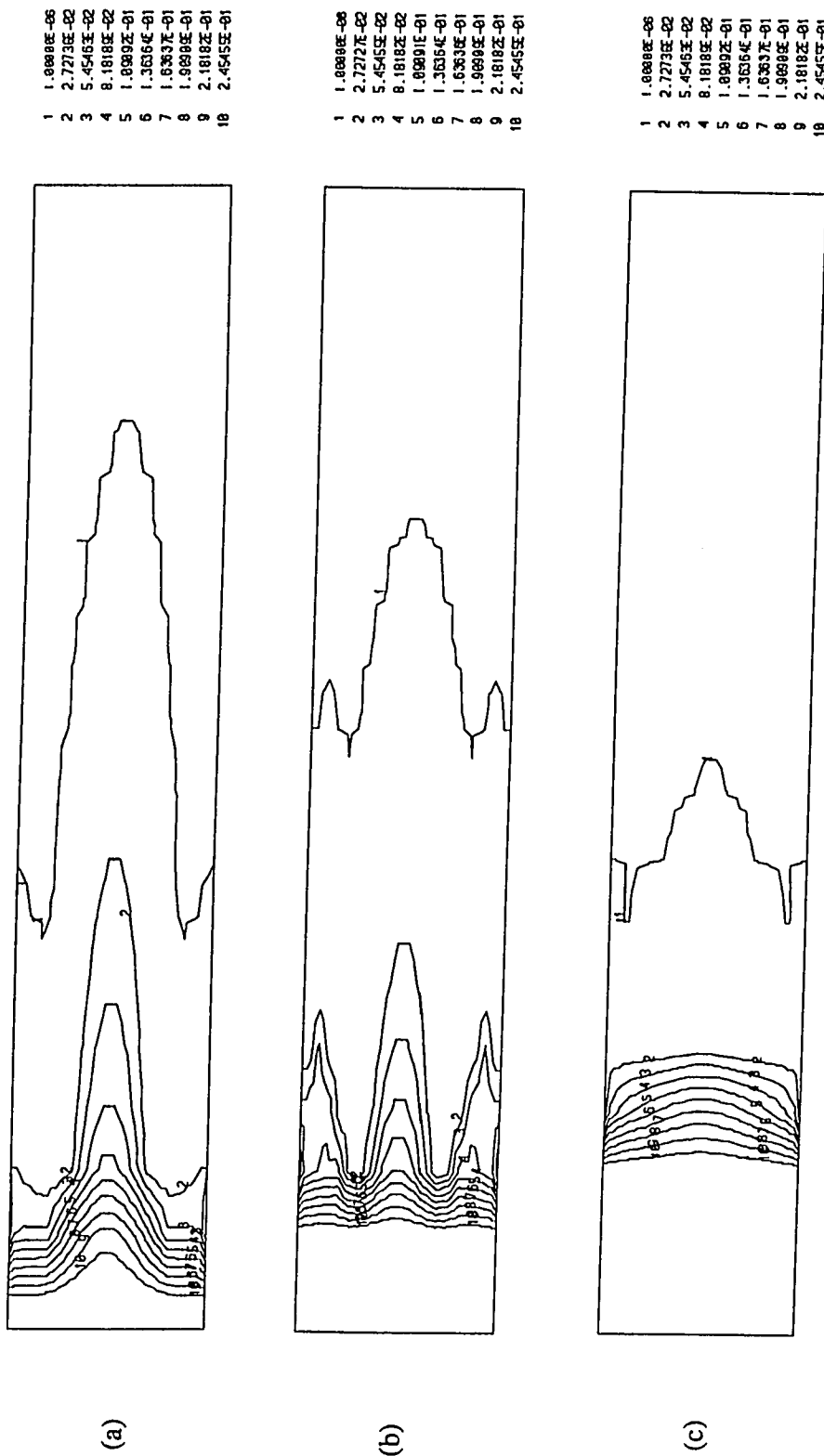


Figure 4.30.1 Predicted Contours of CO Concentration (a) case 1 (b) case 2 (c) case 3..

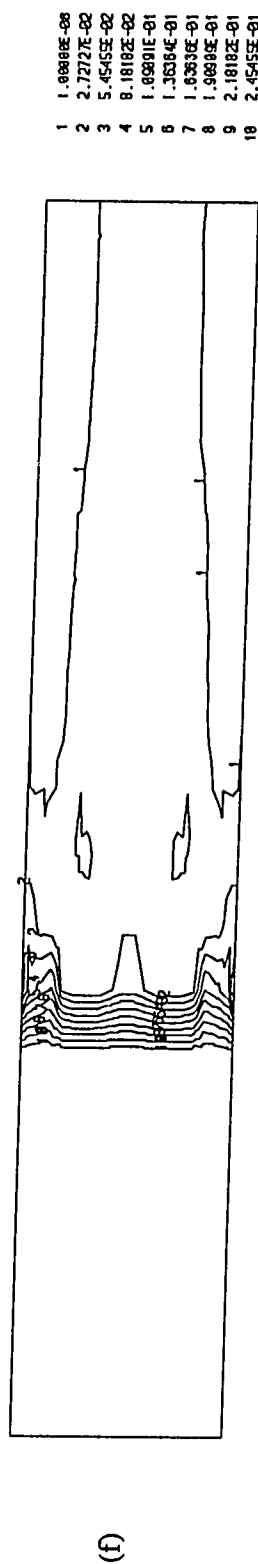
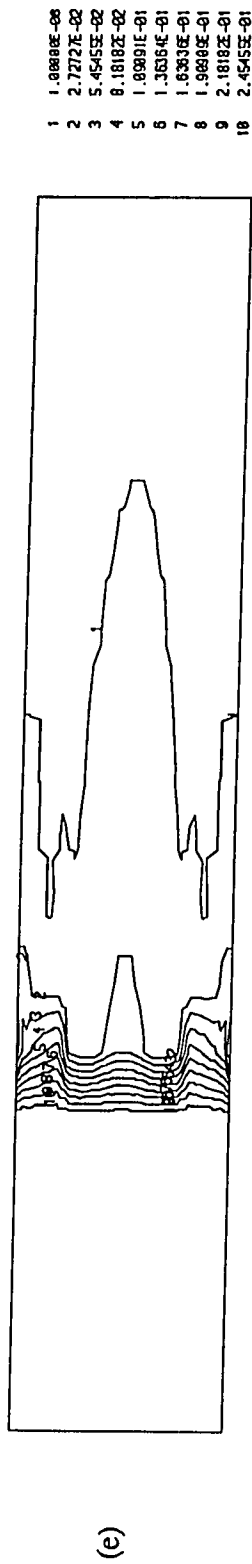
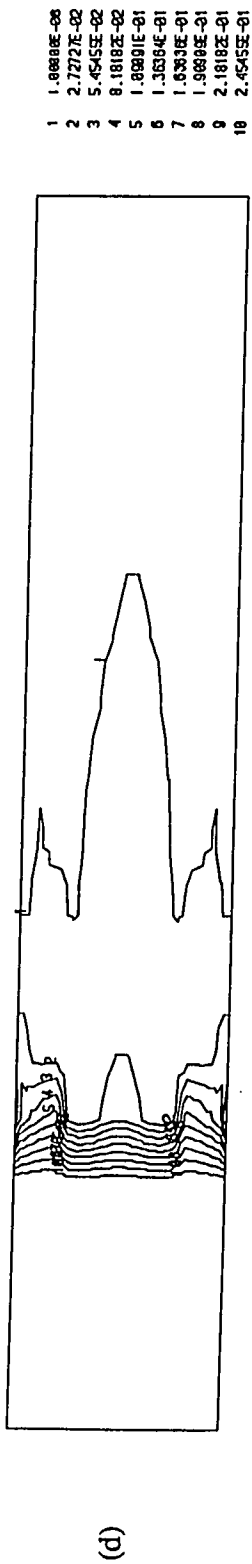


Figure 4.30.2 Predicted Contours of CO Concentration (d) case 4 (e) case 5 (f) case 6.

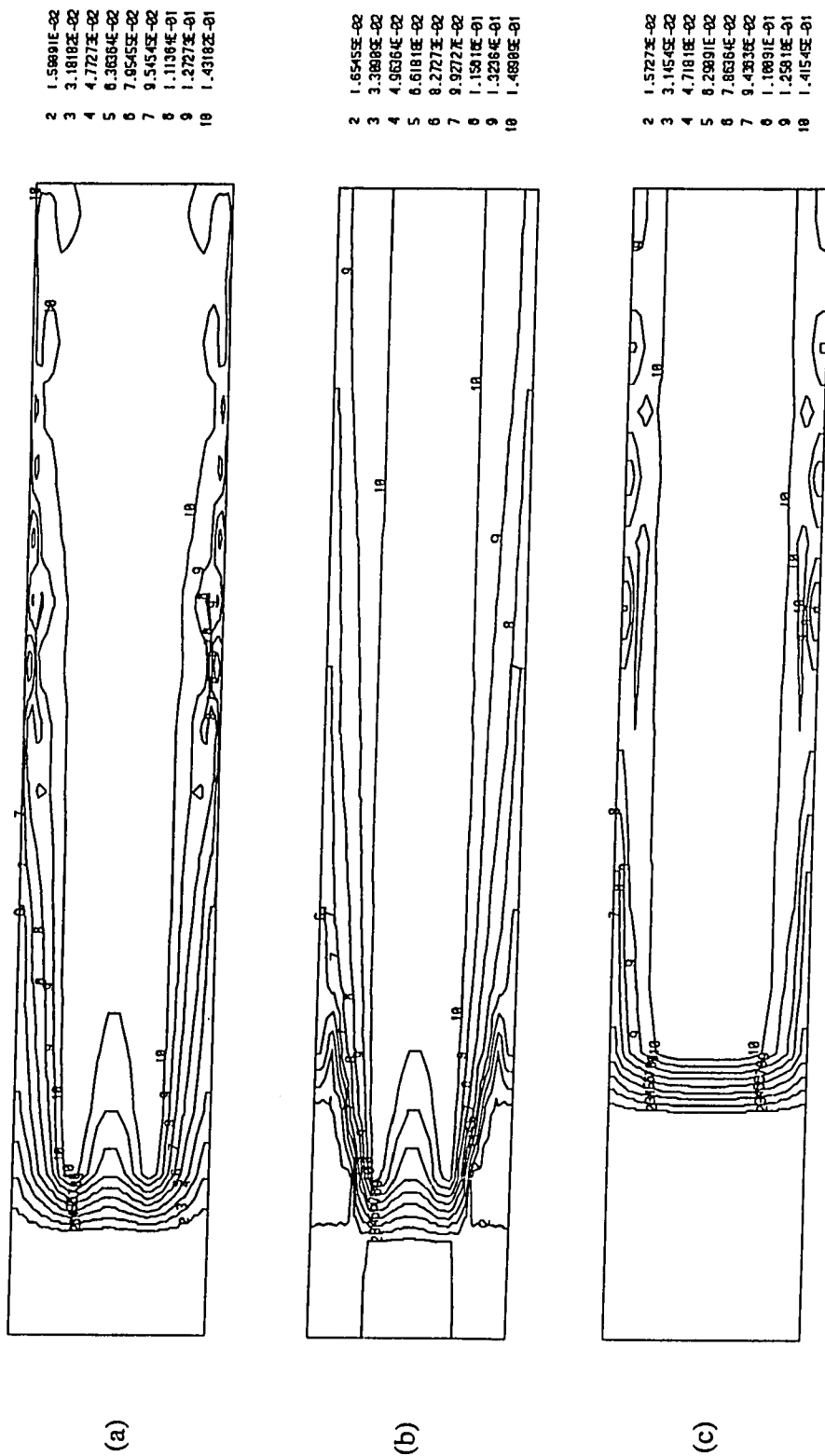


Figure 4.31.1 Predicted Contours of CO₂ Concentration (a) case 1 (b) case 2 (c) case 3.

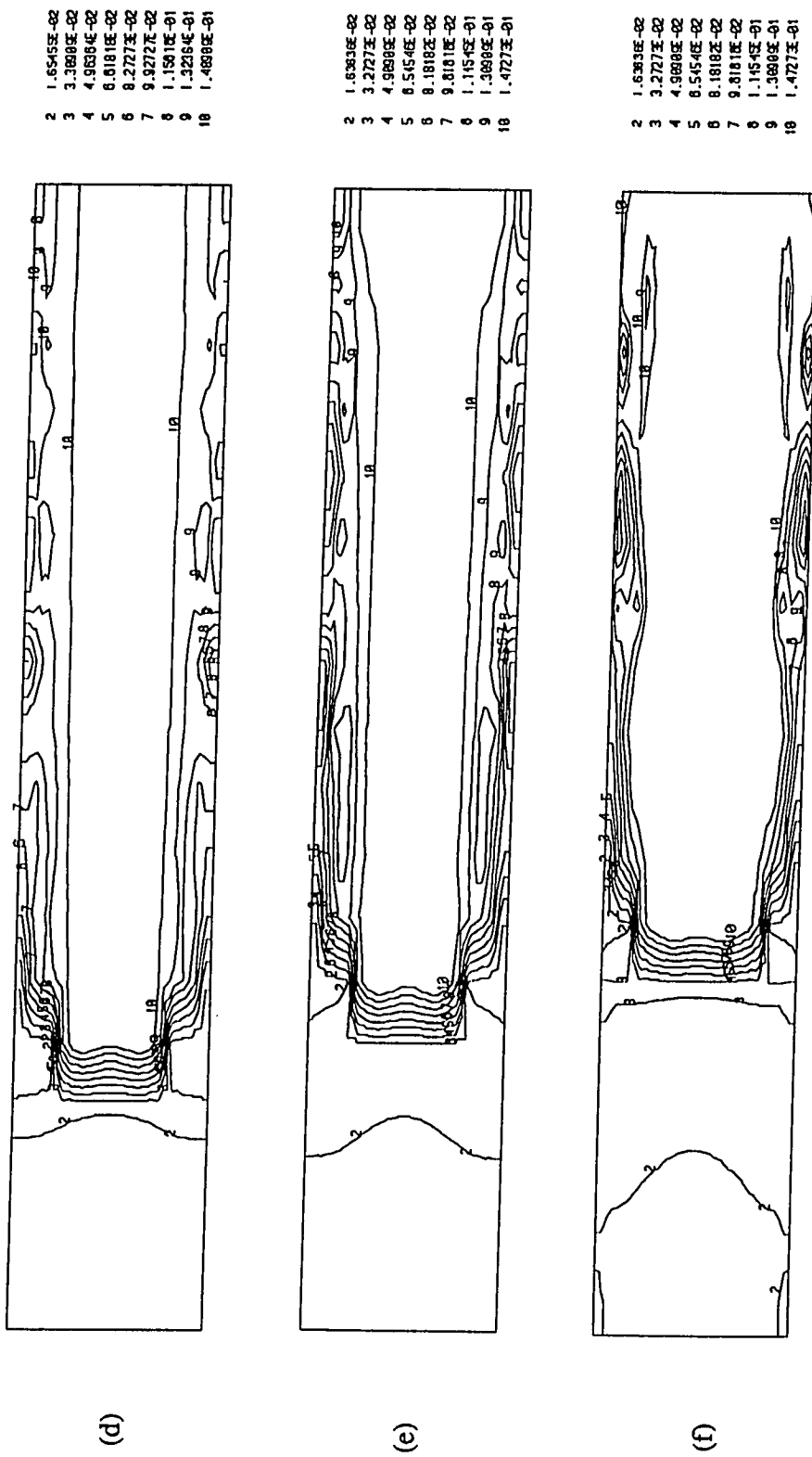


Figure 4.31.2 Predicted Contours of CO₂ Concentration (d) case 4 (e) case 5 (f) case 6.

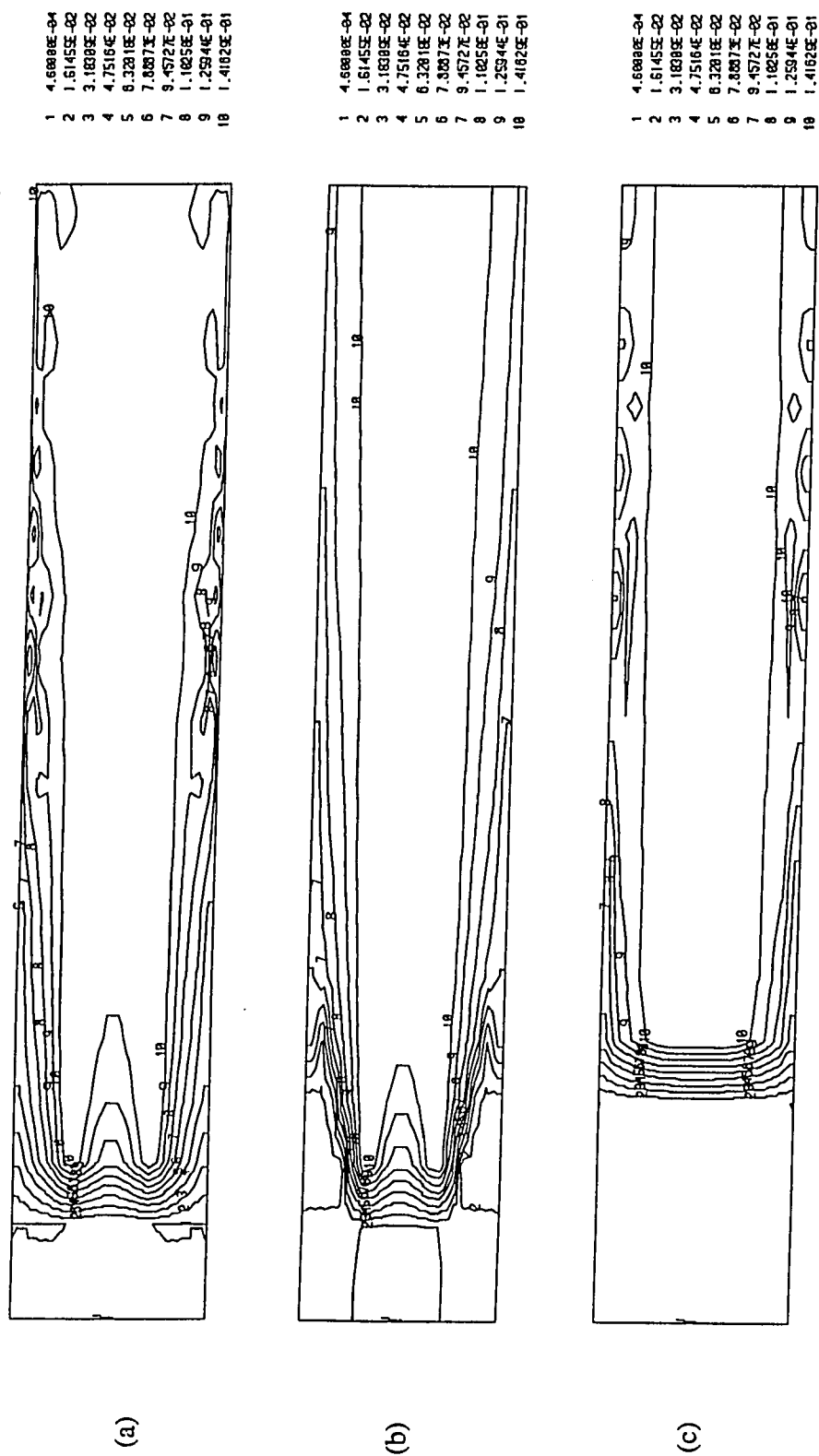


Figure 4.32.1 Predicted Contours of H_2O Concentration (a) case 1 (b) case 2 (c) case 3.

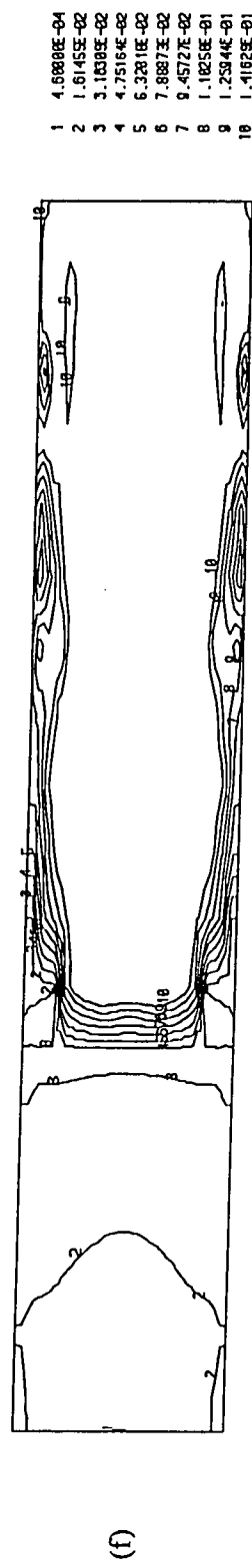
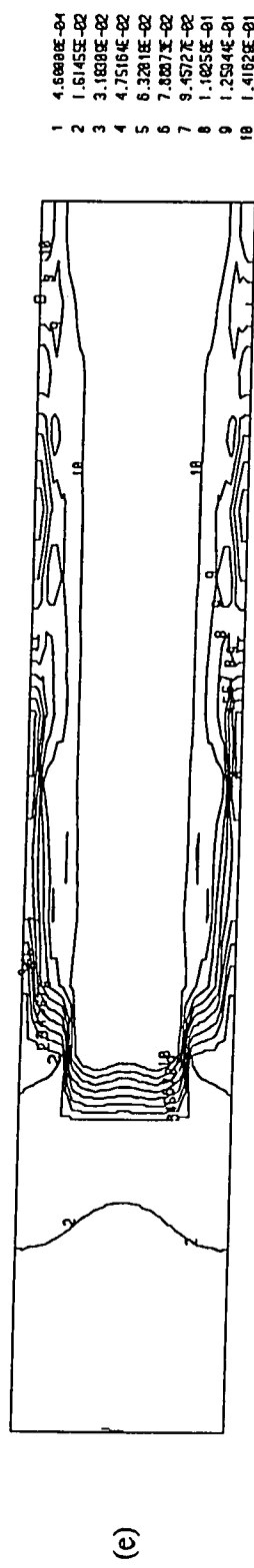
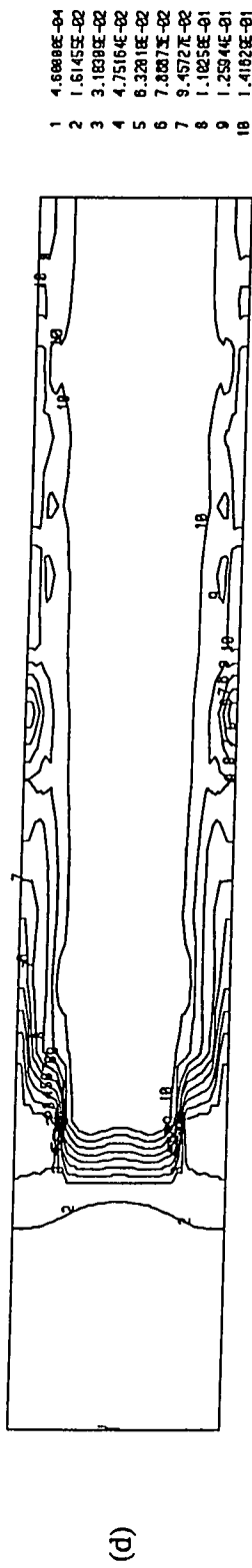


Figure 4.32.2 Predicted Contours of H_2O Concentration (d) case 4 (e) case 5 (f) case 6.

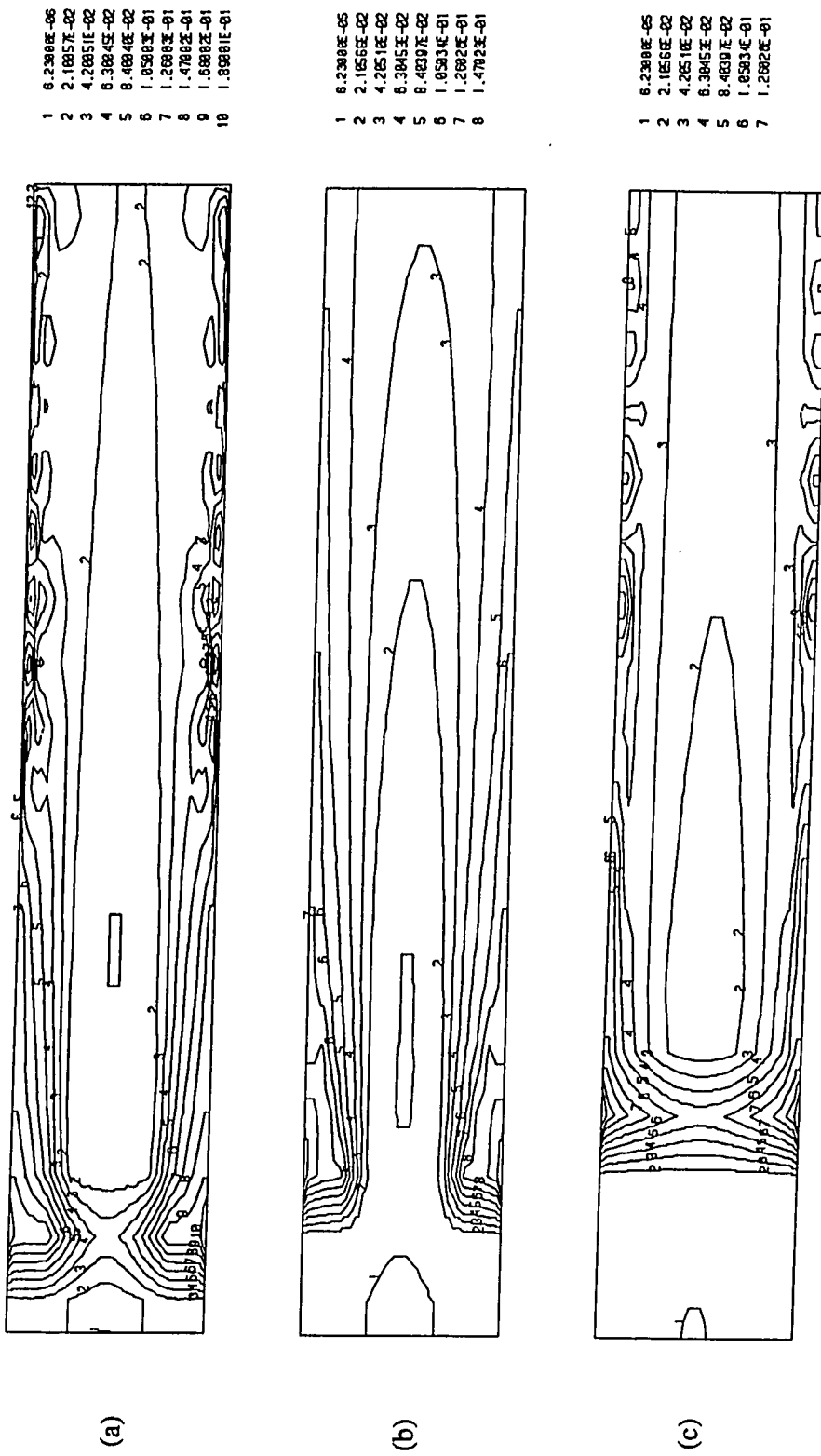


Figure 4.33.1 Predicted Contours of O_2 Concentration (a) case 1 (b) case 2 (c) case 3.

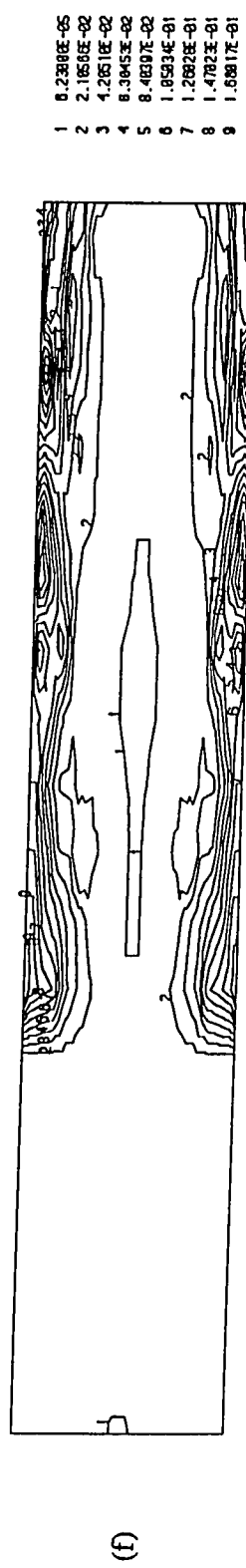
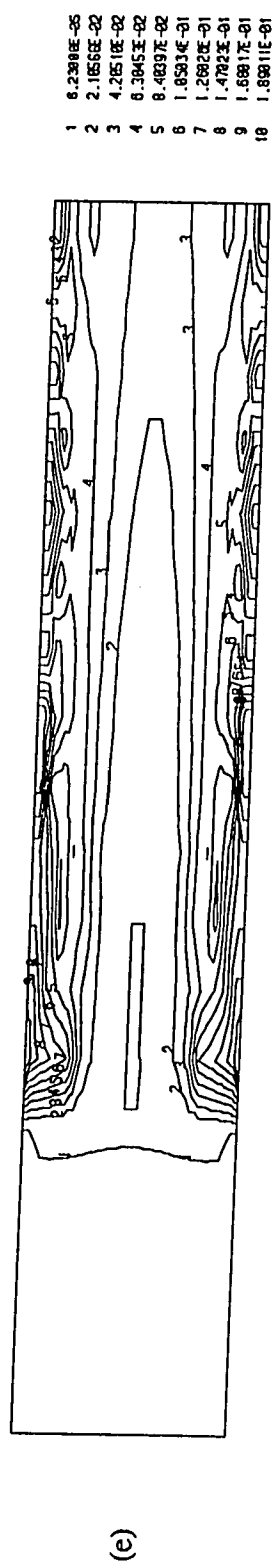
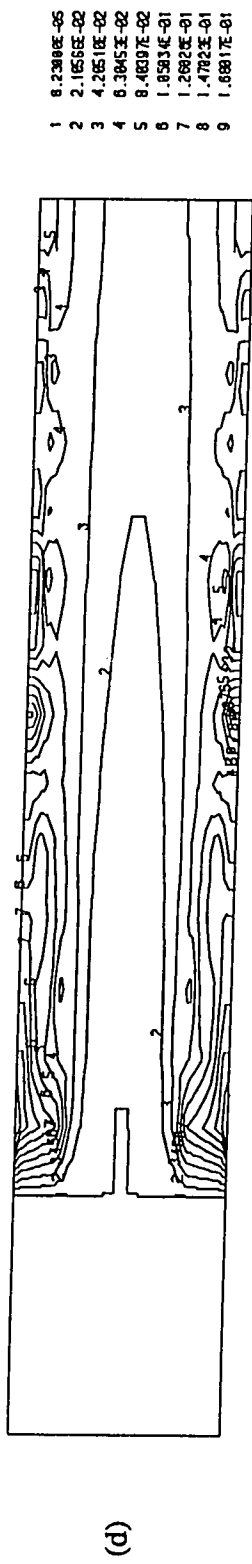


Figure 4.33.2 Predicted Contours of O_2 Concentration (d) case 4 (e) case 5 (f) case 6.

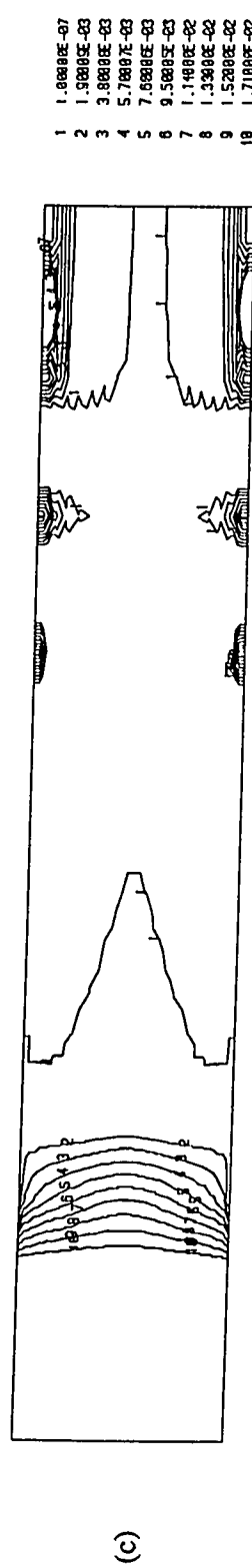
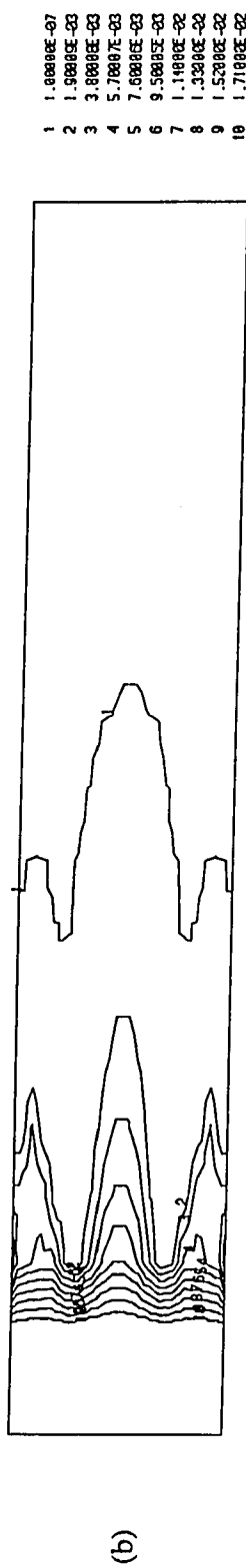
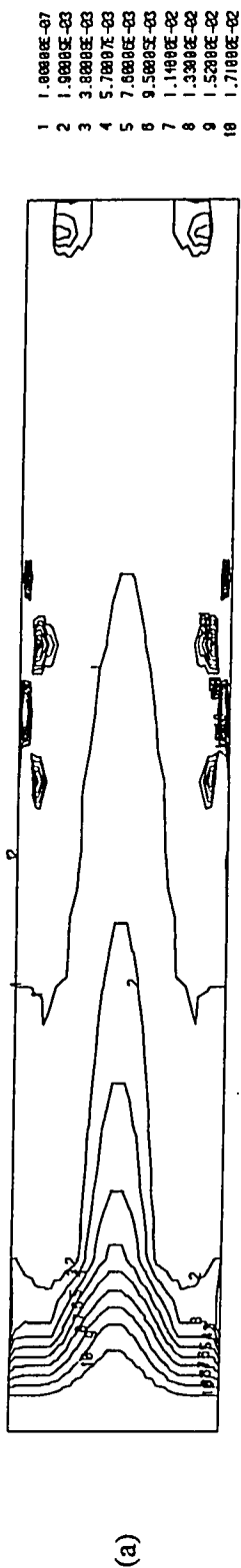
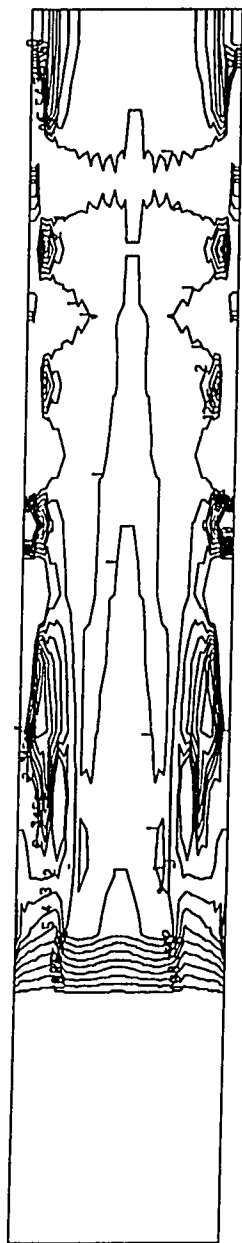


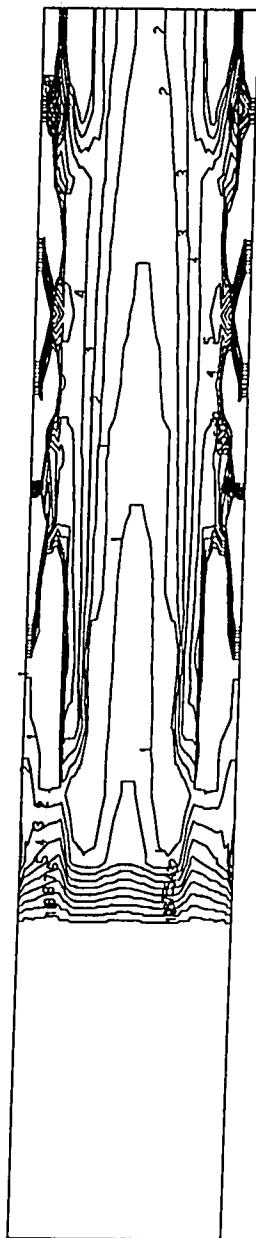
Figure 4.34.1 Predicted Contours of CH₄ Concentration (a) case 1 (b) case 2 (c) case 3.

1 1.0000E-07
2 1.9000E-03
3 3.8000E-03
4 5.7000E-03
5 7.6000E-03
6 9.5000E-03
7 1.1400E-02
8 1.3300E-02
9 1.5200E-02
10 1.7100E-02



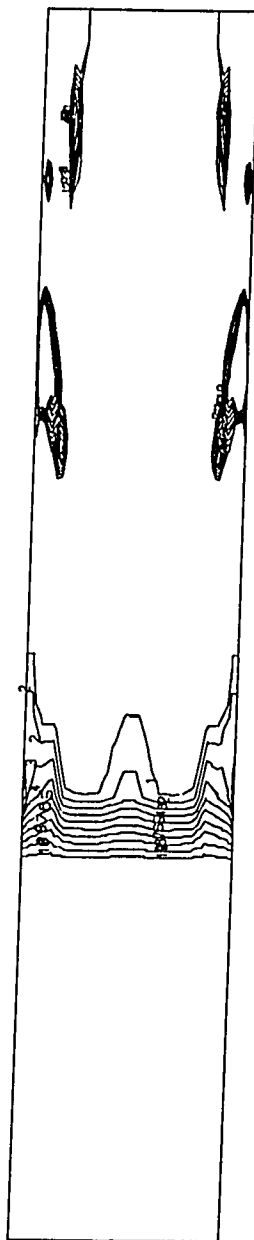
(d)

1 1.0000E-07
2 1.9000E-03
3 3.8000E-03
4 5.7000E-03
5 7.6000E-03
6 9.5000E-03
7 1.1400E-02
8 1.3300E-02
9 1.5200E-02
10 1.7100E-02



(e)

1 1.0000E-07
2 1.9000E-03
3 3.8000E-03
4 5.7000E-03
5 7.6000E-03
6 9.5000E-03
7 1.1400E-02
8 1.3300E-02
9 1.5200E-02
10 1.7100E-02



(f)

Figure 4.34.2 Predicted Contours of CH_4 Concentration (d) case 4 (e) case 5 (f) case 6.

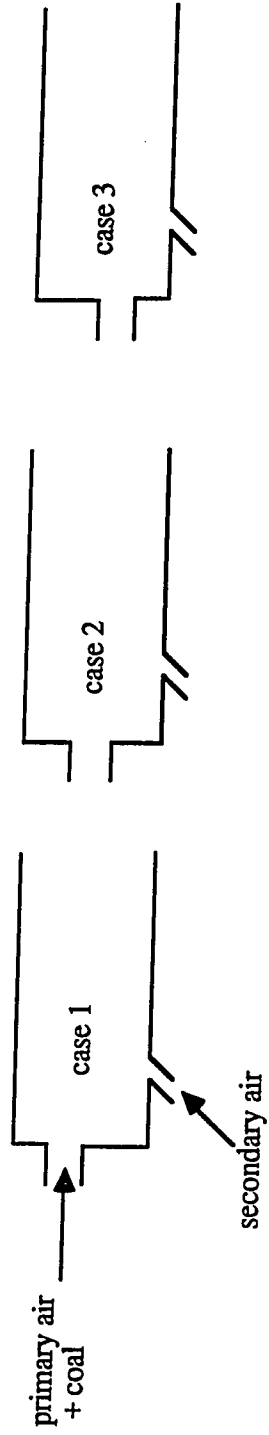


Figure 4.35 The Location of Primary Streams in Three Cases

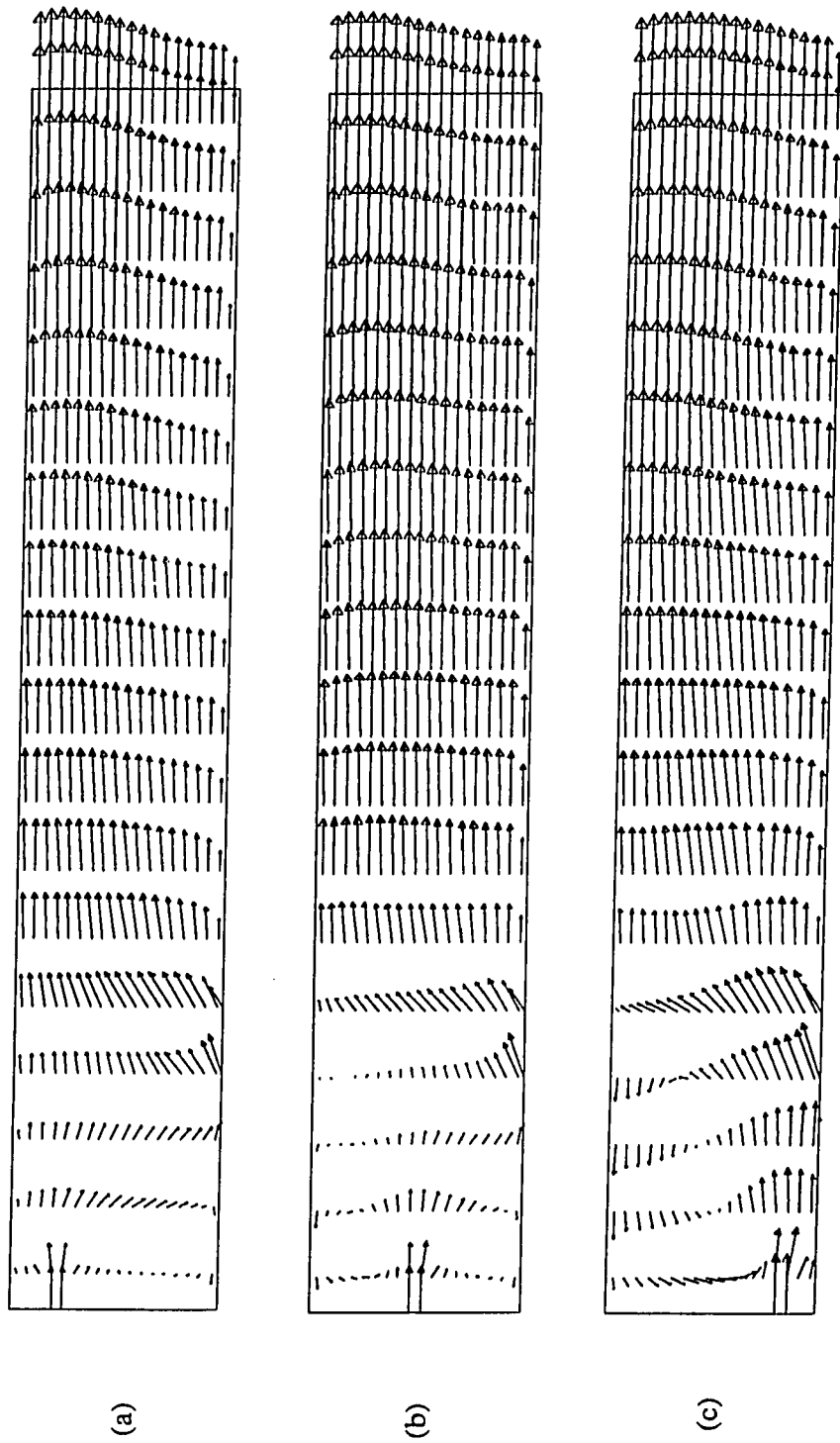


Figure 4.36 Predicted Gas Velocity Vectors (a) case 1 (b) case 2 (c) case 3.

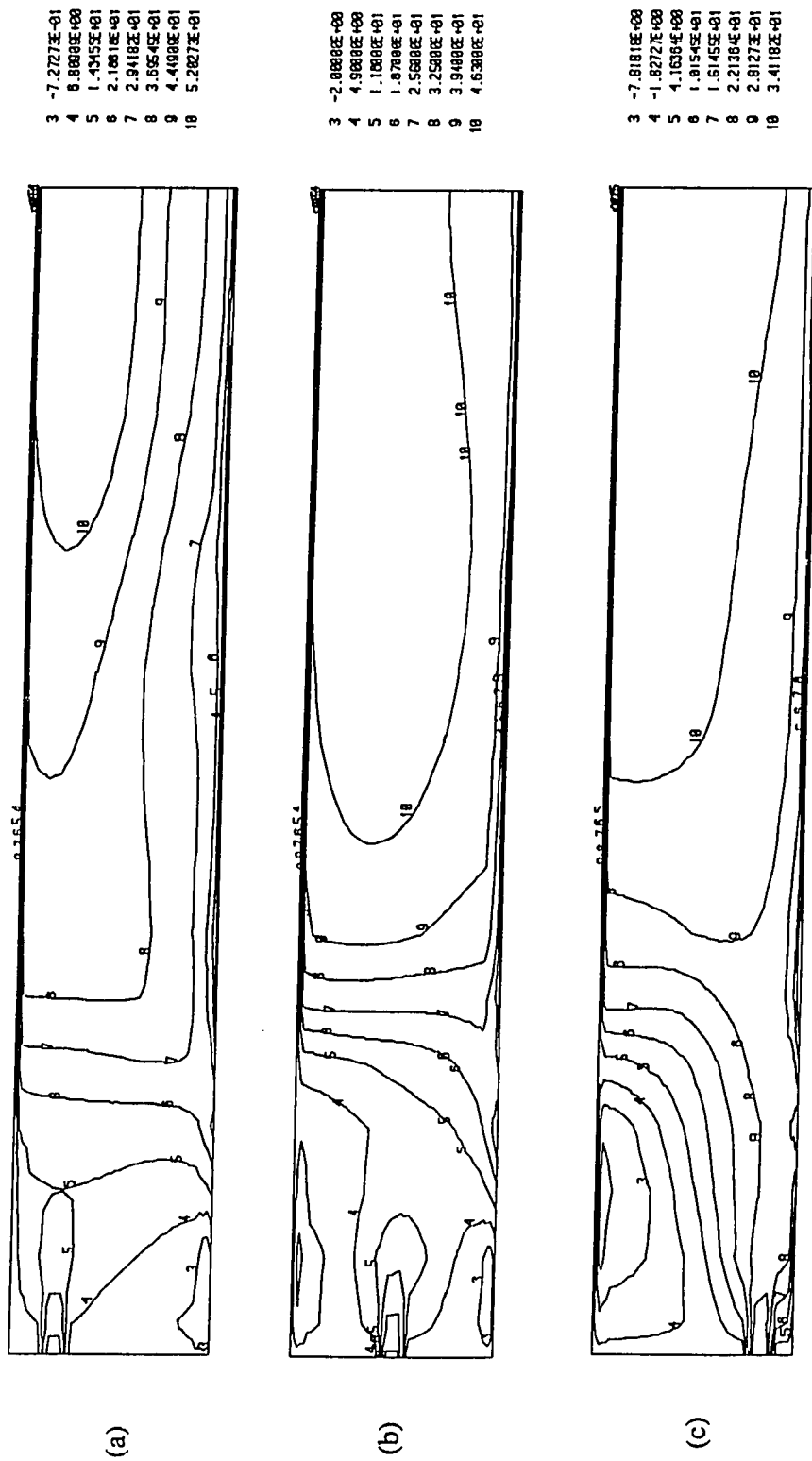


Figure 4.37 Predicted Gas Velocity in X- Direction (a) case 1 (b) case 2 (c) case 3.

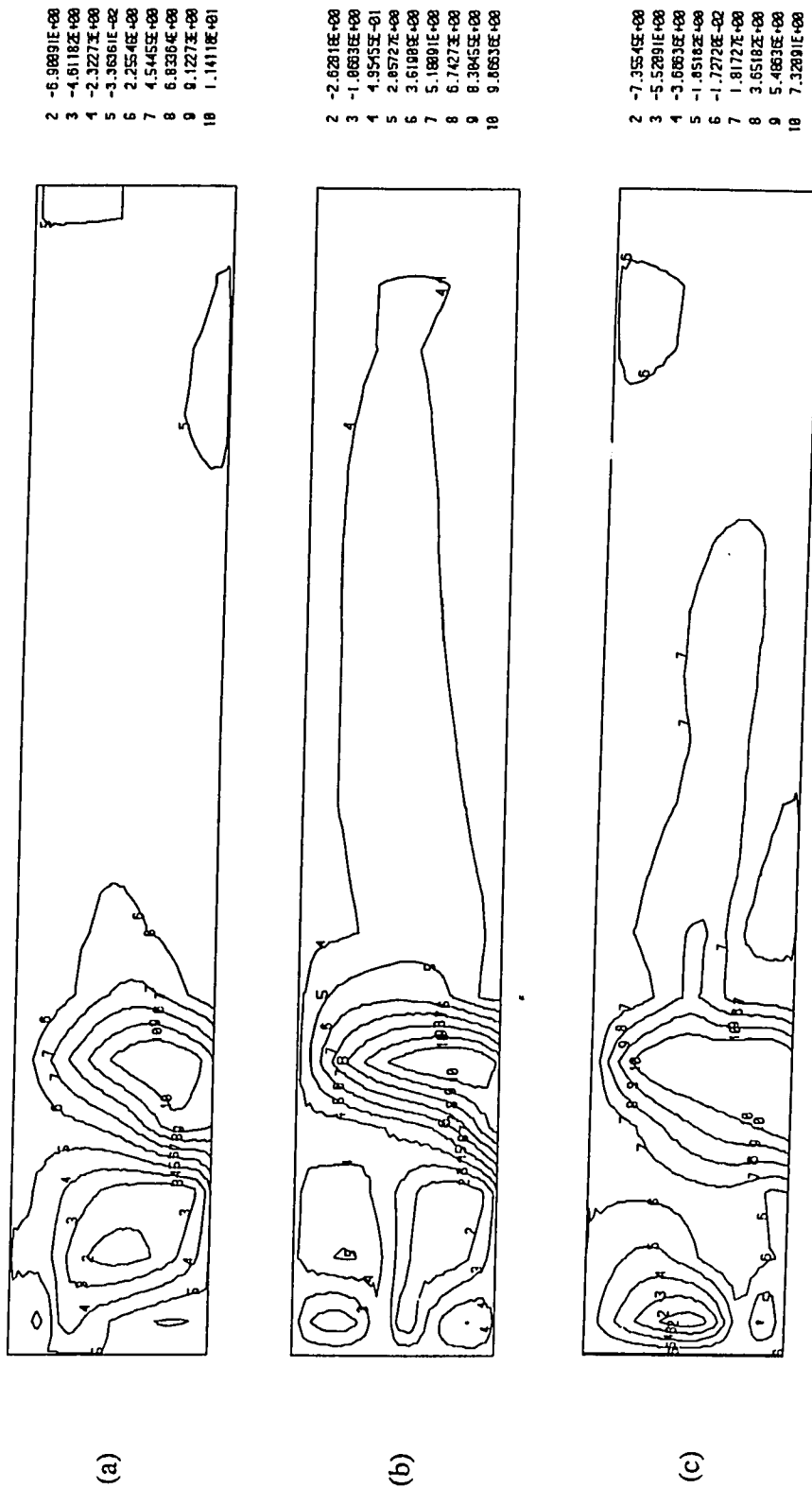
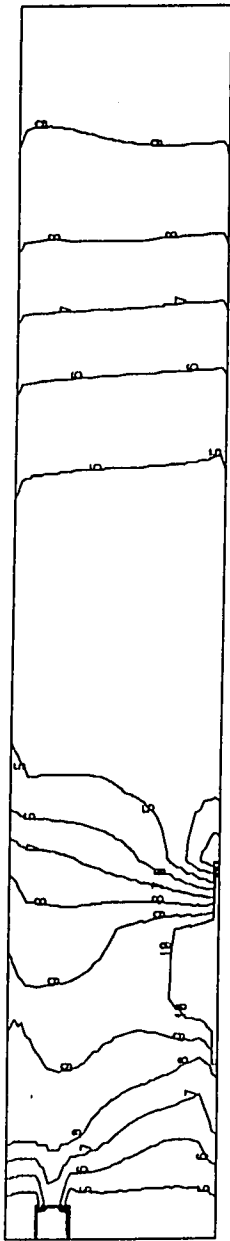


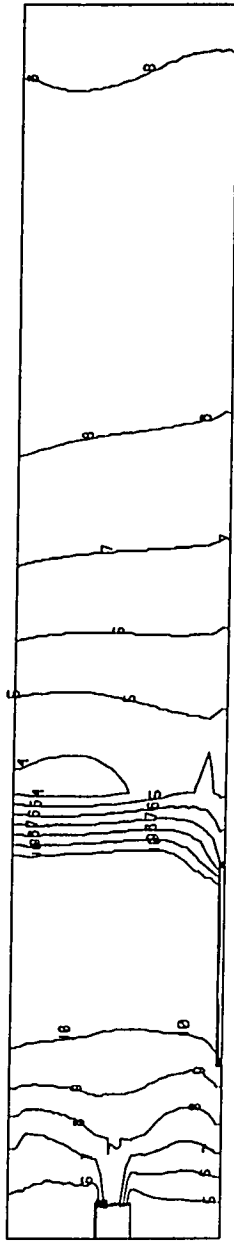
Figure 4.38 Predicted Gas Velocity in Y- Direction (a) case 1 (b) case 2 (c) case 3.

5 1.0008E+05
6 1.0003E+05
7 1.0006E+05
8 1.0009E+05
9 1.0011E+05
10 1.0014E+05



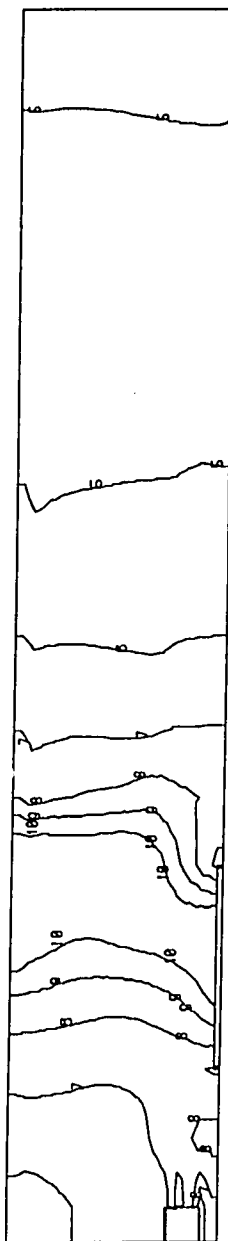
(a)

1 1.0358E+05
2 1.0351E+05
3 1.0353E+05
4 1.0355E+05
5 1.0357E+05
6 1.0359E+05
7 1.0360E+05
8 1.0362E+05
9 1.0364E+05
10 1.0366E+05



(b)

5 1.0040E+05
6 1.0043E+05
7 1.0046E+05
8 1.0049E+05
9 1.0051E+05
10 1.0054E+05



(c)

Figure 4.39 Predicted Contours of Pressure (a) case 1 (b) case 2 (c) case 3.

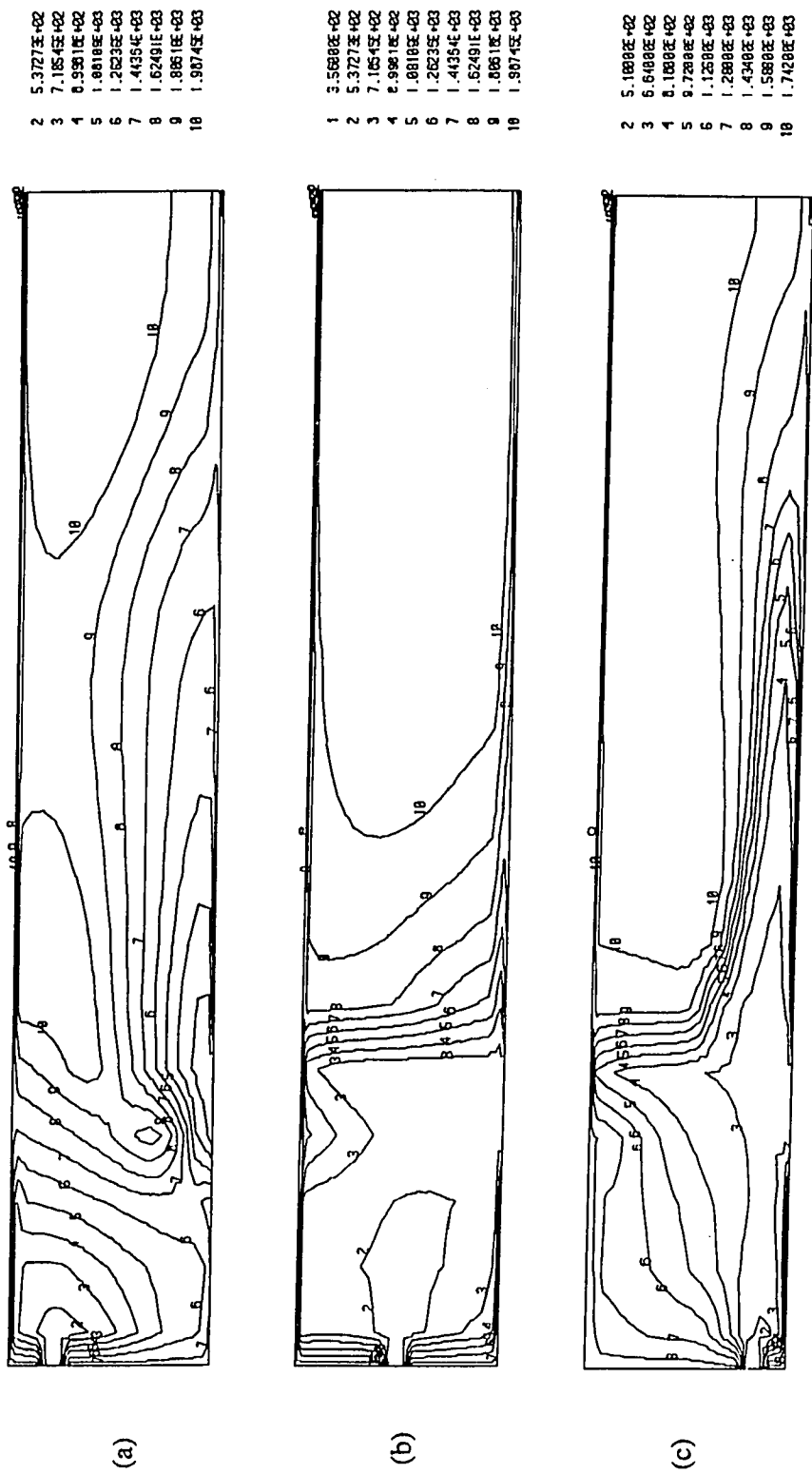


Figure 4.40 Predicted Contours of Temperature (a) case 1 (b) case 2 (c) case 3.

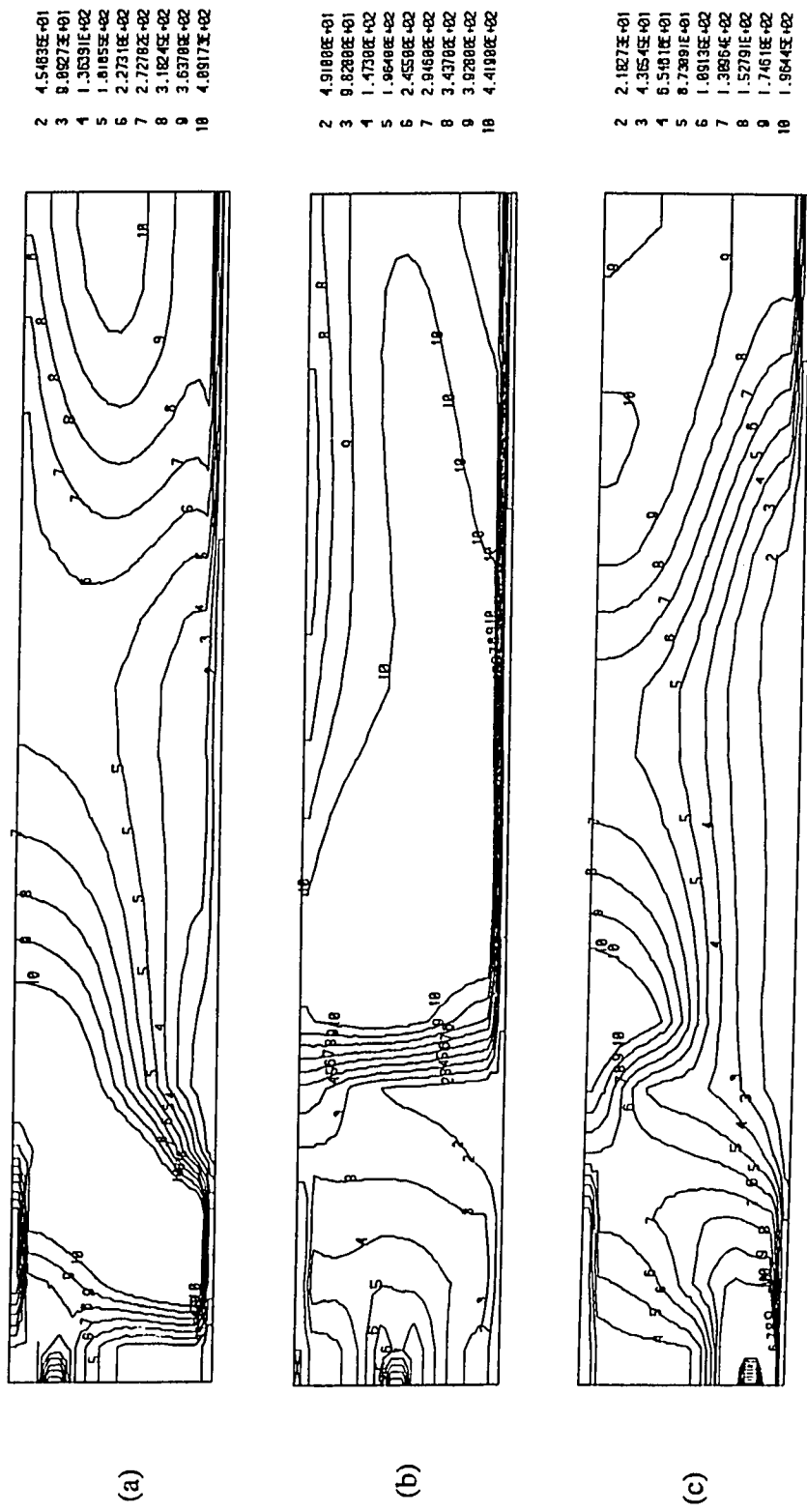


Figure 4.41 Predicted Contours of Turbulence Kinetic Energy (a) case 1 (b) case 2 (c) case 3.

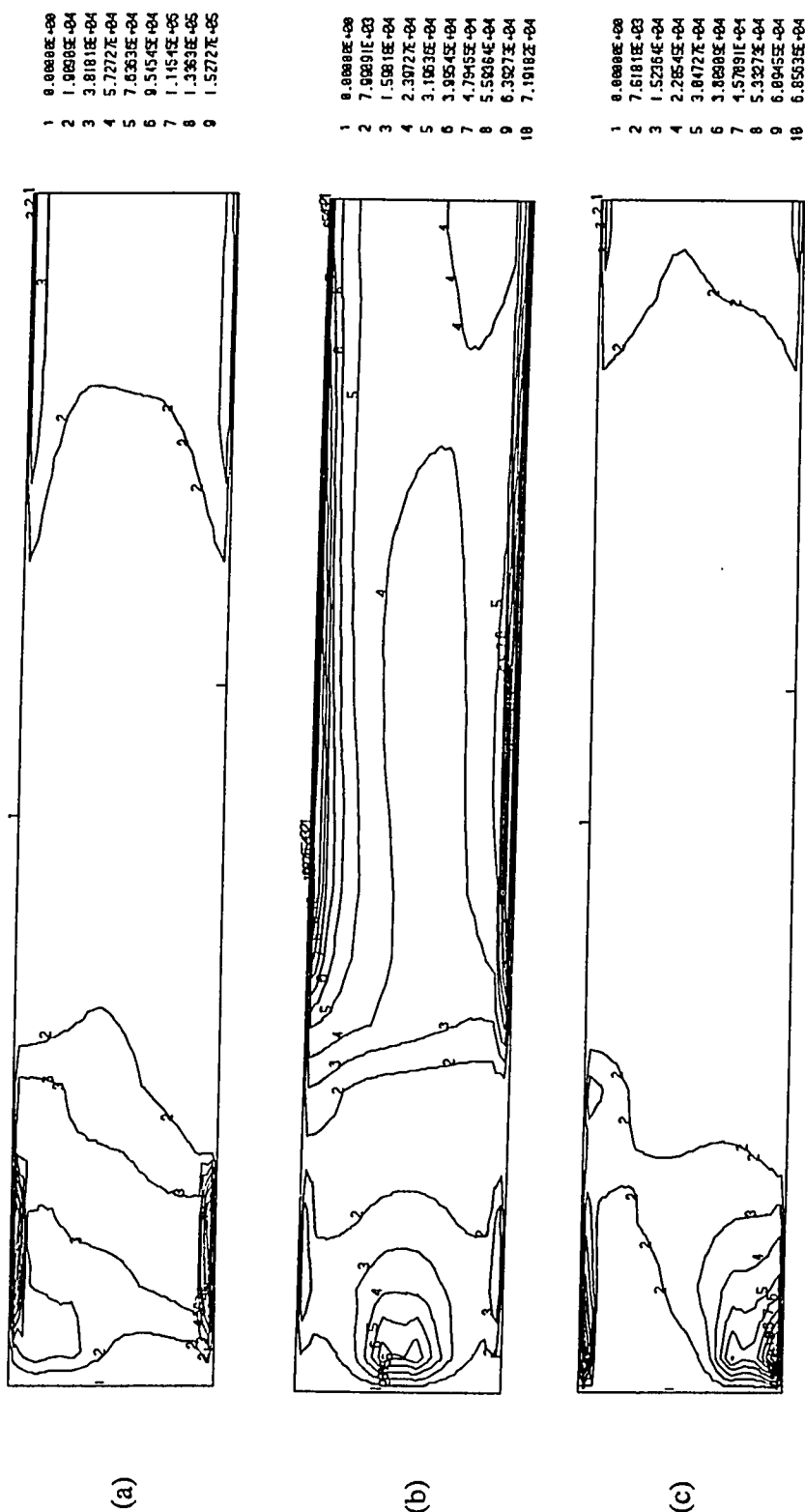


Figure 4.42 Predicted Contours of Turbulence Dissipation Rate (a) case 1 (b) case 2 (c) case 3.

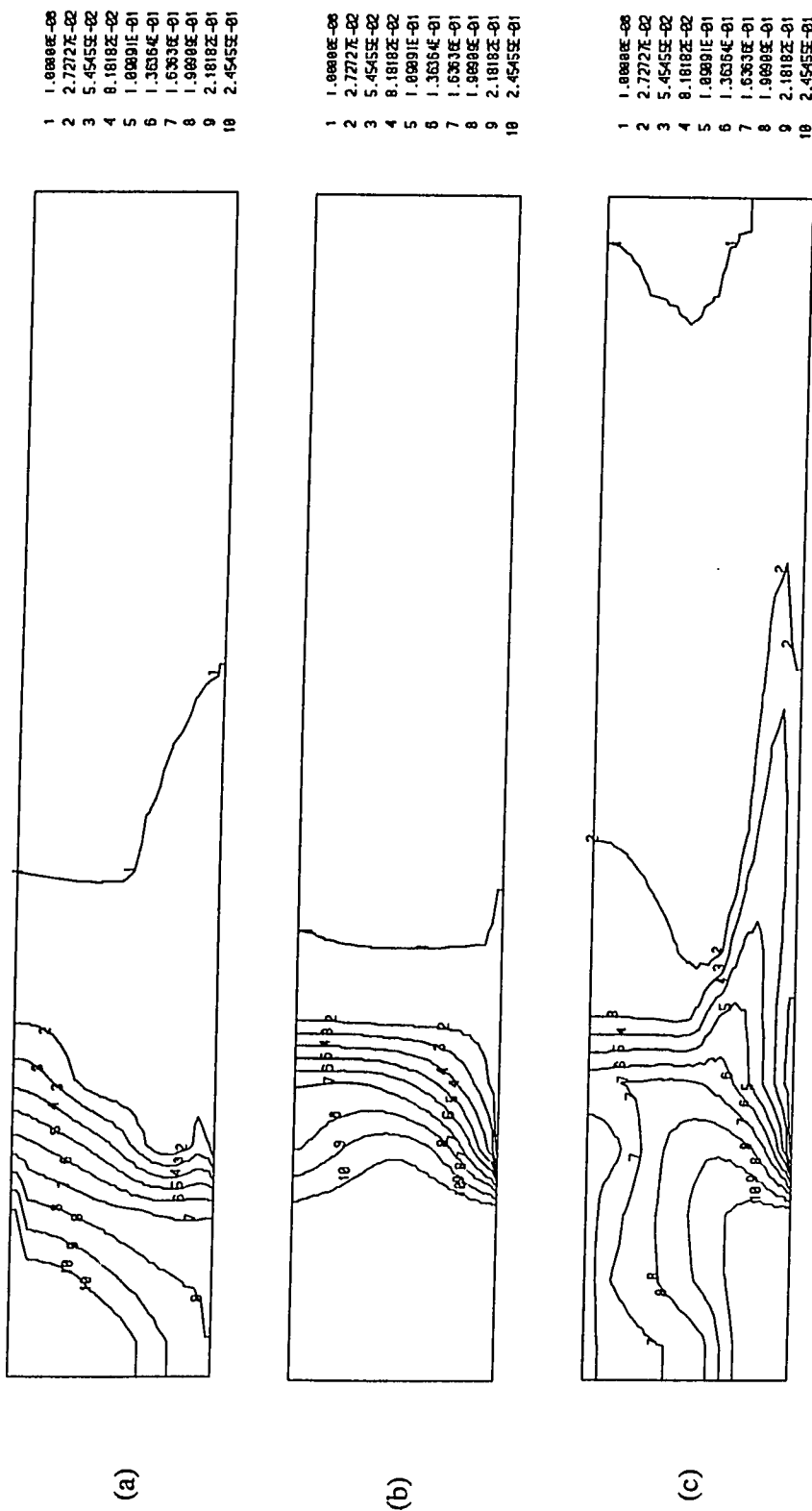


Figure 4-43 Predicted Contours of CO Concentration (a) case 1 (b) case 2 (c) case 3.

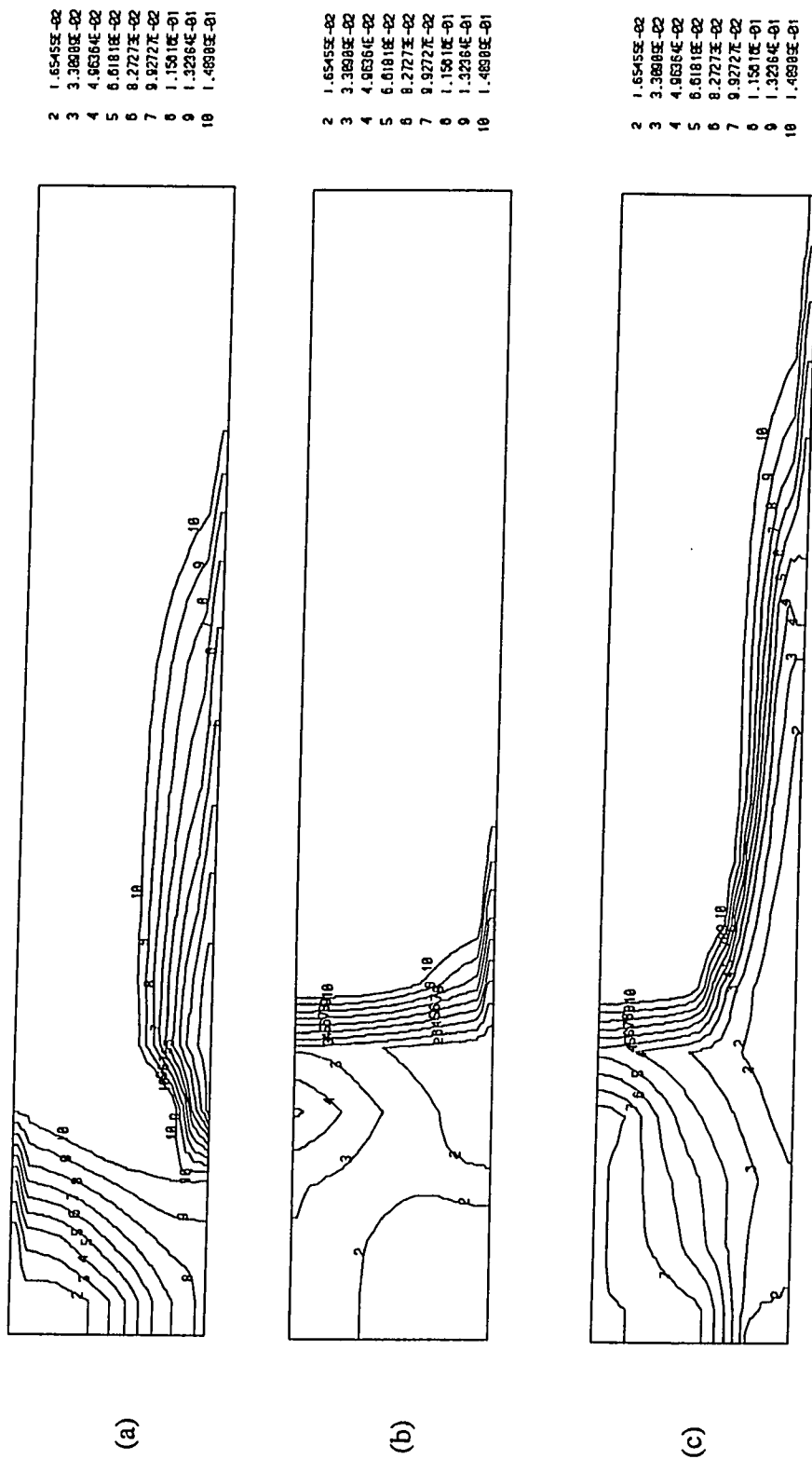


Figure 4.44 Predicted Contours of CO₂ Concentration (a) case 1 (b) case 2 (c) case 3.

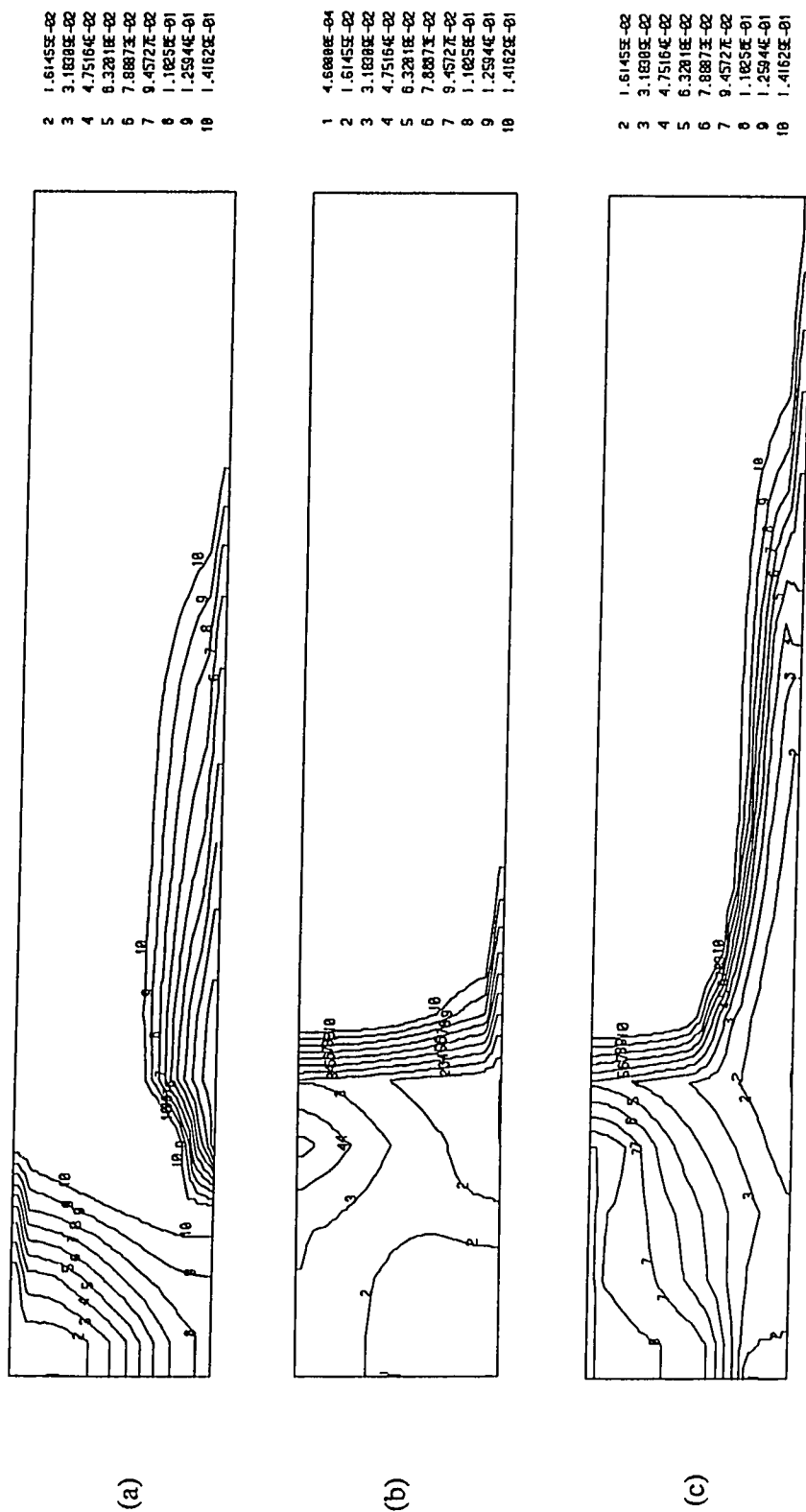


Figure 4.45 Predicted Contours of H_2O Concentration (a) case 1 (b) case 2 (c) case 3.

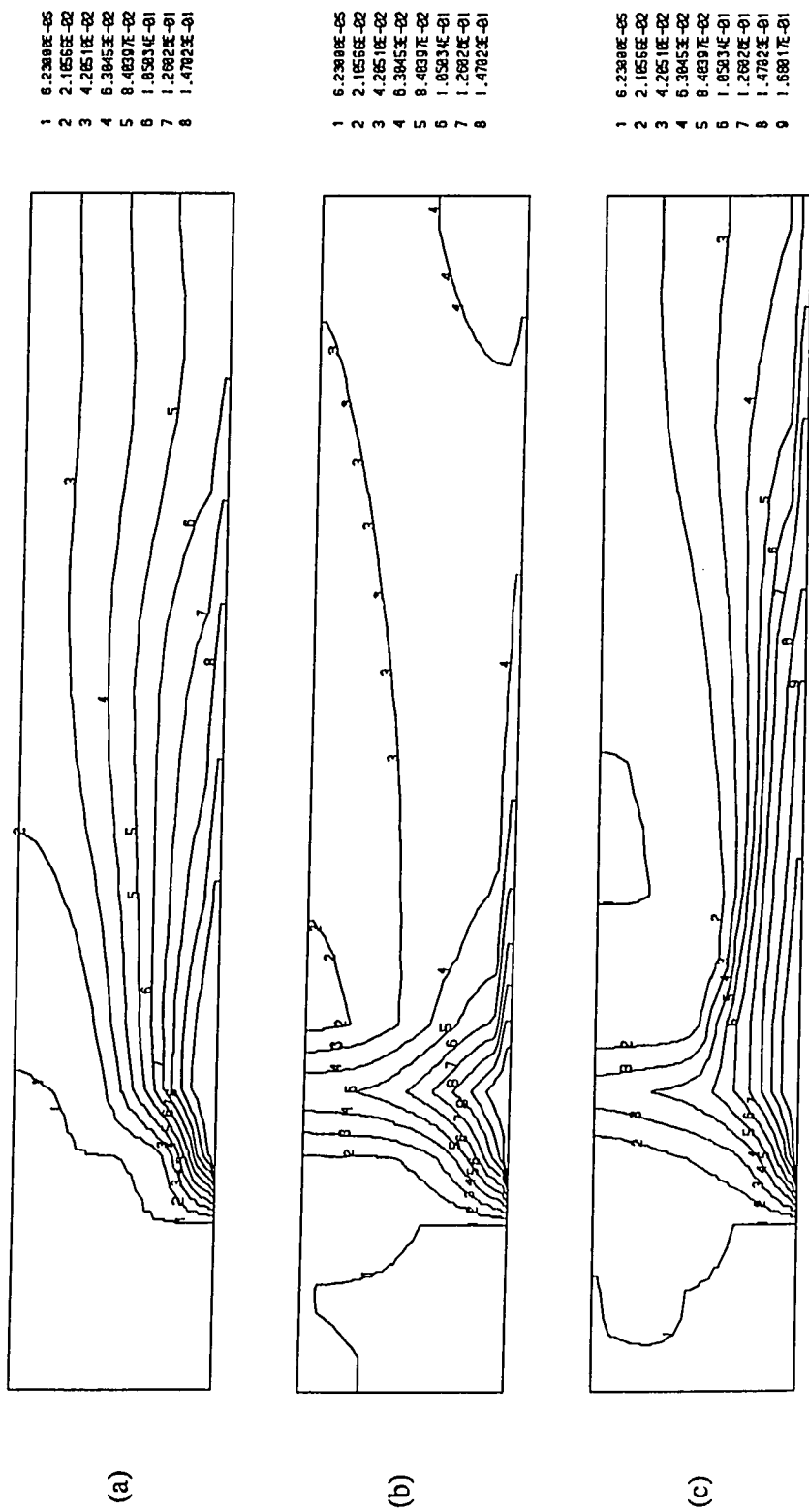


Figure 4.46 Predicted Contours of O_2 Concentration (a) case 1 (b) case 2 (c) case 3.

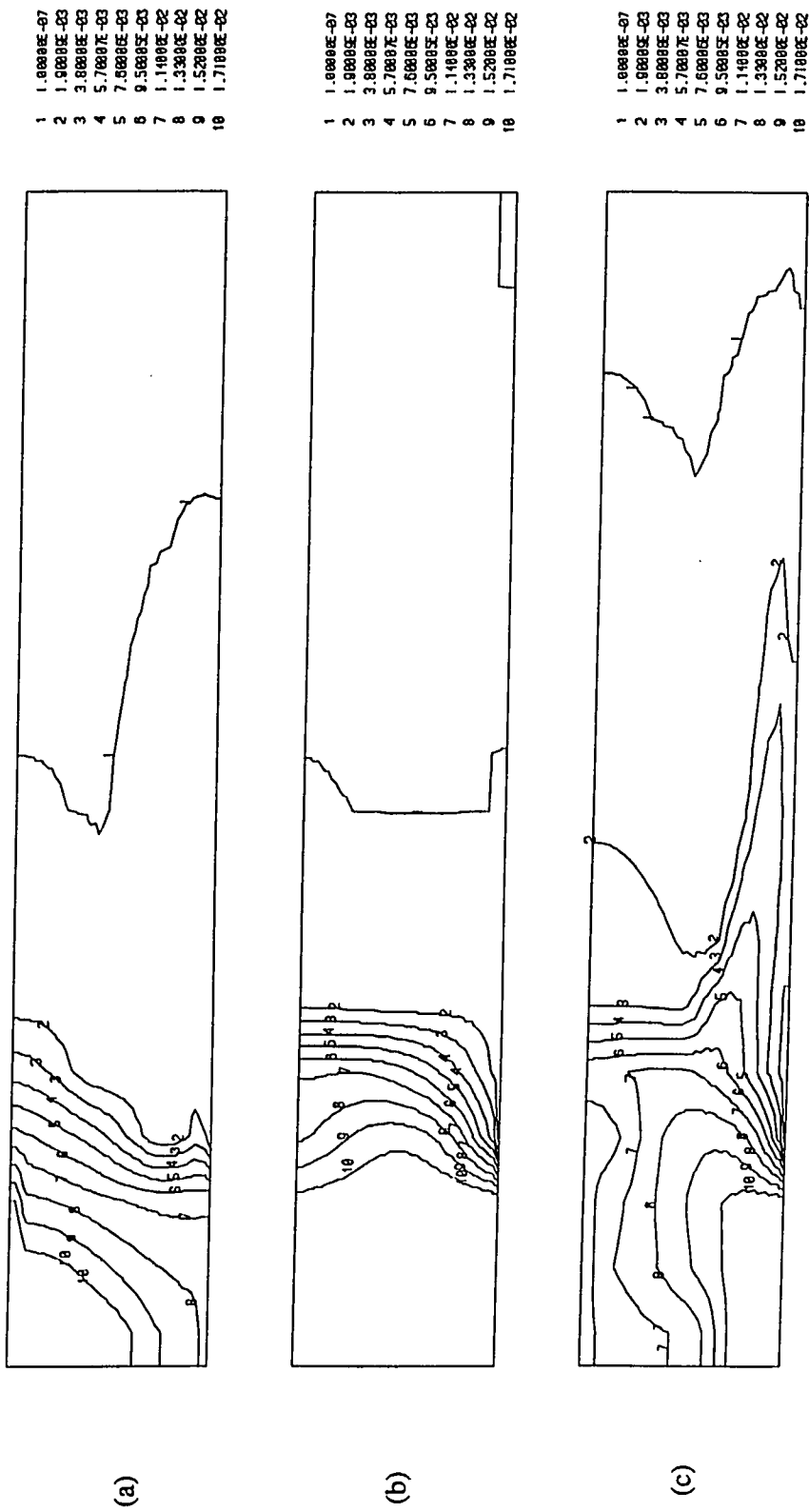


Figure 4.47 Predicted Contours of CH₄ Concentration (a) case 1 (b) case 2 (c) case 3.

Chapter 5

CONCLUSIONS AND RECOMMENDATIONS

A model was developed for solving the two-dimensional flow and combustion of pulverized coal by diffusion flames. The model was used to study the interaction between flow and combustion in flames produced by arranging the location of primary and secondary inlets. The calculation of an axially symmetrical problem is, generally speaking, more difficult than that of a two-dimensional one. The asymmetric cylindrical problems increases the difficulty profoundly over those of 2-dimensional cases.

5.1 CONCLUSIONS

Sudden expansion flow:

This case is to evaluate the program's ability to solve the conservation of mass, momentum, and energy using κ - ϵ two-equation turbulence model, before solving the problem of combustion.

Assuming uniform velocity and temperature profiles at inlet and with inlet turbulence parameters (κ_0 , ϵ_0) chosen, the computational predictions for velocity, kinetic energy in two-dimensional ducts turn out to compare satisfactorily with experimental data taken from in cylindrical geometries.

Outlined below are some of the results and conclusions of this work which could prove useful for practical furnace designs.

Effect of recirculation area on coal combustion:

The size of the recirculation zone can be controlled by varying the location of inlet. With inlet width h_3 kept constant, and by decreasing h_2 and increasing h_1 , the recirculation area ratio, defined as the total flow field area over recirculation area, increases linearly with h_1 and decreases linearly with h_3 . This tendency has also been proven by order of magnitude analysis.

When the location of primary streams is highly off-centered, we observe:

- (a) The formation of one large recirculation zone, instead of two small separated recirculation zones.
- (b) A high temperature burned gas region penetrating deep into the recirculation zone.
- (c) The occurrence of strong turbulence and thorough mixing, followed by more efficient burning.

These are favorable for stable and intensive combustion.

Effect of the location of the secondary air flow on coal combustion:

Secondary air flow is to be supplied from the side wall, the location of the air inlet must correspond to the region where flow re-attaches. This maximizes the combustibility by reducing the amount of unburnt products.

Effect of the location of the primary streams on coal combustion:

By arranging the location of primary streams, efficiency can be also controlled.

5.2 RECOMMENDATIONS REGARDING NUMERICAL PROCEDURES

- (1) From the property contours, it is clear that the changes are quite small in the downstream region. Therefore a coarse mesh can be used for that region.
- (2) The region closest to the inlet has strong interactions with flow, flames, and particles. Thus, one should use a fine mesh in that region in order to get better results.
- (3) To improve existing estimates, experimental properties such as κ_0 , ϵ_0 must be incorporated whenever they become available.
- (4) To save computational time, implicit scheme for solid phase must be used to increase the time step.

Further work:

- (1) The radiation between gas and particles should be taken into account. This effect can influence the particles' characteristics when the temperature difference is large.
- (2) An acoustic field of specific or varying intensity can be applied to the fluid to study the influence between particles and gas such as slip velocity and acoustically induced flow in the gas. Both of these will increase the combustion heat and mass transfer to and from the particles, thus enhancing the gasification or the combustion processes.

Bibliography

- [1] Hendrickson, T. A. (ed.) *Synthetic Fuels Data Handbook*, Cameron Engineers, Inc., Denver, CO (1975).
- [2] Essenhigh, R. H. "Combustion and Flame Propagation in Coal Systems: A Review," *16th Symposium (International) on Combustion*, The Combustion Institute, Pittsburgh, PA, 372 (1976).
- [3] Lowry, H. H. (ed.), *Chemistry of Coal Utilization*, supplementary volume, Wiley, New York, NY (1963).
- [4] Given, P. H. (ed.), *American Conference on Coal Science*, Adv. Chem. Ser. 55, American Chemical Society, Washington, DC (1964).
- [5] Neavil, R. C., "Coal Origin, Analysis, and Classification," Paper No. 111b, AIChE 72nd Annual Meeting, New York, NY (1979).
- [6] Spackman, W., "The Characteristics of American Coals in Relation to Their Conversion into Clean Energy Fuels," Pennsylvania State University, DDE Report FE-2030-13, University Park, PA (May 1980).
- [7] Hamblen, D. G., Solomon, P. R., and Hobbs, R. H., "Physical and Chemical Characterization of Coal," U.S. Environmental Protection Agency EPA-600/7-80-106, United Technologies Research Center, Hartford, CN (May 1980).
- [8] Elliott, M. A. (ed.), *Chemistry of Coal Utilization*, second supplementary volume, Wiley, New York, NY (1981).

- [9] Smoot, L. D., and Pratt, D. T. (eds.), *Pulverized Coal Combustion and Gasification*, Plenum, New York, NY (1979).
- [10] Smoot, L. D., and Smith, P. J., "Modeling Pulverized Coal Reaction Processes" (L. D. Smoot and D. T. Pratt eds.), *Pulverized Coal Combustion and Gasification*, Plenum, New York, NY 217 (1979).
- [11] Gray, D., Cogoli, J. G., and Essenhigh, R. H., "Problems in Pulverized Coal and Char Combustion", No. 6, *Adv. Chem. Ser.* **131**, 72, American Chemical Society, Washington, DC (1976).
- [12] Smoot, L. D., and Smith, P. J., *Coal Combustion and Gasification*, Plenum, New York, NY (1985).
- [13] Field, M. A., Gill, D. W., Morgan, B. B., and Hawksley, P. G. W., "Combustion of Pulverized Fuel: Part 6. Reaction Rate of Carbon Particles", *Brit. Coal Util. Res. Assoc. Monogr. Bull.* **31**, 285 (1967).
- [14] Edelman, R. B., and Harsha, P. T., "Laminar and Turbulent Gas Dynamics in Combustors – Current Status," *Progress in Energy and Combustion Science*, **4**, 1 (1978).
- [15] Lilley, D. G., "Flowfield Modeling in Practical Combustors: A Review," *J. Energy*, **3**, 193 (1979).
- [16] Williams, F. A., and Libby, P. A., AIAA Paper 80-0012, 18th Aerospace Sciences Meeting, Pasadena, CA(1980).
- [17] Smoot, L. D., "Pulverized Coal Diffusion Flames: A Perspective Through Modeling", *18th Symposium (International) on Combustion*, The Combustion Institute, Pittsburgh, PA, 1185 (1980).

- [18] Gibson, M. M., and Morgan, B. B., "Mathematical Model of Combustion of Solid Particles in a Turbulent Streams with Recirculation," *J. Inst. Fuel.* **43**, 517 (1970).
- [19] Gosman, A. D., Pun, W. M., Ruchal, A. K., Spalding, D. B., and Wolfshstein, R., *Heat and Mass Transfer in Recirculating Flow*, Academic Press, New York, NY (1969).
- [20] Richter, W., and Quack, R., "Mathematical Model of a Low-Volatile Pulverized Fuel Flame," *Heat Transfer in Flames* (N. H. Afgan and J. M. Beer, eds.), Scripta Technica, 95 (1974).
- [21] Smith, P. J., and Smoot, L.D., "One Dimensional Model for Pulverized Coal Combustion and Gasification," *Combust. Sci. Technol.*, **23**, 17 (1980).
- [22] Smith, P. J., Fletcher, T. J., and Smoot, L. D., "Model for Pulverized Coal-Fired Reactors", *18th Symposium (International) on Combustion*, The Combustion Institute, Pittsburgh, PA, 1285 (1980).
- [23] Lockwood, F. C., Salooja, A. P., and Syed, S. A., "A Prediction Method for Coal-Fired Furnaces," *Combust. Flame* **38**, 1 (1980).
- [24] Patankar, S. V., *Studies in Convection*, (B. W. Launder, ed.), Vol. 1, Academic Press, New York, NY (1975).
- [25] Blake, T. R., Brownell, D. H., Jr., Garg, S. K., Herline, W. E., Pritchett, J. W., and Schneyer, G. P., *Computer Modeling of Coal Gasification Reactors, Year 2*, U.S. Department of Energy Report, FE-1770-32, (1977).
- [26] Patankar, S. V., *Numerical Heat Transfer and Fluid Flow*, Washington, New York, NY (1980).

- [27] Hutchinson, P., Khalil, E. E., Whitelaw, J. H., and Wigley, G., "The Calculation of Furnace Flow Properties and Their Experimental Verification", *ASME J. Heat Transfer*, **81**, 276 (1976).
- [28] Hutchinson, P., Khalil, E. E., Whitelaw, J. H., and Wigley, G., "Experimental Investigations of Flow and Combustion in Axisymmetric furnaces", *J. Energy*, **1**, 210 (1977).
- [29] Khalil, E. E., "On the Modelling of Turbulent Reacting Flows in Furnaces and Combustion Chambers", *Acta Astronautica*, **6**, 449 (1979).
- [30] Gosman, A. D., Lockwood, F. C., and Salooja, A. P., "The Prediction of Cylindrical Furnaces Gaseous Fueled with Premixed and Diffusion Burners", *17th Symposium (Int.) on Combustion*, The Combustion Institute, Pittsburgh, PA, 747 (1979).
- [31] Launder, B. E., and Spalding, D. B., "The Numerical Computation of Turbulent Flows", *Computational Methods in Applied Mechanics and Engineering*, **3**, 269 (1974).
- [32] Gosman, A. D., Khalil, E. E., and Whitelaw, J. H., "The Calculation of Two Dimensional Turbulent Recirculating Flows", *1st Symposium on Turbulent Shear Flows*, **1**, 1335 (1977).
- [33] Hinze, J. O., *Turbulence*, McGraw-Hill, (1959).
- [34] Khalil, E. E., Spalding, D. B. and Whitelaw, J. H., "The Calculation of Local Flow Properties in Two-Dimensional Furnaces", *Int. J. Heat Mass Transfer*, **18**, 775 (1975).
- [35] Anthony, D. B., and Howard, J. B., "Coal Devolatilization and Hydrogasification", *AIChE J.* **22**, 625 (1976).

- [36] Howard, J. B., "Fundamentals of Coal Pyrolysis and Hydropyrolysis", *Chemistry of Coal Utilization*, second supplementary volume (M. A. Elliott, ed.), Wiley, New York, NY, 665 (1981).
- [37] Horton, M. D., "Fast Pyrolysis", *Pulverized-Coal Combustion and Gasification*, (L. D. Smoot and D. T. Pratt, eds.), Plenum, New York, NY (1979).
- [38] Wendt, J. O. L., "Fundamental Coal Combustion Mechanisms and Pollutant Formation in Furnaces", *Progr. Energy Combustion Science*, **6**, 201 (1980).
- [39] Kobayashi, H., Howard, J. B., and Sarofim, A. F., "Coal Devolatilization at High Temperatures," *18th Symposium (International) on Combustion*, The Combustion Institute, Pittsburgh, PA, 411 (1980).
- [40] Badzioch, S. and Hawksley, P. G. W., "Kinetic of Thermal Decomposition of Pulverized Coal Particles", *Ind. Eng. Chem. Process Design and Development*, **9**, 521 (1970).
- [41] Ubhayakar, S. K., Stickler, D. B., Von Rosenberg, C. W. and Gannon, R. E., "Rapid Devolatilization of Pulverized Coal in Hot Combustion Gases," *16th Symposium (International) on Combustion*, The Combustion Institute, Pittsburgh, PA, 427 (1976).
- [42] Jamaluddin, A. S., Truelove, J. S. and Wall, T. F., "Devolatilization of Bituminous Coals at Medium to High Heating Rates," *Combust. Flame* **63**, 329 (1986).
- [43] Khalil, E. E., *Modeling of Furnaces and Combustors*, Abacus Press, (1982).
- [44] Arora, R., Kuo, K. K., and Razdan, M. K., "Near-Wall Treatment for Turbulent Boundary-Layer Computations," *AIAA J.*, **20**, 1481 (1982).
- [45] Putnam, A., *ARS J.*, **31**, 1467 (1961).

- [46] Faeth, G. M., "Evaporation and Combustion of Sprays," *Progress in Energy and Combustion Science*, **9**, 1, Pergamon Press, New York, (1983).
- [47] Dickerson, R. A., and Schuman, M. D., *J. Spacecraft*, 99 (1960).
- [48] Caretto, L. S., Gosman, A. D., Patankar, S. V., and Spalding, D. B., "Two Calculation Procedures for Steady Three-Dimensional Flows with Recirculation," *Proceedings of The Third International Conference on Numerical Methods in Fluid Dynamics*, Berlin, Heidelberg, New York, Springer (1972).
- [49] Barbin, A. R., and Jones, J. B., "Turbulent Flow in The Inlet Region of a Smooth Pipe," *J. Basic Engineering*, **85** (1) , 23 (1963).
- [50] Laufer, J., *NBS Report*, **1174**, (1952)

Appendix A

DERIVATION OF THE GOVERNING EQUATIONS

A.1 GAS PHASE

A.1.1 MASS

$$\left[\begin{array}{l} \text{the rate of gaseous mass} \\ \text{accumulation in the control} \\ \text{volume occupied by gases} \end{array} \right] =$$

$$\left[\begin{array}{l} \text{the mass flux} \\ \text{convected into} \\ \text{control volume} \end{array} \right] + \left[\begin{array}{l} \text{the rate of gaseous mass addition} \\ \text{due to devolatilization and} \\ \text{heterogeneous reaction of solid particles} \end{array} \right]$$

$$\begin{aligned} \left[\begin{array}{l} \text{the mass flux} \\ \text{convected into} \\ \text{control volume} \end{array} \right] &= \rho_g U_g \phi \Delta y \Delta z - \left(\rho_g U_g \phi \Delta y \Delta z + \frac{\partial(\rho_g U_g \phi \Delta y \Delta z)}{\partial x} dx \right) \\ &\quad + \rho_g V_g \phi \Delta x \Delta z - \left(\rho_g V_g \phi \Delta x \Delta z + \frac{\partial(\rho_g V_g \phi \Delta x \Delta z)}{\partial y} dy \right) \\ &= - \frac{\partial(\rho_g U_g \phi \Delta y \Delta z)}{\partial x} dx - \frac{\partial(\rho_g V_g \phi \Delta x \Delta z)}{\partial y} dy \end{aligned}$$

$$\left[\begin{array}{l} \text{the rate of gaseous mass addition} \\ \text{due to devolatilization and} \\ \text{heterogeneous reaction of solid particles} \end{array} \right] = \dot{W}_m \Delta x \Delta y \Delta z$$

$$= \dot{M}_p \tilde{n} \Delta x \Delta y \Delta z$$

$$\left[\begin{array}{l} \text{the rate of gaseous mass} \\ \text{accumulation in the control} \\ \text{volume occupied by gases} \end{array} \right] = \frac{\partial(\rho_g \phi \Delta x \Delta y \Delta z)}{\partial t}$$

Thus,

$$\begin{aligned} \Rightarrow & \frac{\partial(\rho_g \phi)}{\partial t} \Delta x \Delta y \Delta z + \frac{\partial(\rho_g U_g \phi)}{\partial x} \Delta x \Delta y \Delta z + \frac{\partial(\rho_g V_g \phi)}{\partial y} \Delta x \Delta y \Delta z \\ & = \dot{W}_m \Delta x \Delta y \Delta z = \dot{M}_p \tilde{n} \Delta x \Delta y \Delta z \end{aligned}$$

The mass balance therefore becomes :

$$\frac{\partial(\rho_g \phi)}{\partial t} + \frac{\partial(\rho_g U_g \phi)}{\partial x} + \frac{\partial(\rho_g V_g \phi)}{\partial y} = \dot{M}_p \tilde{n} = \dot{W}_m \quad (\text{A.1})$$

A.1.2 MOMENTUM

$$\left[\begin{array}{l} \text{rate of increase} \\ \text{of momentum in} \\ \text{the control volume} \end{array} \right] = \left[\begin{array}{l} \text{net rate of} \\ \text{momentum flux into} \\ \text{control volume} \end{array} \right] + \left[\begin{array}{l} \text{summation of forces} \\ \text{acting on the} \\ \text{control volume} \end{array} \right]$$

(A) x - momentum equation :

$$\left[\begin{array}{l} \text{rate of increase} \\ \text{of momentum in} \\ \text{the control volume} \end{array} \right] = \frac{\partial(\rho_g U_g \phi \Delta x \Delta y \Delta z)}{\partial t} = \frac{\partial(\rho_g U_g \phi)}{\partial t} \Delta x \Delta y \Delta z$$

$$\left[\begin{array}{l} \text{net rate of} \\ \text{momentum flux into} \\ \text{control volume} \end{array} \right] = (1) + (2)$$

$$(1) = \rho_g U_g \phi U_g \Delta y \Delta z + \rho_g U_g \phi V_g \Delta x \Delta z - (\rho_g U_g \phi U_g \Delta y \Delta z$$

$$+ \frac{\partial(\rho_g U_g U_g \phi \Delta y \Delta z)}{\partial x} dx + \rho_g U_g \phi V_g \Delta x \Delta z + \frac{\partial(\rho_g U_g V_g \phi \Delta x \Delta z)}{\partial y} dy)$$

$$\begin{aligned} (2) &= \text{momentum of gasified particle mass due to the motion of the burning particles} \\ &= \dot{W}_m U_p \Delta x \Delta y \Delta z \end{aligned}$$

$$\left[\begin{array}{c} \text{summation of forces} \\ \text{acting on the} \\ \text{control volume} \end{array} \right] = (3) + (4) + (5)$$

$$\begin{aligned} (3) &= \text{pressure} \\ &= P \phi \Delta y \Delta z - \left(P \phi \Delta y \Delta z + \frac{\partial(P \phi \Delta y \Delta z)}{\partial x} dx \right) \\ &= -\frac{\partial(P \phi)}{\partial x} \Delta x \Delta y \Delta z \end{aligned}$$

$$\begin{aligned} (4) &= -\tau_{xx} \phi \Delta y \Delta z + \left(\tau_{xx} \phi \Delta y \Delta z + \frac{\partial(\tau_{xx} \phi \Delta y \Delta z)}{\partial x} dx \right) \\ &\quad -\tau_{yx} \phi \Delta x \Delta z + \left(\tau_{yx} \phi \Delta x \Delta z + \frac{\partial(\tau_{yx} \phi \Delta x \Delta z)}{\partial y} dy \right) \\ &= \frac{\partial(\tau_{xx} \phi)}{\partial x} \Delta x \Delta y \Delta z + \frac{\partial(\tau_{yx} \phi)}{\partial y} \Delta x \Delta y \Delta z \end{aligned}$$

$$\begin{aligned} (5) &= \text{drag force due to the relative velocity between gas and particles} \\ &= -A_s D_{vx} \Delta x \Delta y \Delta z \end{aligned}$$

The x-direction momentum equation therefore becomes :

$$\begin{aligned} &\frac{\partial(\rho_g U_g \phi)}{\partial t} + \frac{\partial(\rho_g U_g \phi U_g)}{\partial x} + \frac{\partial(\rho_g U_g \phi V_g)}{\partial y} \\ &= \dot{W}_m U_p - \frac{\partial(P \phi)}{\partial x} + \frac{\partial(\tau_{xx} \phi)}{\partial x} + \frac{\partial(\tau_{yx} \phi)}{\partial y} - D_{vx} A_s \end{aligned} \quad (A.2)$$

(B) y - momentum equation :

Similarly ,the y-direction momentum equation can be written as :

$$\begin{aligned}
& \frac{\partial(\rho_g V_g \phi)}{\partial t} + \frac{\partial(\rho_g U_g \phi V_g)}{\partial x} + \frac{\partial(\rho_g V_g \phi V_g)}{\partial y} \\
= & \dot{W}_m V_p - \frac{\partial(P\phi)}{\partial y} + \frac{\partial(\tau_{xy}\phi)}{\partial x} + \frac{\partial(\tau_{yy}\phi)}{\partial y} - D_{vy} A_s
\end{aligned} \tag{A.3}$$

A.1.3 ENERGY

$$\left[\begin{array}{c} \text{increase in stored} \\ \text{energy of} \\ \text{the system} \end{array} \right] = \left[\begin{array}{c} \text{energy} \\ \text{input to} \\ \text{system} \end{array} \right] + \left[\begin{array}{c} \text{work down} \\ \text{on system} \end{array} \right]$$

The rate of change of the total stored energy can be written as

$$\frac{dE}{dt} = \frac{\delta Q}{\delta t} + \frac{\delta W}{\delta t}$$

$$\begin{aligned}
\left[\begin{array}{c} \text{increase in stored} \\ \text{energy of} \\ \text{the system} \end{array} \right] &= \frac{\partial(\rho_g E \phi \Delta x \Delta y \Delta z)}{\partial t} \\
&= \frac{\partial(\rho_g E \phi)}{\partial t} \Delta x \Delta y \Delta z
\end{aligned}$$

$$\left[\begin{array}{c} \text{work down} \\ \text{on system} \end{array} \right] = (1) + (2) + (3) + (4)$$

$$\begin{aligned}
(1) &= \text{energy flux convected into C. V.} \\
&= \rho_g U_g E \phi \Delta y \Delta z - \left(\rho_g U_g E \phi \Delta y \Delta z + \frac{\partial(\rho_g U_g E \phi \Delta y \Delta z)}{\partial x} dx \right) \\
&\quad + \rho_g V_g E \phi \Delta x \Delta z - \left(\rho_g V_g E \phi \Delta x \Delta z + \frac{\partial(\rho_g V_g E \phi \Delta x \Delta z)}{\partial y} dy \right) \\
&= - \left(\frac{\partial(\rho_g U_g E \phi)}{\partial x} + \frac{\partial(\rho_g V_g E \phi)}{\partial y} \right) \Delta x \Delta y \Delta z
\end{aligned}$$

$$(2) = \text{heat conducted into the C. V.}$$

$$\begin{aligned}
&= q_x \phi \Delta y \Delta z - \left(q_x \phi \Delta y \Delta z + \frac{\partial(q_x \phi \Delta y \Delta z)}{\partial x} dx \right) \\
&\quad + q_y \phi \Delta x \Delta z - \left(q_y \phi \Delta x \Delta z + \frac{\partial(q_y \phi \Delta x \Delta z)}{\partial y} dy \right) \\
&= - \left(\frac{\partial(q_x \phi)}{\partial x} + \frac{\partial(q_y \phi)}{\partial y} \right) \Delta x \Delta y \Delta z
\end{aligned}$$

$$(3) = \left[\begin{array}{c} \text{the rate of heat loss} \\ \text{to solid particles} \end{array} \right]$$

$$= -A_s \hat{h}(T_g - T_p) \Delta x \Delta y \Delta z$$

$$(4) = \left[\begin{array}{c} \text{the rate of energy input} \\ \text{due to particles burning} \end{array} \right]$$

$$= -\dot{W}_h \Delta x \Delta y \Delta z$$

$$\left[\begin{array}{c} \text{energy} \\ \text{input to} \\ \text{system} \end{array} \right] = (5) + (6) + (7) + (8) + (9)$$

$$\begin{aligned}
(5) &= [\text{the rate of pressure work on the end surfaces of C.V.}] \\
&= PU_g \phi \Delta y \Delta z - \left(PU_g \phi \Delta y \Delta z + \frac{\partial(PU_g \phi \Delta y \Delta z)}{\partial x} dx \right) \\
&\quad + PV_g \phi \Delta x \Delta z - \left(PV_g \phi \Delta x \Delta z + \frac{\partial(PV_g \phi \Delta x \Delta z)}{\partial y} dy \right) \\
&= - \left(\frac{\partial(PU_g \phi)}{\partial x} + \frac{\partial(PV_g \phi)}{\partial y} \right) \Delta x \Delta y \Delta z
\end{aligned}$$

$$\begin{aligned}
(6) &= [\text{the rate of work done by viscous stresses}] \\
&= \frac{\tau_{xx} U_g \phi \Delta y \Delta z}{J} - \left(\frac{\tau_{xx} U_g \phi \Delta y \Delta z}{J} + \frac{1}{J} \frac{\partial(\tau_{xx} U_g \phi \Delta y \Delta z)}{\partial x} dx \right) \\
&\quad + \frac{\tau_{yy} V_g \phi \Delta x \Delta z}{J} - \left(\frac{\tau_{yy} V_g \phi \Delta x \Delta z}{J} + \frac{1}{J} \frac{\partial(\tau_{yy} V_g \phi \Delta x \Delta z)}{\partial y} dy \right) \\
&\quad + \frac{\tau_{yx} V_g \phi \Delta x \Delta z}{J} - \left(\frac{\tau_{yx} V_g \phi \Delta x \Delta z}{J} + \frac{1}{J} \frac{\partial(\tau_{yx} V_g \phi \Delta x \Delta z)}{\partial x} dx \right)
\end{aligned}$$

$$\begin{aligned}
& + \frac{\tau_{xy} U_g \phi \Delta y \Delta z}{J} - \left(\frac{\tau_{xy} U_g \phi \Delta y \Delta z}{J} + \frac{1}{J} \frac{\partial(\tau_{xy} U_g \phi \Delta y \Delta z)}{\partial y} dy \right) \\
& = - \left(\frac{\partial(\tau_{xx} U_g \phi)}{\partial x} + \frac{\partial(\tau_{yy} V_g \phi)}{\partial y} \right) \frac{\Delta x \Delta y \Delta z}{J} \\
& \quad - \left(\frac{\partial(\tau_{yx} V_g \phi)}{\partial x} + \frac{\partial(\tau_{xy} U_g \phi)}{\partial y} \right) \frac{\Delta x \Delta y \Delta z}{J} \\
(7) & = \left[\begin{array}{l} \text{the rate of work done by the drag force} \\ \text{acting on the gas phase due to solid particles} \end{array} \right] \\
& = - \left(A_s D_{vx} U_p + A_s D_{vy} V_p \right) \frac{\Delta x \Delta y \Delta z}{J}
\end{aligned}$$

$$\begin{aligned}
(8) & = [\text{the rate of pressure work for the dilatation of the gas in C.V.}] \\
& = -P \frac{\partial \phi}{\partial t} \frac{\Delta x \Delta y \Delta z}{J}
\end{aligned}$$

$$\begin{aligned}
& \frac{\partial(\rho_g E \phi)}{\partial t} + \frac{\partial(\rho_g U_g E \phi)}{\partial x} + \frac{\partial(\rho_g V_g E \phi)}{\partial y} + \frac{\partial(q_x \phi)}{\partial x} + \frac{\partial(q_y \phi)}{\partial y} \\
& + \frac{\partial(P U_g \phi)}{\partial x} + \frac{\partial(P V_g \phi)}{\partial y} + \frac{1}{J} \frac{\partial(\tau_{xx} U_g \phi)}{\partial x} + \frac{1}{J} \frac{\partial(\tau_{yy} V_g \phi)}{\partial y} \\
& + \frac{1}{J} \frac{\partial(\tau_{xy} U_g \phi)}{\partial x} + \frac{1}{J} \frac{\partial(\tau_{yx} V_g \phi)}{\partial y} + \frac{(A_s D_{vx} U_p + A_s D_{vy} V_p)}{J} \\
& + \frac{P}{J} \frac{\partial \phi}{\partial t} = A_s \hat{h} (T_g - T_p) + \dot{W}_h
\end{aligned} \tag{A.4}$$

A.2 SOLID PHASE

A.2.1 MASS

$$\left[\begin{array}{l} \text{the rate of particle mass} \\ \text{accumulation in the control} \\ \text{volume occupied by particles} \end{array} \right] =$$

$$\left[\begin{array}{c} \text{the particle mass} \\ \text{convection into the} \\ \text{control volume} \\ \text{occupied by particles} \end{array} \right] + \left[\begin{array}{c} \text{the rate of particle mass} \\ \text{reduction due to gasification} \\ \text{of solid particles} \end{array} \right]$$

$$\begin{aligned} \left[\begin{array}{c} \text{the particle mass} \\ \text{convection into the} \\ \text{control volume} \\ \text{occupied by particles} \end{array} \right] &= \rho_p U_p (1 - \phi) \Delta y \Delta z - (\rho_p U_p (1 - \phi) \Delta y \Delta z \\ &+ \frac{\partial(\rho_p U_p (1 - \phi) \Delta y \Delta z)}{\partial x} dx) + \rho_p U_p (1 - \phi) \Delta y \Delta z \\ &- (\rho_p U_p (1 - \phi) \Delta y \Delta z + \frac{\partial(\rho_p U_p (1 - \phi) \Delta y \Delta z)}{\partial y} dy) \\ &= -\left(\frac{\partial(\rho_p U_p (1 - \phi))}{\partial x} - \frac{\partial(\rho_p U_p (1 - \phi))}{\partial y} \right) \Delta x \Delta y \Delta z \end{aligned}$$

$$\left[\begin{array}{c} \text{the rate of particle mass} \\ \text{reduction due to gasification} \\ \text{of solid particles} \end{array} \right] = \dot{W}_m \Delta x \Delta y \Delta z = \dot{M}_p \tilde{n} \Delta x \Delta y \Delta z$$

$$\begin{aligned} \left[\begin{array}{c} \text{the rate of particle mass} \\ \text{accumulation in the control} \\ \text{volume occupied by particles} \end{array} \right] &= \frac{\partial(\rho_p (1 - \phi) \Delta x \Delta y \Delta z)}{\partial t} \\ &= \frac{\partial(\rho_p (1 - \phi))}{\partial t} \Delta x \Delta y \Delta z \end{aligned}$$

$$\begin{aligned} \Rightarrow & \left(\frac{\partial(\rho_p (1 - \phi))}{\partial t} + \frac{\partial(\rho_p U_p (1 - \phi))}{\partial x} + \frac{\partial(\rho_p V_p (1 - \phi))}{\partial y} \right) \Delta x \Delta y \Delta z \\ &= \dot{W}_m \Delta x \Delta y \Delta z = \dot{M}_p \tilde{n} \Delta x \Delta y \Delta z \end{aligned}$$

The mass balance therefore becomes :

$$\frac{\partial(\rho_p (1 - \phi))}{\partial t} + \frac{\partial(\rho_p U_p (1 - \phi))}{\partial x} + \frac{\partial(\rho_p V_p (1 - \phi))}{\partial y} = -\dot{W}_m = -\dot{M}_p \tilde{n} \quad (\text{A.5})$$

A.2.2 MOMENTUM

$$\left[\begin{array}{c} \text{rate of increase} \\ \text{of particle momentum} \\ \text{in the control volume} \end{array} \right] =$$

$$\left[\begin{array}{c} \text{summation of forces} \\ \text{acting on the} \\ \text{control volume} \end{array} \right] + \left[\begin{array}{c} \text{net rate of} \\ \text{momentum flux into} \\ \text{control volume} \end{array} \right]$$

(A) x - momentum equation :

$$\left[\begin{array}{c} \text{rate of increase} \\ \text{of particle momentum} \\ \text{in the control volume} \end{array} \right] = \frac{\partial(\rho_p U_p(1 - \phi))}{\partial t} \Delta x \Delta y \Delta z$$

$$\left[\begin{array}{c} \text{net rate of} \\ \text{momentum flux into} \\ \text{control volume} \end{array} \right] = (1) + (2)$$

$$\begin{aligned} (1) = & \rho_p U_p(1 - \phi) U_p \Delta y \Delta z + \rho_p U_p(1 - \phi) V_p \Delta x \Delta z \\ & - \left(\rho_p U_p(1 - \phi) U_p \Delta y \Delta z + \frac{\partial(\rho_p U_p(1 - \phi) U_p \Delta y \Delta z)}{\partial x} dx \right. \\ & \left. + \rho_p U_p(1 - \phi) V_p \Delta x \Delta z + \frac{\partial(\rho_p U_p(1 - \phi) V_p \Delta x \Delta z)}{\partial y} dy \right) \end{aligned}$$

$$\begin{aligned} (2) = & \text{loss of particle linear momentum due to gasification of particle into} \\ & \text{gas phase} \\ = & \dot{W}_m U_p \Delta x \Delta y \Delta z \end{aligned}$$

$$\begin{aligned}
 \left[\begin{array}{c} \text{summation of forces} \\ \text{acting on the} \\ \text{control volume} \end{array} \right] &= \text{drag force due to the relative velocity between} \\
 &\text{gas and particles} \\
 &= A_s D_{vx} \Delta x \Delta y \Delta z
 \end{aligned}$$

The x-direction momentum equation therefore becomes :

$$\frac{\partial(\rho_p U_p(1-\phi))}{\partial t} + \frac{\partial(\rho_p U_p(1-\phi)U_p)}{\partial x} + \frac{\partial(\rho_p U_p(1-\phi)V_p)}{\partial y} = \dot{W}_m U_p + A_s D_{vx} \quad (\text{A.6})$$

(B) y - momentum equation : Similarly, the y-direction momentum equation can be written as :

$$\frac{\partial(\rho_p V_p(1-\phi))}{\partial t} + \frac{\partial(\rho_p V_p(1-\phi)U_p)}{\partial x} + \frac{\partial(\rho_p V_p(1-\phi)V_p)}{\partial y} = \dot{W}_m V_p + A_s D_{vy} \quad (\text{A.7})$$

After rearranging with mass equation, momentum equation can be finally written as

$$\rho_p(1-\phi) \left[\frac{\partial U_p}{\partial t} + U_p \frac{\partial U_p}{\partial x} + V_p \frac{\partial U_p}{\partial y} \right] = A_s D_{vx} \quad (\text{A.8})$$

$$\rho_p(1-\phi) \left[\frac{\partial V_p}{\partial t} + U_p \frac{\partial V_p}{\partial x} + V_p \frac{\partial V_p}{\partial y} \right] = A_s D_{vy} \quad (\text{A.9})$$

Appendix B

DIMENSIONLESS GOVERNING EQUATIONS

B.1 NONDIMENSIONAL VARIABLES

Define parameters

$$\rho_g^* = \frac{\rho_g}{\rho_{go}}$$

$$\phi^* = \frac{\phi}{\phi_o}$$

$$t^* = \frac{t}{\left(\frac{\mu_o}{\rho_{go} U_{go}^2}\right)}$$

$$U_g^* = \frac{U_g}{U_{go}}$$

$$V_g^* = \frac{V_g}{U_{go}}$$

$$x^* = \frac{x}{\left(\frac{\mu_o}{\rho_{go} U_{go}}\right)}$$

$$y^* = \frac{y}{\left(\frac{\mu_o}{\rho_{go} U_{go}}\right)}$$

$$U_p^* = \frac{U_p}{U_{go}}$$

$$V_p^* = \frac{V_p}{U_{go}}$$

$$P^* = \frac{P}{\rho_{go} U_{go}^2}$$

$$S_c = \frac{\nu_o}{D_o}$$

$$\rho_p^* = \frac{\rho_p}{\rho_{po}}$$

$$\rho_o^* = \frac{\rho_{go}}{\rho_{po}}$$

$$\dot{W}_m^* = \frac{\dot{W}_m}{\dot{m}_{ref}}$$

$$\dot{m}_{ref} = \frac{\rho_{go}^2 \phi_o U_{go}^2}{\mu_o}$$

$$\dot{M}_{hr}^* = \frac{\dot{M}_{hr}}{\dot{m}_{cdref}}$$

$$\dot{M}_{vo}^* = \frac{\dot{M}_{vo}}{\dot{m}_{cdref}}$$

$$\dot{m}_{cdref} = \frac{\rho_{po}^2 \mu_o^2}{\rho_{go} U_{go}}$$

$$\mu^* = \frac{\mu}{\mu_o}$$

$$U_1 = U_g - U_p$$

$$V_1 = V_g - V_p$$

$$U_1^* = U_g^* - U_p^*$$

$$V_1^* = V_g^* - V_p^*$$

$$Re_{dpx} = \frac{\rho_g U_1 d_p}{\mu}$$

$$Re_{dpy} = \frac{\rho_g V_1 d_p}{\mu}$$

$$\theta^* = \frac{T_g}{T_{go}}$$

$$\theta_{ps}^* = \frac{T_g - T_{ps}}{T_{go}}$$

$$A_s^* = \frac{A_s}{\left(\frac{\rho_{go} \phi_o U_{go}}{3\mu_o} \right)}$$

$$\bar{H}^* = \frac{\bar{H}}{C_p T_{go}} = \frac{\bar{H}}{H_{ref}}$$

$$\begin{aligned}
D^* &= \frac{D}{D_o} \\
Y_K^* &= \frac{Y_K}{Y_{O_2,o}} \\
\dot{W}_K^* &= \frac{\dot{W}_K}{Y_{O_2,o} \dot{m}_{ref}} \\
d_p^* &= \frac{d_p}{\left(\frac{\mu_o}{\rho_{go} U_{go}}\right)}
\end{aligned}$$

B.2 DIMENSIONLESS GOVERNING EQUATIONS

$$\frac{\partial(\rho_g^* \phi^*)}{\partial t^*} + \frac{\partial(\rho_g^* U_g^* \phi^*)}{\partial x^*} + \frac{\partial(\rho_g^* \rho_g \phi^*)}{\partial y^*} = \dot{W}_m^* \quad (B.1)$$

$$\begin{aligned}
& \frac{\partial(\rho_g^* U_g^* \phi)}{\partial t^*} + \frac{\partial(\rho_g^* U_g^* \phi^* U_g^*)}{\partial x^*} + \frac{\partial(\rho_g^* U_g^* \phi^* V_g^*)}{\partial y^*} = \dot{W}_m^* U_p^* - \frac{\partial(P^* \phi^*)}{\partial x^*} \\
& + \phi^* \mu^* \left[\frac{\partial^2 U_g^*}{\partial x^{*2}} + \frac{\partial^2 U_g^*}{\partial y^{*2}} \right] + \frac{1}{3} \phi^* \mu^* \frac{\partial}{\partial x^*} \left[\frac{\partial U_g^*}{\partial x^*} + \frac{\partial V_g^*}{\partial y^*} \right] \\
& + \frac{\partial(\phi^* \mu^*)}{\partial x^*} \left[\frac{4}{3} \frac{\partial U_g^*}{\partial x^*} - \frac{2}{3} \frac{\partial V_g^*}{\partial y^*} \right] + \frac{\partial(\phi^* \mu^*)}{\partial y^*} \left[\frac{\partial U_g^*}{\partial y^*} + \frac{\partial V_g^*}{\partial x^*} \right] - \frac{A_s^* \rho_g^* U_1^{*2}}{Re_{d_{px}}} \quad (B.2)
\end{aligned}$$

$$\begin{aligned}
& \frac{\partial(\rho_g^* V_g^* \phi^*)}{\partial t^*} + \frac{\partial(\rho_g^* U_g^* \phi^* V_g^*)}{\partial x^*} + \frac{\partial(\rho_g^* V_g^* \phi^* V_g^*)}{\partial y^*} = \dot{W}_m^* V_p^* - \frac{\partial(P^* \phi^*)}{\partial y^*} \\
& + \phi^* \mu^* \left[\frac{\partial^2 V_g^*}{\partial x^{*2}} + \frac{\partial^2 V_g^*}{\partial y^{*2}} \right] + \frac{1}{3} \phi^* \mu^* \frac{\partial}{\partial y^*} \left[\frac{\partial U_g^*}{\partial x^*} + \frac{\partial V_g^*}{\partial y^*} \right] \\
& + \frac{\partial(\phi^* \mu^*)}{\partial y^*} \left[\frac{4}{3} \frac{\partial V_g^*}{\partial y^*} - \frac{2}{3} \frac{\partial U_g^*}{\partial x^*} \right] + \frac{\partial(\phi^* \mu^*)}{\partial x^*} \left[\frac{\partial U_g^*}{\partial y^*} + \frac{\partial V_g^*}{\partial x^*} \right] - \frac{A_s^* \rho_g^* V_1^{*2}}{Re_{d_{py}}} \quad (B.3)
\end{aligned}$$

$$\begin{aligned}
& \frac{\partial(\rho_g^* \theta^* \phi^*)}{\partial t^*} + \frac{\partial(\rho_g^* \theta^* U_g^* \phi^*)}{\partial x^*} + \frac{\partial(\rho_g^* \theta^* V_g^* \phi^*)}{\partial y^*} \\
& + \frac{1}{Pr} \left[\frac{\partial}{\partial x^*} \left(-\phi^* \frac{\partial \theta^*}{\partial x^*} \right) + \frac{\partial}{\partial y^*} \left(-\phi^* \frac{\partial \theta^*}{\partial y^*} \right) \right] + Ec \left[\frac{\partial(P^* U_g^* \phi^*)}{\partial x^*} + \frac{\partial(P^* V_g^* \phi^*)}{\partial y^*} \right] \\
& - \frac{Ec}{J} \frac{4}{3} \phi^* \mu^* \left[U_g^* \frac{\partial^2 U_g^*}{\partial x^{*2}} + V_g^* \frac{\partial^2 V_g^*}{\partial y^{*2}} \right] - \frac{Ec}{J} \frac{\partial(\phi^* \mu^* U_g^*)}{\partial x^*} \left[\frac{4}{3} \frac{\partial U_g^*}{\partial x^*} - \frac{2}{3} \frac{\partial V_g^*}{\partial y^*} \right] \\
& + \frac{Ec}{J} \frac{2}{3} \left[\frac{\partial U_g^*}{\partial x^*} \frac{\partial^2 V_g^*}{\partial x^* \partial y^*} + \frac{\partial V_g^*}{\partial y^*} \frac{\partial^2 U_g^*}{\partial x^* \partial y^*} \right] - \frac{Ec}{J} \frac{\partial(\phi^* \mu^* V_g^*)}{\partial y^*} \left[\frac{4}{3} \frac{\partial V_g^*}{\partial y^*} - \frac{2}{3} \frac{\partial U_g^*}{\partial x^*} \right] \\
& + Ec \left[\frac{A_s^* \rho_g^* U_1^{*2} U_p^*}{Re_{d_{px}}} + \frac{A_s^* \rho_g^* V_1^{*2} V_p^*}{Re_{d_{py}}} \right] + \frac{Ec}{J} \frac{P^*}{\partial t^*} \frac{\partial \phi^*}{\partial t^*} = \dot{W}_h^* \quad (B.4)
\end{aligned}$$

$$\begin{aligned} & \rho_g^* \phi^* \frac{Y_K^*}{\partial t^*} + \rho_g^* \phi^* U_g^* \frac{Y_K^*}{\partial x^*} + \rho_g^* \phi^* V_g^* \frac{Y_K^*}{\partial y^*} \\ & + Sc \left(\frac{\partial}{\partial x^*} (\rho_g^* \phi^* D^* \frac{\partial Y_K^*}{\partial x^*}) + \frac{\partial}{\partial y^*} (\rho_g^* \phi^* D^* \frac{\partial Y_K^*}{\partial y^*}) \right) = \dot{W}_K^* - \dot{W}_m^* Y_K^* \end{aligned} \quad (B.5)$$

$$\begin{aligned} & \frac{\partial}{\partial x^*} (\rho_g^* U_g^* \phi^* \kappa^*) + \frac{\partial}{\partial y^*} (\rho_g^* V_g^* \phi^* \kappa^*) \\ & = \frac{\partial}{\partial x^*} \left[\left(\frac{\mu_t^*}{\sigma_k^*} + \mu^* \right) \frac{\partial \phi^* \kappa^*}{\partial x^*} \right] + \frac{\partial}{\partial y^*} \left[\left(\frac{\mu_t^*}{\sigma_k^*} + \mu^* \right) \frac{\partial \phi^* \kappa^*}{\partial y^*} \right] + G^* \phi^* - \rho_g^* \epsilon^* \phi^* \end{aligned} \quad (B.6)$$

$$\begin{aligned} & \frac{\partial}{\partial x^*} (\rho_g^* U_g^* \phi^* \epsilon^*) + \frac{\partial}{\partial y^*} (\rho_g^* V_g^* \phi^* \epsilon^*) \\ & = \frac{\partial}{\partial x^*} \left[\left(\frac{\mu_t^*}{\sigma_\epsilon^*} + \mu^* \right) \frac{\partial \phi^* \epsilon^*}{\partial x^*} \right] + \frac{\partial}{\partial y^*} \left[\left(\frac{\mu_t^*}{\sigma_\epsilon^*} + \mu^* \right) \frac{\partial \phi^* \epsilon^*}{\partial y^*} \right] + C_1 \frac{\epsilon^*}{\kappa^*} G^* \phi^* \\ & - \frac{C_2 \rho^* \epsilon^{*2}}{\kappa^*} \phi^* \end{aligned} \quad (B.7)$$

$$\frac{\partial(\rho_p^*(1 - \phi_o \phi^*))}{\partial t^*} + \frac{\partial(\rho_p^* U_p^*(1 - \phi_o \phi^*))}{\partial x^*} + \frac{\partial(\rho_p^* V_p^*(1 - \phi_o \phi^*))}{\partial y^*} = -\rho_o^* \phi_o \dot{W}_m^* \quad (B.8)$$

$$\rho_p^*(1 - \phi_o \phi^*) \left[\frac{\partial U_p^*}{\partial t^*} + U_p^* \frac{\partial U_p^*}{\partial x^*} + V_p^* \frac{\partial U_p^*}{\partial y^*} \right] = A_s^* \rho_g^* U_1^{*2} \frac{\rho_o^* \phi_o}{Re_{dpx}} \quad (B.9)$$

$$\rho_p^*(1 - \phi_o \phi^*) \left[\frac{\partial V_p^*}{\partial t^*} + U_p^* \frac{\partial V_p^*}{\partial x^*} + V_p^* \frac{\partial V_p^*}{\partial y^*} \right] = A_s^* \rho_g^* V_1^{*2} \frac{\rho_o^* \phi_o}{Re_{dpy}} \quad (B.10)$$

$$\frac{d}{dt} (m_p \cdot C_p \cdot T_p) = (\dot{q}_{cond} + \dot{q}_{rad}) \cdot (\pi d_p^2) + \dot{q}_{conv} - \dot{q}_{decomp} + \dot{q}_{het} \quad (B.11)$$

$$\frac{1}{2} \rho_p^* \pi d_p^{*2} \left[\frac{dd_p^*}{dt^*} \right] = \dot{M}_{hr}^* \quad (B.12)$$

$$\left[\frac{\pi d_p^{*3}}{6} \right] \left[\frac{d\rho_p^*}{dt^*} \right] = \dot{M}_{vo}^* \quad (B.13)$$

where $G^* = \left(\frac{\mu_t^*}{\sigma_k^*} + \mu^* \right) \left[\left(2 \left(\frac{\partial V_g^*}{\partial y^*} \right)^2 + 2 \left(\frac{\partial U_g^*}{\partial x^*} \right)^2 + \left(\frac{\partial V_g^*}{\partial x^*} + \frac{\partial U_g^*}{\partial y^*} \right)^2 \right] \right]$